PUNCHING SHEAR OF FLAT SLABS WITH OPENINGS, MOMENT TRANSFER AND SHEAR REINFORCEMENT

M.Sc. Júlia Borges dos Santos

TESE DE DOUTORADO EM ESTRUTURAS E CONSTRUÇÃO CIVIL
DEPARTAMENTO DE ENGENHARIA CIVIL E AMBIENTAL

FACULDADE DE TECNOLOGIA

UNIVERSIDADE DE BRASÍLIA

UNIVERSIDADE DE BRASÍLIA
FACULDADE DE TECNOLOGIA
DEPARTAMENTO DE ENGENHARIA CIVIL

PUNCHING SHEAR OF FLAT SLABS WITH OPENINGS, MOMENT TRANSFER AND SHEAR REINFORCEMENT

M.Sc. JÚLIA BORGES DOS SANTOS

ORIENTADOR: GUILHERME SALES SOARES DE AZEVEDO MELO
COORIENTADOR: AURELIO MUTTONI *(EPFL-Suíça)*

TESE DE DOUTORADO EM ESTRUTURAS E CONSTRUÇÃO CIVIL

BRASÍLIA-DF, 13 DE JULHO DE 2023

M.Sc. JÚLIA BORGES DOS SANTOS

PUNCHING SHEAR OF FLAT SLABS WITH OPENINGS, MOMENT TRANSFER AND SHEAR REINFORCEMENT

TESE SUBMETIDA AO DEPARTAMENTO DE ENGENHARIA CIVIL E AMBIENTAL DA FACULDADE DE TECNOLOGIA DA UNIVERSIDADE DE BRASÍLIA COMO PARTE DOS REQUISITOS NECESSÁRIOS PARA A OBTENÇÃO DO GRA DE DOUTOR EM ESTRUTURAS E CONSTRUÇÃO CIVIL**.**

APROVADA POR:

_____

Prof. Guilherme Sales Soares de Azevedo Melo (UnB)
(Orientador)

_____

Profª. : Marcos Honorato de Oliveira (UnB)
(Examinador interno)

_____

Profª. : Eva Lantsoght (TU Delft)
(Examinador externo)

_____

Profª. : Leandro Mouta Trautwein (UNICAMP)
(Examinador externo)

BRASÍLIA/DF, 13 DE JULHO DE 2023

DEDICATÓRIA

Dedico esse trabalho ao meu marido

Marco, minha fonte constante de amor,

apoio e inspiração.

If you are depressed you are living in the past. If you are anxious you are living in the future. If you are at peace you are living in the present.

Lao Tzu

AGRADECIMENTOS

Gostaria de agradecer primeiramente ao meu orientador Prof. Guilherme Melo, pelos conhecimentos e experiências compartilhadas, pelas oportunidades confiadas a mim durante esse período, que foram tão essenciais para meu crescimento.
Ao meu co-orientador, Prof. Aurelio Muttoni, por ter me recebido no período de doutorado sanduíche na EPFL-Suíça. Agradeço pela sua humildade admirável e pelo convívio engrandecedor. Ao Prof. Olivier Burdet pelas conversas proveitosas. À Yvonne pela prontidão e receptividade em relação às minhas demandas. Aos técnicos do laboratório, Gilles, Jonathan, Gérald, Serge, Armin, François, Frédérique, pela disponibilidade e momentos de convivência agradáveis. Aos meus colegas do iBETON, Andri e Diego, pelos desafios vividos no laboratório e por todo conhecimento transmitido. Aos demais colegas Xhemsi, Marko, Enrique, Qianhui, Frédéric, pela convivência prazerosa. Me sinto grata pela oportunidade de ter conhecido cada um de vocês.

Ao finado Prof. Paul Regan, que foi o idealizador dos ensaios que originaram esta pesquisa.

Ao Prof. Honorato, Diretor do laboratório de estruturas da UnB (LABEST), pelo apoio essencial durante os ensaios. Ao técnico do laboratório Sr. Magno, pela prontidão e prestatividade. Ao meu colega e parceiro de laboratório João Paulo, cuja ajuda foi indispensável para concluir a etapa experimental do trabalho, e pelas discussões sempre valiosas. Aos colaboradores que trabalharam comigo no laboratório ao longo desses anos, especialmente ao Zé Paulo e toda a sua família (Sr. Jacinto, Hagamenon pai e filho, João e Daniel).

Ao Prof. Miguel Ruiz, pela colaboração em uma parte do trabalho. Sua paciência e comprometimento em ajudar são qualidades preciosas e admiráveis.

Ao meu marido, Marco, e aos meus pais, Celso e Izilda, pelo suporte e ajuda nas minhas frequentes viagens à Brasília. Aos meus amigos Laila e Thomas, Sheila e Ribamar, Raissa, Paula e Asher, pelas conversas encorajadoras nos momentos difíceis.

Aos colegas que contribuíram nas concretagens e ensaios: Henrique, Vitor, Renata, Natanael, Renan, John, Renan, Kleiça, Brunna, Pedro, Thalia e Mara. Agradeço ao aluno de mestrado Junio por sua contribuição durante a segunda série de ensaios. Aos colegas que me ajudaram de diversas formas: Prof. Roger, Prof. Jonathas, Pedro Paulo, Prof. Manoel e Jerfson.

Gostaria de expressar minha profunda gratidão a todos aqueles que contribuíram para o sucesso da minha pesquisa, mesmo que eu possa não me lembrar de todos os nomes neste momento. Ao longo de muitos anos de trabalho, a contribuição essencial de alunos, professores, técnicos, amigos e até desconhecidos foi fundamental para sua conclusão. Seu apoio em qualquer medida foi inestimável.

Expresso minha gratidão à empresa *Trejor* pelo fornecimento dos studs, à *Ciplan* pelo fornecimento do concreto e ao *SENAI-DF* pelo suporte nos ensaios de caracterização de materiais. Por fim, gostaria de agradecer às agências de apoio financeiro brasileiras CAPES, CNPq e FAP-DF.

ACKNOWLEDGEMENT

I would like to express my most sincere gratitude to my supervisor, Prof. Guilherme Melo, for the knowledge and shared experiences, as well as the opportunities entrusted to me during this period, which have been essential for my growth.

To my co-supervisor, Prof. Aurelio Muttoni, for hosting me during my exchange PhD period at EPFL-Switzerland. I am grateful for his admirable humility and enriching companionship. I thank Prof. Olivier Burdet for the insightful conversations and Yvonne for her promptness and responsiveness to my requests. I extend my appreciation to the laboratory technicians, Gilles, Jonathan, Gérald, Serge, Armin, François, Frédérique, for their availability and pleasant interactions. To my colleagues at iBETON, Andri and Diego, for the challenges faced in the laboratory and the knowledge shared. To the other colleagues Xhemsi, Marko, Enrique, Qianhui, Frédéric, for the pleasant companionship. I am grateful for the opportunity to have known each and every one of you.

To the late Prof. Paul Regan, who conceived the tests that originated this research.

To Prof. Honorato, Director of the Structures Laboratory at UnB (LABEST), for the essential support during the tests. To laboratory technician Mr. Magno, for his readiness and helpfulness. To my colleague and laboratory partner João Paulo, whose assistance was indispensable to complete the experimental phase of this work, and for the always valuable discussions. To the collaborators who have worked with me in the laboratory over these years, especially to Zé Paulo and his entire family (Mr. Jacinto, Hagamenon father and son, João, and Daniel).

To Prof. Miguel Ruiz, for his collaboration in a part of this work. His patience and commitment to help are precious and admirable qualities.

To my husband, Marco, and my parents, Celso and Izilda, for their support and assistance during my frequent trips to Brasília. To my friends Laila and Thomas, Sheila and

Ribamar, Raíssa. Paula and Asher, for the encouraging conversations during challenging times.

To the colleagues who contributed to the concrete pouring and tests: Henrique, Vitor, Renata, Natanael, Renan, John, Renan, Kleiça, Brunna, Pedro, Thalia, and Mara. I appreciate the contribution of the master's student Junio during the second series of tests.

To the colleagues who have helped me in various ways: Prof. Roger, Prof. Jonathas, Pedro Paulo, Prof. Manoel, and Jerfson.

I would like to express my deep gratitude to all those who have contributed to the success of my research, even if I cannot remember all the names at this moment. Throughout many years of work, the essential contribution of students, professors, technicians, friends, and even strangers has been fundamental to its completion. Your support in any measure has been invaluable.

I express my gratitude to the company *Trejor* for the supply of studs, to *Ciplan* for the supply of concrete, and to *SENAI-DF* for the support in material characterisation tests. Finally, I would like to thank the Brazilian funding agencies *CAPES*, *CNPq*, and *FAP-DF* for their financial support.

ABSTRACT

PUNCHING SHEAR OF FLAT SLABS WITH OPENINGS, MOMENT TRANSFER AND SHEAR REINFORCEMENT

Author: Júlia Borges dos Santos
Supervisor: Guilherme Sales Soares de Azevedo Melo
Co-supervisor: Aurelio Muttoni
Programa de Pós-graduação em Estruturas e Construção Civil
Brasília, 13 de julho de 2023

Openings in flat slabs near to columns are often needed to supply the building with utilities. The presence of these openings can lead to a decrease of the punching resistance which is related to (i) the reduction of the control perimeter, (ii) the stress concentrations at the edges of the openings, (iii) the reduction of the unitary shear resistance caused by increased flexural deformations and (iv) the moment transfer in the slab connection in case of unsymmetrical openings. The impact of openings on punching shear resistance depends on their geometry, location, number, and size. Although current code approaches consider a reduction in the control perimeter, there is a lack of sufficient experimental evidence and certain effects are disregarded in design codes. Furthermore, the available literature on slabs with openings and unbalanced moments is limited. Despite the common use of shear reinforcement to enhance punching resistance, there is a surprising absence of published experimental work on shear-reinforced interior connections with openings and unbalanced moments. This study presents three experimental programmes focusing on flat slabs with openings. The first consists of eight interior slab-column connections with axis-symmetric loading and openings at different locations and dimensions. The second consists of nine interior slab-column connections with openings at different locations and dimensions, subjected to different unbalanced moment orientations and eccentricities, and without shear reinforcement. The last series of experimental tests consists of five slabs with openings and moment transfer, representing several practical cases and potential arrangements of shear reinforcement. Additionally,

this work proposes a new approach and a new definition of the control perimeter to improve the prediction of the punching shear resistance of slabs with openings based on the results of the database, previous studies, and linear-elastic analyses of the shear force distribution along the control perimeter. Simple and refined approaches of the Critical Shear Crack Theory are suggested and validated with experimental results to consider the redistribution of forces caused by the openings and/or moment transfer.

Keywords: flat slabs, openings, moment transfer, shear reinforcement, CSCT

RESUMO

PUNÇÃO EM LAJES LISAS COM ABERTURAS, TRANSFERÊNCIA DE MOMENTO FLETOR E ARMADURA DE CISALHAMENTO
Autora: Júlia Borges dos Santos
Orientador: Guilherme Sales Soares de Azevedo Melo
Co-orientador: Aurelio Muttoni
Programa de Pós-graduação em Estruturas e Construção Civil
Brasília, 13 de julho de 2023

Aberturas em lajes lisas próximas aos pilares são frequentemente necessárias para passagem de tubulações diversas na edificação. A presença dessas aberturas pode levar a uma diminuição da resistência ao cisalhamento por punção, que está relacionada a: (i) redução do perímetro de controle, (ii) concentrações de tensão nos cantos das aberturas, (iii) redução da resistência ao cisalhamento devido a maiores deformações de flexão e (iv) transferência de momento na ligação da laje em caso de aberturas assimétricas. O impacto das aberturas na resistência ao cisalhamento por punção depende de sua geometria, localização, quantidade e dimensões. Embora as das normas vigentes considerem uma redução no perímetro de controle, há uma falta de evidências experimentais e certos efeitos são negligenciados. Além disso, a literatura disponível sobre lajes com aberturas e momentos é limitada. Apesar do uso comum de armadura de cisalhamento para aumentar a resistência à punção, surpreendentemente, não há trabalhos experimentais publicados sobre ligações internas com armadura de cisalhamento, com aberturas e transferência de momentos. Este trabalho apresenta três programas experimentais focados em lajes lisas com aberturas. O primeiro consiste em oito ligações laje-pilar com carregamento simétrico e aberturas em diferentes locais e dimensões. O segundo consiste em nove ligações com aberturas em diferentes locais e dimensões, sujeitas a diferentes orientações e excentricidades de momentos, e sem armadura de cisalhamento. A última série de testes consiste em cinco lajes com aberturas e transferência de momento, representando vários casos práticos e detalhamentos

potenciais de armadura de cisalhamento. Além disso, este trabalho propõe uma nova abordagem e uma nova definição do perímetro de controle para melhorar a previsão da resistência à punção de lajes com aberturas com base na análise do banco de dados, estudos anteriores e análises lineares-elásticas da distribuição da força de cisalhamento ao longo do perímetro de controle. Abordagens simples e refinadas da Teoria da Fissura Crítica são sugeridas e validadas com resultados experimentais para considerar a redistribuição de esforços causadas pelas aberturas e/ou transferência de momento.

Palavras-chave: lajes lisas, aberturas, transferência de momento, armadura de cisalhamento, TFC.

SUMÁRIO

LIST OF FIGURES ..... **xvii**

LIST OF TABLES ..... **xxi**

LIST OF SYMBOLS ..... **xxiii**

1. INTRODUCTION **29**

1.1. PROBLEM STATEMENT 29

1.2. OBJECTIVES 31

1.3. SCIENTIFIC CONTRIBUTIONS 32

1.4. STRUCTURE OF THE THESIS 33

1.5. REFERENCES 34

2. PUNCHING RESISTANCE OF FLAT SLABS WITH OPENINGS ADJACENT TO THE COLUMN **39**

2.1 INTRODUCTION 39

2.2 EXPERIMENTAL INVESTIGATION 41

2.2.1 First remarks 41

2.2.2 Material and Specimens 41

2.2.3 Test setup and instrumentation 43

2.3 EXPERIMENTAL RESULTS AND DISCUSSION 44

2.3.1 Vertical displacements 44

2.3.2 Ultimate load 50

2.3.3 Crack pattern 51

2.3.4 Steel strain 54

2.3.5 Concrete strain 55

2.4 COMPARISON WITH DESIGN CODES 57

2.5 CONCLUSIONS 63

2.6 REFERENCES 64

3. ENHANCEMENT OF THE PUNCHING SHEAR VERIFICATION OF SLABS WITH OPENINGS 68

3.1 INTRODUCTION 68

3.2 DESIGN CODE APPROACHES FOR SLABS WITH OPENINGS 71

3.3 ANALYSIS OF EXPERIMENTAL DATA 76

3.3.1 Preliminary remarks 76

3.3.2 Comparison of punching shear strength predicted by codes 77

3.4 PROPOSED PUNCHING VERIFICATION FOR SLABS WITH OPENINGS . 78

3.4.1 Modification of the control perimeter to account for the presence of an opening 78

3.4.2 Approach for slabs with unsymmetrical openings 82

3.4.3 Application of the proposed approach to the database 84

3.5 APPLICATION OF THE CRITICAL SHEAR CRACK THEORY TO SLABS WITH OPENINGS 86

3.5.1 Introdutory remarks 86

3.5.2 Approach for slabs with openings 88

3.6 CONCLUSIONS 91

3.7 REFERENCES 93

4. INVESTIGATING PUNCHING SHEAR IN SLABS WITH UNBALANCED MOMENTS AND OPENINGS 99

4.1 INTRODUCTION 99

4.1.1 General 99

4.1.2 ACI 318:19 provision for slab with openings 100

4.1.3 fib MC 2010:13 levels of approximation for slab with openings 104
4.1.4 prEN 1992-1-1:23 provision for slab with openings 105
4.2 EXPERIMENTAL PROGRAMME 105
4.2.1 Specimens and materials 106
4.2.2 Test setup and instrumentation 109
4.3 EXPERIMENTAL RESULTS AND DISCUSSION 110
4.3.1 Punching shear resistance 110
4.3.2 Flexural reinforcement strains 112
4.3.3 Load-deflection relationship 112
4.3.4 Concrete strains 118
4.4 COMPARISON OF THEORETICAL PREDICTIONS AND EXPERIMENTAL RESULTS 124
4.5 CONCLUSIONS 130
4.6 REFERENCES 131
4.7 APPENDIX A 136
4.7.1 J_c property according to ACI 318:19 136
5. PUNCHING PERFORMANCE OF FLAT SLABS WITH OPENINGS ACCOUNTING FOR THE INFLUENCE OF MOMENT TRANSFER AND SHEAR REINFORCEMENT 139
5.1 Introduction 139
5.2 Experimental programme 142
5.2.1 Specimen description 142
5.2.2 Material properties 146
5.2.3 Test setup and instrumentation 146
5.3 EXPERIMENTAL RESULTS 148
5.3.1 Global response and failure mode 148

5.3.2 Cracking pattern 150
5.3.3 Strains on the concrete surface 154
5.3.4 Activation of shear reinforcement 156
5.4 COMPARISON TO CODE PREDICTIONS 158
5.5 A MECHANICAL APPROACH FOR PUNCHING DESIGN OF FLAT SLABS WITH OPENINGS AND UNBALANCED MOMENTS 160
5.5.1 Mechanical background 160
5.5.2 Shear field analysis 162
5.5.3 Failure criteria 164
5.5.4 Comparison with test results and discussion 166
5.6 CONCLUSIONS 167
5.7 REFERENCES 168
5.8 ANNEX A: FLEXURAL STRENGTH 176
5.9 ANNEX B: EXPERIMENTAL DATA 176
6. CONCLUSIONS AND OUTLOOK 185
6.1 CONCLUSIONS 185
6.1.1 Punching resistance of flat slabs with openings adjacent to the column 185
6.1.2 Enhancement of the punching shear verification of slabs with openings 186
6.1.3 Investigating punching shear in slabs with unbalanced moments and openings 187
6.1.4 Punching performance of flat slabs with openings accounting for the influence of moment transfer and shear reinforcement 189
6.2 OUTLOOK 190
ANNEX A: CODE PROVISIONS 192

LIST OF FIGURES

Figure 1.1 - Available punching tests on various types of connections: (a) distribution among all connection types (b) distribution among connections that include openings (adapted from [28]) 30

Figure 2.1 - Slab characteristics 42

Figure 2.2 - Tests setup (a) Plain view (b) Section A-A (c) Section B-B 45

Figure 2.3 - Measurement of displacements in slabs 46

Figure 2.4 - Flexural reinforcement instrumentation (a) L1 (b) L2, L3 e L4 (c) L7 e L9 (d) L16 e L19 46

Figure 2.5 - Positioning of concrete strain gages (a) L1, L2, L3, L4 (b) L7 e L9 (c) L16 e L19 47

Figure 2.6 - Force *versus* displacement (a) L1 (b) L2 (c) L3 (d) L4 (e) L7 (f) L9 (g) L16 (h) L19 49

Figure 2.7 - Comparison of the Force versus displacement (a) L1 (b) L2 (c) L3 (d) L4 (e) L7 (f) L9 (g) L16 (h) L19 50

Figure 2.8 - Slab cracking (a) L1 (b) L2 (c) L3 (d) L4 (e) L7 (f) L9 (g) L16 (h) L19 52

Figure 2.9 - Failure surface (a) L1 (b) L2 (c) L3 (d) L4 (e) L7 (f) L9 (g) L16 (h) L19 53

Figure 2.10 - Punching cone (a) L2 (b) L3 (c) L4 55

Figure 2.11 - Force versus strain of flexural bars 55

Figure 2.12 - Deformations in concrete Slabs L1 a L4 56

Figure 2.13 - Deformations in concrete of slabs L7, L9 L16 e L19 57

Figure 2.14 - Control perimeter and centroid (a) fib MC 2010 (b) Eurocode 2 e ABNT NBR 6118 (c) ACI 318 61

Figure 3.1 - Effect of the position of the opening on the shear force distribution along the control perimeter located at 0.5d from the column for slabs from Teng et al. (2004) [12]: (a) OC11H30; (b) OC11V20; and (c) OC11V23 (black curves (**1**): control perimeter; blue curves (**2**): shear force distribution for slab without opening; red curves (**3**): shear force distribution for slab with opening) 69

Figure 3.2 - Effect of the distance of the opening on the shear force distribution for slabs from Augustin et al. (2019) [10] for openings distance equal to: (a) 0d; (b) 1d; (c) 2d; and (d) 2d with opening dimensions equal to 300x200 mm 69

Figure 3.3 - Effect of the position of the opening on the shear force distribution along the control perimeter of a rectangular column for slabs from Souza (2008) [7], c_{max}/ c_{min} =2.5: (a) L2, L3 and L4; (b) L7; (c) L9; (d) L16; and (e) L19 70

Figure 3.4 - Reduction of control perimeter to account for openings according to several approaches: (a), (b) and (c) ACI ASCE Committee 326:2 [6]; (d) BS 8110:1995 [9] and Regan (1974) [1]; and (e) Teng et al. (2004) [12] 72

Figure 3.5 - Reduction of the control perimeter in presence of openings according to: (a) fib MC 2010:2013 [27] and prEN 1992-1-1:2021 [26]; (b) ACI 318:2019 [24]; and (c) EN 1992-1-1:2004 [25] 74

Figure 3.6 - Current control perimeter according to fib MC 2010:2013 for tests by Souza (2008) [7]: (a) L9; (b) L19; and (c) Experimental resistance-effective control perimeter of slabs L9 and L19 75

Figure 3.7 - ASCE Committee 352.1R:1989 [28] recommendation for connection with large openings..... 75

Figure 3.8 - Database analysis according to codes provisions: (a) ACI318:2019; (b) EN 1992-1-1:2004; (c) prEN 1992-1-1:2021; and (d) fib MC 2010:2013-LoAII (Legend for symbols in Table 3.2) 78

Figure 3.9 - Control perimeter reduction rule according to the proposed approach: (a) when b < c+d; and (b) when b ≥ c+d (c- column dimension, b- opening dimension, a- distance from the opening to the face of the column, a*- distance of the opening from the face of the column that leads no reduction of the control perimeter, according to 3. 1 and 3. 2)..... 80

Figure 3.10 - Comparison between current and proposed control perimeter for slabs L9 and L19 from Souza (2008) [7]..... 81

Figure 3.11 - Linear-elastic distribution of shear force along the control perimeter at 0.5d and maximum nominal shear calculated for slabs from Teng et al. (2004) [12]: (a) OC11 with e=240mm without opening; and (b) OC11H30 with opening, but without eccentricity of the resultant. (Note: maximum nominal shear force shown for a total applied load V = 373 kN)..... 82

Figure 3.12 - Effect of opening dimension on the stress field at 0.5d and maximum nominal shear for slabs with a square column width equal to 200 mm and for several opening width: (a) b/c = 0.5; (b) b/c = 1, square opening; (c) b/c = 2, rectangular opening; and (d) b/c = 1, rectangular opening. (Note: maximum nominal shear stress shown for a total applied load V = 373 kN)..... 83

Figure 3.13 - Proposed approach to account the moment transfer in slabs with unsymmetrical openings: (a) opening on the side of the column; and (b) opening on the corner of the column; (c) control perimeter to calculate the punching shear resistance; and (d) simplification of the control perimeter with sharp corners to calculate its centroid..... 84

Figure 3.14 - Database analysis with proposed changes (eccentricity in case of unsymmetric openings) and new control perimeter for the approaches according to: (a) ACI318:19; (b) prEN 1992-1-1: 2021 (c) fib MC 2010:13-LoAII; and (d) CSCT LoAIII-ψm (Legend for symbols in Table 3.3) 85

Figure 3.15 - Load-rotation relationship and failure criterion for several cases: (a) L45FFS_CG from Borges (2004) [14], ρ_x/ρ_y=0.86, c_{max}/c_{min} =3.0; (b) L9 from Souza (2008) [7], ρ_x/ρ_y=0.92, c_{max}/c_{min} =2.5; (c) S1-1 from Augustin et al (2019) [10], ρ_x/ρ_y=0.88, c_{max}/c_{min} =1.0; and (d) LF2-A from Liberati et al (2019) [17], ρ_x/ρ_y=1.0, c_{max}/c_{min} =1.0. 90

Figure 4.1 - Stress distribution of an interior column subjected to moment about y-axis according to ACI 318:2019 (a) moment orientation clockwise (b) moment orientation contraclockwise 103

Figure 4.2 - Slabs characteristics: dimensions and loading configuration 106

Figure 4.3 - Tests setup (a) Plain view (b) Section A-A (c) Section B-B 108

Figure 4.4 - Instrumentation: displacement measurement locations, flexural reinforcement strain gauges and concrete bottom surface strain gauges..... 109

Figure 4.5 - Comparison of ultimate strength of slabs with openings to reference slab: (a) the reference capacity are the slab without openings with unbalanced moments (L14 and L15) and (b) the reference capacity is the slab without openings with concentric loading (L1 from [12]) 111

Figure 4.6 - Flexural reinforcement strain comparison of all slabs 112

Figure 4.7 - Displacement-location of slabs in both directions, west-east direction: (a) L14 (b) L8 (c) L10, north-south direction: (e) L14 (f) L8 (g) L10 115

Figure 4.8 - Displacement-location of slabs in both directions, west-east direction: (a) L11 (b) L12 (c) L13, north-south direction: (e) L11 (f) L12 (g) L13 116

Figure 4.9 - Displacement-location of slabs in both directions, west-east direction: (a) L15 (b) L17 (c) L18, north-south direction: (e) L15 (f) L17 (g) L18 117

Figure 4.10 - Load-displacement in the west-east and north-south direction (a) Legend (b) Slabs without openings (14 and L15) (c) Slabs with openings and moment transfer in the west-east direction (L8, L10, L11, L12 and L13) (d) Slabs with openings and moment transfer in the north-south direction (L17 and L18) 118

Figure 4.11 - Concrete strain comparison between slabs L1, L8, L11, L14 (a) legend (b) radial-northeast column corner (c) tangential-the northeast column corner (d) radial-column axis (e) tangential-column axis (f) radial-west column corner (g) tangential-west column corner 121

Figure 4.12 - Concrete strain comparison between slabs L1, L15, L16, L17, L18, L19 (a) legend (b) radial-northeast column corner (c) tangential-northeast column corner (d) radial-east column corner (e) tangential-northeast opening corner 122

Figure 4.13 - Concrete strain comparison between slabs with moment transfer and slabs with axis-symmetric loading (a) legend and slabs characteristics (b) radial-northeast column corner (c) tangential-northeast column corner (d) radial-north column axis (e) tangential-north column axis (f) radial-northwest column corner (f) tangential-northwest column corner 123

Figure 4.14 - Experimental-to-theoretical resistance considering the current control perimeter and (a) $b_{0,eff}/b_{0,full}$ (b) number of openings, considering the control perimeter from [7] and (c) $b_{0,eff}/b_{0,full}$ (d) number of openings 124

Figure 4.15 - (a) Comparison of coefficient k_{pb} from two different approaches of prEN 1992-1-1:21, perimeter at column edge b_0 and at 0.5d $b_{0,5}$ for: (b) slab without opening (c) L17 (d) L18 128

Figure 4.16 - Control perimeter of slabs with openings according to the current radial line approach, and according to the approach of Santos et al. (2022) 128

Figure 4.17 - Normalized stresses distribution according to ACI 318:19 (a) west-east direction of slabs L14, L8, L10, L11, L12 (b) north-south direction of slabs L15, L17, L18 129

Figure 4.18 - Control perimeter areas for the J_c calculation of an interior connections subjected to moment transfer in the y-direction (a) connection without opening (b) connection with opening (P: control perimeter centroid, O: column centroid) 136

Figure 4.19 - Control perimeter and parameters for J_c calculation for different opening's location (O: column centroid, P: control perimeter centroid) 138

Figure 5.1 - Slab with an opening adjacent to a column: (a) section at the opening, and (b) view of the slab-column connection 139

Figure 5.2 - Load-rotation of with and without openings (a) comparison of specimens with axis-symmetric loading, with and without shear reinforcement, tested by [13] (b) comparison of specimens with and without moment transfer, tested by [20] (Note: in both cases the reference specimen is 1-without openings, without shear reinforcement and with axis-symmetric loading) 140

Figure 5.3 - Main dimensions and load arrangement (Note: dimensions in mm) 144

Figure 5.4 - Reinforcement arrangement and instrumentation of the slabs: (a) flexural and column reinforcement arrangement; (b) LVDTs; (c) bottom concrete strain gauge position; (d) shear stud arrangement; and (e) shear reinforcement detailing (Note: units in mm)... 145

Figure 5.5 - Test setup: (a) plan view; and (b) side view 147

Figure 5.6 - Load-rotation relationships of the tested specimens (Note: LRSS: slab with moment, without openings and without shear reinforcement, LRFS: slab with openings, with moment and without shear reinforcement, LFS1-S3: Slabs with openings, with moment and with shear reinforcement, ψ_N, ψ_E, ψ_W: rotation in the north, east and west side, respectively) 149

Figure 5.7 - Activation of flexural reinforcement 150

Figure 5.8 - Cracking pattern on the top surface of the slabs 152

Figure 5.9 - Saw cuts and lateral views of specimens: (a) LRSS; and (b) LRFS, LFS1-S3 153

Figure 5.10 - Concrete strains: (a) EC03; (b) EC04; (c) EC05; (d) EC06; (e) EC07; (f); EC08; (g) EC09; and (h) EC10 (refer to Figure 5.4) 155

Figure 5.11 - Load-strain of shear reinforcement for different locations: (a) northwest (b) column north axis (c) northeast 1st layer (d) northeast 2nd layer (e) northeast opening region 157

Figure 5.12 - Activation of shear reinforcement according to stud position: (a) 1st layer; and (b) 2nd layer 157

Figure 5.13 - Shear force distribution along the control perimeter of slabs with moment transfer: (a) slab without openings; and (b) slab with openings 163

Figure 5.14 - Punching shear resistance approach according to the CSCT [39] adapted for slabs with openings and unbalanced moments: (a) LRSS, (b) LRFS and (c) LFS2..... 167

Figure 5.15 - Governing yield-line pattern: (a) LRSS (b) LRFS, LFS1-S3 176

Figure 5.16 – LRSS: instrumentation of flexural rebars 179

Figure 5.17 – LRFS: instrumentation of flexural rebars 180

Figure 5.18 – Strains of flexural rebars: (a) LRSS (b) LRFS (c) LFS1 (d) LFS2 (e) LFS3 181

Figure 5.19 – Instrumentation of shear reinforcement (a) LFS1 (b) LFS2 (c) LFS3 182

Figure A. 1 - Control perimeter reduction of slabs with openings according to: (a) fib MC 2010:13 and FprEN 1992-1-1:23 (b) ACI 318:19 192

LIST OF TABLES

Table 2.1 - Properties of concrete and reinforcing steel 43

Table 2.2 - Ultimate and normalized strengths 43

Table 2.3 - Summary of code provisions of Eurocode 2 and ABNT NBR 6118 58

Table 2.4 - Experimental and theoretical resistances 59

Table 2.5 -Summary of code provisions for load eccentricity 62

Table 2.6 - Experimental and theoretical resistances with moment transfer 62

Table 3.1 - Summary of database containing 68 specimens with openings and without transverse reinforcement 76

Table 3.2 - Summary of experimental-to-calculated resistances according to the current codes provision (see Figure 3.8) 85

Table 3.3 - Summary of experimental-to-calculated resistances according to the proposed approach (see Figure 3.14) 86

Table 3.4 - Percentage of unsafe code provisions over 40 slabs with unsymmetrical openings according to the current and proposed control perimeter to account for openings 86

Table 3.5 - Summary of results of the CSCT and MC 2010:13 (experimental-to-calculated resistances) according to the new control perimeter, and for different approaches. Note: results for 68 slabs from the database. 91

Table 4.1 - Characteristics of tested slabs 107

Table 4.2 - Properties of concrete and flexural reinforcement rebars 107

Table 4.3 - Ultimate loads and moments (M'_u is the moment at ultimate load with respect to the column axis, e'_u is the eccentricity of ultimate load with respect to the column axis) 110

Table 4.4 - Summary of experimental-to-theoretical results of the codes shown in Figure 4.14 125

Table 4.5 - Summary of experimental-to-theoretical provisions of codes according to the current control perimeter and the control perimeter proposed by Santos et al. (2022) [7] 125

Table 5.1 - Main geometrical and material properties 144

Table 5.2 - Load levels at which shear cracking was observed and failure crack inclination 152

Table 5.3 - Comparison of experimental-to-calculated resistances according to codes of practice 159

Table 5.4 – Slab LRSS: results of rotations 177

Table 5.5 - Slab LRFS: results of rotations 177

Table 5.6 - Slab LFS1: results of rotations 178

Table 5.7 - Slab LFS2: results of rotations 178

Table 5.9 - Slab LFS3: results of rotations 179

Table 5.9 – Slab LFS1: ratio of recorded-to-yield shear reinforcement strain ($\varepsilon / \varepsilon_{ys}$) 182

Table 5.10 – Slab LFS2: ratio of recorded-to-yield shear reinforcement strain ($\varepsilon / \varepsilon_{ys}$)..... 183
Table 5.11 – Slab LFS3: ratio of recorded-to-yield shear reinforcement strain ($\varepsilon / \varepsilon_{ys}$)..... 183
Table A. 1 - Summary of ACI 318 :19 provisions 192
Table A. 2 - Summary of fib MC 2010:13 provisions..... 193
Table A. 3 - Summary of FprEN 1992-1-1:23 provisions..... 193

LIST OF SYMBOLS

Symbols

B specimen side

E_s modulus of elasticity

J_c property analogous to polar moment of inertia, according to ACI 318:19

V punching shear force

V_R punching shear resistance

V_E shear force acting at the control perimeter, according to prEN 1992-1-1:23

V_{cr} level of shear force at which first crack was observed on the sides of the opening

V_{Rc} calculated punching resistance of a slab without shear reinforcement

$V_{R,max}$ calculated maximum punching resistance of a slab with shear reinforcement

$V_{R,cs}$ calculated punching resistance of a shear-reinforced slab

V_{flex} flexural resistance of a slab-column connection in punching

V_{test} experimental punching shear resistance

V_{calc} theoretical punching shear resistance

V_{crush} failure by crushing of concrete

V_{within} failure within the shear reinforced zone

V_A, V_B, V_c shear force acting in the sectors A, B and C respectively

$V_{R,A}$, $V_{R,B}$, $V_{R,C}$ governing shear resistance of sectors A, B and C respectively

$A_{ø}$ cross-sectional area of one rebar

A_{sw} cross-sectional area of shear reinforcement

a distance of the opening from the face of the column

a^* distance of the opening from the face of the column that leads no reduction of the control perimeter

a_{px}, a_{py} distances from the axis of the support area to the zero radial bending moment according to prEN 1992-1-1:23

b opening width parallel to the column (refer to Figure 3.9)

$b_{0.5}$ length of control perimeter at 0.5d from the edge of the supported column

b_0 length of control perimeter at the edge of the supported column

$b_{1,red}$ reduced control perimeter for large supported areas according to fib Model Code 2010

$b_{0,eff}$ effective control perimeter of slab with opening

$b_{0,full}$ control perimeter of slab without opening

b_{cp} length of control perimeter within radial lines, according to ASCE Committee 352.1R:1989 (refer to Figure 3.7)

b_x,b_y side length of the opening in x, resp. y-direction

b_1 dimension of the critical section measured in the direction of the span for which moments are determined, according to ACI 318:19

b_2 dimension of the critical section measured in the direction perpendicular to b_1, according to ACI 318:19

b_u diameter of a circle with the same surface as the region inside the control perimeter according to *fib* MC 2010:13

b_s width of the support strip for calculating m_E

b_b geometric mean of the minimum and maximum overall widths of the control perimeter, according to prEN 1992-1-1:23

$b_{b,min}$,$b_{b,max}$ minimum and maximum overall widths of the control perimeter, according to prEN 1992-1-1:23

$b_{1,A}$, $b_{1,B}$, $b_{1,C}$ basic control perimeter of sectors A, B and C respectively

c square column dimension

c_{max}, c_{min} maximum and minimum side length of a rectangular column

c_x, c_y side length of a square column in x, resp. y-direction

d effective depth

d_g maximum aggregate size

d_{g0} reference aggregate size

d_v shear-resisting effective depth of reinforcement

$e_{predicted}$ predicted eccentricity to be applied in the test

e_u eccentricity with respect to the control perimeter centroid

e'_u eccentricity of ultimate load with respect to the column centroid

$e_{b,x}$,$e_{b,y}$ components of the eccentricity of the resultant of shear forces with respect to the centroid of the control perimeter, according to prEN 1992-1-1:23

f_b bond strength of shear reinforcement

f_c concrete compressive strength measured on a cylinder

f_{ys} yield strength of flexural reinforcement

f_{yw} yield strength of shear reinforcement

f_u ultimate strength of flexural reinforcement

k size effect according to EC2:04 and ABNT NBR 6118:14

k_1 coefficient dependent on the ratio between column dimensions, according to Eurocode 2:04

k_m coefficient related to level of approximation

k_{pb} shear gradient enhancement coefficient for punching according to prEN 1992-1-1:23

k_e coefficient of eccentricity

k_ψ coefficient for rotations

k_m factor of proportionality related to the level of approximation

k_{dg} coefficient for aggregate size

k_{sys} maximum punching shear resistance coefficient

J property analogous to polar moment of inertia, according to ACI 318:19

M_u moment at ultimate load, with respect to the control perimeter centroidal axis

M'_u moment at ultimate load, with respect to the column axis

M_x bending moment due the presence of opening in the axis x (refer to Figure 3.13)

M_y bending moment due the presence of opening in the axis x (refer to Figure 3.13)

m_E bending moment per unit width

m_R flexural strength per unit width

m_{eq} bending moment calculated per equilibrium

$m_{eq,x}$, $m_{eq,y}$ bending moment calculated per equilibrium in directions *x* and *y*

n_r number of studs

r_s the distance between the axis of the supported area ant the line of contraflexure

r_1 the distance between the yield line and the loading point *P/4* (see Figure A.1)

r_2 the distance between the yield line and the loading point *P/8* (see Figure A.1)

β coefficient of eccentricity according to Eurocode 2 and ABNT NBR 6118

β_e coefficient accounting for concentrations of the shear forces according to prEN 1992-1-1:23

ε_{ys} yield strain of flexural reinforcement

ε_c concrete bottom strain measured on the test

ϕ_s flexural reinforcement diameter

ϕ_w shear reinforcement diameter

γ_v ratio of moment between slab and column that is considered transferred by eccentricity of shear according to ACI 318:19

v_{op} shear force perpendicular to the control perimeter for slab with opening (refer to Figures 3.1-3.3)

$v_{perp,max}$ maximum value of the shear force projected in the direction perpendicular to the control perimeter (refer to Figures 3.1-3.3)

η_c coefficient accounting for contribution of concrete, according to prEN 1992-1-1:23

η_s coefficient accounting for contribution of shear reinforcement, according to prEN 1992-1-1:23

η_{sys} coefficient for maximum punching, according to prEN 1992-1-1:23

u_1 control perimeter at 2*d* according to EC2:04 and ABNT NBR 6118:14

μ_p coefficient accounting for the shear force-to-bending moment ratio and for shear force concentrations according to prEN 1992-1-1:23

w opening of the CSC

ψ slab rotation

ψ_{m} geometric mean of the rotations

ψ_{max} maximum rotation

ψ_{x} rotation in the *x*-direction

ψ_{y} rotation in the *y*-direction

ψ_{W} rotation in the west side

ψ_{E} rotation in the east side

ψ_{N} rotation in the north side

W_1 corresponds to a distribution of shear as function of the basic control perimeter u_1, according to Eurocode 2 and ABNT NBR 6118

θ punching cone inclination

ρ flexural reinforcement ratio

ρ_x, ρ_y flexural reinforcement ratio in directions *x* and *y*

σ_{sw} shear reinforcement stress

$\lambda_A, \lambda_B, \lambda_C$ corresponding shear force at sector A, B and C, respectively

Acronyms and abbreviations:

O Column centroid

C centroid of the column (refer to Figure 3.13)

P centroid of the control perimeter (refer to Figure 3.13 and 4.1)

CSC Critical Shear Crack

CSCT Critical Shear Crack Theory

Col. Column

LVDT Linear Variable Differential Transducer

LRSS Slab with moment, without openings and without shear reinforcement

LRFS Slab with openings, with moment and without shear reinforcement

LFS1-S3 Slabs with openings, with moment and with shear reinforcement

N North cardinal direction

NS North-South cardinal direction

E East cardinal direction

S South cardinal direction

SE South-East cardinal direction

W West cardinal direction

WE West-East cardinal direction

1. INTRODUCTION

1.1. PROBLEM STATEMENT

In flat slab buildings, openings are commonly positioned near the slab-column region to accommodate utility pipes. However, this choice, which offers clear benefits for building services and architectural purposes, can have significant implications for the punching performance of slab-column connections. The proximity of the openings to the columns restricts the use of transverse reinforcement in this region of high shear stresses, leading to a significant decrease in punching shear resistance.

In 1960, Di Satsio and Van Buren [1] discussed the stress modification caused by openings in flat slabs and proposed a reduction in the resisting control perimeter. From an experimental perspective, Moe (1961) [2] conducted the first study on the influence of openings on the punching shear behaviour of slabs without transverse reinforcement. It took more than thirty years for similar research to emerge [3].

However, while studies on slabs with openings and axis-symmetric loading have made significant contributions to the field, both for slabs without shear reinforcement [1-10] and with shear reinforcement [11-16], they do not reflect real-world scenarios where unbalanced moments are more prevalent. Additionally, the literature presents only a limited number of studies [17-20] in this context. In the numerical scope, it is possible to highlight some studies that analysed the influence of the presence of openings on the behaviour of slab-column connections [21-27].

As observed in the literature review, there is a noticeable lack of experimental research on slabs with openings, despite their relatively common use in practice. According to Hernandez Fraile et al. [28], out of the published tests focussed on slab-column connections,

only a small percentage (8%) specifically investigated slabs with openings. Furthermore, data compiled from various sources [2-27] indicates that among the test of slabs with openings, the majority (61%) were conducted on slabs with axis-symmetric loading, while only 21% incorporated shear reinforcement, and a mere 18% studied moment transfer (see Figure 1.1). Remarkably, no published work was found that investigated the performance of punching tests on slabs with openings and shear reinforcement in the presence of moment transfer, which is the most common scenario in flat slab buildings.

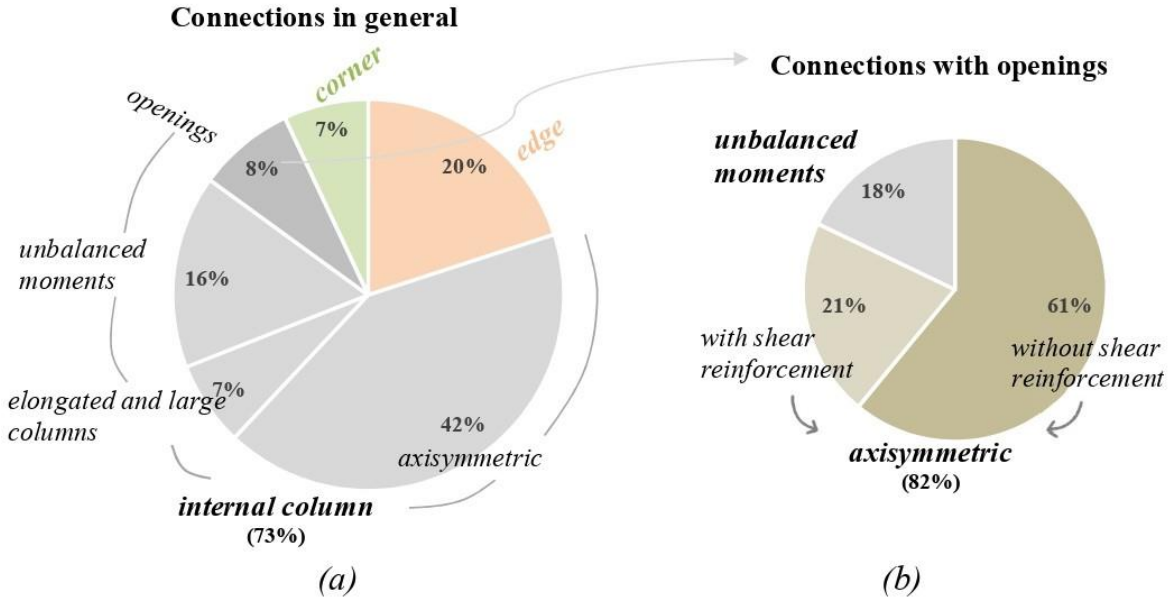

Figure 1.1 - Available punching tests on various types of connections: (a) distribution among all connection types (b) distribution among connections that include openings (adapted from [28])

The need for further experimental research on slabs with openings that accurately represent practical scenarios is also evident from the perspective of code provisions. The current approach adopted by codes consists of simply reducing the resisting control perimeter to account for the decrease in resistance [29-32], which is based on Moe's experimental research published in 1961. However, other factors that are often present can influence the resistance, such as the opening's location, column geometry, and eccentricity caused by nonsymmetric opening positions [4,6,12]. This approach leads to scatter results of experimental-to-theoretical resistance ratios compared to design provisions, resulting in a

high coefficient of variation [4,6,12,14]. It is evident that the simplified rules adopted by the codes are not fully representative and safe. A rational and comprehensive approach is required to effectively address the diverse range of situations encountered in practice.

1.2. OBJECTIVES

Following the context described above, the main objectives of this work are to:

- Contribute with new experimental data on the axis-symmetrical and non-axis-symmetrical punching strengths of full-scale reinforced concrete flat slabs with openings;
- Analyse a database of interior slab-column connections with axis-symmetric punching and openings, aiming to identify current issues and propose new methodologies for incorporating the presence of openings in the design process;
- Perform linear-elastic analysis to better understand the perturbations in the shear field caused by different parameters of openings, including their size, quantity, location, distance from the columns, and the presence of moment transfer;
- Increase the knowledge on the non-axis-symmetric punching behaviour of interior slab-column connections by conducting novel experimental tests that include openings, moment transfer, and shear reinforcement;
- Develop a rational approach based on the Critical Shear Crack Theory for the design of slabs with openings, moment transfer, and shear reinforcement, considering adequately their non-axisymmetric behaviour.

1.3. SCIENTIFIC CONTRIBUTIONS

The mains scientific contributions of the thesis are listed below:

- An experimental programme consisting eight specimens of flat slabs with rectangular column, axis-symmetric loading, and openings of various sizes and quantities (results from Souza (2008));
- Comprehensive critical literature review, analysis of design codes provisions and experimental results from the database of slabs with openings;
- Better understanding of the shear field perturbation caused by openings through elastic-linear analysis for slabs with axis-symmetric and non-axis-symmetric loading;
- Proposal for an approach to consider openings in the punching shear design, taking into account moment transfer for cases of asymmetric openings, and introducing a new geometrical rule to reduce the control perimeter;
- Proposal based on the Critical Shear Crack Theory to account for forces redistribution in slabs with openings;
- An experimental programme consisting of nine specimens of flat slabs with rectangular columns, moment transfer, and openings of various sizes and quantities (results from Souza (2008));
- Critical review of FprEN1992-1-1:23 regarding the consideration of openings;
- An experimental programme comprising five specimens of flat slabs with moment transfer, shear reinforcement and openings;
- Investigation of physics behind the punching failures of slabs with openings and unbalanced moments through the investigation of the shear field;
- Proposal of a rational approach to design slabs with openings, moment transfer and shear reinforcement based on the CSCT.

1.4. STRUCTURE OF THE THESIS

This document is a compilation of four scientific journal articles with an additional chapter. Hence, in addition to the Introduction, this thesis includes six chapters as described below:

- **Chapter 2** presents an experimental campaign on the axis-symmetrical punching shear behaviour of slabs with openings. The influence of the presence of openings adjacent to a rectangular column is analysed, regarding the amount and dimensions of the openings, as well as the orientation of the openings with respect to the column;
- **Chapter 3** examines a database of 68 flat slab specimens with openings, considering current code provisions, the Critical Shear Crack Theory, and linear-elastic analyses of shear force distribution. A new approach and definition of the control perimeter are proposed to enhance the prediction of punching shear resistance in slabs with openings;
- **Chapter 4** describes an experimental campaign focused on investigating the impact of openings and moment transfer on punching shear resistance in interior slab-column connections. The study analyses various parameters, including the position of the openings relative to the rectangular column, the dimensions and number of openings, the value of eccentricity, and the orientation of moment transfer;
- **Chapter 5** presents an experimental programme of slabs with openings, moment transfer, and different arrangements of shear reinforcement. The experimental findings were thoroughly analysed and compared with codes of practice. Based on the mechanical model of the Critical Shear Crack Theory, a comprehensive framework for modelling and designing such slabs are proposed;
- **Chapter 6** summarises the main conclusions of this thesis and discusses topics for future research.

It must be noted that the chapters include their own introduction, state-of-the art (literature review), conclusions, references and annexes, as the present thesis is a compilation of journal articles (paper-based thesis).

1.5. REFERENCES

1. DI STASIO J.; VAN BUREN M. P. *Transfer of bending moment between flat plate floor and column*. ACI Journal Proceedings, t. 57(9), p. 299–314, 1960.
2. MOE, J. *Shearing Strength of Reinforced Concrete Slab and Footings under concentrated loads*. Bulletin D47, Portland Cement Association, Research and Development Laboratories. Skokie-Illinois, 1961.
3. GOMES, R. B.; ANDRADE, M.A.S. *Punching in Reinforced Concrete Flat Slabs with Holes*. Proceedings of Developments in Computer Aided Design and Modelling for Structural Engineering. Edinburgh-UK, pp.185-193, 1995.
4. TENG S.; CHEONG H.K.; KUANG K.L.; GENG J.Z. *Punching shear strength of slabs with openings and supported on rectangular columns*, ACI Structural Journal, 2004, V. 101, pp. 678–87.
5. ANIL Ö.; KINA T.; SALMANI V. *Effect of opening size and location on punching shear behaviour of two-way RC slabs*, Magazine of Concrete Research, Vol. 66, n°18, 2014, pp. 955-966. doi.org/10.1680/macr.14.00042
6. AUGUSTIN T.; FILLO L.; HALVONIK, J. *Punching resistance of slab-column connections with openings*, Structural Concrete. 2019, pp. 1–13. doi.org/10.1002/suco.201900158
7. LIBERATI E.A. P.; MARQUES M.G.; LEONEL E.D.; ALMEIDA L.C.; TRAUTWEIN L.M. *Failure analysis of punching in reinforced concrete flat slabs with openings adjacent to the column*, Engineering Structures, Elsevier, Vol. 182, 2019, pp. 331-343. doi.org/10.1016/j.engstruct.2018.11.073

8. LOURENÇO D. S.; LIBERATI E. A. P.; MARQUES M. G.; ALMEIDA L. C.; TRAUTWEIN L. M. *Reinforced concrete flat slabs with openings at different distances from the column*, IBRACON Structures and Materials Journal, Vol. 14, 2021. doi.org/10.1590/S1983-41952021000100011
9. EL-SHAFIEY, T.F.; ATTA, A.M.; HASSAN, A.; ELNASHARTY, M. *Effect of opening shape, size and location on the punching shear behaviour of RC flat slabs*, Engineering Structures, Elsevier, Vol. 44, 2022, pp. 1138-1151. doi.org/10.1016/j.istruc.2022.08.076
10. KORMOŠOVÁ L.; HALVONIK J. *Punching shear behavior of flat slabs supported by elongated columns with openings*, Structural Concrete, 2023, pp. 1–21. doi.org/10.1002/suco.202200450
11. MÜLLER F.; MUTTONI A.; THÜRLIMANN B. *Durchstanzversuche an Flachdecken mit Aussparungen*. Institut für Baustatik und Konstruktion, ETH Zürich, n° 7305-5 ISBN 3-7643-1686-1, 1984. (In German)
12. REGAN, P. E. *Punching Tests of Reinforced Concrete Slabs with and without Shear Reinforcement with Openings Adjacent to Columns.* School of the Built Environment, University of Westminster, London, July. 1999.
13. SOUZA R.M. *Punção em lajes cogumelo de concreto armado com furos adjacentes ou distantes de um pilar interno*, Dissertação de Mestrado, Faculdade de Tecnologia, Departamento de Engenharia Civil e Ambiental, Universidade de Brasília, 2004. pp 171. (*In Portuguese*)
14. BORGES L.L.J.; MELO G.S.; GOMES R.B. *Punching shear of reinforced concrete flat plates with openings*, ACI Structural Journal, Vol. 110, 2013, pp. 547-556.
15. MARQUES M.G.; LIBERATI E.A.P.; GOMES, R.B.; ALMEIDA L.C.; TRAUTWEIN L.M. *Study of Failure Mode of Reinforced Concrete Flat Slabs with*

Openings and Studs, ACI Structural Journal, Vol. 117, 2020, pp. 39-48 (Title no. 117-S75). doi: 10.14359/51723518

16. MARQUES M.G.; LIBERATI E.A.P.; GOMES, R.B.; CARVALHO, A.L.; TRAUTWEIN L.M. *Punching Shear Strength Model for Reinforced Concrete Flat Slabs with Openings*, J. Struct. Eng. Vol. 147(7), 2020, pp. 01-16 (Title no. 117-S75). doi: 10.1061/(ASCE)ST.1943-541X.0003043

17. HANSON, N.W.; HANSON, J.M. Shear and Moment Transfer Between Concrete Slabs and Columns. Journal PCA Research and Development Laboratories, Vol. 10, 1968, pp. 2-16.
18. SOUZA, R. M. *Punção em Lajes Cogumelo de Concreto Armado com Furos Adjacentes ao Pilar e Transferência de Momento*. Tese de Doutorado, Faculdade de Tecnologia, Departamento de Engenharia Civil e Ambiental, Universidade de Brasília, 2008. 442p. *(In Portuguese)*
19. OLIVEIRA, D.C.; GOMES, R.B.; MELO, G.S. Punching shear in reinforced concrete flat slabs with hole adjacent to the column and moment transfer, IBRACON Structures and Material Journal, 2014, Vol. 7, pp. 1983-4195.
20. BURSAĆ, S.; BEŠEVIĆ, M.; PURČAR, M.V.; KOZARIĆ, L.; ĐURIĆ, N. Experimental analysis of punching shear strength of eccentrically loaded slab with the opening along the face of the internal column, Engineering Structures, Elsevier, Vol. 249, 2021, 113359. doi.org/10.1016/j.engstruct.2021.113359
21. BALOMENOS, G. P.; GENIKOMSOU, A. S.; POLAK, M. A. *Investigation of the effect of openings of interior reinforced concrete flat slabs*. Structural Concrete, V.19:1672–1681, 2018. https://doi.org/10.1002/suco.201700201

22. GENIKOMSOU, A. S.; POLAK, M. A. *Finite-Element Analysis of Reinforced Concrete Slabs with Punching Shear Reinforcement***.** American Society of Civil Engineers, 2017. doi: 10.14359/51689871
23. MOSTOFINEJADA, D.; JAFARIANA, N.; NADERIA, A.; MOSTOFINEJAD, A.; SALEHIA, M. *Effects of openings on the punching shear strength of reinforced concrete slabs*. Engineering Structures, 2020. doi.org/10.1016/j.istruc.2020.03.061
24. ŽIVKOVIĆ, S., BEŠEVIĆ, M., PURČAR, M. V., KOZARIĆ, L. *Nonlinear Finite Element Analysis of Punching Shear Strength of Eccentrically Loaded RC Flat Slabs with Opening*. KSCE Journal of Civil Engineering, V. 23, p. 4771–4780, 2019. doi.org/10.1007/s12205-019-0075-5
25. ALROUSAN, R. Z., ALNEMRAWI, B. R. *The influence of concrete compressive strength on the punching shear capacity of reinforced concrete flat slabs under different opening configurations and loading conditions*. Engineering Structures, V. 44, p. 101-119, 2022. doi.org/10.1016/j.istruc.2022.07.091
26. ALROUSAN, R. Z., ALNEMRAWI, B. R. *Punching shear code provisions examination against the creation of an opening in existed RC flat slab of various sizes and locations*. *Engineering Structures*, V. 49, p. 875-888, 2023. doi.org/10.1016/j.istruc.2023.02.007
27. ISMAIL E-S. I. M. *Nonlinear finite element analysis of reinforced concrete flat plates with opening adjacent to column under eccentric punching loads*. Housing and Building National Research Center Journal, V. 14, p. 438–449, 2018. doi.org/10.1016/j.hbrcj.2018.01.001
28. HERNÁNDEZ FRAILE, D.; SETIAWAN, A.; SANTOS J.B.; MUTTONI, A, *Punching Tests on Edge Slab-Column Connections With Refined Measurements,*

Engineering Structures, Elsevier, Vol. 288, 2023, pp. 1-24. doi.org/10.1016/j.engstruct.2023.116166

29. ACI COMMITTEE 318. *Building code requirements for structural concrete (ACI 318-19) and commentary (318R-19).* American Concrete Institute, Farmington Hills, MI, 2019, pp 623.
30. EN 1992-1-1. *Eurocode 2-Design of concrete structures- Part 1-1: general rules and rules for buildings*, CEN, EN 1992-1-1, Brussels, Belgium, 2004, pp 225.
31. prEN 1992-1-1:2021 *draft*. *Eurocode 2-Design of concrete structures- Part 1-1: general rules and rules for buildings*, CEN, EN 1992-1-1, Brussels, Belgium, 2022, pp 410.
32. FÉDÉRATION INTERNATIONALE DU BÉTON. *Fib Model Code for Concrete Structures 2010 (MC2010),* fib , Lausanne, Switzerland, 2013, pp 390.

2. PUNCHING RESISTANCE OF FLAT SLABS WITH OPENINGS ADJACENT TO THE COLUMN

2.1 INTRODUCTION

The use of openings in the slab-column region is common in flat slab building projects due to the need to pass pipes with different purposes. The openings are often positioned adjacent to the column, preventing the use of transverse reinforcement in this region of high shear stresses.

The results of several experimental test have showed that openings adjacent to column reduce drastically the strength of flat slabs [1-17]. Since 1960, Di Satsio and Van Buren [1] had discussed about the stress modification caused by the opening in flat slabs. In this research, the authors indicated the reduction of the control perimeter to consider the decrease of strength. Similar recommendations of the reduction regarding the control perimeter were incorporated in the design codes.

The first experimental program which studied the influence of openings in slabs resistance without transverse reinforcement was made by Moe (1961) [2]. Only fifty years later other similar research appeared [3-8]. Flat slabs with holes and with transversal reinforcement were studied by [9-14].

In the numerical scope, it is possible to highlight some studies that analysed the influence of the presence of openings on the behaviour of slab-column connections [15]. Through a numerical investigation the authors showed that openings located at distances greater than 4d from the column do not cause changes in the resistance to the connection punching. Thus, the ACI 318 2019 version modified the criterion for reducing the critical perimeter for openings located up to *4h*. In the previous version, the reduction occurred for holes located less than 10h distance. [16] and [17] also made contributions with numerical research.

Despite the advances in experimental and numerical research lately, the behaviour of the punching on flat slabs with the presence of openings still needs to be better understood. In addition to the well-known difficulties in determining the strength of slab-column connections subject to failure by punching, the presence of openings introduces more uncertainty due to the increase in shear stresses in a region where they are already remarkably high.

In practice, some accidents confirm the need for a broad understanding of this topic. In Brazil, in 2013, part of a flat slab with openings near the columns [18] fell. The collapse technical report pointed out flaws in the used punching reinforcement, as well as other deficiencies caused by the existence of holes in the slab-column connection.

On the other hand, the current code's provision indicate the reduction in the critical perimeter to consider the loss of strength due to the presence of openings. However, owing to the small database used in the validation of these models, high coefficients of variation are found when the theoretical punching strength is compared with experimental strength [3-8].

In previous tests, the presence of holes in flat slabs without shear reinforcement was carried out, in most studies, in slabs with square columns. But rectangular columns represent more faithfully the reality of the buildings, and it is important to investigate how the position of the holes in relation to the column impact the punching resistance. In this research, the influence of the presence of holes adjacent to a rectangular column is analysed, regarding the amount and dimensions of the holes, as well as the orientation of the holes in relation to the column dimensions. Design provisions reduce the control perimeter in order to consider the loss of stiffness due to the presence of openings, and not considering its position regarding to the column. Besides, the number of tests in slab-column connections with openings is still very limited, and more research is needed to expand the database. Finally, the results from the experimental campaign and from the literature in comparing with the

results from design codes can contribute a lot for the improvement of the recommendations for the cases of punching with holes.

2.2 EXPERIMENTAL INVESTIGATION

2.2.1 First remarks

This work contains results from eight slabs tested at full scale without shear reinforcement, which are part of Souza's thesis (2008) [19]. The variables assessed were: the position of the holes adjacent to the rectangular column, the dimensions and the number of holes. The results analysed were the slab displacements, the flexural reinforcement strains and concrete strains, the cracking, the failure surface, the inclination of the punching cone and the ultimate experimental loads compared with the theoretical predictions.

2.2.2 Material and Specimens

The experimental program consisted of eight square slabs without shear reinforcement with sides equal to 2.400 mm, height equal to 150 mm and rectangular columns of dimensions equal to 200 mm and 500 mm. The hole dimensions were 400 mm and 200 mm in the case of square holes, and 200 mm x 300 mm regarding the rectangular holes (Figure 2.1). The tests investigated the dimensions and number of holes adjacent to the column.

The compressive strength expected for the concrete was 30 MPa. The following tests were carried out for the characterization of concrete: tensile strength by diametrical compression, secant elasticity module and compressive strength. Steel was tested for uniaxial tension to determine its mechanical properties. Table 2.1 shows the properties of concrete and steel.

In all slabs, the diameter of the bars was 12.5 mm in the flexural reinforcement, and the reinforcement ratios are shown in Table 2.2. For the slabs with a large hole, the flexural reinforcement ratio was varied: 0.87% for slab L2, and 1.17% and 0.52% respectively for

slabs L3 and L4. In slabs L7 and L9 it was equal to 1.48% and in slabs L16 and L19 equal to 1.00%. The reinforcement ratios chosen (0.52% and 1.48%) represent the usual range of reinforcement ratios usually found in design projects. The effective depth of the slabs remained in the order of 123 mm, with minimal changes related to execution.

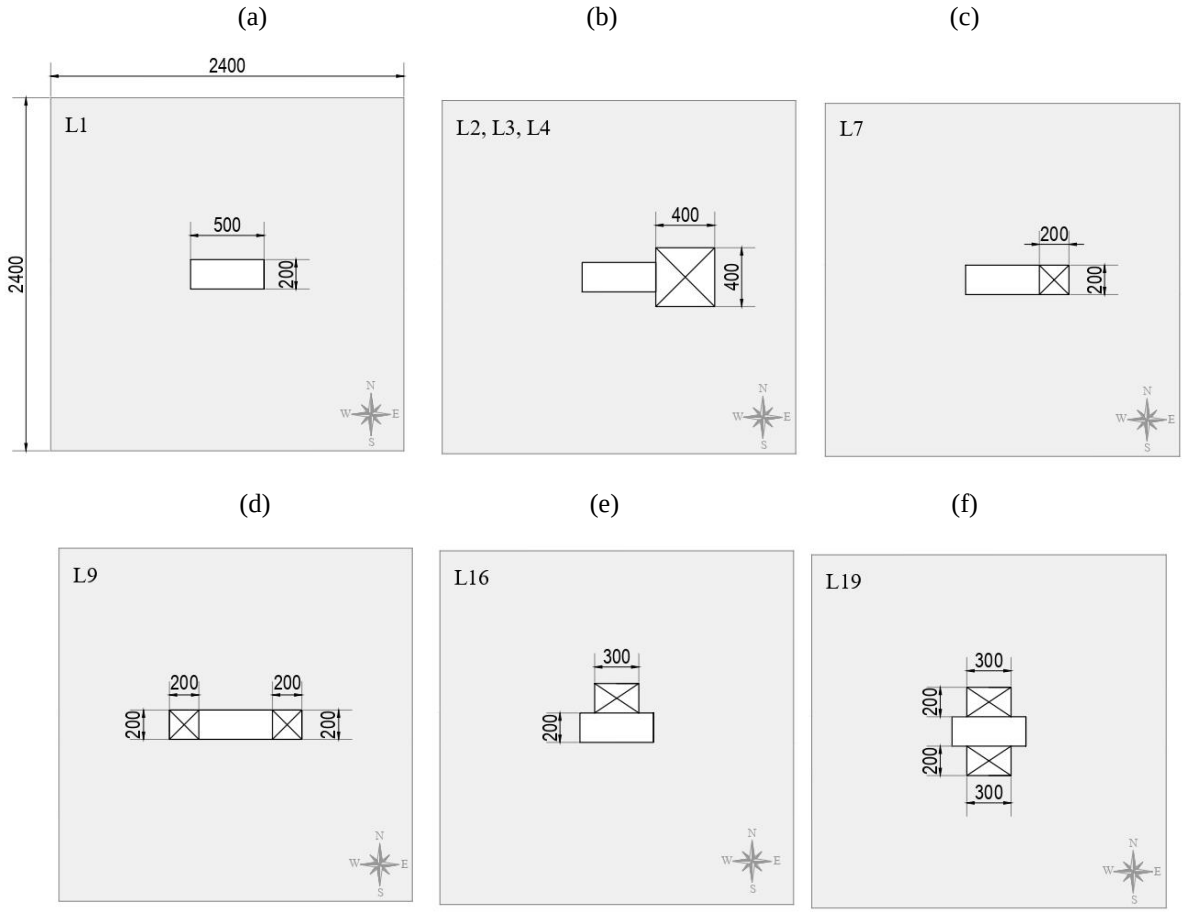

Figure 2.1 - Slab characteristics

Table 2.1 - Properties of concrete and reinforcing steel

Slab	Concrete		Flexural reinforcement			
	f_c (MPa)	$Ø_s$ (mm)	f_{ys} (MPa)	f_u (MPa)	ε_s ‰	E_s (GPa)
L1	37,8	12,5	623	739	2,7	208
L2	32,3					
L3	39,5					
L4	39,1					
L7	37,2					
L9	34,2					
L16	44,0		583	710	2,4	243
L19	39,0					

Table 2.2 - Ultimate and normalized strengths

Slab	f_c (MPa)	Openings (mm)	d (mm)	ρ (%)	V_u (kN)	$\frac{V_u}{d\sqrt{f_c}}$
L1	37,8	-	121	0,93	475	0,64
L2	32,3	1 400x400	123	0,87	240	0,34
L3	39,5	1 400x400	125	1,17	250	0,32
L4	39,1	1 400x400	124	0,52	237	0,31
L7	37,2	1 200x200	123	1,48	455	0,61
L9	34,2	2 200x200	123	1,48	375	0,52
L16	44,0	1 300x200	125	1,01	474	0,57
L19	39,0	2 300x200	126	1,05	411	0,52

2.2.3 Test setup and instrumentation

Loads of the slabs were applied by four hydraulic actuators on steel beams, which distributed the loads on eight application points at the slabs (Figure 2.2). The column was monolithically connected to the slab and prestressed to the strong floor by a jack positioned on top of the

column to strengthen the system. The apparatus could also be used for slabs with unbalanced moments.

Vertical displacements were recorded with up to twelve mechanical dial gauges positioned at the top of each slab, and Figure 2.3 compare the displacements for the four gauge positions common for all slabs. The instrumentation of the flexion bars was performed at points as shown in Figure 2.4, and each point had a pair of diametrically opposed extensometers. The instrumentation of concrete in slabs L1 to L4 was performed on the column monolithically connected to the slab (Figure 2.5a). In the remaining slabs, the strain gauges were positioned on the compressed face of the slab, as shown in Figure 2.5b,c.

2.3 EXPERIMENTAL RESULTS AND DISCUSSION

2.3.1 Vertical displacements

In order to plot the Load versus Displacement graphs, the deflectometers with the highest values were chosen, that is, those located near the edge of the slabs, which are D1 and D6, in the west-east direction, and D7 and D12 in the north-south direction as shown in Figure 2.3**.**

In general, the existence of holes caused an increase in slab displacements and a reduction in stiffness. The larger the dimensions of the holes, the more pronounced this influence was. As it can be seen in Figure 2.6, in slabs L2, L3, L4, L16 and L19 the largest displacements occurred on the direction of the opening. On the other hand, in L7 and L9, which had smaller holes positioned adjacent to the shorter column side, the maximum displacements did not occur in the opening's direction.

(a)

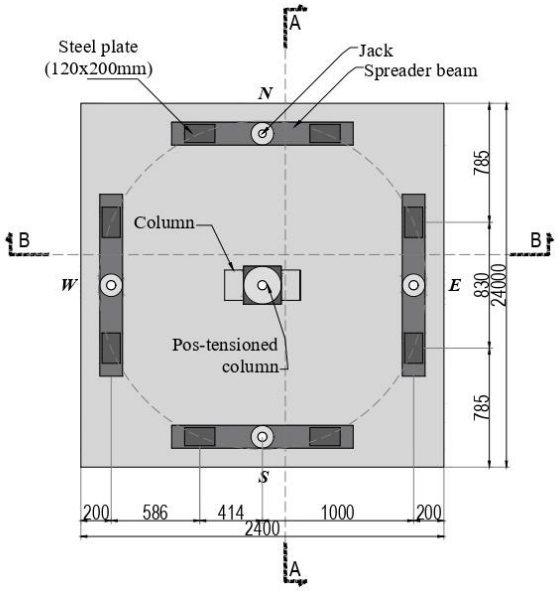

(b) (c)

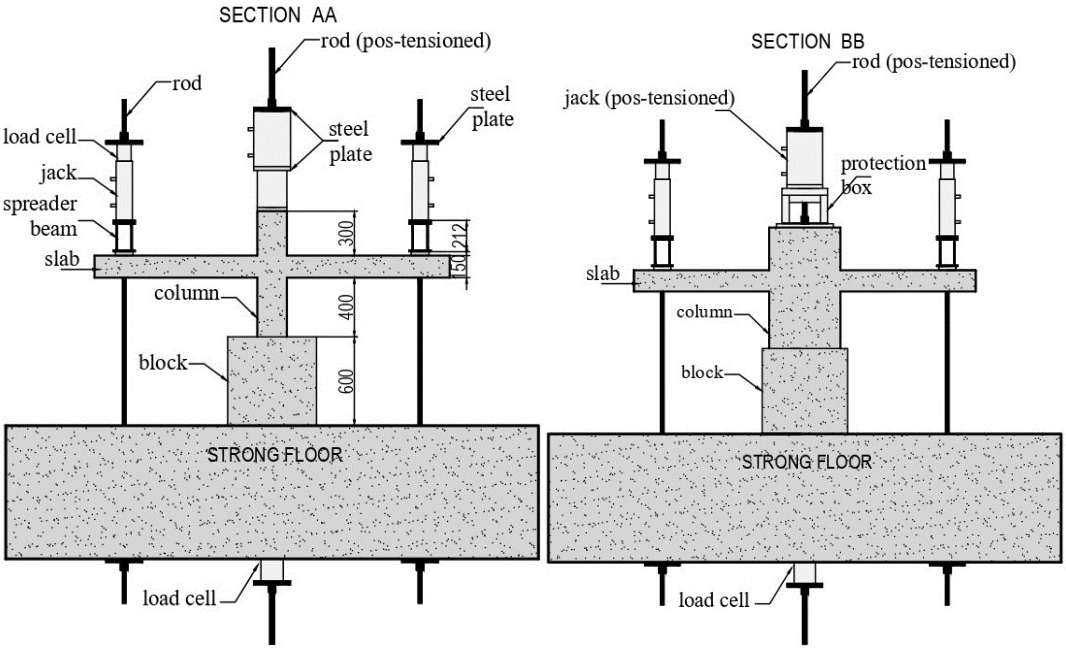

Figure 2.2 - Tests setup (a) Plain view (b) Section A-A (c) Section B-B

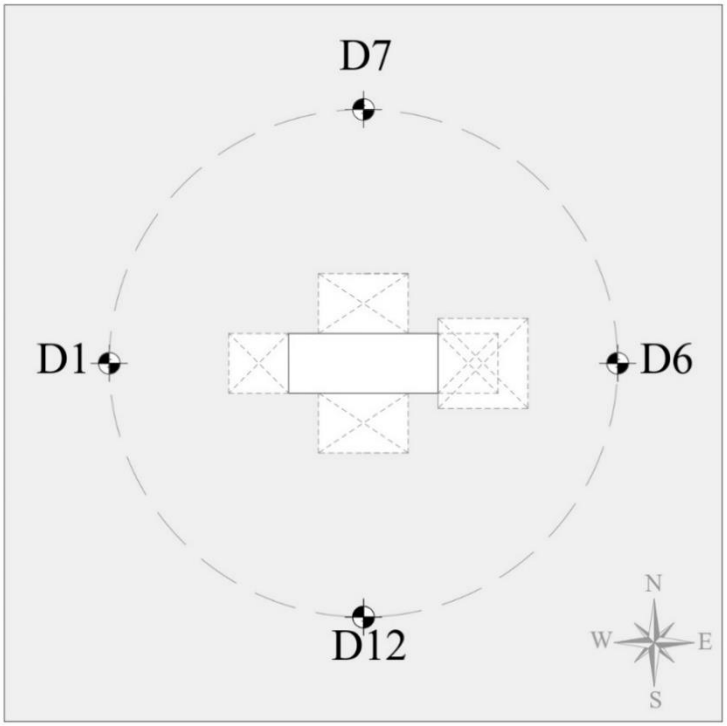

Figure 2.3 - Measurement of displacements in slabs

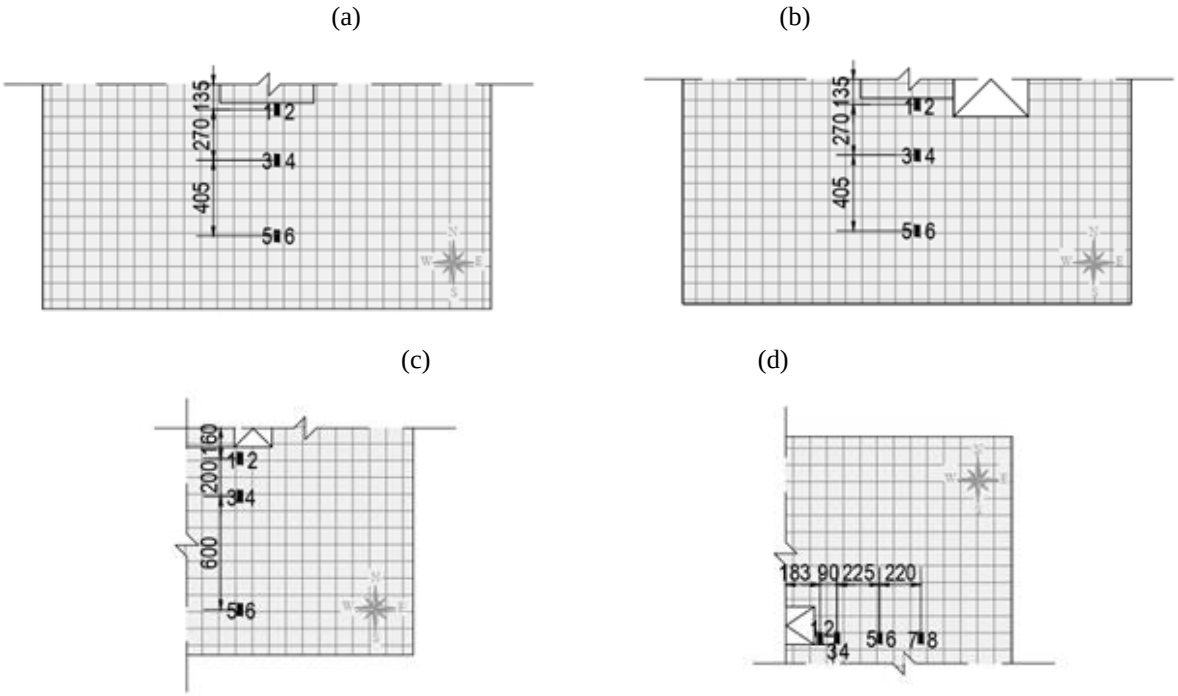

Figure 2.4 - Flexural reinforcement instrumentation (a) L1 (b) L2, L3 e L4 (c) L7 e L9 (d) L16 e L19

(a)

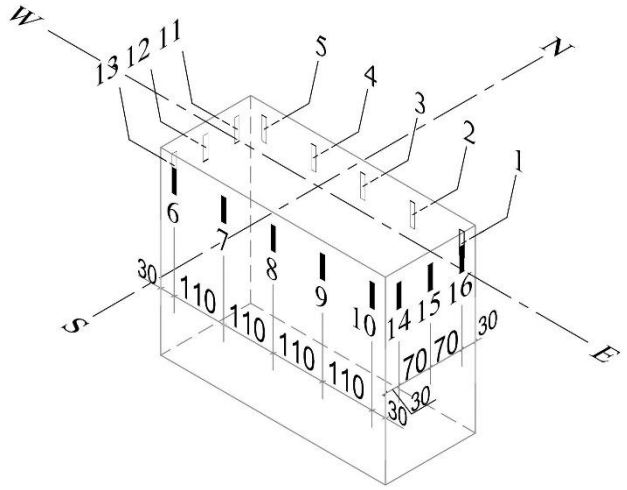

(b) (c)

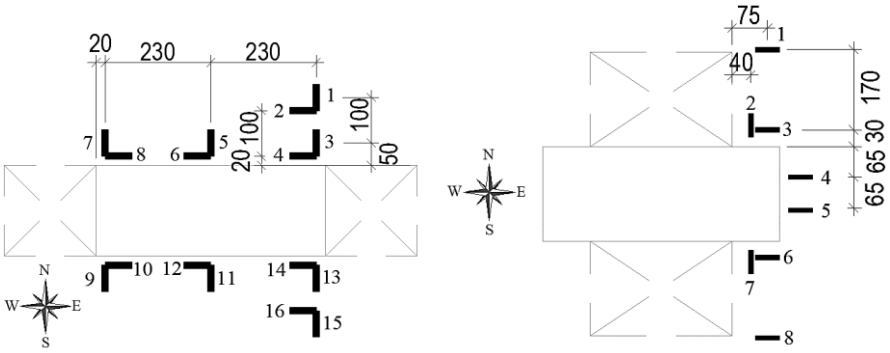

Figure 2.5 - Positioning of concrete strain gages (a) L1, L2, L3, L4 (b) L7 e L9 (c) L16 e L19

Due to the presence of a rectangular column, and therefore with different stiffnesses, the analysis of the influence of the openings in the displacements is not trivial. In slabs with rectangular columns without holes, usually maximum displacements are observed in the direction of lower column stiffness. However, due to the slab's two-dimensional behaviour, the presence of openings in one direction also affects the displacement profile in the other direction.

In this context, it is possible to notice that in slabs L2, L3 and L4 with large holes, the maximum displacements occurred in the west-east direction, as the presence of openings caused a great loss of stiffness (Figure 2.6b-d). On the other hand, in slabs L7 and L9, the maximum displacement occurred in the direction of weaker axis (north-south), because the

presence of smaller holes was not enough to reverse the direction of maximum displacement (Figure 2.6e,f).

The comparison of the load-displacement was performed in three groups, in all cases using the L1 slab without holes as a reference. Figure 2.7a and b, show that the influence of the flexural reinforcement ratio in the Load versus Displacement ratio of slabs L2, L3 and L4 occurred as expected, that is, with stiffness proportional to the increase in reinforcement ratio.

Observing the curves on the side of the opening (east), it is possible to identify the reduction in stiffness caused by the hole in the west side. Figure 2.7c,d shows the results of slabs with holes positioned adjacent to the shorter side of the column. It is evident the reduction of stiffness caused by the hole when observing the results on the west side: on the L7 slab there was no hole on this side, and on the L9 slab there was.

In the north-south direction where there were no holes in the L7 and L9 slabs, the load-displacement behaviour of the slabs was similar. The same occurred in the west-east direction in slabs L16 and L19, as it can be seen in Figure 2.7e. In Figure 2.7f, on the south side, it is also possible to notice the reduction of stiffness that occurred in the slab L19 in relation to L16 due to the presence of the hole.

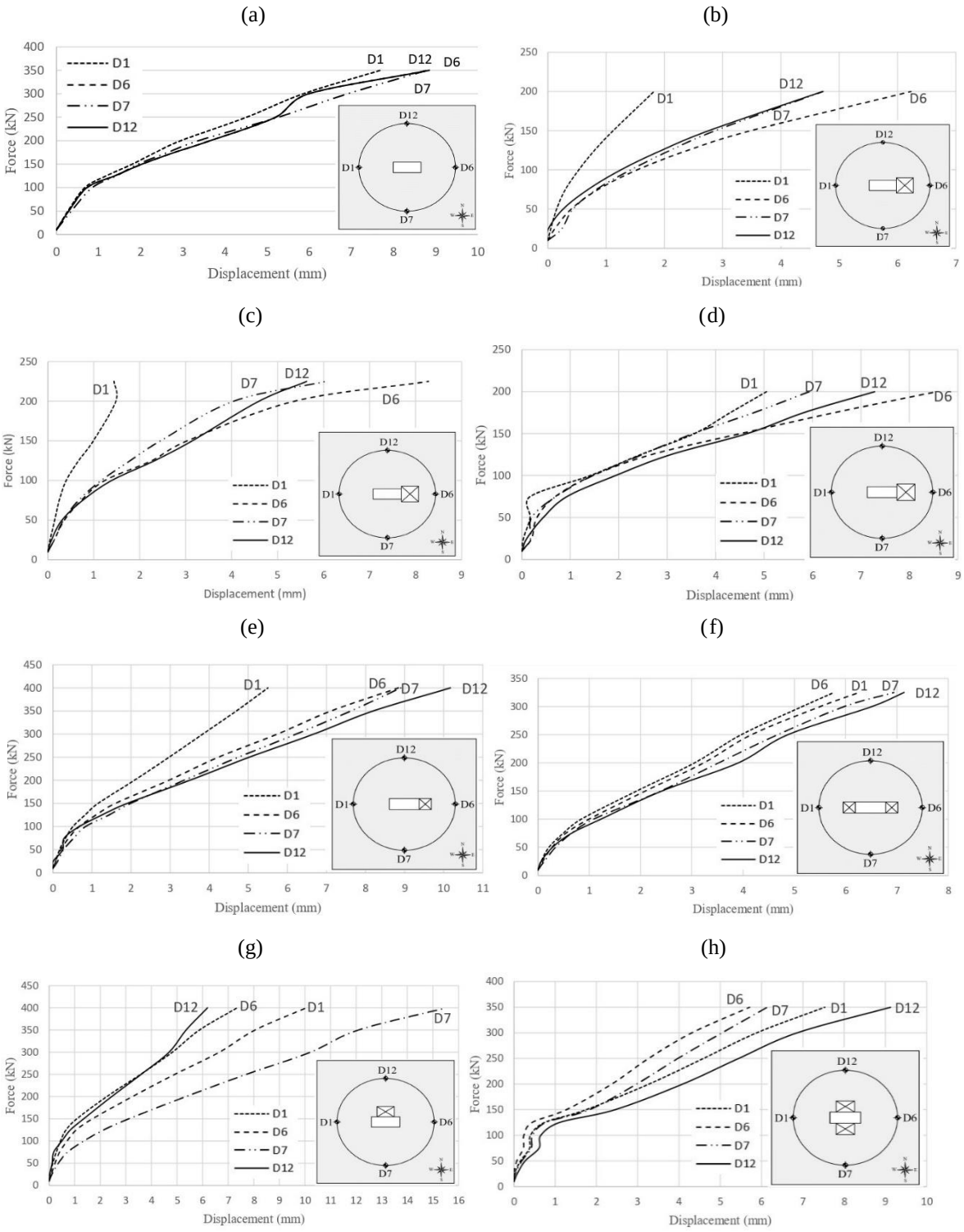

Figure 2.6 - Force *versus* displacement (a) L1 (b) L2 (c) L3 (d) L4 (e) L7 (f) L9 (g) L16 (h) L19

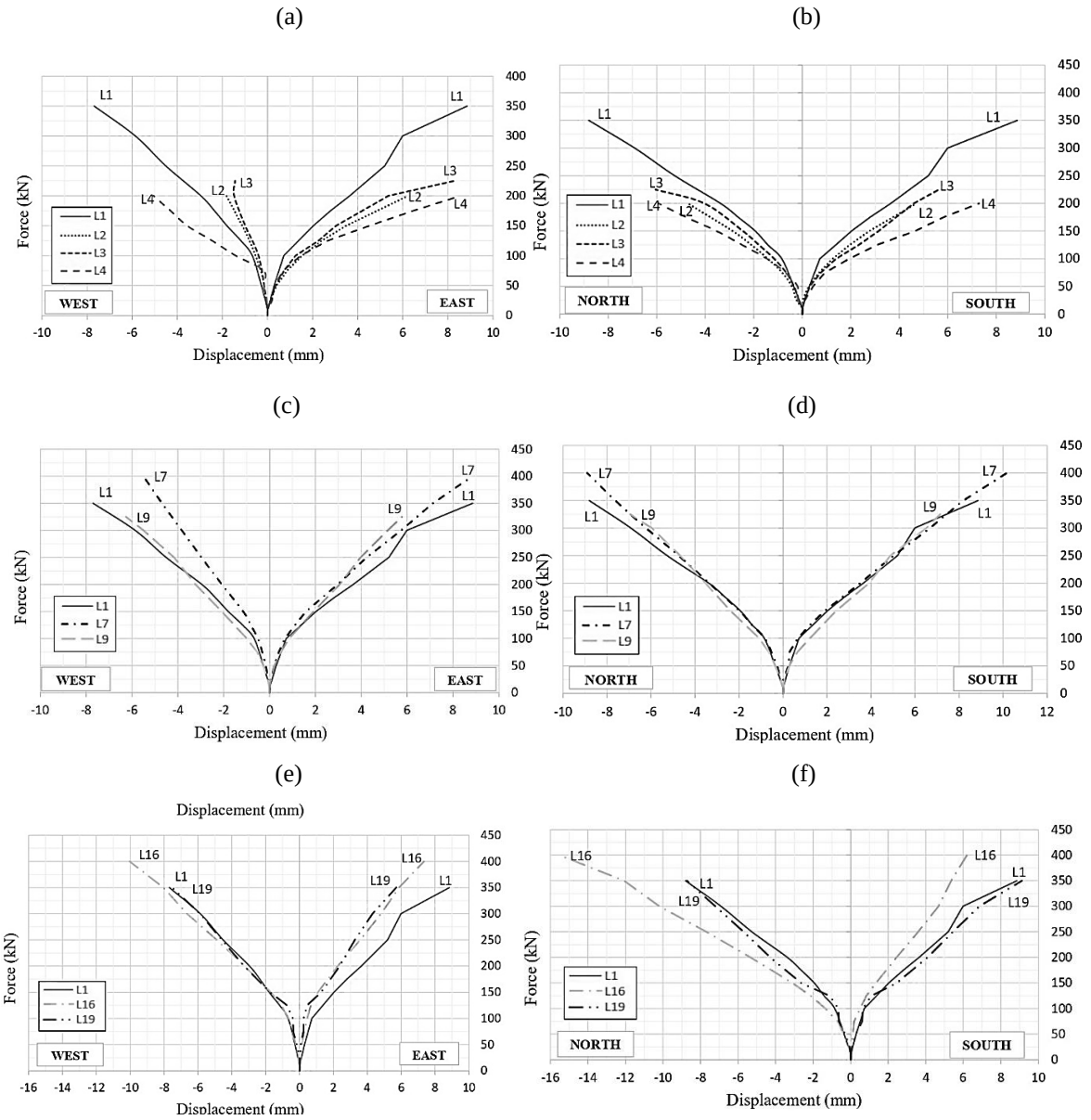

Figure 2.7 - Comparison of the Force versus displacement (a) L1 (b) L2 (c) L3 (d) L4 (e) L7 (f) L9 (g) L16 (h) L19

2.3.2 Ultimate load

The ultimate load (V_u) was determined by adding the largest load measured in the test, the slab's own weight and the equipment. All slabs failure by punching in an abrupt and sudden way. As the concrete strength and the effective depth inevitably varies a normalization was utilized to minimize the influence of these variations, dividing the ultimate strength per the

effective depth and per the square root of the compressive strength of concrete, as suggested by [7].

By analysing the values of normalized ultimate load from Table 2.2**,** it is noticed that the greatest losses of strength took place in the slabs with a 400 mm square hole (L2, L3 and L4). Comparing the final normalized load for the cases of holes positioned adjacent to the shorter column side (L7 and L9), the slab with two holes (L9) showed lower resistance. The same occurred for the case of the holes positioned adjacent to the longer column side: the slab with two holes (L19) presented lower resistance. It is interesting to note that resistance of L7 (opening adjacent to the shorter column side) was close to the resistance of slab without holes (L1).

2.3.3 Crack pattern

The cracking of the slabs can be seen in Figure 2.8. Observing the crack maps, it is possible to identify the influence of the openings in the control perimeter. In the slabs that showed the least resistance (L2, L3 and L4), it is possible to notice that the presence of the hole drastically reduced the control perimeter.

From the failure surface observed on the upper face of the slabs, the diagonal shear cracks were drawn (Figure 2.9). The inclination was calculated by dividing the crack height per its horizontal length. In the slabs L2, L3 L4, L7 and L9, the punching cone was represented in the North-South direction. On the L16 and L19 slabs, it was represented in the East-West direction. On the L1 slab, both directions were represented.

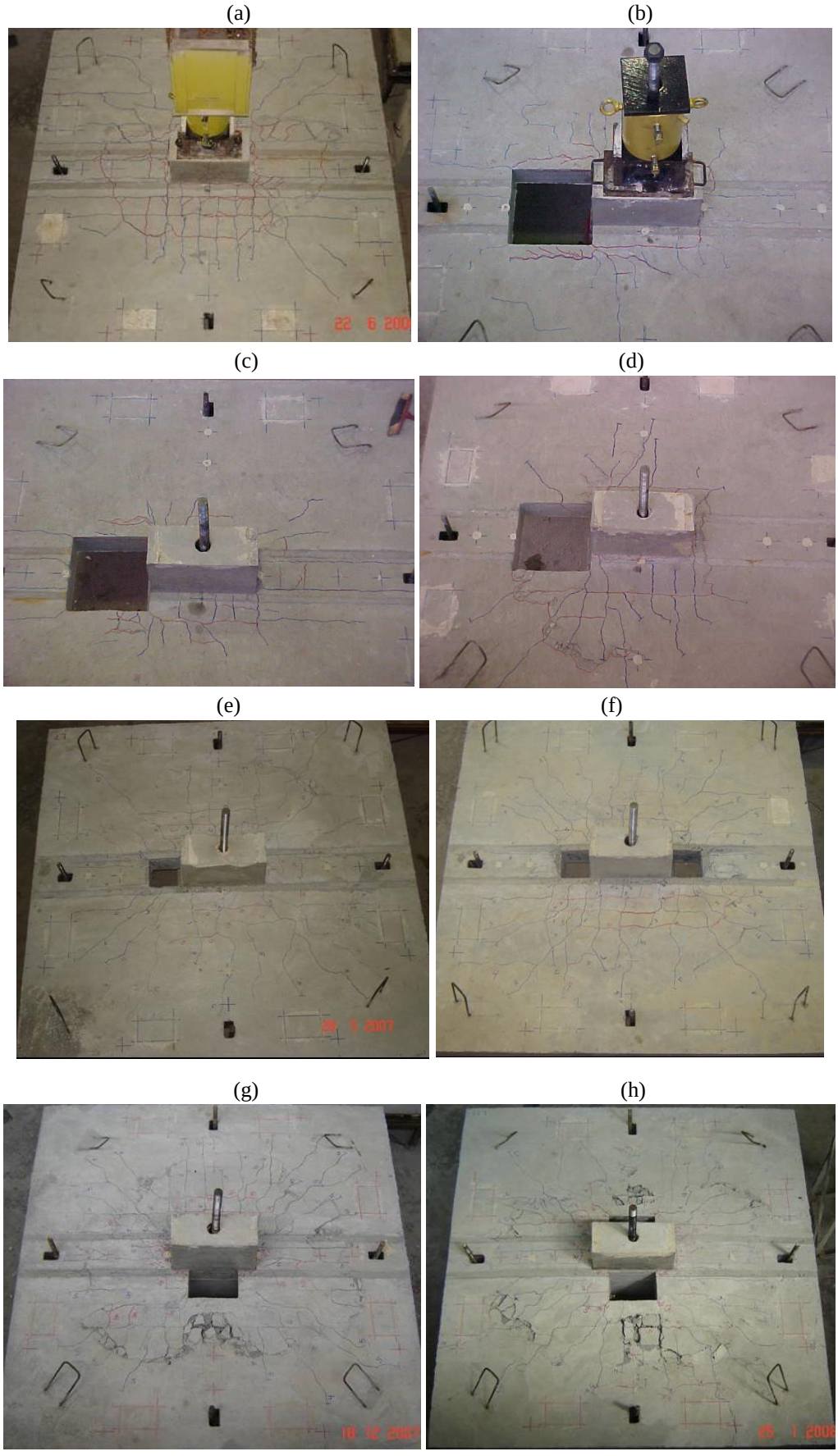

Figure 2.8 - Slab cracking (a) L1 (b) L2 (c) L3 (d) L4 (e) L7 (f) L9 (g) L16 (h) L19

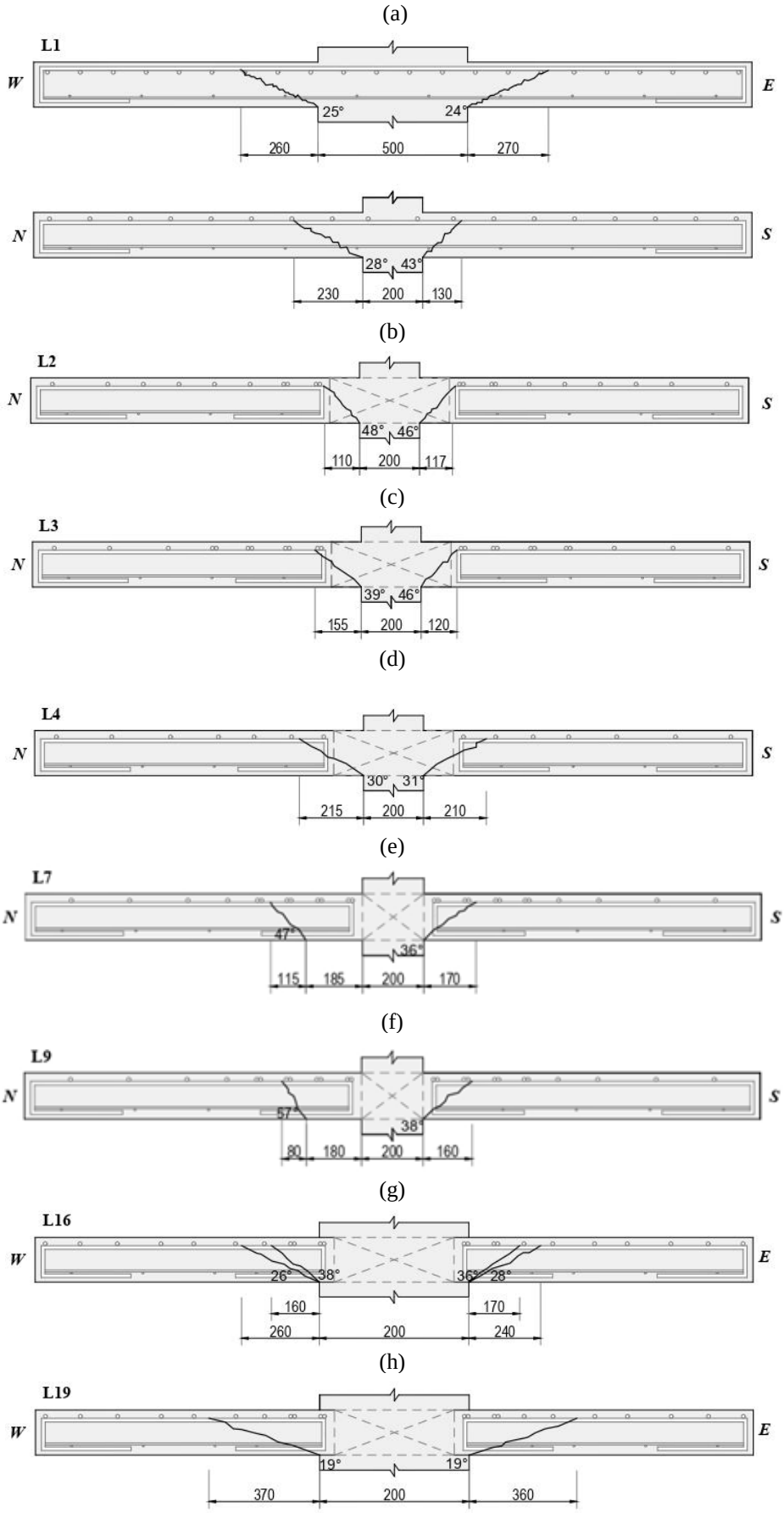

Figure 2.9 - Failure surface (a) L1 (b) L2 (c) L3 (d) L4 (e) L7 (f) L9 (g) L16 (h) L19

Among the slabs L2, L3 and L4, in which there was variation only in the reinforcement ratio, there were values of inclination of the failure cone from 30 ° to 48 ° (Figure 2.9b,c,d). In slabs L7 and L9 (Figure 2.9e,f) the inclination varied between 36° and 57°. Regarding the slabs L16 and L19 (Figure 2.9g,h), the slope was between 19° and 38°.

For slabs with greater openings (L2, L3 and L4), it was possible to observe the deviation in the critical shear crack slope due to the variation in the reinforcement ratio. Comparing the slope cracking of slabs L7 and L9, it is observed that the presence of two holes in L19 slab increased the slope cracking on the north side. The presence of two holes in the L19 slab significantly decreased the crack inclination in the West-East direction in relation to the L16 slab.

In general, the slabs with holes positioned adjacent to the longest side of the column (L19 and L16) showed inclination of the critical crack far lower than the slabs with holes positioned adjacent to the shortest side (L7 and L9). On the face of the slab holes, it was possible to experimentally verify the slope of the failure surface. The punching cone of slabs L2, L3 and L4 can be seen in Figure 2.10.

2.3.4 Steel strain

Figure 2.11 shows the Load-Strain relationship of the strain gauges pair 1,2 from the flexural reinforcements, positioned as shown in Figure 2.4. The averages of the pairs of strain gauges located at the same point, diametrically opposite on the bar, were used.

In slabs L1 to L4, L9 and L16, the extensometers located close to the column had the highest strain values. In slabs L7 and L9, the bars cut due to the presence of the hole did not present relevant strain, which indicates that these bars may not play a role in combating bending. Only in slabs L1, L16 and L9 the steel yield was reached.

(a) (b)

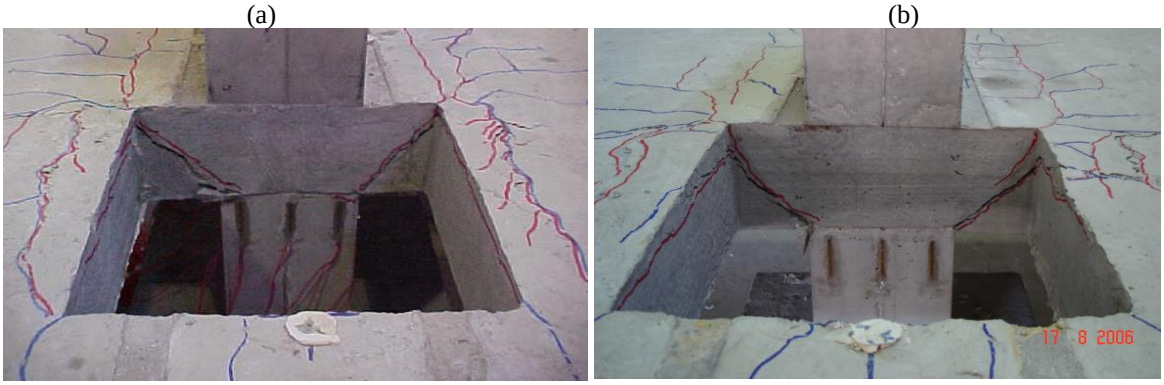

(c)

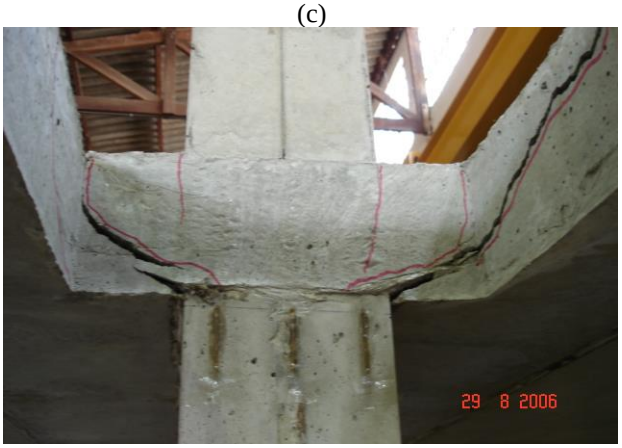

Figure 2.10 - Punching cone (a) L2 (b) L3 (c) L4

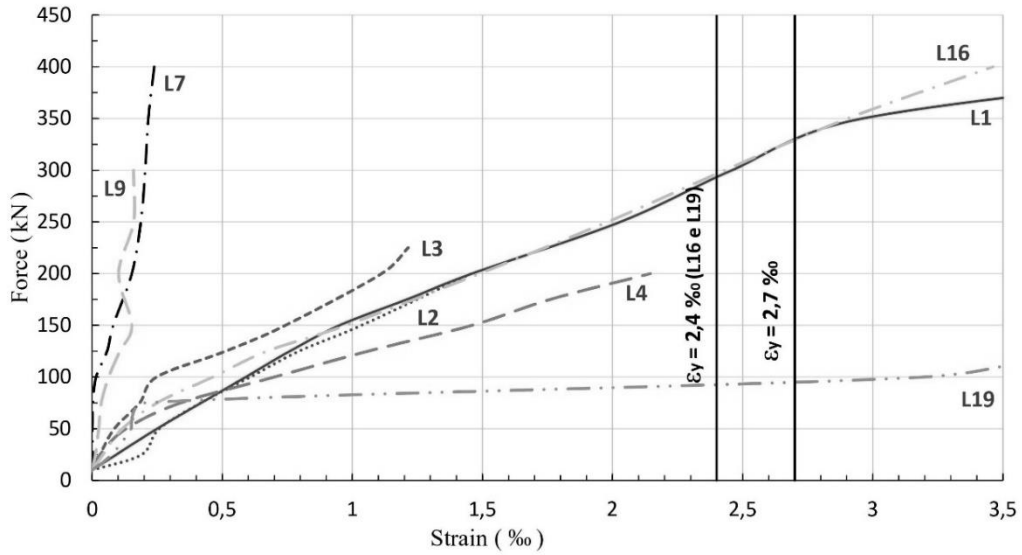

Figure 2.11 - Force versus strain of flexural bars

2.3.5 Concrete strain

The positioning of the strain gauges on the concrete was performed as shown in Figure 2.5. However, it was decided to present only the most significant results in the graphs. Regarding

the reference slab L1, in the slabs with holes (L2 to L4) there was an increase in the compression strains of the concrete on the west side (strain gauges 9, 10 and 16), as shown in Figure 2.12.

According to Figure 2.13a,b, the largest strains of the slabs L7 and L9 occurred in the radial direction close to the center of the column. Due to the presence of the hole on the West side, on the L9 slab (Figure 2.10b) there was an increase in the tangential compression of the strain gauge number 8 compared to slab L7. For the same loading level, slab L9 showed greater strains in the concrete when compared to slab L7, indicating that the presence of the hole increased the level of stresses in the slab. On slabs L16 and L19, the strain gauge number 2 recorded large compression strains due to the presence of the hole, as shown in Figure 2.10c,d.

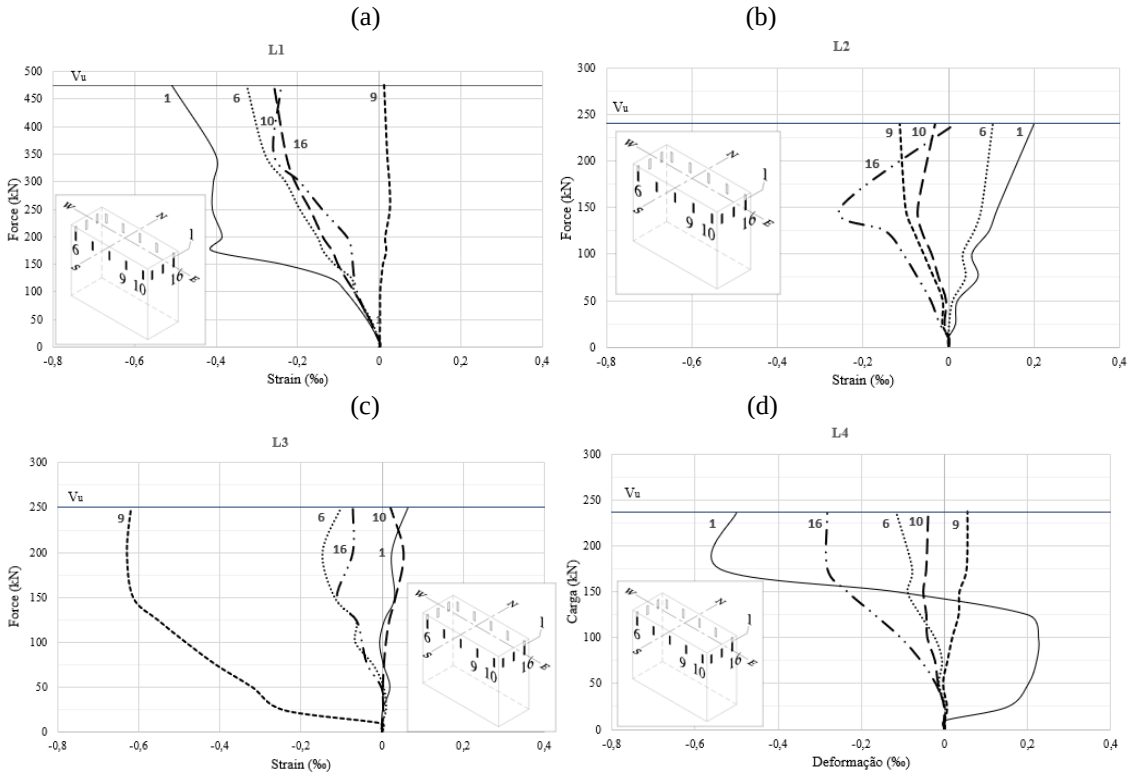

Figure 2.12 - Deformations in concrete Slabs L1 a L4

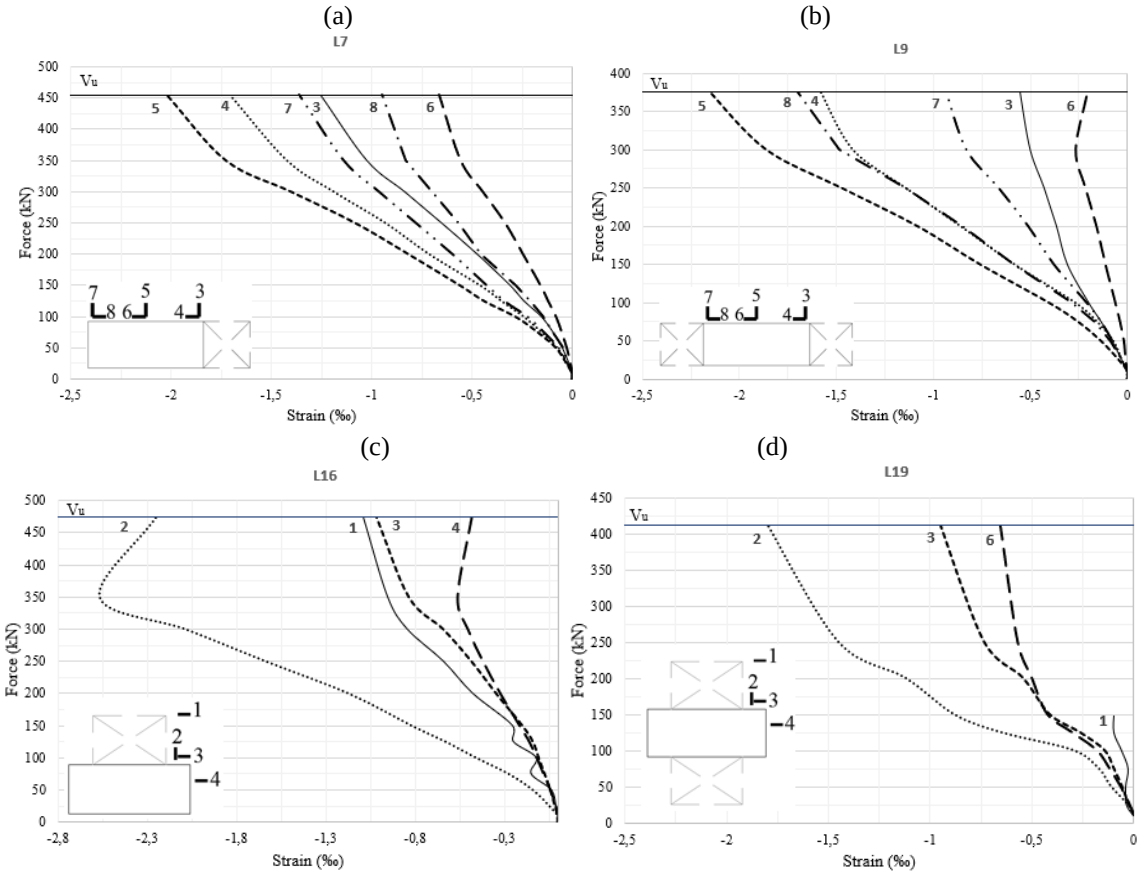

Figure 2.13 - Deformations in concrete of slabs L7, L9 L16 e L19

2.4 COMPARISON WITH DESIGN CODES

The calculation of the punching strength of the slabs was done according to normative predictions of ACI 318:19 [20], Eurocode 2:04 [21], ABNT NBR 6118:14 [22] and *fib* MC 2010:13 [23]. The codes propose similar empirical expressions to verify the shear stress in a control perimeter, which is a function of the effective depth of the slab and assumes different values for each code. The fib Model Code is based on the Critical Cracking Theory [24], which estimates punching resistance as a function of slab rotation. The expressions of punching resistance for slabs without shear reinforcement according to Eurocode 2:14 and ABNT NBR 6118:14 are summarized in Table 2.3. The formulae according to ACI 318:19 and *fib* MC 2010:13 are summarized in the ANNEX A: CODE PROVISIONS.

Regarding the presence of holes in the slabs, the codes have similar recommendations on the reduction of strength by reducing the control perimeter. Considerations vary as to the distance between the hole position and the column axis. In the slabs of this research, all the holes were adjacent to the column, that is, the perimeter reductions concerning the positioning of the holes were the same for the analysed codes. The reduced control perimeters can be seen in Figure 2.14

Table 2.3 - Summary of code provisions of Eurocode 2 and ABNT NBR 6118

Code	Resistance of slabs without shear reinforcement
Eurocode 2:04	$V_c=0.18k\left(100\rho f_c\right)^{1/3}u_1 d \geq 0{,}035k^{2/3}\sqrt{f_c}u_1 d$ where: $k = 1+\sqrt{200/d} \leq 2$ $\rho = \sqrt{\rho_x \rho_y} \leq 0.02$
ANBT NBR 6118:14	$V_c = 0.182(1+k)\left(100\rho f_c\right)^{1/3}u_1 d$ where: $k = 1+\sqrt{200/d}$ $\rho = \sqrt{\rho_x \rho_y}$ OBS: refer to list of symbols

In Table 2.4, the normative predictions are compared with the resistance obtained experimentally. For L2, L3 and L4 slabs, which had a 400 mm square hole on the side, all codes provided unsafe results. For the L7 and L9 slabs, which had one and two 200 mm holes adjacent to the shorter column side, respectively, only the ABNT NBR 6118 presented unsafe predictions. For the L19 slab, which had two 300x200 mm holes adjacent to the longer column side, the most conservative estimate for all codes occurred. According to [10], the codes indicate a very conservative reduction in critical perimeter for these hole situations. By assessing the value of the coefficient of variation, the fib Model Code showed the smallest deviation. However, the high dispersion of estimates from all codes indicates that the provisions are not appropriate for the different hole configurations. In general, for the

slabs with large holes, the provisions were unsafe, and for the other slabs, the provisions were very conservative. In order to obtain estimates closer to reality, it would be desirable to have a different treatment according to the dimensions, geometry and location of the holes.

Table 2.4 - Experimental and theoretical resistances

Slab	**V_u (kN)**	**ACI 318:19**		**EC 2:04**		**NBR 6118:14**		***fib* MC 2010:13**	
		V_{ACI} (kN)	**V_u/V_{ACI}**	**V_{EC02} (kN)**	**V_u/V_{EC02}**	**V_{NBR} (kN)**	**V_u/V_{NBR}**	**V_{MC} (kN)**	**V_u/V_{MC}**
L1	475	429	1.11	417	1.14	482	0.99	462	1.03
L2	240	289	0.83	304	0.79	349	0.69	291	0.82
L3	250	326	0.77	367	0.68	421	0.59	359	0.70
L4	237	321	0.74	276	0.86	317	0.75	258	0.92
L7	455	377	1.21	431	1.06	496	0.92	424	1.07
L9	375	307	1.22	356	1.05	409	0.92	359	1.04
L16	474	358	1.32	333	1.42	382	1.24	399	1.19
L19	411	223	1.84	190	2.16	217	1.89	307	1.34
		Av	1.13		1.15		1.00		1.01
		CoV	0.32		0.41		0.41		0.20

According to the ACI-ASCE 421 Committee [25], openings that are large compared to the dimensions of the critical section must be treated as free edges, which means that the moment between the slab and the column must be considered. NBR 6118, Eurocode 2 and the fib Model Code do not provide additional instructions on determining the acting stresses for slabs with openings.

The presence of non-symmetrical holes creates an eccentricity between the centroid of the column and the centroid of the critical perimeter. Thus, slabs with only one hole were calculated considering the moment transfer and their ultimate loads were compared with those obtained by conventional analysis for internal columns.

The objective was to identify if the codes would present better predictions of ultimate load considering the moment transfer between the slab and the column caused by the eccentricity of the critical perimeter. Figure 2.14 illustrates the eccentricities of the critical perimeters of

the slabs, according to each code rules. The letter "C" indicates the centroid of the column, and the letter "P" indicates the centroid of the perimeter. On slabs L2, L3, L4 and L7, the eccentricity of the critical perimeter causes a moment about the vertical axis, while on the L16 slab the moment is about the horizontal axis.

Table 2.5 presents a summary of the code's recommendations for moment transfer according to Eurocode 2:14 and ABNT NBR 6118:14. The formulae according to ACI 318:19 and *fib* MC 2010:13 are summarized in the ANNEX A: CODE PROVISIONS.

The eccentricity reduces the area of the slab-column connection that effectively contributes to the punching. To take this effect into account, ACI 318, Eurocode 2 and NBR 6118 consider an amplification in the acting stress due to the existence of the bending moment. Table 2.5 contains the indications for moment about y-axis, if the moment is about x-axis, just change the indexes in the expressions. fib Model Code 2010 recommends a reduction in the control perimeter by a k_e coefficient. The parameters indicated in Table 2.5 can be consulted directly in the codes.

Table 2.5 shows the results of the relationship between experimental load (V_u) and theoretical load with the bending moment transfer ($V_{ACI,M}$, $V_{EC,M}$, $V_{NBR,M}$ and $V_{MC,M}$) and the comparison with the results without moment.

(a)

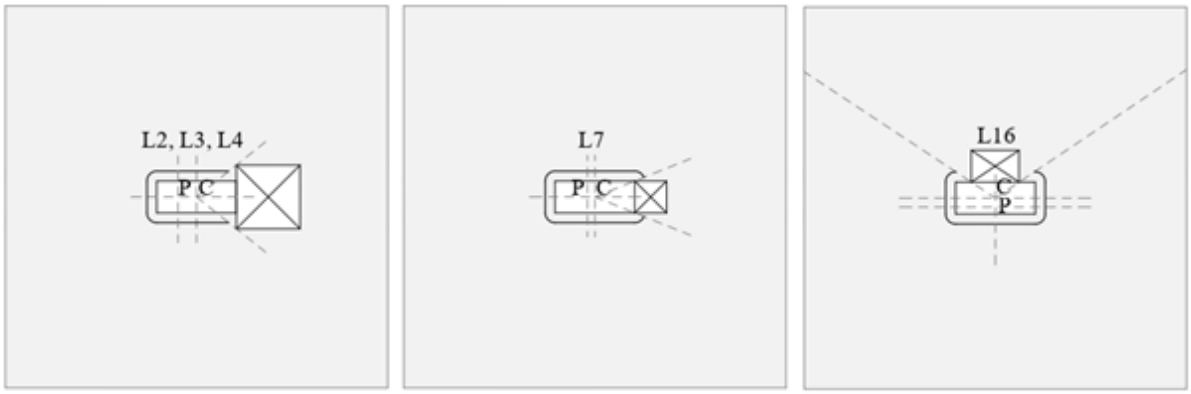

(b)

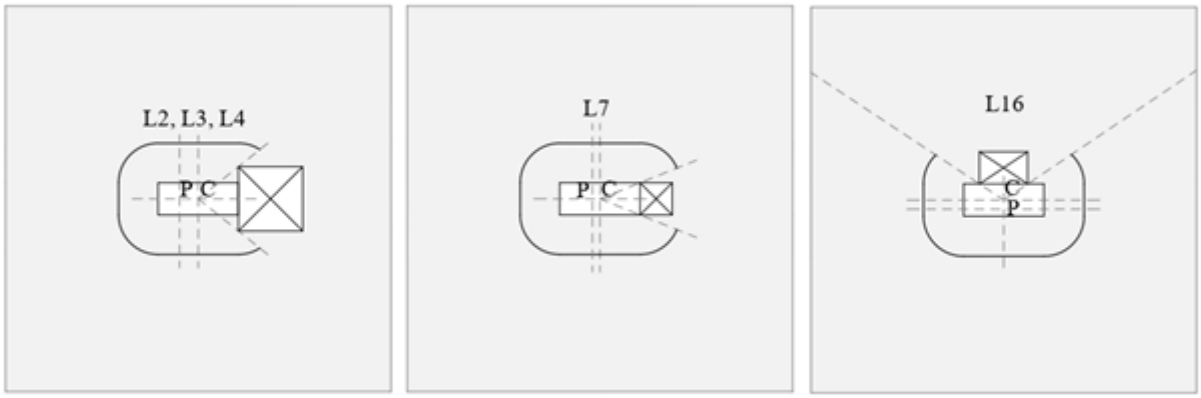

(c)

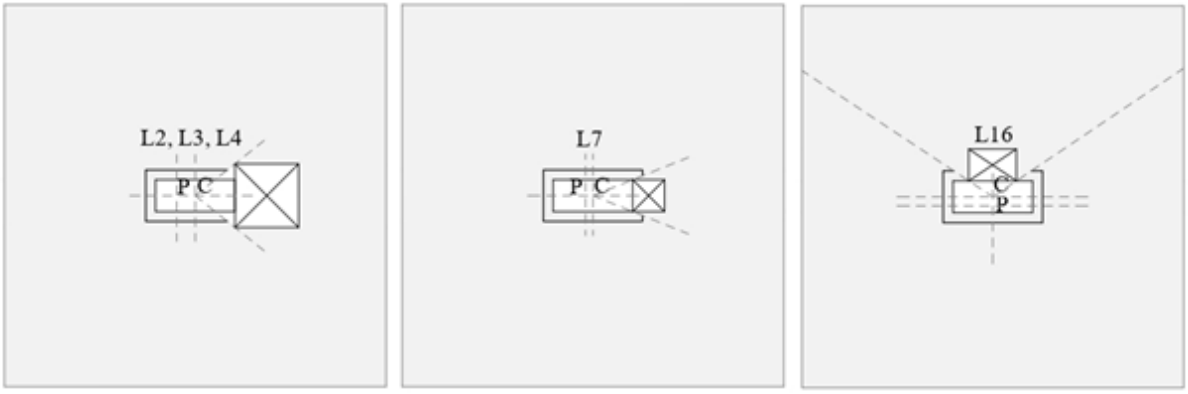

Figure 2.14 - Control perimeter and centroid (a) fib MC 2010 (b) Eurocode 2 e ABNT NBR 6118 (c) ACI 318

Table 2.5 -Summary of code provisions for load eccentricity

Code	**Effect of load eccentricity**
Eurocode 2:04	$V_{c,M}=\frac{0.18k(100\rho f_c)^{1/3}u_1 d}{\beta}$ $\beta = 1 + k_1 \frac{M_E}{V}\frac{\mu_1}{W_1}$
ANBT NBR 6118:14	$V_{c,M}=\frac{0.182(1+k)(100\rho f_c)^{1/3}u_1 d}{\beta}$ OBS: refer to list of symbols

The calculation of slabs with asymmetric holes, considering the moment transfer due to the eccentricity of the critical perimeter, resulted in lower CoV for all analysed codes, when compared to the CoV without this consideration, as shown in Table 2.6**.** For the slabs L2, L3 and L4, which had previously presented unsafe values up to 50%, due to the amplification of the acting stress caused by the moment, presented values of the ultimate load calculated much closer to the experimental results. On slabs L7 and L16, the results became more conservative.

Table 2.6 - Experimental and theoretical resistances with moment transfer

Slab	**V_u (kN)**	**ACI 318:19**		**EC 2:04**		**NBR 6118:14**		***fib* MC 2010:13**	
		V_u/V_{ACI}	**$V_u/V_{ACI,M}$**	**V_u/V_{EC}**	**$V_u/V_{EC,M}$**	**V_u/V_{NBR}**	**$V_u/V_{NBR,M}$**	**V_u/V_{MC}**	**$V_u/V_{MC,M}$**
L2	240	0.83	1.26	0.79	1.07	0.69	0.93	0.82	0.94
L3	250	0.77	1.16	0.68	0.92	0.59	0.81	0.70	0.80
L4	237	0.74	1.12	0.86	1.16	0.75	1.01	0.92	1.04
L7	455	1.21	1.31	1.06	1.36	0.92	1.18	1.07	1.14
L16	474	1.32	1.61	1.42	1.83	1.24	1.48	1.19	1.34
Av.		0.97	1.29	0.96	1.27	0.84	1.08	0.94	1.05
CoV		0.28	0.15	0.30	0.28	0.30	0.24	0.21	0.19

For L2, L3 and L4 slabs, which had large holes, the normative predictions considering the moment transfer showed values much closer to the experimental results. The presence of large holes causes greater eccentricities between the centroid of the perimeter and the

column, which makes the behaviour of the slab-column connection closer to an edge column than to an internal column, as suggested by the ACI 318. However, in the case of smaller holes, the eccentricity is lower, and the prediction of failure load considering the moment transfer was more conservative.

From these results, it is recommended that in cases of asymmetric holes with large dimensions, the eccentricity of the critical perimeter should be calculated to verify the magnitude of the moment transferred from the slab to the column. In future work, an analysis of experimental data from the bibliography can be carried out to conclude on what would be the relationship among the dimensions of the hole and the control perimeter to take into consideration the moment, and therefore avoid the occurrence of unsafe resistance in these cases.

2.5 CONCLUSIONS

Eight slab-column connections subject to punching were experimentally studied, observing the influence of dimensions, location and number of holes in the behaviour of the slabs. The presence of holes reduced the slabs stiffness, causing higher displacements. The cracking distribution as well as the inclination of the critical shear crack were affected by the presence, quantity and location of the holes.

In view of the coefficients of variation obtained in this research, as well as those presented in the literature, it is desirable that the code's recommendations for the reduction of the critical perimeter considers to the geometry and position of the openings, and not depend exclusively on the distance of the hole in relation to the column, as is currently done.

In slabs with large and non-symmetrical openings, the consideration of the bending moment transfer caused theoretical resistances closer to the experimental results, for all the analysed codes. For slabs with small holes (L7 and L16), the consideration of moment resulted in more conservative values for punching resistance. It is important to investigate what the

desirable relationships of the dimensions of the opening to the dimensions of the critical perimeter to consider the moment transfer in slabs with asymmetric holes. To achieve this, more experimental results from the bibliography should be analysed in further research.

2.6 REFERENCES

1. DI STASIO J.; VAN BUREN M.P. *Transfer of bending moment between flat plate floor and column*. ACI Journal Proceedings, V. 57(9), p. 299–314, 1960
2. MOE, J. *Shearing Strenght of Reinforced Concrete Slab and Footings under concentrated loads*. Bulletin D47, Portland Cement Association, Research and Development Laboratories. Skokie-Illinois, 1961.
3. TENG S., CHEONG H. K., KUANG K. L., GENG J. Z. *Punching shear strength of slabs with openings and supported on rectangular columns*. ACI Struct J V. 101(5), p. 678–87, 2004.
4. SOUZA, R. M. *Punção em Lajes Cogumelo de Concreto Armado com Furos Adjacentes ou Distantes de um Pilar Interno*. Dissertação de Mestrado, Faculdade de Tecnologia, Departamento de Engenharia Civil e Ambiental, Universidade de Brasília, 2004. 171p. *(In Portuguese.)*
5. HA, T.; LEE, M.; PARK, J.; KIM, D. *Effects of openings on the punching shear strength of RC flat-plate slabs without shear reinforcement*. Struct. Design Tall Spec. Build. V. 24, p. 895–911, 2015. dx.doi.org/10.1002/tal.1217
6. LOURENÇO, D. S. *Punção em Lajes Lisas de Concreto Armado com Aberturas: Análise Experimental*. Dissertação de Mestrado, Faculdade de Engenharia Civil, Arquitetura e Urbanismo, Universidade Estadual de Campinas, 2018, 179p. In Portuguese.

7. AUGUSTIN, T.; FILLO, L.; HALVONIK, J. *Punching resistance of slab-column connections with openings*. Structural Concrete. p. 1–13, 2019. doi.org/10.1002/suco.201900158
8. LIBERATI, E. A. P.; MARQUES, M. G.; LEONEL, E. D.; ALMEIDA L. C.; TRAUTWEIN, L. M. *Failure analysis of punching in reinforced concrete flat slabs with openings adjacent to the column*. Engineering Structures, 2019. doi.org/10.1016/j.engstruct.2018.11.073
9. GOMES, R. B.; ANDRADE, M.A.S. de. *Punching in Reinforced Concrete Flat Slabs with Holes*. Proceedings of Developments in Computer Aided Design and Modelling for Structural Engineering. Edinburgh-UK, pp.185-193, 1995.
10. REGAN, P. E. *Punching Tests of Reinforced Concrete Slabs with and without Shear Reinforcement with Openings Adjacent to Columns*. School of the Built Environment, University of Westminster, London, July. 1999.
11. SILVA, A. S. *Punção em lajes cogumelo: Pilares Retangulares, Furos e Armadura de Cisalhamento*. Dissertação de Mestrado, Escola de Engenharia Civil, Universidade Federal de Goiás, 2003. 210 p. *(In Portuguese)*
12. BU W.; POLAK M. A. *Effect of openings and shear bolt pattern in seismic retrofit of reinforced concrete slab-column connections*, Engineering Structures, Elsevier, Vol. 33, No. 12, pp. 3329-3340, 2011.
13. BORGES L. L. J.; MELO G. S., GOMES R. B. *Punching shear of reinforced concrete flat plates with openings*. ACI Structural Journal, V. 110, No.4, pp 547-556, 2013.
14. MARQUES, M. G. *Punção em Lajes Lisas de Concreto Armado com Aberturas Adjacentes ao Pilar e Armadura de Cisalhamento*. Tese de Doutorado, Faculdade

de Engenharia Civil, Arquitetura e Urbanismo, Universidade Estadual de Campinas, 2018, 274p. *(In Portuguese)*

15. BALOMENOS, G. P.; GENIKOMSOU, A. S.; POLAK, M. A. *Investigation of the effect of openings of interior reinforced concrete flat slabs*. Structural Concrete, V.19:1672–1681, 2018. doi.org/10.1002/suco.201700201
16. GENIKOMSOU, A. S.; POLAK, M. A. *Finite-Element Analysis of Reinforced Concrete Slabs with Punching Shear Reinforcement***.** American Society of Civil Engineers, 2017. doi: 10.14359/51689871
17. MOSTOFINEJADA, D.; JAFARIANA, N.; NADERIA, A.; MOSTOFINEJAD, A.; SALEHIA, M. *Effects of openings on the punching shear strength of reinforced concrete slabs*. Engineering Structures, 2020. doi.org/10.1016/j.istruc.2020.03.061
18. CREA-PI. *Relatório técnico sobre o desabamento da obra do Shopping Rio Poty*. Conselho Regional de Engenharia, Arquitetura e Agronomia do Piauí. Teresina, Piauí, 2013. *(In Portuguese)*
19. SOUZA, R. M. *Punção em Lajes Cogumelo de Concreto Armado com Furos Adjacentes ao Pilar e Transferência de Momento*. Tese de Doutorado, Faculdade de Tecnologia, Departamento de Engenharia Civil e Ambiental, Universidade de Brasília, 2008. 442p. *(In Portuguese)*
20. AMERICAN CONCRETE INSTITUTE. *ACI 318 – Building code requirements for structural concrete (ACI 318-19) and Commentary*. Farmington Hills, EUA, 2019.
21. Eurocode 2: *Design of concrete structures – Part 1-1: General rules and rules for buildings*. Brussels: European Committee for Standardization, 2014.
22. Associação Brasileira De Normas Técnicas. *NBR 6118: Projeto de estruturas de concreto*. Rio de Janeiro: 2014.EUROPEAN STANDARD.

23. *fib* Model Code 2010. *Model Code 2010: Model code for concrete structures 2010*. Lausanne: Special Activity Group 5, 2013. 390 p.

24. MUTTONI, A. *Punching Shear Strength of Reinforced Concrete Slabs without Transverse Reinforcement*, ACI Structural Journal, V. 105, No. 4, pp. 440-450, 2008.

25. ACI 421.1R-20. *Guide for Shear-Reinforcement for Slabs*. Reported by Joint ACI-ASCE Committee 421, ACI, Farmington Hills, Michigan, 1999.

3. ENHANCEMENT OF THE PUNCHING SHEAR VERIFICATION OF SLABS WITH OPENINGS

3.1 INTRODUCTION

In flat slabs, openings are necessary to allow the passage of various utilities, such as plumbing, electricity, heating, and ventilation. From a practical point of view, the most convenient place for these openings is close to the columns. From a structural point of view, however, this is the least favourable location as it can lead to a significant reduction of the punching shear resistance.

The reduction of the load-carrying concrete cross section due to opening usually leads to a decrease of the punching shear resistance. This is caused by an increase of the average shear force along the reduced control perimeter, by stress concentrations near the openings, by the reduction of the unitary shear resistance caused by increased flexural deformations and by moment transfers in the case of unsymmetrical openings.

The shear force distribution along a control perimeter located at 0.5*d* from the column edge area provides useful information to understand the perturbations of the shear field caused by openings. The results of a linear-elastic analysis using *SAP2000*® software show that the effect of openings on the shear force distribution depends on their size, location, distance from the columns and number.

Figure 3.1 shows that, for an opening of a given size, the shear force distribution depends on the location of the opening with respect to the column and on its orientation if it is elongated. Large openings located at the corners of the column (Figure 3.1c) have a smaller influence on the shear force distribution along the control perimeter than openings located on the sides of small columns (Figure 3.1a, b). Figure 3.2 shows that, as the opening is moved away from the column, the shear force distribution along the control perimeter in the slab with an

opening gets closer to the shear distribution of the slab without openings. However, not only the distance of the opening from the column, but also the orientation of the opening with respect to the column influences the shear force distribution, as it can be seen comparing Figure 3.2c and Figure 3.2d.

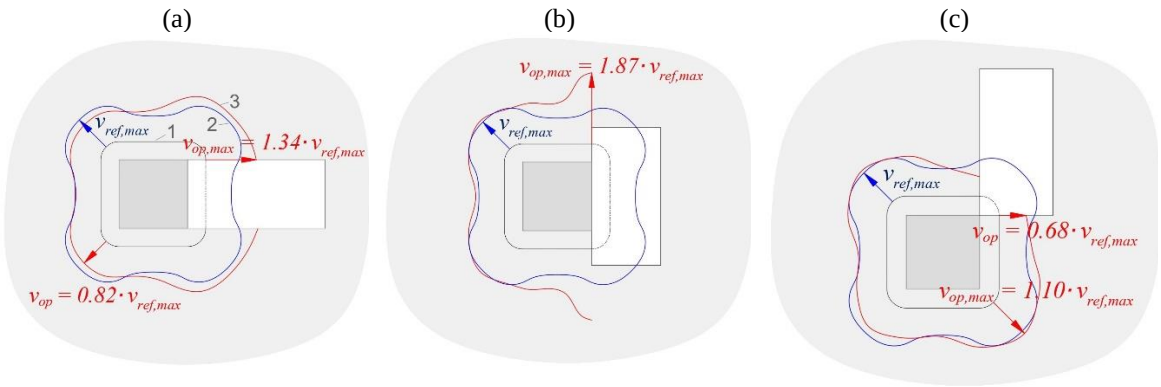

Figure 3.1 - Effect of the position of the opening on the shear force distribution along the control perimeter located at 0.5d from the column for slabs from Teng et al. (2004) [12]: (a) OC11H30; (b) OC11V20; and (c) OC11V23 (black curves (**1**): control perimeter; blue curves (**2**): shear force distribution for slab without opening; red curves (**3**): shear force distribution for slab with opening)

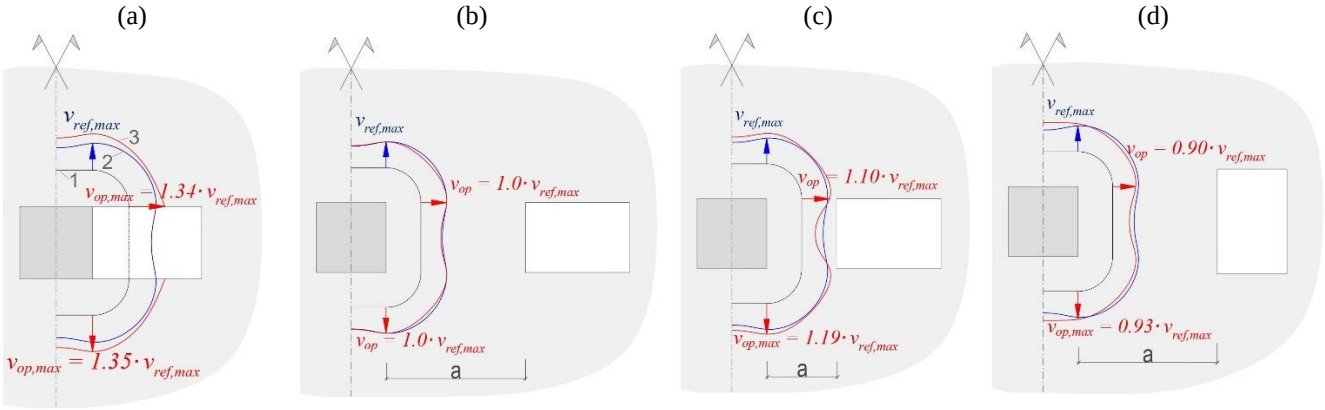

Figure 3.2 - Effect of the distance of the opening on the shear force distribution for slabs from Augustin et al. (2019) [10] for openings distance equal to: (a) 0d; (b) 1d; (c) 2d; and (d) 2d with opening dimensions equal to 300x200 mm

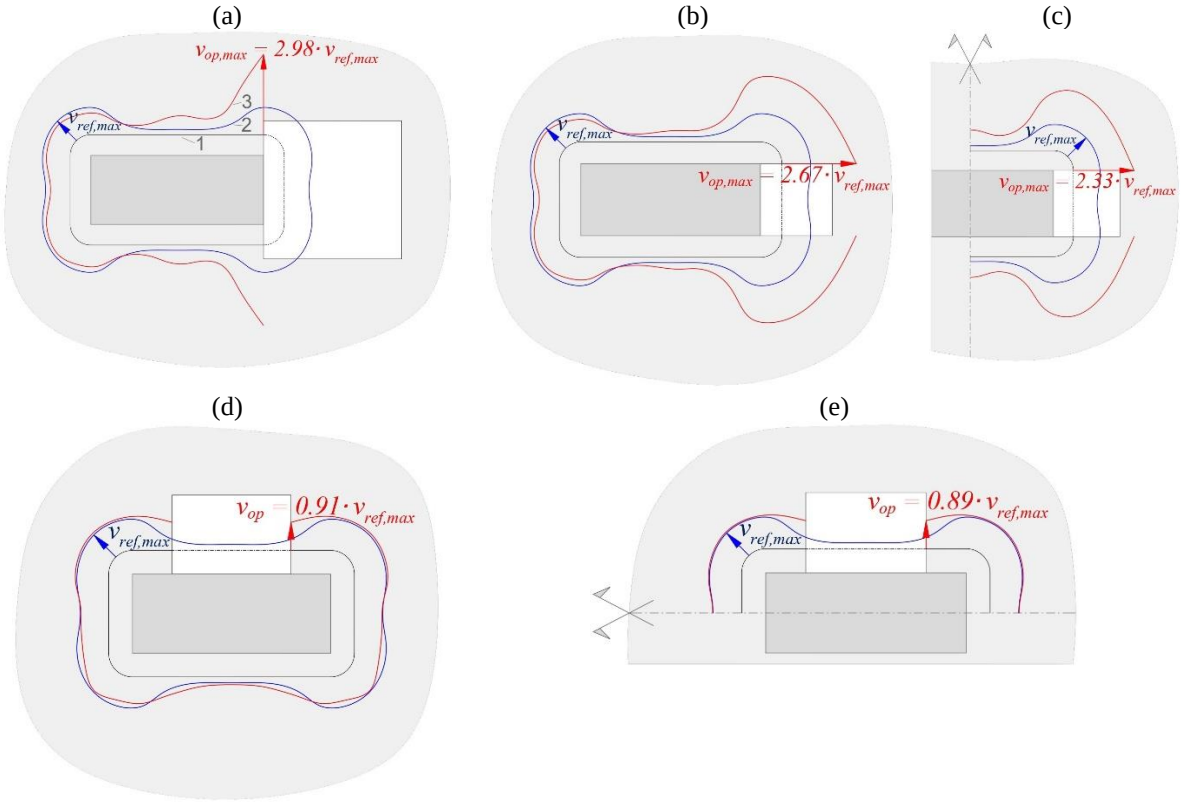

Figure 3.3 - Effect of the position of the opening on the shear force distribution along the control perimeter of a rectangular column for slabs from Souza (2008) [7], c_{max}/ c_{min} =2.5: (a) L2, L3 and L4; (b) L7; (c) L9; (d) L16; and (e) L19

Another aspect that can influence the resistance of slabs with openings is the lack of symmetry. The presence of unsymmetrical openings can lead to moment transfers in the slab-column connection, which results in additional shear force concentrations that can reduce the punching resistance (Figure 3a, b and d) [1,2].

It has to be noted that since the elastic shear fields do not consider cracking and local yielding, the peaks of shear forces shown in Figure 3.1-Figure 3.3 overestimate the actual shear force distribution [3,4]. In addition, the presence of vertical legs provided by bends of the flexural reinforcement or pins positioned on the edge of the openings can act as shear reinforcement contributing to smooth the peaks of the shear force. However, these effects were not considered in the present analyses.

3.2 DESIGN CODE APPROACHES FOR SLABS WITH OPENINGS

The first experimental results for flat slabs with openings were published by Moe (1961) [5]. Based on Moe's results, the ASCE Committee 326:62 [6] recommended that the reduction of the control perimeter to account for the presence of openings should be done depending on the distance to the column face. For an opening located at less than $d/2$ from the column face, the length of the control perimeter between radial lines should be neglected as shown in Figure 3.4a. For openings between $d/2$ and $2d$ from the column face, the smallest value of the control perimeter given by Figure 3.4b should be taken. For openings that are large compared to the dimensions of the control perimeter, the committee suggested to calculate them as free edges. Since then, ACI 318 and EN 1992-1-1 considered the reduction of the control perimeter by taking radial lines from the centroid of the column, and this approach remains in the current codes (Figure 3.5). The CEB-FIP and *fib* Model Codes did not include indications for slabs with openings until *fib* MC 2010:2013.

While the radial lines approach to account for the presence of openings is simple, it does not always accurately represent the actual behaviour of flat slabs with openings. As it can be seen in Figure 3.6 where two tests by Souza (2008) [7] are compared, the measured punching resistance of the test with openings on the short side of the column (test L9) is lower than the resistance of the test with openings at the long side (test L19), even though the control perimeter according to the rule described above is longer for test L9 (Figure 3.6a) than for test L19 (Figure 3.6b). This is related to the fact that the distribution of shear forces in case of openings located on the short side of a rectangular columns are more detrimental to the resistance than those located on the long side, as shown in Figure 3.6. This comparison shows that not only the reduction of the control perimeter, but also the position of the openings and the resulting distribution of the shear forces has an influence on the punching shear

resistance. This fact should be accounted for in defining a nominal control perimeter to rationally evaluate the punching shear resistance.

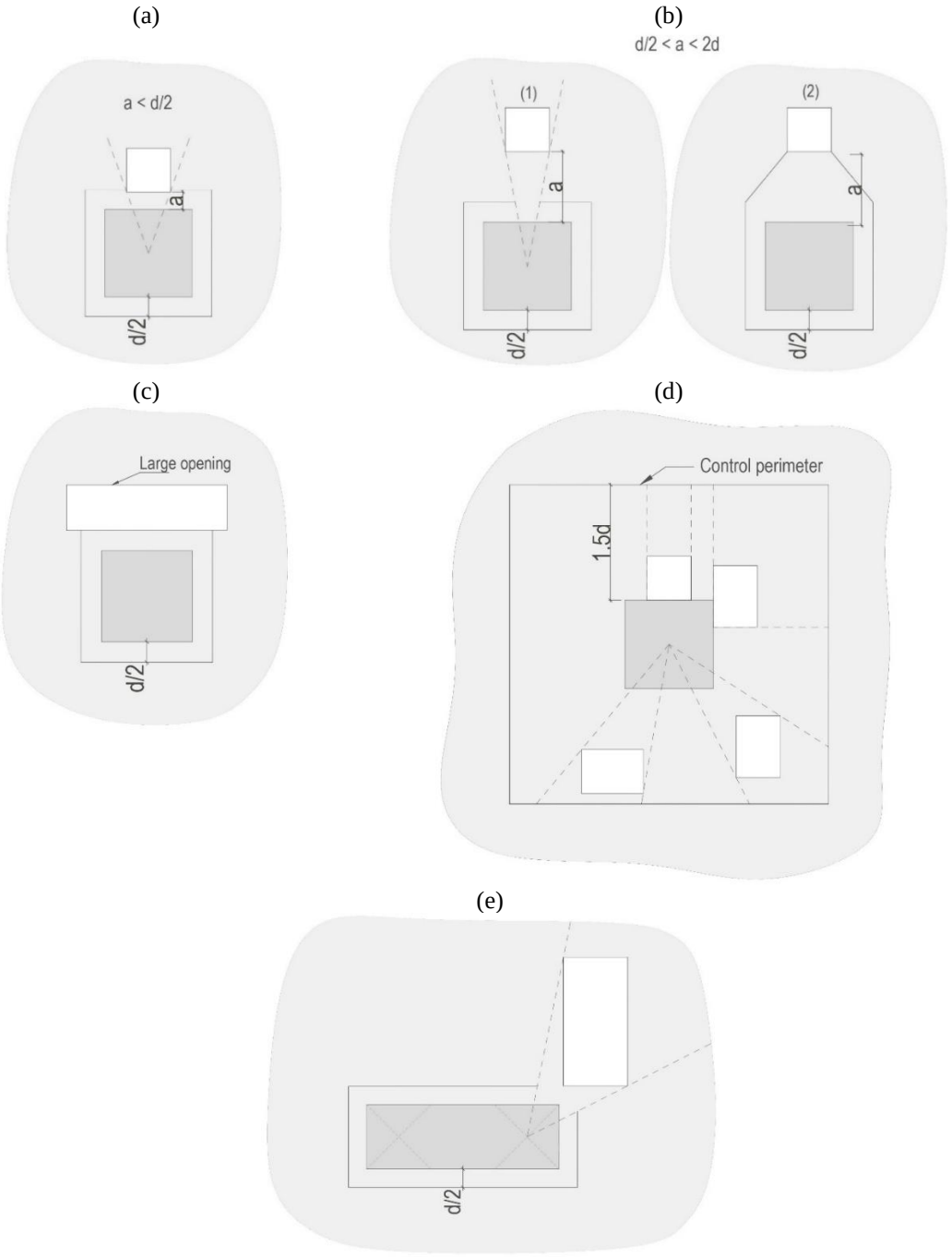

Figure 3.4 - Reduction of control perimeter to account for openings according to several approaches: (a), (b) and (c) ACI ASCE Committee 326:2 [6]; (d) BS 8110:1995 [9] and Regan (1974) [1]; and (e) Teng et al. (2004) [12]

According to Regan (1974) [1] and Borges, Melo and Gomes (2013) [8], the radial lines approach can overestimate the reduction of the nominal control perimeter related to the

presence of openings. To correct this shortcoming, Regan (1974) [1] proposed a less restrictive procedure on the basis of parallel lines (accounting also for the fact that the control perimeter according to the British Standard of 1985 was taken at 1.5*d* form the column face). BS 8110:1985 [9] also recommended the radial lines approach, excepting when openings are immediately adjacent to the column (touching the column face). In this case, the recommendation was to take parallel projections as suggested by Regan (1974) [1] (Figure 3.4d). For slabs with openings close to the columns, Augustin *et al.* (2019) [10] and Kormošová *et al.* (2020) [11] obtained more accurate predictions by performing the reduction of the nominal control perimeter on the basis of parallel lines as proposed by Regan (1974) [1]. Teng *et al.* (2004) [12] observed that for very elongated columns, the approach with radial lines is not sufficiently accurate. They suggested taking the projection lines from the end portion of the column to avoid underestimating the resistance (Figure 3.4e).

In the last decades, many studies have been performed to investigate punching shear in flat slabs with openings and without shear reinforcement, either numerically or experimentally [1-2,5-22]. Test results are now available for a wide variety of column dimensions as well as geometries and locations of the openings. Nevertheless, the current code approaches to account for the strength reduction due to openings, originally validated on the basis of limited experimental results (square columns, square and circular openings) have not been updated to account for recent results.

The present paper analyses a database of test results on slabs with openings and without shear reinforcement according to the Critical Shear Crack Theory [23] and the following codes: ACI 318:2019 [24], EN 1992-1-1:2004 [25], the draft prEN 1992-1-1:2021 [26] and *fib* MC 2010:2013 [27]. Based on the results of this analysis and on previous studies, it proposes a new approach and a new definition of the control perimeter to improve the prediction of the punching shear resistance of slabs with openings.

The provisions of the considered codes are very similar. Only EN 1992-1-1:2004 presents a more conservative reduction when the shorter dimension of a rectangular opening is positioned towards the column (Figure 3.5c). For the maximum distance between the column and the openings to reduce the control perimeter, prEN 1992-1-1:2021 and MC 2010:13 define a distance of $5.5d_v$ from the column edge and EN 1992-1-1:2004 a distance of $6d$. Based on the numerical results by Genikomsou and Polak (2017) [20], ACI 318:2019 uses a distance of $4h$. The reduction of the control perimeter with respect to each code is shown in Figure 3.5. It is worth mentioning that *fib* MC 2010:13 and prEN 1992-1-1:2021 define reduction of the control perimeter to account for the effect of concentration of shear forces in large supporting areas based on geometrical considerations, while ACI 318:2019 uses an analytical approach to consider this effect.

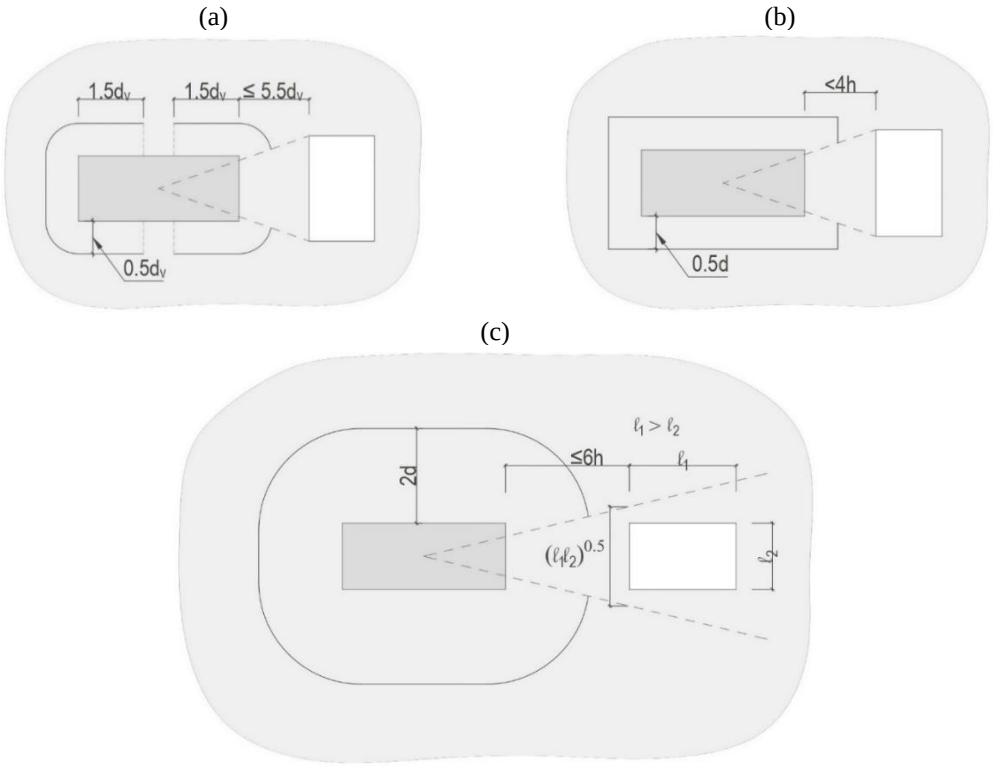

Figure 3.5 - Reduction of the control perimeter in presence of openings according to: (a) fib MC 2010:2013 [27] and prEN 1992-1-1:2021 [26]; (b) ACI 318:2019 [24]; and (c) EN 1992-1-1:2004 [25]

In the presence of large openings, ACI 318:2019 recommends considering the slab-column connection as an edge connection. Detailed recommendation can be found in ASCE-ACI

352.1R:1989 [28] which specifies the conditions to consider an internal connection with opening as an edge connection, as shown in Figure 3.7. No comments are given regarding different opening patterns that can lead to moment transfer. EN 1992-1-1:2004, *fib* MC 2010:13 and prEN 1992-1-1:2021 do not provide any recommendations concerning moment transfers in slab with openings. The formulae to calculate the punching resistance according to the investigated codes are summarized in the ANNEX A: CODE PROVISIONS.

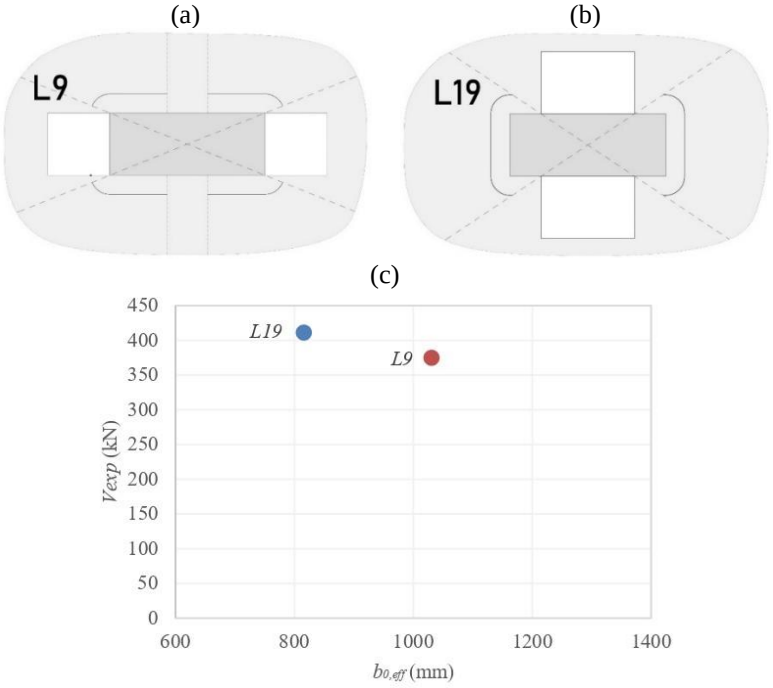

Figure 3.6 - Current control perimeter according to fib MC 2010:2013 for tests by Souza (2008) [7]: (a) L9; (b) L19; and (c) Experimental resistance-effective control perimeter of slabs L9 and L19

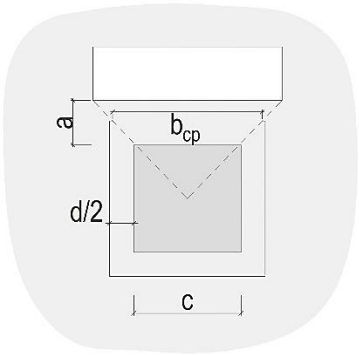

b_{cp}: length of control perimeter within radial lines

a: clear distance between support and opening

c: column dimension

d: effective depth

Note:

Regard as free edge if $b > c$ and $a < 4h$

Figure 3.7 - ASCE Committee 352.1R:1989 [28] recommendation for connection with large openings

3.3 ANALYSIS OF EXPERIMENTAL DATA

3.3.1 Preliminary remarks

The presence of openings requires the rearrangement of the flexural reinforcement. Some rebars around the openings must be interrupted, which can lead to different reinforcement ratios in each direction depending on the number, size and position of the openings.

Table 3.1 - Summary of database containing 68 specimens with openings and without transverse reinforcement

Authors	n°	B (mm)	d (mm)	c_x x c_y (mm)	b_x x b_y (mm)	f_c (MPa)	d_g (mm)	ρ_{MC} (%)	ρ_{EN} (%)	f_y (MPa)
Moe (1961)	12	1829	114.3	254 x 254	127 x 127 254 x 254 127*	24-28	37.5	1.15	1.12	327
Müller *et al.* (1984)	2	2750	152-153.5	300*	250 x 200 500 x 200	29.7-34.2	16	1.29-1.30	1.39-1.41	551
Teng *et al.* (1999)	8	2200	108-117.8	200 x 200 600 x 200	200 x 300 300 x 200	33.9-43.1	20	1.61-1.74+	1.61-1.74+	453-470
Souza (2004)	7	1800	89-92	150 x 150	150 x 150 150 x 300 150 x 450	32.1-36.2	19	1.21-1.42	1.01-1.42	538-555
Borges (2004)	6	3000	144-164	600 x 200	200 x 300	37-41.6	19	1.20-1.40	1.00-1.55	601-604
Souza (2008)	7	2400	123-126	500 x 200	200 x 200 300 x 200 400 x 400	32.3-44	19	0.65-1.04	0.52-1.48	583-595
Anil *et al.* (2014)	8	2000	95	200 x 200	300 x 300 500 x 500	19.6-21.2	15	0.39+	0.39+	480
Liberati *et al.* (2019)	8	1800	88-95	150 x 150	75* 150*	35.2-44.5	16	1.29-1.43	1.08-1.49	576-585
Augustin *et al.* (2019)	6	2500	200	200 x 200	200 x 300	31.1-43.3	12	1.41-1.44	1.49-1.68	561
Lourenco *et al.* (2021)	4	1800	91-93	150 x 150	150 x 150	41.2-46	16	1.36-1.39	1.23-1.29	563-576
Total	68	1800-3000	88-164	150 x150 600 x 200	150 x 150 500 x 500	19.6-46	12-37.5	0.39-1.74	0.39-1.74	327-604

Modulus of elasticity of steel E_s = 200 MPa for all slabs
+provided by the author
*diameter of round column/opening
B - dimension of the isolated slab (square for all cases); d - effective depth; c_x, c_y - column dimensions in directions x and y; b_x, b_y - opening dimensions in directions x and y; f_c - concrete compressive strength; d_g - maximum aggregate size; ρ_{MC}, ρ_{EN}: reinforcement ratio according to Model Code and Eurocode, respectively; f_y- yield strength of flexural reinforcement
x and y are the coordinate axes where the x direction is parallel to the long side of the column

To ensure a consistent analysis of the database, the reinforcement ratio was recalculated neglecting the rebars interrupted by the opening (this is justified by the fact that these bars cannot have large strains and thus do not significantly contribute to the flexural behaviour

[2,8,12] and averaging the reinforcement ratio over the width specified by the standards (different definitions for fib MC 2010:2013 and EN 1992-1-1:2004). When the reinforcement detailing was not available, the reinforcement ratio was taken as indicated by the authors [12, 16].

The database includes a total of 68 slabs without transverse reinforcement [5,7,10,12-19]. Table 3.1 shows the reinforcement ratios obtained from fib MC 2010:2013 and EN 1992-1-1:2004, as well as properties of the slabs.

3.3.2 Comparison of punching shear strength predicted by codes

Figure 3.8 shows the ratio of experimental to theoretical resistance as a function of the ratio of the effective control perimeter $b_{0,eff}$ of the slab with openings to the control perimeter of the slab without opening $b_{0,full}$ according to ACI 318:2019, EN 1992-1-1:2004, prEN 1992-1-1:2021 and *fib* MC 2010:2013 level II. As shown in Table 3.2, ACI 318:2019 presents the largest mean value and coefficient of variation and *fib* MC 2010:13 the smallest. Symmetrical openings immediately adjacent to the columns have a large mean value.

According to the empirical approaches of ACI 318:2019 and EN 1992-1-1:2004, the reduction of the punching resistance due to the presence of openings depends proportionally to the reduction of the control perimeter. As shown in Figure 3.8a,b, this assumption does not reflect the actual behaviour. The approaches of *fib* MC 2010:2013 and prEN 1992-1-1:2021, which are based on a mechanical model and account for a nonlinear relationship between the length of the control perimeter and the resistance, provide a better estimate.

Nevertheless, in some cases, *fib* Model Code 2010 and prEN 1992-1-1:2021 also give overly conservative estimates of the punching shear resistance. This is mainly related to the reduction of the control perimeter which is still based on the approach proposed by Moe (1961) [5] (radial lines approach shown in Figure 3.4).

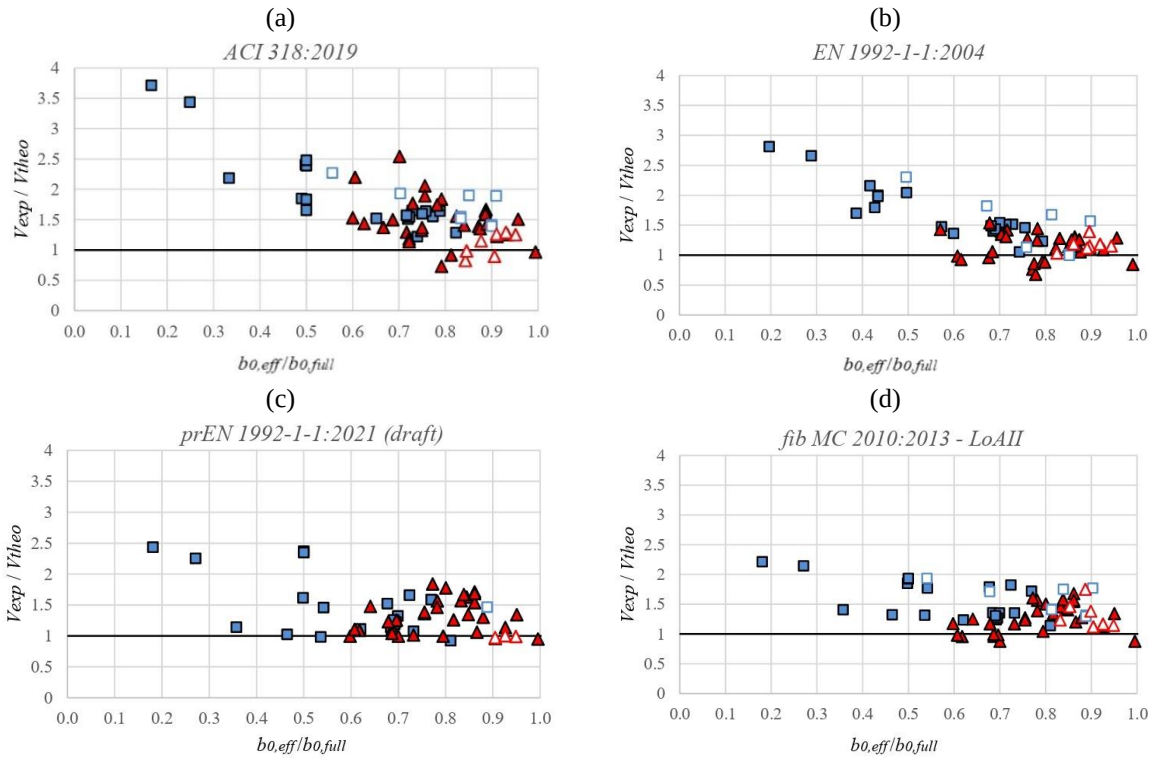

Figure 3.8 - Database analysis according to codes provisions: (a) ACI318:2019; (b) EN 1992-1-1:2004; (c) prEN 1992-1-1:2021; and (d) fib MC 2010:2013-LoAII (Legend for symbols in Table 3.2)

The unsafe predictions of the resistance can be explained by the moment transfer caused by the lack of symmetry in slabs with unsymmetrical openings. In these cases, ACI 318:2019 generally recommends considering the connection as a free edge. The other codes do not give any recommendation regarding moment transfers in slabs with unsymmetrical openings. Based on the considerations and on the comparison with experimental results, improvements are needed for code provisions on punching shear for slabs with openings and without transverse reinforcement.

3.4 PROPOSED PUNCHING VERIFICATION FOR SLABS WITH OPENINGS

3.4.1 Modification of the control perimeter to account for the presence of an opening

The results of the shear forces distribution at 0.5*d* from the column face obtained by a linear-elastic finite element analysis provide useful information to better understand the shear field perturbations caused by openings [29]. Figure 3.1-Figure 3.3 show that the neglected part of

the control perimeter indicated by the radial lines does not correspond to the shear distribution around the column.

Based on the results of linear-elastic analyses and on the experimental results described in previous section, a new proposal for the reduction of the control perimeter in the presence of openings is proposed. When the opening is either immediately adjacent to the column or inside the control perimeter region, the control perimeter can be extended up to the edges of the opening (Figure 3.9a-1). When the distance between the column face and the opening is larger than 0.5*d*, the control perimeter should be taken as the minimum distance to the opening (Figure 3.9a-2). Evidently, the total reduced perimeter should never be larger than the control perimeter of a slab without openings (Figure 3.9a-3). Figure 3.9b shows an example of openings wider than the control perimeter width. In that case, the minimized control perimeter is given by the straight lines to the edge of the opening (Figure 3.9b-2).

The dimension a^* shown in Figure 3.9a-3 and Figure 3.9b-3 is the minimum distance from the opening to the column that leads to a control perimeter with no reduction (the presence of the opening does not decrease the resistance) and is given by Eq. (3. 1)- (3. 3). It is worth mentioning that according to this proposal, this distance depends on the dimensions of the column and of the opening, and not only on the effective depth as in current codes. This modification of the control perimeter agrees with many experimental and numerical results [1,2,7,10,12,20-22].

Equations (3. 1)- (3. 3) are valid for the cases of Figure 3.9, for slabs with rectangular columns and a single opening. For a larger number of openings and other column geometries, the expressions need to be adapted accordingly.

(a)

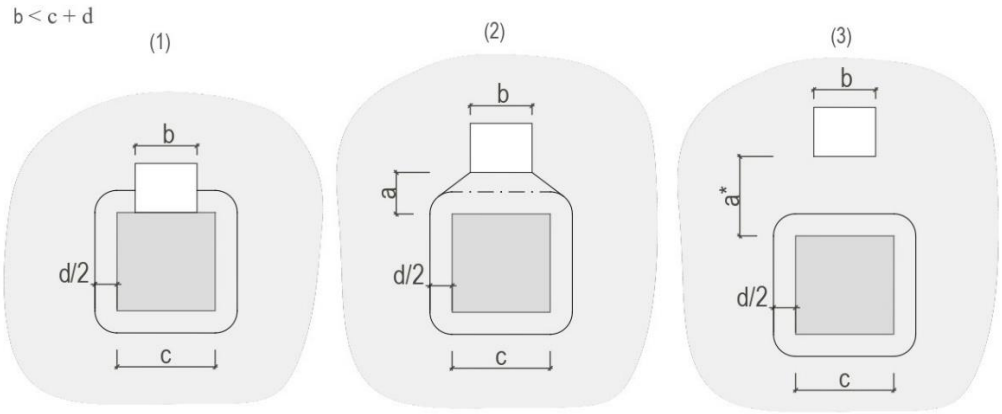

(b)

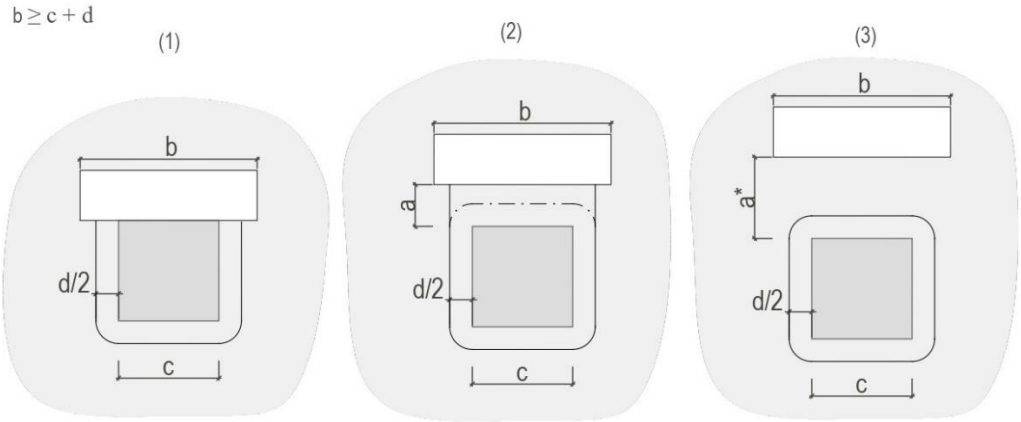

Figure 3.9 - Control perimeter reduction rule according to the proposed approach: (a) when b < c+d; and (b) when b ≥ c+d (c- column dimension, b- opening dimension, a- distance from the opening to the face of the column, a*- distance of the opening from the face of the column that leads no reduction of the control perimeter, according to 3. 1 and 3. 2)

If $b < c$

$$a^* = c + \frac{\pi d}{2} - d \cdot \arctan\left(\frac{\sqrt{b^2-2bc+c^2-d^2}}{d}\right) - \sqrt{b^2-2bc+c^2-d^2} \quad (3.\ 1)$$

If $b = c$

$$a^* = \frac{1}{2}\sqrt{\frac{\pi^2 d^2}{4} + \pi dc + c^2 - d^2} \quad (3.\ 2)$$

If $b \geq c+d$

$$a^* = c + \frac{\pi d}{2} \quad (3.\ 3)$$

where c is the side length of the column near to the opening (with $c \leq 3d$), b is the width of the opening and d is the effective depth.

With the proposed control perimeter, several shortcomings of the old approach by Moe (1961) [5] (radial lines approach, still considered in current standards) can be resolved. The issue presented in Figure 3.6 for instance, can now be corrected by considering the neglected parts of the control perimeter that effectively contribute to the punching resistance (see Figure 3.10). The contribution of one-way shear at elongated columns with openings near to the short side of the column can be significant, as the openings are in the region of two-way forces transfer (for instance, as L9 presented in Figure 3.6 and Figure 3.10) [4]. However, the one-way shear contribution was not considered in this work for simplicity. A more refined analyses could be performed using refined shear field analyses.

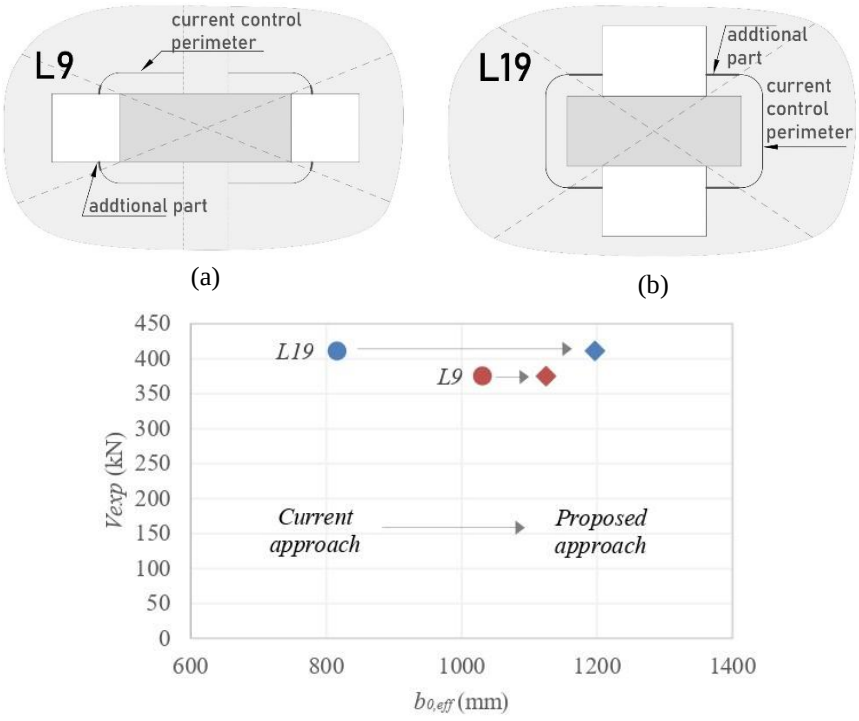

Figure 3.10 - Comparison between current and proposed control perimeter for slabs L9 and L19 from Souza (2008) [7]

3.4.2 Approach for slabs with unsymmetrical openings

The comparison between measured punching shear resistances and code predictions in Figure 3.8 shows that the lowest values are obtained for unsymmetrical openings (tests shown with red squares). Figure 3.3a, b and d clearly show the effect of an unsymmetrical position of the openings on the distribution of shear forces along the control perimeter (linear-elastic-uncracked numerical analysis). Figure 3.11b shows that the distribution of shear forces in a slab with an unsymmetrical opening is similar to that of a slab without opening, but with an unbalanced moment, Figure 3.11a. In addition, Figure 3.12 shows that the unsymmetrical behaviour caused by the lack of symmetry depends on the size and the orientation of the opening with respect to the column. EN 1992-1-1:2004 and MC 2010:2013 neglect this effect, which appears unsafe.

Figure 3.11 - Linear-elastic distribution of shear force along the control perimeter at 0.5d and maximum nominal shear calculated for slabs from Teng et al. (2004) [12]: (a) OC11 with e=240mm without opening; and (b) OC11H30 with opening, but without eccentricity of the resultant. (Note: maximum nominal shear force shown for a total applied load V = 373 kN)

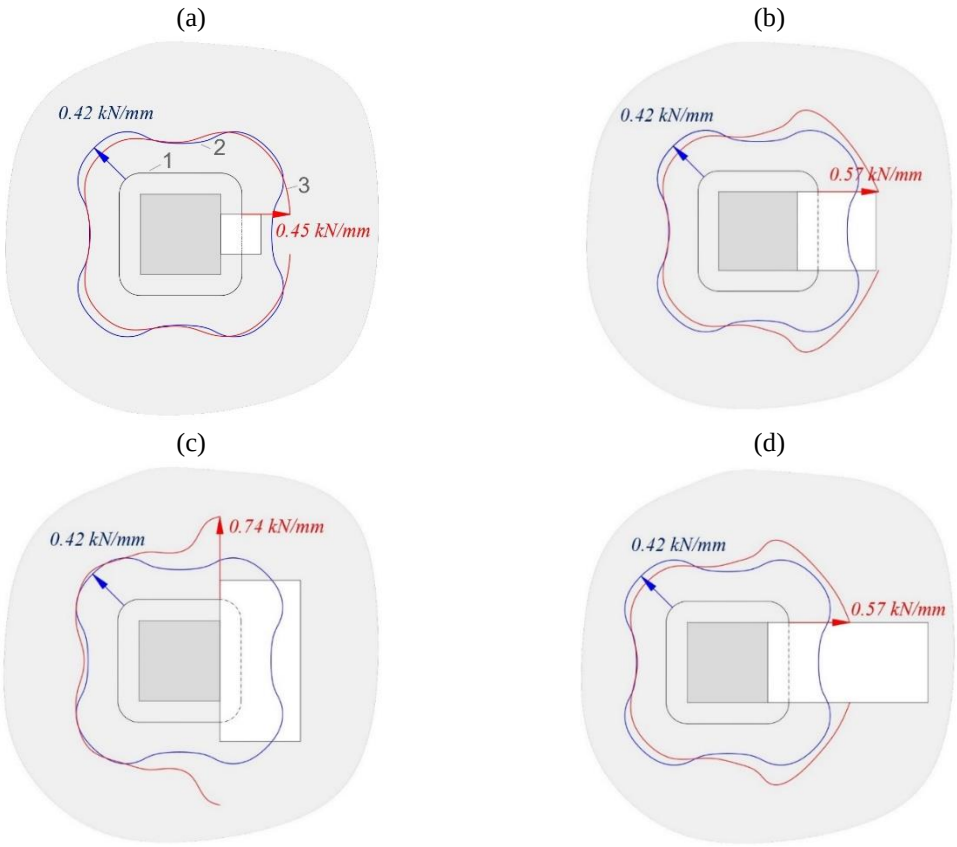

Figure 3.12 - Effect of opening dimension on the stress field at 0.5d and maximum nominal shear for slabs with a square column width equal to 200 mm and for several opening width: (a) b/c = 0.5; (b) b/c = 1, square opening; (c) b/c = 2, rectangular opening; and (d) b/c = 1, rectangular opening. (Note: maximum nominal shear stress shown for a total applied load V = 373 kN)

As shown in Figure 3.11, these shortcomings can be resolved by considering a corrected unbalanced moment which results from the eccentricity between the centroid of the reduced control perimeter (point P in Figure 3.13) and the resultant of the acting shear force (point C in Figure 3.13 for the case without unbalanced moment in the column). With this calculated eccentricity (or corrected unbalanced moment), the described effect can be considered in the same manner as for the case of unbalanced moments in a slab without openings (see ANNEX A: CODE PROVISIONS for the approaches in the different codes). It has to be noted that this effect has already been accounted for in prEN 1992-1-1:2021 as a result of present research (this explains the less unsafe predictions according to prEN 1992-1-1:2021 compared to other standards, see Table 3.2 and Figure 3.8).

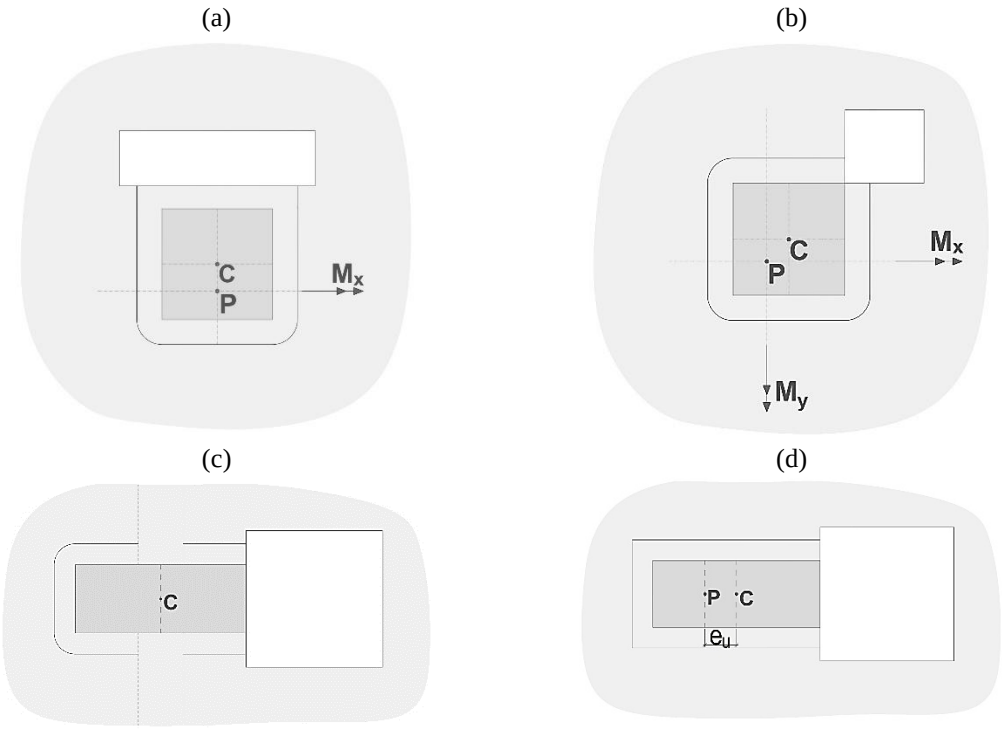

Figure 3.13 - Proposed approach to account the moment transfer in slabs with unsymmetrical openings: (a) opening on the side of the column; and (b) opening on the corner of the column; (c) control perimeter to calculate the punching shear resistance; and (d) simplification of the control perimeter with sharp corners to calculate its centroid

It is important to note that to calculate the eccentricity of the resultant of shear forces according to MC 2010:13, the larger control perimeter width should not be limited to $3d_v$ as recommended by the code. In addition, for the computation of the eccentricity, the control perimeter can be simplified by replacing the round parts by sharp corners (Figure 3.13c,d).

3.4.3 Application of the proposed approach to the database

The new control perimeter presented in 3.4.1 and the consideration of eccentricity for unsymmetrical cases presented in 3.4.2 were applied in the database. The results are shown in Figure 3.14 and in Table 3.3.

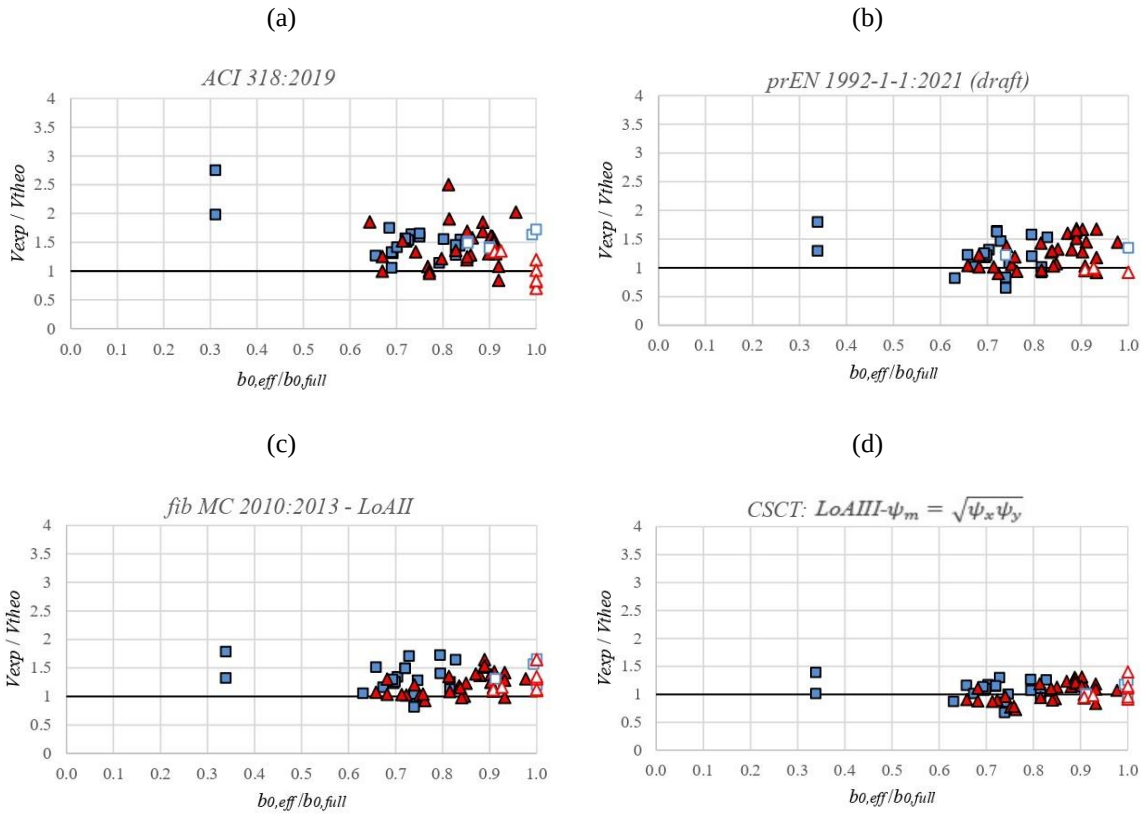

Figure 3.14 - Database analysis with proposed changes (eccentricity in case of unsymmetric openings) and new control perimeter for the approaches according to: (a) ACI318:19; (b) prEN 1992-1-1: 2021 (c) fib MC 2010:13-LoAII; and (d) CSCT LoAIII-ψ_m (Legend for symbols in Table 3.3)

Table 3.2 - Summary of experimental-to-calculated resistances according to the current codes provision (see Figure 3.8)

Legend		ACI 318:2019			EN 1992-1-1:2004			prEN 1992-1-1:2021			*fib* MC 2010:2013 LoAII		
	n°	Av.	CoV	Min	Av.	CoV	Min	Av.	CoV	Min	Av.	CoV	Min
Adjacent / symmetrical	20	1.81	0.24	1.22	1.70	0.27	1.05	1.48	0.33	0.92	1.57	0.21	1.14
Adjacent / unsymmetrical	37	1.47	0.25	0.73	1.13	0.19	0.68	1.30	0.21	0.95	1.24	0.19	0.87
Non-adjacent / symmetrical	8	1.74	0.18	1.40	1.46	0.32	1.00	1.45	0.08	1.31	1.57	0.15	1.29
Non-adjacent / unsymmetrical	7	1.10	0.17	0.83	1.17	0.09	1.03	1.19	0.19	0.97	1.32	0.17	1.09
All tests	68	1.60	0.33	0.73	1.34	0.31	0.68	1.36	0.25	0.92	1.39	0.22	0.87

The mean values and the coefficients of variation are smaller than in Table 3.2 for all investigated codes. For openings immediately adjacent to the column and for symmetric openings, the mean values are significantly reduced. For cases with unsymmetrical openings

(40 slabs), the prediction of several tests is improved by considering the eccentricity, and the number of tests with unsafe predictions is significantly smaller, as shown in Table 3.4.

Table 3.3 - Summary of experimental-to-calculated resistances according to the proposed approach (see Figure 3.14)

Legend		ACI 318:2019			prEN 1992-1-1:2021			*fib* MC 2010:2013 LoAII		
		n°	**Av.**	**CoV**	**Min**	**Av.**	**CoV**	**Min**	**Av.**	**CoV**	**Min**
■	Adjacent / symmetrical	20	1.54	0.23	1.06	1.24	0.25	0.65	1.35	0.19	0.82
▲	Adjacent / unsymmetrical	33	1.44	0.24	0.84	1.26	0.20	0.90	1.22	0.16	0.93
□	Non-adjacent / symmetrical	8	1.47	0.10	1.26	1.26	0.07	1.12	1.36	0.12	1.20
△	Non-adjacent / unsymmetrical	7	1.03	0.26	0.70	1.05	0.14	0.92	1.26	0.16	1.10
	All tests	68	1.43	0.24	0.70	1.23	0.21	0.65	1.28	0.17	0.82

Table 3.4 - Percentage of unsafe code provisions over 40 slabs with unsymmetrical openings according to the current and proposed control perimeter to account for openings

Code	$V_{exp} / V_{theo}<1$	
	Current	**Proposed**
ACI 318:2019	18%	15%
prEN 1992-1-1:2021 (*draft*)	20%	20%
fib MC 2010:2013 LoAII	20%	5%

3.5 APPLICATION OF THE CRITICAL SHEAR CRACK THEORY TO SLABS WITH OPENINGS

3.5.1 Introdutory remarks

Inspired by the theoretical approach of Kinnunen and Nylander [31], the critical shear crack theory (CSCT) was proposed by Muttoni and Schwartz [32] on the basis that the opening of a critical shear crack reduces the ability of a concrete to transfer shear forces and eventually leads to failure. According to this mechanical model, the opening of the critical shear crack (w) can be assumed to be proportional to the slab rotation ψ times the effective depth d, so that, according to Muttoni (2008) [23], the following failure criterion can be used:

$$V_{Rc} = \frac{0.75 \cdot b_0 \cdot d \cdot \sqrt{f_c}}{1 + 15 \cdot \frac{\psi \cdot d}{d_{g0} + d_g}} \tag{3. 4}$$

where b_0 is the control perimeter at $d/2$ from the supporting area (with rounded corners); d_{g0} is the reference aggregate size (16 mm) and d_g is the maximum aggregate size.

To determine the punching shear resistance according to Eq. (3. 4), the rotation ψ of the slab at failure needs to be known. Despite the high non-linearity of such relationship, a refined calculation can be performed by considering a quadri-linear moment-curvature diagram incorporating cracking and tension-stiffening effects, as presented by Muttoni (2008) [23]. For practical purposes, a simplified relationship assuming a non-linear parabolic law has been derived [23] and shown to be efficient in terms of accuracy and ease of use:

$$\psi = k_m \cdot \frac{r_s}{d} \frac{f_y}{E_s} \left(\frac{m_E}{m_R}\right)^{3/2} \tag{3. 5}$$

where k_m depends on the level of refinement used to estimate the acting bending moment [33]; r_s is the distance between the axis of the supporting area and the line of zero radial moment; d is the effective depth; f_y is the yield strength of flexural reinforcement; E_s is the modulus of elasticity of flexural reinforcement; m_E is the average acting bending moment in the support strip and m_R is the average moment capacity in the support strip. For design purposes, m_E can be calculated based on the acting loads and the verification is fulfilled if V_{Rc} is not smaller than the acting shear force V_E (where V_{Rc} and V_E have to be reduced, respectively increased by partial safety factors), whereas for calculating the actual punching shear resistance, an iteration is required until $V_{Rc} = V_E$.

The intersection of the hyperbolic failure criterion (Eq. (3. 4)) and the parabolic load rotation relationship (Eq. (3. 5), which corresponds to the described iteration, provides the punching shear resistance along with the corresponding deformation capacity. The level of approximation can be chosen as the accuracy of the analysis requires [33].

3.5.2 Approach for slabs with openings

Contrary to empirical expression calibrated on available test data [34], mechanical models attempt to faithfully represent the physical phenomena. Another advantage is that physical models can easily account for various aspects in terms of geometry, reinforcement and actions by means of refined approaches. The CSCT has been improved and refined models have been proposed for rectangular columns, non-axis-symmetrical punching and unbalanced moments [30, 35-38].

According to Sagaseta *et al.* (2011) [35], the following reasons can cause non-axis-symmetrical punching in flat slabs: the loading pattern, the slab and column geometry, and the reinforcement layout. In slabs with openings, the asymmetry can be caused by the lack of symmetry of the openings, leading to a moment transfer in the connection (Figure 3.1 and Figure 3.3). In addition, the presence of openings is usually associated with an irregular reinforcement layout, and different reinforcement ratios can occur in each direction. The database used in the present paper (Table 3.1) includes cases of asymmetrical openings, rectangular columns and different reinforcement ratios [7,12-15]. For cases with different reinforcement ratios in both orthogonal directions, which are non-axis-symmetrical [35], experimental results in slabs without openings have shown a considerably difference between the rotations in both directions. In these cases, the conventional analysis for axis-symmetrical punching shear might not be suitable.

In this paper, in a first step, the Level of Approximation II has been investigated by adopting the moment acting in the support strip as $m_E = V/8$ and by considering the direction of maximum rotation [23].

In a second step, the Level of Approximation III has been investigated by calculating the average moment acting in the support strip directly from equilibrium (this is possible only for isolated slab-column connections which are statically determinate). Here again, the

maximum rotation in both directions has been considered, leading to a safe estimate of the punching shear resistance.

In some cases, the prediction of the resistance is very different in each direction, and the estimation of resistance along the direction with maximum rotation provides an overly conservative result. As shown by Sagaseta *et al.* (2011) [35], in these cases, a redistribution of internal forces can occur between the direction with higher resistance (lower rotation) and the governing direction with larger rotation and lower resistance. For the sake of simplicity, this complex phenomenon of redistribution of internal forces can be approximated by considering the geometric mean of the rotations in the two directions *x* and *y* ($\psi_m = \sqrt{\psi_x \psi_y}$) in a similar manner as for calculating the mean reinforcement ratio of *x* and *y* directions according to EN 1992-1-1:2004 and prEN 1992-1-1:2021 [25,26]. Figure 3.15 shows the results for slabs with rectangular columns and different reinforcement ratios in each direction. The dotted lines in Figure 3.15a,b show the solution obtained using the mean rotation ψ_m. It can be observed that this approach presents a load-rotation relationship very close to the experimental load-rotation curve (Figure 3.15b).

As shown in Figure 3.15, according to the proposed control perimeter, the strength prediction is improved from Level II-ψ_{max} approach (point A') to Level III-ψ_m approach (point B'). On the contrary, for slabs with square columns, if there is no significant difference between the reinforcement ratios in each direction, the Level II-ψ_{max} approach can provide sufficiently accurate results (Figure 3.15d).

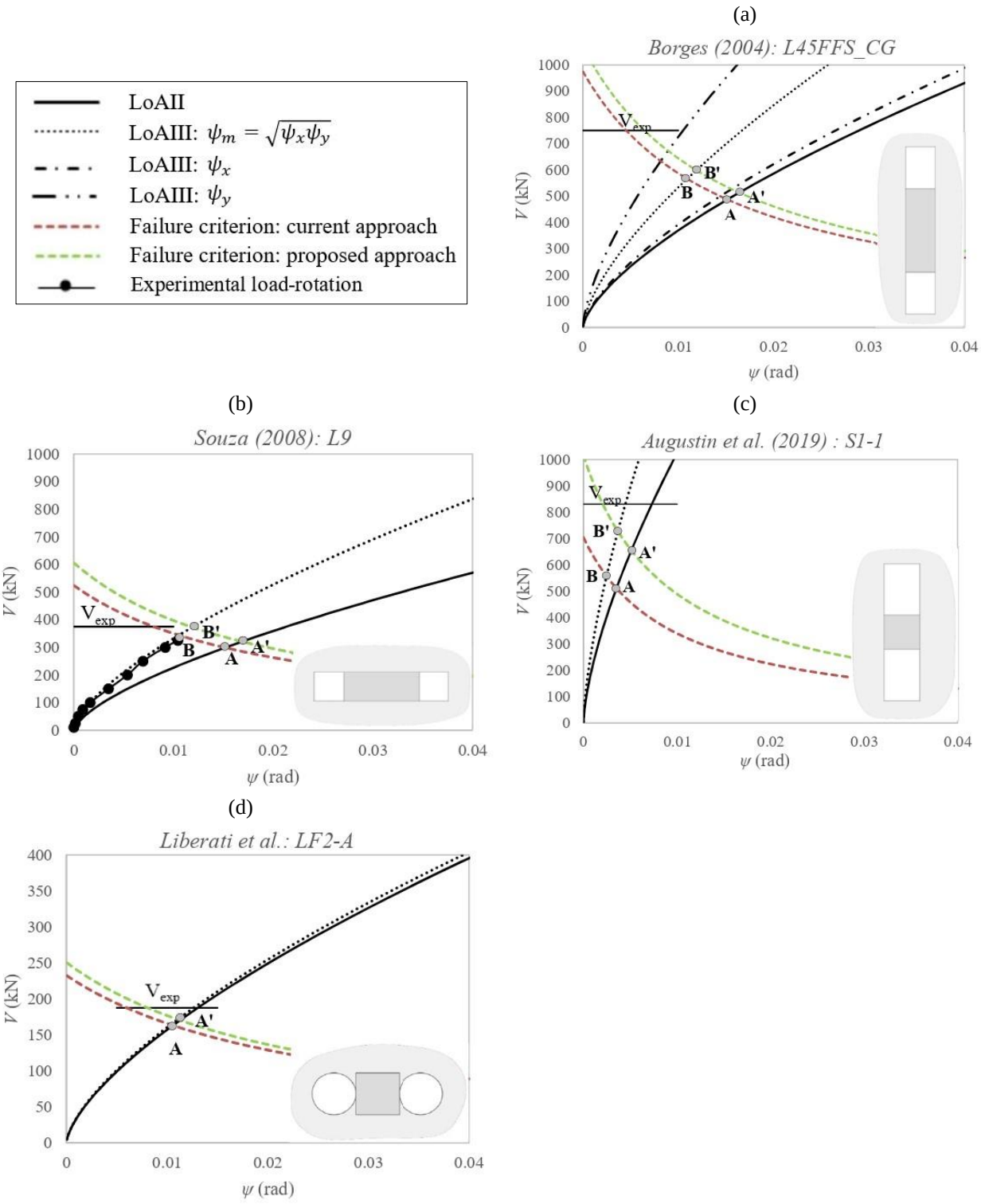

Figure 3.15 - Load-rotation relationship and failure criterion for several cases: (a) L45FFS_CG from Borges (2004) [14], ρ_x/ρ_y=0.86, c_{max}/c_{min} =3.0; (b) L9 from Souza (2008) [7], ρ_x/ρ_y=0.92, c_{max}/c_{min} =2.5; (c) S1-1 from Augustin et al (2019) [10], ρ_x/ρ_y=0.88, c_{max}/c_{min} =1.0; and (d) LF2-A from Liberati et al (2019) [17], ρ_x/ρ_y=1.0, c_{max}/c_{min} =1.0.

The CSCT is very useful to understand the behaviour of slabs with openings, and to evaluate new design proposals. Table 3.5 shows the results for the CSCT and *fib* MC 2010:2013 comparing different approaches, using the proposed control perimeter and considerations of moment transfer. The approach of the geometric mean of the rotations provides the smallest coefficient of variation and average. These results can be seen in Figure 3.14d. Taking into consideration the very different situations that can lead to non-axis-symmetrical punching in slabs with openings, the results are excellent from a practical perspective.

Table 3.5 - Summary of results of the CSCT and MC 2010:13 (experimental-to-calculated resistances) according to the new control perimeter, and for different approaches. Note: results for 68 slabs from the database.

	CSCT		***fib* MC 2010:2013**	
Approach	**Average**	**CoV**	**Average**	**CoV**
LoAII-ψ_{max}	1.18	0.17	1.30	0.17
LoAIII- ψ_{max}	1.12	0.16	1.26	0.17
LoAIII-ψ_m	1.05	0.15	1.21	0.18
LoAII-ψ_{max}: m_E = V/8, $\psi_{max} = \max(\psi_x, \psi_y)$				
LoAIII- ψ_{max}: $m_E = m_{eq}$, $\psi_{max} = \max(\psi_x, \psi_y)$				
LoAIII-$\psi_m = \sqrt{\psi_x \psi_y}$: $\psi_x = f(m_{eq,x},\rho_x)$, $\psi_y = f(m_{eq,y},\rho_y)$				

For slabs with unsymmetrical small openings, despite the proposed consideration of eccentricity, as the proposed control perimeter has been increased for adjacent openings, it compensates the reduction of the resistance caused by the eccentricity. For large openings, the consideration of eccentricity provides a better provision.

3.6 CONCLUSIONS

Design rules to account for detrimental influence of the presence openings on the punching shear capacity are very similar in different design codes. Typically, the control perimeter is reduced to account for the presence of openings, often up to radial lines from the centroid of the column.

From an analysis of 68 slabs with openings and without shear reinforcement found in the literature, some main issues were found:

1. The code predictions for slabs with openings immediately adjacent to the column are often overly conservative;
2. The approach to reduce the control perimeter based on radial lines is not suitable to evaluate a wide variety of column and openings geometries that occur in practice;
3. Some code provisions for slabs with unsymmetrical openings are unsafe because the effect of the non-symmetrical behaviour is neglected;
4. Based on the average and coefficient of variation of experimental-to-calculated resistances obtained from database analysis, improvements are needed.

A new approach based on the investigation of the shear field in the opening region and the Critical Shear Crack Theory (CSCT) is proposed, which increases the control perimeter for openings adjacent to the columns and explicitly accounts for the eccentricity of slabs with unsymmetrical configurations. The main conclusions regarding the improvements are:

5. With the two proposed changes, all investigated codes would present a notable improvement in terms of statistical values of the experimental/calculated ratio of the resistance (mean values closer to one, smaller CoV and less unsafe predictions);
6. The amount of unsafe predictions of resistance can be reduced by considering the eccentricity between the acting shear force and the centroid of the control perimeter of the connection with unsymmetrical openings;
7. The proposed approach to reduce the control perimeter accounts for the influence of the column, the geometry of the opening and the effective depth, leads to a better correlation both with experimental results and numerical investigations.

As mechanical models can faithfully represent the physical phenomena of punching shear, MC 2010:13 and CSCT have shown promising results for slabs with openings. The main conclusions regarding the analyses are:

8. The MC 2010:13, which is based on the CSCT, presents the mean value closest to one and the smallest CoV of experimental-to-calculated resistances;
9. MC 2010:13 and CSCT can account for the observed non-linearity between the reduced control perimeter and the resistance of a slab with openings;
10. MC 2010:13 and CSCT allow to evaluate non-axis-symmetrical punching in flat slabs with openings caused by the column geometry, and by the different reinforcement ratios in each direction;
11. The Critical Shear Crack Theory can successfully model the non-axis-symmetrical behaviour in slabs with openings by considering the geometric mean of the rotations in both directions;

3.7 REFERENCES

1. REGAN, P. E. *Design for punching shear. The Structural Engineer*, V. 52, n° 6, pp 197-207, 1974.
2. SANTOS J. B.; SOUZA R. M.; MELO G. S.; GOMES R. B. *Punching resistance of flat slabs with openings adjacent to the columns*. ACI Structural Journal, V. 119, n°.1, pp 41-53, 2022. doi: 10.14359/51734216
3. SETIAWAN A.; VOLLUM R. L.; MACORINI L.; IZZUDDIN B. A. *Numerial modelling of punching shear failure of reinforced concrete flat slabs with shear reinforcement*. Magazine of Concrete Research V. 73(23), p. 1205-1224, 2021. doi.org/10.1680/jmacr.19.00562
4. SETIAWAN A.; VOLLUM R. L.; MACORINI L.; IZZUDDIN B. A. *Punching of RC slabs without transverse reinforcement supported on elongated columns*. Engineering Structures, 2048-2068, 2020. doi.org/10.1016/j.ist6uc.2020.08.017

5. MOE J. *Shearing strength of reinforced concrete slabs and footing under concentrated loads*. Development department bulletin D47. Portland Cement Association; pp 135, 1961.
6. ACI-ASCE Committee 326. *Shear and diagonal tension. Part 3: slabs and footings*. ACI Journal, Proceedings, V.59, n° 3, p. 353-396, 1962.
7. SOUZA R. M. *Punção em Lajes Lisas de Concreto Armado com Furos Adjacentes ao Pilar e Transferência de Momento*. Tese de Doutorado, Faculdade de Tecnologia, Departamento de Engenharia Civil e Ambiental, Universidade de Brasília, 2008. pp 442. *(In Portuguese)*
8. BORGES L. L. J.; MELO G. S.; GOMES R. B. *Punching shear of reinforced concrete flat plates with openings*. ACI Structural Journal, V. 110, n°.4, p. 547-556, 2013.
9. HANDBOOK to BS 8110:1985-1. *Structural Use of Concrete, Part1: code of practice for design and construction*. Palladian Publications Ltd, London, UK, 1987.
10. AUGUSTIN T.; FILLO L.; HALVONIK, J. *Punching resistance of slab-column connections with openings*. Structural Concrete, p. 1–13, 2019. doi.org/10.1002/suco.201900158
11. KORMOŠOVÁ L.; HALVONIK J., MAJTÁNOVÁ L. *Safety of the Models for Assessment of Punching Resistance of Flat Slabs with Openings Adjacent to the Columns*. Solid State Phenomena, V. 309, p. 186-192, 2020. doi:10.4028/www.scientific.net/SSP.309.186
12. TENG S.; CHEONG H. K.; KUANG K. L.; GENG J. Z. *Punching shear strength of slabs with openings and supported on rectangular columns*. ACI Struct J, V. 101(5), p. 678–87, 2004.

13. MÜLLER F.; MUTTONI A.; THÜRLIMANN B. *Durchstanzversuche an Flachdecken mit Aussparungen. Institut für Baustatik und Konstruktion*, ETH Zürich, n° 7305-5 ISBN 3-7643-1686-1, 1984. *(In German)*
14. BORGES, L. L. J. *Comportamento ao puncionamento de lajes cogumelo de concreto armado com pilares retangulares e furos de grandes dimensões*. Tese de doutorado, Faculdade de Tecnologia, Departamento de Engenharia Civil e Ambiental, Universidade de Brasília, 2004. pp 367. *(In Portuguese)*
15. SOUZA R. M. *Punção em lajes cogumelo de concreto armado com furos adjacentes ou distantes de um pilar interno*. Dissertação de Mestrado, Faculdade de Tecnologia, Departamento de Engenharia Civil e Ambiental, Universidade de Brasília, 2004. pp 171. *(In Portuguese)*
16. ANIL Ö.; KINA T.; SALMANI V. *Effect of opening size and location on punching shear behaviour of two-way RC slabs*. Magazine of Concrete Research, V. 66, n°18, V. 955-966, 2014. dx.doi.org/10.1680/macr.14.00042
17. LIBERATI E. A. P.; MARQUES M. G.; LEONEL E. D.; ALMEIDA L. C.; TRAUTWEIN L. M. *Failure analysis of punching in reinforced concrete flat slabs with openings adjacent to the column. Engineering Structures*, V. 182, 2019, p. 331-343, 2019. doi.org/10.1016/j.engstruct.2018.11.073
18. LOURENÇO D. S.; LIBERATI E. A. P.; MARQUES M. G.; ALMEIDA L. C.; TRAUTWEIN L. M. *Reinforced concrete flat slabs with openings at different distances from the column*. IBRACON Structures and Materials Journal, V. 14, n°1, 2021. doi.org/10.1590/S1983-41952021000100011
19. MARQUES M. G.; LIBERATI E. A.; GOMES R. B.; CARVALHO A. L.; TRAUTWEIN L. M. *Punching shear strength model for reinforced concrete flat slabs with openings*. J. Struct. Eng., V. 147, n°7, 2021.

20. GENIKOMSOU A. S.; POLAK M. A. *Effect of Openings on Punching Shear Strength of Reinforced Concrete Slabs—Finite Element Investigation*. ACI Strucutral Journal, V. 114, n°5, p. 1249-1261, 2017. doi: 10.14359/51689871
21. BALOMENOS G. P.; GENIKOMSOU A. S.; POLAK M. A. *Investigation of the effect of openings of interior reinforced concrete flat slabs*. Structural Concrete, V. 19, p. 1672–1681, 2017. doi.org/10.1002/suco.201700201
22. MOSTOFINEJAD D.; JAFARIAN N.; NADERI A.; MOSTOFINEJAD A.; SALEHI M. *Effects of openings on the punching shear strength of reinforced concrete slabs*. Structures, V. 25, p. 760-773, 2020. doi: 10.1016/j.istruc.2020.03.061
23. MUTTONI A. *Punching shear strength of reinforced concrete slabs without transverse reinforcement*. ACI Struct J, V. 105(4), p. 440–50, 2008
24. ACI COMMITTEE 318. *Building code requirements for structural concrete (ACI 318-19) and commentary (318R-19).* American Concrete Institute, Farmington Hills, MI, 2019, pp 623.
25. EN 1992-1-1. *Eurocode 2-Design of concrete structures- Part 1-1: general rules and rules for buildings*, CEN, EN 1992-1-1, Brussels, Belgium, 2004, pp 225.
26. prEN 1992-1-1:2021 *draft*. *Eurocode 2-Design of concrete structures- Part 1-1: general rules and rules for buildings*, CEN, EN 1992-1-1, Brussels, Belgium, 2022, pp 410.
27. FÉDÉRATION INTERNATIONALE DU BÉTON. *Fib Model Code for Concrete Structures 2010 (MC2010),* fib , Lausanne, Switzerland, 2013, pp 390.
28. ACI-ASCE COMMITTEE 352.1R-89. *Recommendations for design of slab'column connections in monolithic reinforced concrete structures*. ACI Journal, Proceedings, V.59, n° 3, p. 353-396, 1997.

29. VAZ RODRIGUES R.; FERNÁNDEZ RUIZ M.; MUTTONI A. *Shear strength of R/C bridge cantilever slabs*. Eng Struct, V. 30: p. 3024–33, 2008. doi:10.1016/j.engstruct.2008.04.017

30. MUTTONI A.; FERNÁNDEZ RUIZ M.; SIMÕES J. T. *The theoretical principles of the critical shear crack theory for punching shear failures and derivation of consistent closed-form design expressions*. Structural Concrete, V. 19, p.174-190, 2018. doi.org/10.1002/suco.201700088

31. KINNUNEN S.; NYLANDER H. *Punching of concrete slabs without shear reinforcement*. Trans Roy Inst Technol, V. 158, p.1-112, 1960.

32. MUTTONI A.; SCHWARTZ J. *Behaviour of beams and punching in slabs without shear reinforcement*. IABSE Colloquium, Zurich, Switzerland; Vol. 62, p. 703–708, 1991.

33. MUTTONI A.; FERNÁNDEZ RUIZ M. *The levels-of-approximation approach in MC 2010: application to punching shear provisions*. Structural Concrete, V. 13, n 1, 2012. 10.1002/suco.201100032

34. MUTTONI A.; FERNÁNDEZ RUIZ M. *From experimental evidence to mechanical modeling and design expressions*: The Critical Shear Crack Theory for shear design. Structural Concrete. V. 20, p. 1464-1480, 2019. doi.org/10.1002/suco.201900193

35. SAGASETA J, MUTTONI A, FERNÁNDEZ RUIZ M, TASSINARI L. *Non-axis-symmetrical punching shear around of RC slabs without transverse reinforcement*. Mag Concr Res, V. 63(6), p. 441–57, 2011. doi.org/10.1680/macr.10.00098

36. SAGASETA J.; TASSINARI L.; FERNÁNDEZ RUIZ M.; MUTTONI A. *Punching of flat slabs supported on rectangular columns*. Engineering Structures, 2014. doi.org/10.1016/j.engstruct.2014.07.007

37. DRAKATOS I-S.; MUTTONI A.; BEYER K. *Internal slab-column connections under monotonic and cyclic imposed rotations*. Engineering Structures, V. 123, p. 501-516, 2016. doi.org/10.1016/j.engstruct.2016.05.038

38. DRAKATOS I-S.; MUTTONI A.; BEYER K. *Mechanical Model for Drift-Induced Punching of Slab- Column Connections without Transverse Reinforcement*, ACI Structural Journal, Farmington Hills, V. 115, n 2, p. 463-474, 2018.

39. ACI COMMITTEE 421. *Guide for Shear Reinforcement for Slabs (ACI 421.1R-20)*. American Concrete Institute, Farming Hills, Mich., 2020, p. 27.

4. INVESTIGATING PUNCHING SHEAR IN SLABS WITH UNBALANCED MOMENTS AND OPENINGS

4.1 INTRODUCTION

4.1.1 General

In flat slab buildings, openings are frequently integrated into the slab-column region to facilitate the passage of pipes serving various purposes. Nevertheless, such openings are typically situated in the proximity of the column, thereby impeding the use of transverse reinforcement in this region of high shear stress.

To address the reduction of resistance caused by the opening, in 1960 Moe [1] proposed a method to neglect the length of the control perimeter between radial lines drawn from the column centroid. Although this approach is still used in current codes, subsequent studies have shown it overestimates the reduction of the control perimeter for different openings and column geometries beyond those studied by Moe [2-7].

Recently, Santos et al. (2022) [7] proposed a new method to reduce the critical perimeter in slabs with openings by analysing a database consisting of 68 slabs with openings subjected to axis-symmetric loading and without shear reinforcement. The theoretical resistance based on the proposed control perimeter exhibited notable improvements compared to experimental results. However, while research on slabs with openings and axis-symmetric loading has made a significant contribution to the field [1-13], it does not reflect real-world scenarios where unbalanced moments are more prevalent.

Unbalanced moments in reinforced concrete flat slabs can arise due to various reasons, such as variations in the stiffness or strength of supporting columns or walls, asymmetric loading, irregular column layout and different span values [14-16]. Due to the limited experimental data available for large-scale flat slabs subjected to eccentric punching shear, it is

challenging to establish a reliable design expression. Design codes generally incorporate coefficients that increase shear stress to account for the effect of eccentric loading, resulting in reduced theoretical resistance.

Regarding the occurrence of openings in interior slab-column connections coupled with moment transfer, the literature presents only a limited number of studies. Hanson and Hanson [17] conducted the first experimental study in the late 1960s on slabs with holes positioned on the faces of the column and moment transfer. In 2014, Oliveira et al. [18] studied slabs with unbalanced moments and a single square opening with eccentricities of 250 mm and 500 mm. In 2021, Bursać et al. [19] investigated the presence of a square hole in slabs with square and rectangular columns with an eccentricity of 150 mm. Notwithstanding, there is a pressing need for more experimental investigations in this area to understand the behaviour of slab-column connections in the presence of openings and moment transfer.

The existing codes offer insufficient direction for a thorough analysis of slabs with openings. Additional guidance and orientation are required to ensure accurate calculations in accordance with the codes. As such, this study presents an overview of the design approaches, with a focus on clarifying the specifications of slab-column connections with openings, to facilitate a comprehensive understanding of the code's calculations. For the complete formulation of the codes, please refer to ANNEX A: CODE PROVISIONS.

4.1.2 ACI 318:19 provision for slab with openings

Slab-column connections under the influence of a factored shear force V_u and an unbalanced moment M_u are assumed to have a linear shear stress distribution along the critical perimeter [20]. The maximum shear stress v_u occurs at a vertex of the control perimeter, which can be determined using Eq. (4. 1).

$$v_u = \frac{V}{b_0 d} \pm \frac{\gamma_v M_u x}{J_c} \quad (4.1)$$

γ_v fraction of moment between slab and column that is considered transferred by eccentricity of shear, given by Eq. (4. 2).

$$\gamma_v = 1 - \frac{1}{1+\frac{2}{3}\sqrt{\frac{b_1}{b_2}}} \quad (4.2)$$

b_1 dimension of the critical section measured in the direction of the span for which moments are determined;

b_2 dimension of the critical section measured in the direction perpendicular to b_1;

J_c property analogous to polar moment of inertia;

M_u is the moment transferred to the connection;

x coordinate that results maximum shear stress.

According to ACI 421.1R-20:20 [21], equilibrium is satisfied by using the components M_u, x and γ_v about the centroidal principal axes of the assumed critical section. When the centroid of the shear critical section does not coincide with the centroid of the column, the moment M'_u must be transferred to the centroidal critical section axes. It is worth mention that, usually either from the structural analysis or from experimental test, V_u and M_u are obtained with respect to the centroidal column axes. Here it is considered the correct moment M'_u when V_u is transferred from the centroidal column axes to the centroidal critical section axes, as shown in Eq. (4. 3).

$$M_u = M'_u \pm V_u x_{cp} \quad (4.3)$$

x_{cp} is the control perimeter x-coordinate with respect to the centroid of the column; For usual slab-column edge connections, the maximum shear stress and the calculation of M_u are clear (in this type of connection the moment usually has the same orientation). Although, for inner connections with openings, the position of the critical section centroid depends on the opening's location, and the stresses along the control perimeter depends on

the moment transfer orientation. Therefore, the signal '±' of Eq. (4. 1) and Eq. (4. 3) must be analysed for each case.

Figure 4.1 illustrates examples of connections with openings in which the centroid of the control perimeter is not coincident with the centroid of the column. In Figure 4.1a, the opening is situated on the same side as the moment orientation, resulting in maximum stress occurring at vertexes A and B. This requires calculations using Eq. (4. 4)-(4. 6). In Figure 4.1b, the moment orientation is opposite to the opening location, and the maximum shear stresses are located at points D and C, leading to calculations according to Eq. (4. 7)-(4. 9).

$$v_{u,(a)} = \frac{V}{b_0 d} + \frac{\gamma_v M_{u(a)} x_{(a)}}{J_c} \quad (4.4)$$

$$v_{u,(a)} = \frac{V}{b_0 d} + \frac{\gamma_v M_{u(a)} x_{(a)}}{J_c} \quad (4.5)$$

$$M_{u(a)} = M_u' + V_u x_{cp} \quad (4.6)$$

$$x_{(a)} = b_1/2 + x_{cp}$$

$$v_{u,(b)} = \frac{V}{b_0 d} + \frac{\gamma_v M_{u(b)} x_{(b)}}{J_c} \quad (4.7)$$

$$M_{u(b)} = M_u' - V_u x_{cp} \quad (4.8)$$

$$x_{(b)} = b_1/2 - x_{cp} \quad (4.9)$$

According to ACI 318:2019, the J_c parameter is analogous to the polar moment of inertia. For interior connections without openings, the centroid of the column coincides with the centroid of the control perimeter, and J_c can be calculated directly using the equation provided in the code. However, for slabs with openings, J_c must be calculated with respect to the control perimeter axis, and the J_c equation given in ACI 318:2019 is not applicable. A detailed explanation of the J_c equations used for the slabs with openings in this study is provided in the 4.7APPENDIX A

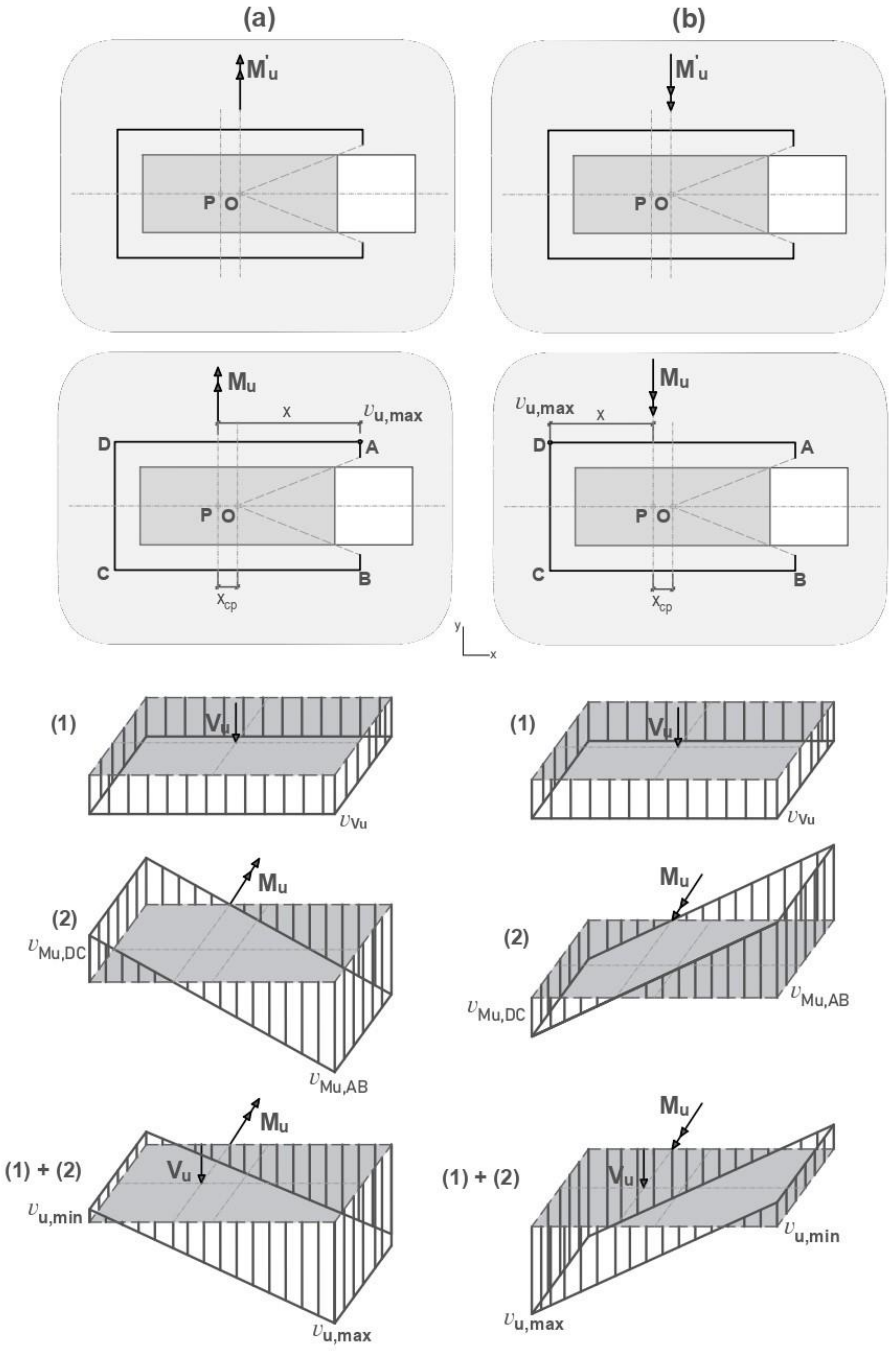

Figure 4.1 - Stress distribution of an interior column subjected to moment about y-axis according to ACI 318:2019 (a) moment orientation clockwise (b) moment orientation contraclockwise

4.1.3 fib MC 2010:13 levels of approximation for slab with openings

The design methodology adopted by *fib* MC 2010:13 [22] relies on the critical shear crack theory, a mechanical model proposed by Muttoni [23]. This model is backed by analytical principles, allowing for an accurate representation of the physical phenomena. Mechanical models offer the advantage of incorporating various factors such as geometry, reinforcement, and loading in a detailed and refined manner.

The level of approximation II provides a simplified estimation of the moment acting in the support strip (m_E). To investigate this approximation level, the moment in the support strip was assumed to be $m_E = V/8$, and the direction of maximum rotation was considered in the analysis [23,24]. This approach is referred to as *fib* MC 2010:13 LoA II-ψ_{max}.

The level of approximation III is used when a more precise determination of the acting bending moment can be made, such as a linear-elastic analysis [24]. However, in statically determinate slab-column connections where the load position is well-established, m_E can be calculated using equilibrium, making level III applicable [7]. This approach is referred to as *fib* MC 2010:13 LoA III- ψ_{max}.

In slabs with openings, there is often a significant discrepancy in resistance predictions between different directions due to the redistribution of internal forces [25-26]. As a result, considering the maximum rotation can lead to overly conservative results. To address this issue and improve the accuracy of the analysis, the phenomenon can be approximated by considering the geometric mean of rotations in both directions [7]. This approach is referred to as *fib* MC 2010:13 LoA III-$\psi_m = \sqrt{\psi_x \psi_y}$.

4.1.4 prEN 1992-1-1:23 provision for slab with openings

The 2nd generation of Eurocode 2 prEN 1992-1-1:21 is grounded on a physical basis and the guidelines for punching shear design are based on *fib* Model Code 2010. The coefficient k_{pb} has been newly introduced to account for the shift from one-way to two-way shear. It increases the unitary shear strength for smaller columns (where k_{pb} is close to 2.5) and decreases it for larger column sizes (where k_{pb} is close to 1.0) [27]. In earlier versions of the code, the coefficient was expressed using Eq. (4. 10) [28], whereas in the latest versions, it is presented as Eq. (4. 13) [29]. According to prEN 1992-1-1:21 [28], this change has been implemented to improve usability and applicability, without causing any technical issues, as the control perimeter $b_{0.5}$ is often equivalent to b_0 plus the length of rounded corners with a radius of $d_v/2$ (as per Eq. 4. 11). If this holds true, Eq. (4. 10) can be rephrased as Eq. (4. 13). However, it should be noted that the assumption made in Eq. (4. 11) may not be applicable to slabs with openings, as it depends on the location of the holes.

$$k_{pb(1)} = \sqrt{5\mu_p \frac{d_v}{b_{0,5}}} \tag{4. 10}$$

$$\mu_p \frac{\pi d_v}{8} = b_{0.5} - b_0 \tag{4. 11}$$

μ_p can be considered as 8 for design purposes of internal columns

$$k_{pb} = \sqrt{\left(\frac{5 \cdot 8}{\pi}\right) \frac{b_{0.5} - b_0}{b_{0,5}}} \tag{4. 12}$$

$$k_{pb} = k_{pb(2)} = 3.6 \sqrt{1 - \frac{b_0}{b_{0,5}}} \tag{4. 13}$$

4.2 EXPERIMENTAL PROGRAMME

This study presents the results of the second series of tests conducted in the doctorate of Souza [30]. The investigation examined nine full-scale slabs without shear reinforcement, with openings and unbalanced moment. The first series of tests, published by Santos *et al.* (2022) [12], focused on slabs with openings and axis-symmetric loading. The variables

examined in the present study include the position of the openings with respect to the rectangular column, the dimensions and number of openings, the value of eccentricity, and the orientation of the moment transfer. The results analysed include ultimate loads, slab displacements, flexural reinforcement strains, and concrete strains.

4.2.1 Specimens and materials

The experimental program consists of nine square slabs without shear reinforcement, measuring 2.400 mm in sides and 150 mm in height, with rectangular columns measuring 200 mm by 500 mm. The slabs had openings on the column faces with square dimensions of 200 mm and rectangular dimensions of 200 mm x 300 mm. The tests varied the number and location of openings, the orientations of moment transfer, as well as eccentricities Of 250 mm and 500 mm.

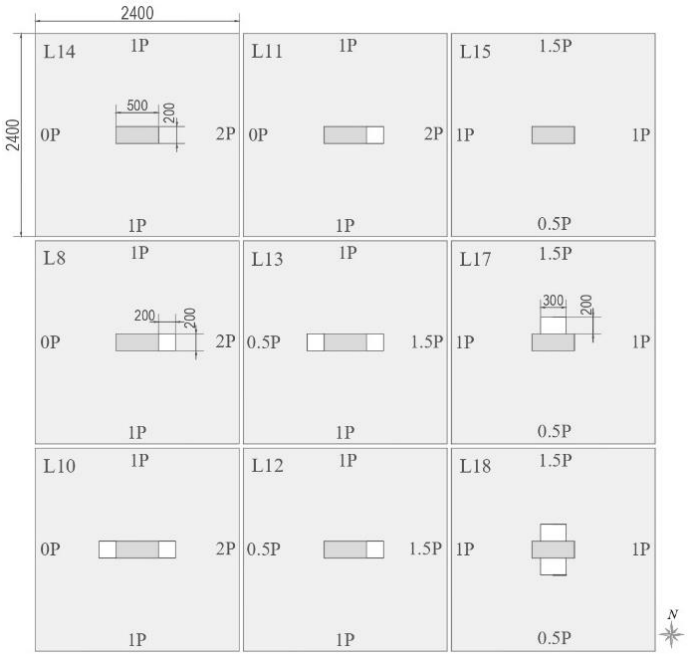

Figure 4.2 - Slabs characteristics: dimensions and loading configuration

Slab L14 was the reference slab without openings with moment about the y-axis (e_x = 500 mm). Slabs L8 and L10 had openings and moment transfer about the y-axis (e_x = 500 mm), while slabs L12 and L13 had a lower eccentricity in the same direction (e_x = 250 mm). L11

was also subjected to e_x = 500 mm, although the moment was applied in the opposite orientation with respect to slabs L14, L8 and L10 (see Figure 4.2). Slab L15 was the reference slab without openings with moment transfer about the x-axis (e_y = 250 mm), while slabs L17 and L18 had openings with the same value of eccentricity. Table 4.1 summarizes the characteristics of the slabs, and Figure 4.2 illustrates slabs and openings geometries, as well the distribution of loading applied on the slabs to transfer unbalanced moments. The eccentricity e_x is equivalent to a moment about the y-axis, as it occurs in slabs L14, L8, L10, L11, L12 and L13, while e_y means a moment about the x-axis, as it occurs in L15, L17 and L18 (see Figure 4.2 and Table 4.1).

To characterize the concrete, tensile strength was measured by diametrical compression, while the secant elasticity module and compressive strength were also determined. Uniaxial tension tests were conducted on the steel to ascertain its mechanical properties. The properties of the concrete and steel materials are shown in Table 4.2.

All slabs had a top flexural rebar diameter of 12.5 mm and a bottom rebar diameter of 6.3 mm. The chosen reinforcement ratios (0.91% and 1.48%) fell within the typical range of reinforcement ratios used in design projects. The effective depth of the slabs remained around 123 mm, with minimal changes related to execution.

Table 4.1 - Characteristics of tested slabs

Slab	**f_c (MPa)**	**Openings (mm)**	**$e_{predicted}$ (mm)**	**d (mm)**	**ρ (%)**	**ρ_x (%)**	**ρ_y (%)**
L14	42,4	-	e_x = 500	121	0,93	0,83	1,05
L8	34,2	1 200x200	e_x = 500	123	1,48	1,62	1,36
L10	34,2	2 200x200	e_x = 500	123	1,48	1,62	1,36
L11	36,7	1 200x200	e_x = -500	125	1,44	1,57	1,32
L12	37,8	1 200x200	e_x = 250	123	1,48	1,62	1,36
L13	36,4	2 200x200	e_x = 250	124	1,46	1,60	1,34
L15	43,2	-	e_y = 250	123	0,91	0,81	1,02
L17	35,8	1 300x200	e_y = 250	125	1,01	0,89	1,16
L18	37,3	2 300x200	e_y = 250	126	1,05	0,97	1,14

Table 4.2 - Properties of concrete and flexural reinforcement rebars

Slab	Concrete	Steel				
	f_c (MPa)	$Ø_s$ (mm)	f_{ys} (MPa)	f_u (MPa)	ε_s ‰	E_s (GPa)
L8	34,2	12,5	595	739	2,7	200
L10	34,2					
L11	36,7					
L12	37,8					
L13	36,4	12,5	623	770	2,4	205
L14	42,4					
L15	43,2	12,5	583	710	2,4	236
L17	35,8					
L18	37,3					

(a)

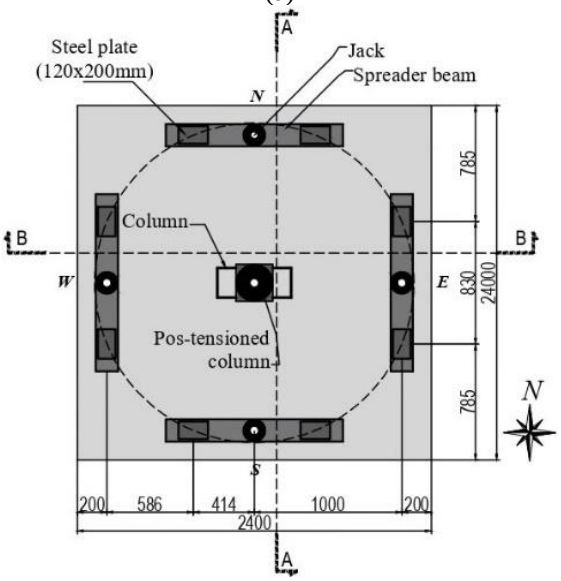

(b) (c)

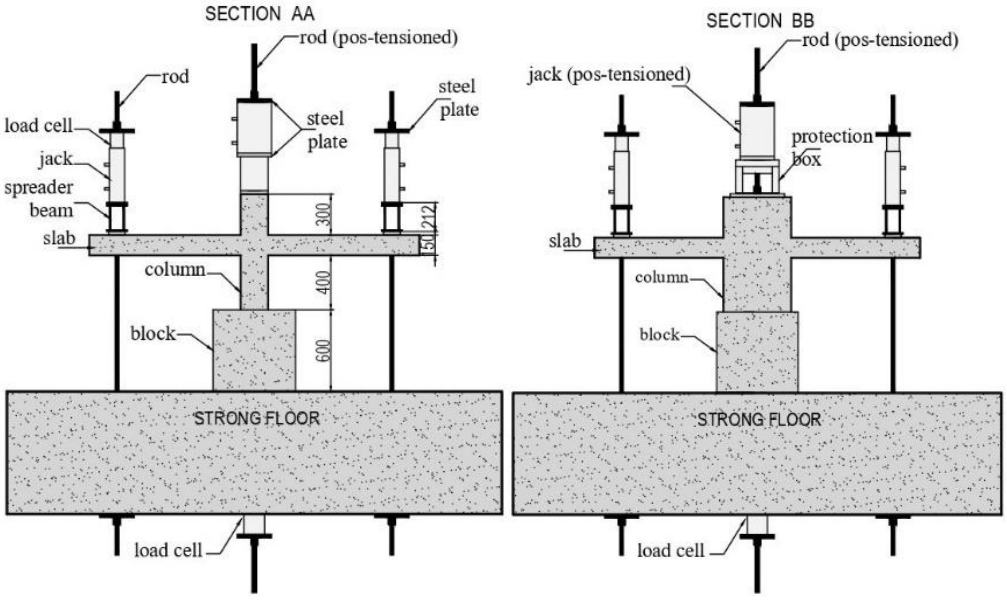

Figure 4.3 - Tests setup (a) Plain view (b) Section A-A (c) Section B-B

4.2.2 Test setup and instrumentation

The loads on the slabs were applied through four hydraulic actuators located on steel beams, which distributed the loads on eight points across the slabs (as depicted in Figure 4.3). The unbalanced moment was achieved by applying unsymmetrical loading, with the load distribution selected based on the desired eccentricity (as shown in Figure 4.2). In order to enhance the system's ability to resist unbalanced moments, the column was monolithically connected to the slab and pre-stressed to the strong floor by a jack located at the top of the column, as depicted in Figure 4.3.

The monitoring of vertical displacements was performed by means of up to twelve mechanical dial gauges placed at the top of each slab. The flexural rebars were instrumented and each location was equipped with a pair of diametrically opposed strain gauges. Concrete strain gauges were positioned on the bottom face of the slab. Figure 4.4 illustrates the instrumentation.

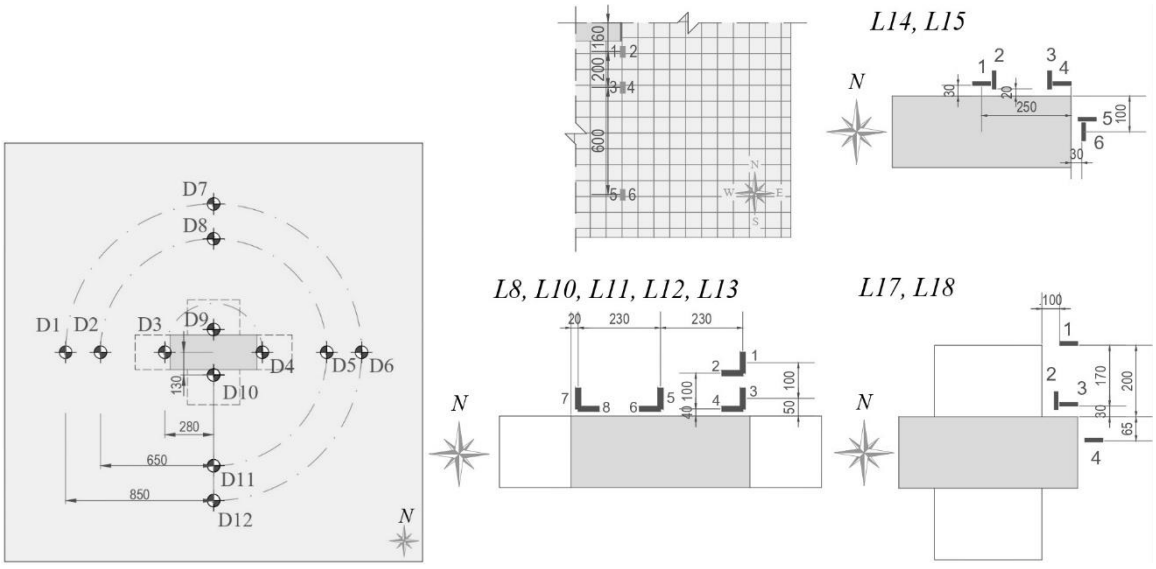

Figure 4.4 - Instrumentation: displacement measurement locations, flexural reinforcement strain gauges and concrete bottom surface strain gauges

4.3 EXPERIMENTAL RESULTS AND DISCUSSION

4.3.1 Punching shear resistance

The ultimate load of the slabs was determined by adding the maximum recorded load, the weight of the slab, and the equipment's weight. The equilibrium of the ultimate load was used to estimate the moment at failure. Table 4.3 provides information about the ultimate load (V_u), the ultimate moment at failure (M'_u), and the corresponding eccentricity at failure (e'_u) of the tested slabs. These two parameters were determined with respect to the column centroidal axis.

To reduce the effect of variations in concrete strength and effective depth, the results of ultimate capacity shown in Figure 4.5 were normalized. As recommended by [5], the normalization was done by dividing it to effective depth and the square root of the compressive strength of the concrete. Since the control perimeters varied based on the geometries and quantities of the openings, it was not considered in the normalization process.

Table 4.3 - Ultimate loads and moments (M'_u is the moment at ultimate load with respect to the column axis, e'_u is the eccentricity of ultimate load with respect to the column axis)

Slab	f_c (MPa)	Openings (mm)	d (mm)	ρ (%)	V_u (kN)	M'_u (kN.m)	e'_u (mm)
L14	42,4	-	121	0,93	274	125,9	459,5
L8	34,2	1 200x200	123	1,48	192	86,3	449,5
L10	34,2	2 200x200	123	1,48	189	83,0	439,2
L11	36,7	1 200x200	125	1,44	299	139,1	465,2
L12	37,8	1 200x200	123	1,48	319	74,4	233,2
L13	36,4	2 200x200	124	1,46	277	61,9	223,5
L15	43,2	-	123	0,91	364	66,5	182,7
L17	35,8	1 300x200	125	1,01	279	59,3	212,5
L18	37,3	2 300x200	126	1,05	322	53,1	164,9

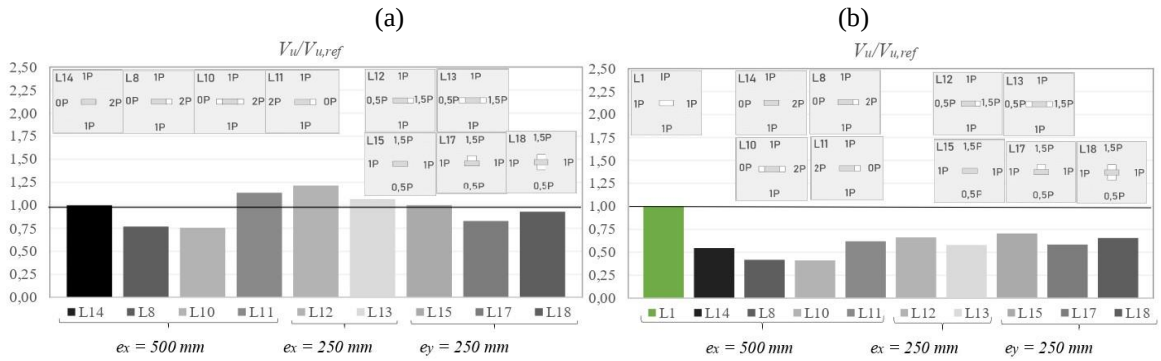

Figure 4.5 - Comparison of ultimate strength of slabs with openings to reference slab: (a) the reference capacity are the slab without openings with unbalanced moments (L14 and L15) and (b) the reference capacity is the slab without openings with concentric loading (L1 from [12])

Figure 4.5a shows the ratio of ultimate strength of the slabs with openings to the ultimate strength of the reference slab with moment and without opening. L14 is the reference slab for L8, L10, L11, L12 and L13, and L15 is the reference slab for L17 and L18.

From Figure 4.5a, is evident that the moment has a greater impact on resistance than the number of openings. While L8 had only one opening, L10 with two openings achieved nearly the same capacity for the same eccentricity (e_x = 500 mm). However, at a lower eccentricity (e_x = 250 mm), L13 with two openings showed a resistance that was 20% lower than L12, which had only one opening.

Slab L11 had an opposite unbalanced moment orientation and presented a resistance 50% higher than L8. This behaviour was also observed in other studies, both experimental [18-19] and numerical [31-34]. On the other hand, L17 had a 17% strength decrease compared to the reference slab L15, while L18 showed a 7% decrease. Despite having two openings, L18 presented a higher capacity due to its lower eccentricity at failure.

Figure 4.5b displays the ratio of the ultimate strength of all the slabs to the ultimate strength of slab L1 from Santos *et al.* (2022) [12], which represents slabs without openings and with concentric loading. The figure shows that the moment significantly decreased the capacity of slabs without openings (L14 and L15). Additionally, the presence of openings had a greater impact on slabs with higher eccentricities (L8 and L10). Overall, the resistance

decreased by approximately 60% due to unbalanced moments and the presence of openings when compared to the slab without openings and with concentric loading.

4.3.2 Flexural reinforcement strains

Figure 4.6 displays the load on the y-axis and the ratio of measured strain to the yield strain on the x-axis. Slabs L14 and L15, which had no openings, exhibited flexural strains that reached yielding, whereas slabs with openings displayed significantly lower levels of deformation. In slabs L17 and L18, the analysed rebar was not cut due to the location of the openings, and the strains reached 40% of the yield strain. However, in the remaining slabs with openings, the analysed rebar was cut due to the location of the openings, preventing the full activation of the rebar. Several studies have reported low levels of strains in rebars that were cut due to the presence of openings [3-5,10,12].

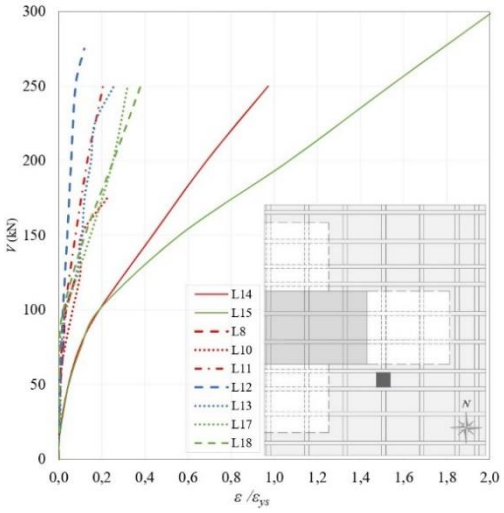

Figure 4.6 - Flexural reinforcement strain comparison of all slabs

4.3.3 Load-deflection relationship

Figure 4.7-Figure 4.9 show the vertical displacement with respect to the dial gauges locations, west-east (x-axis) and north-south (y-axis) directions. In these figures, negative values indicate a downward displacement of the slab, whereas positive values indicate an upward displacement.

The asymmetric displacement profiles of Figure 4.7-Figure 4.9 unequivocally indicates the influence of unbalanced moments, while symmetrical displacement patterns are evident in the direction of symmetric loading. The displacement results in the west-east direction reveal the effect of the opposite orientation of the applied moment in slab L11 in comparison to the other slabs subjected to moments in the other orientation (L14, L8, L10, L12 and L13).

Of particular interest, the slabs L17 and L18 registered the highest values of displacement. These slabs were subjected to unbalanced moments about the weaker x-axis, resulting in greater displacements compared to the moments applied about the stronger y-axis. A clear comparison between the results of slabs L17 and L18, with slabs L12 and L13, which had the same eccentricity but moments about the strongest y-axis, further supports this observation.

For a more comprehensive understanding of the numerous results presented, Figure 4.10 is provided to compare the load-displacement behaviour of the slabs. To ensure a valid analysis, the comparison was performed among slabs with the same reinforcement ratios. Figure 4.10b presents the load-displacement results of L14 and L15, while Figure 4.10c examines L8, L10, L11, L12, and L13. Additionally, Figure 4.10d analyses the displacement results of L17 and L18. In these figures, a negative signal on the x-axis indicates that the displacement occurred on the west or north side, while a positive signal indicates that it occurred on the east or south side. The results of the outermost dial gauges with respect to the column (D1, D6, D7, and D12, see Figure 4.4) were chosen to be presented in Figure 4.10.

Figure 4.10b shows how moment orientation affects slab displacement. Despite having half the eccentricity of slab L14, slab L15 showed similar displacement values in different directions. The reason is because the moment in slab L15 was applied about the weaker x-

axis, while in slab L14 it was applied about the stronger y-axis. It is worth noting that the stiffness of the slabs was significantly influenced by the moment transfer direction.

Figure 4.10c depicts the influence of eccentricity in the x-axis on the load-displacement behaviour of the slabs. The slabs L8, L10, L12, and L13, were subjected to a moment oriented from west to east, resulting in higher displacement on the east side, particularly for slabs with greater eccentricity and lower stiffness (L8 and L10). However, slab L11 was subjected to a moment oriented from east to west, leading to significant displacements on the west side. In the north-south direction, despite the symmetrical load distribution in this direction, the effect of higher eccentricity was still discernible. Slabs L12 and L13 demonstrated a slightly lower level of displacement compared to the slabs with greater eccentricity.

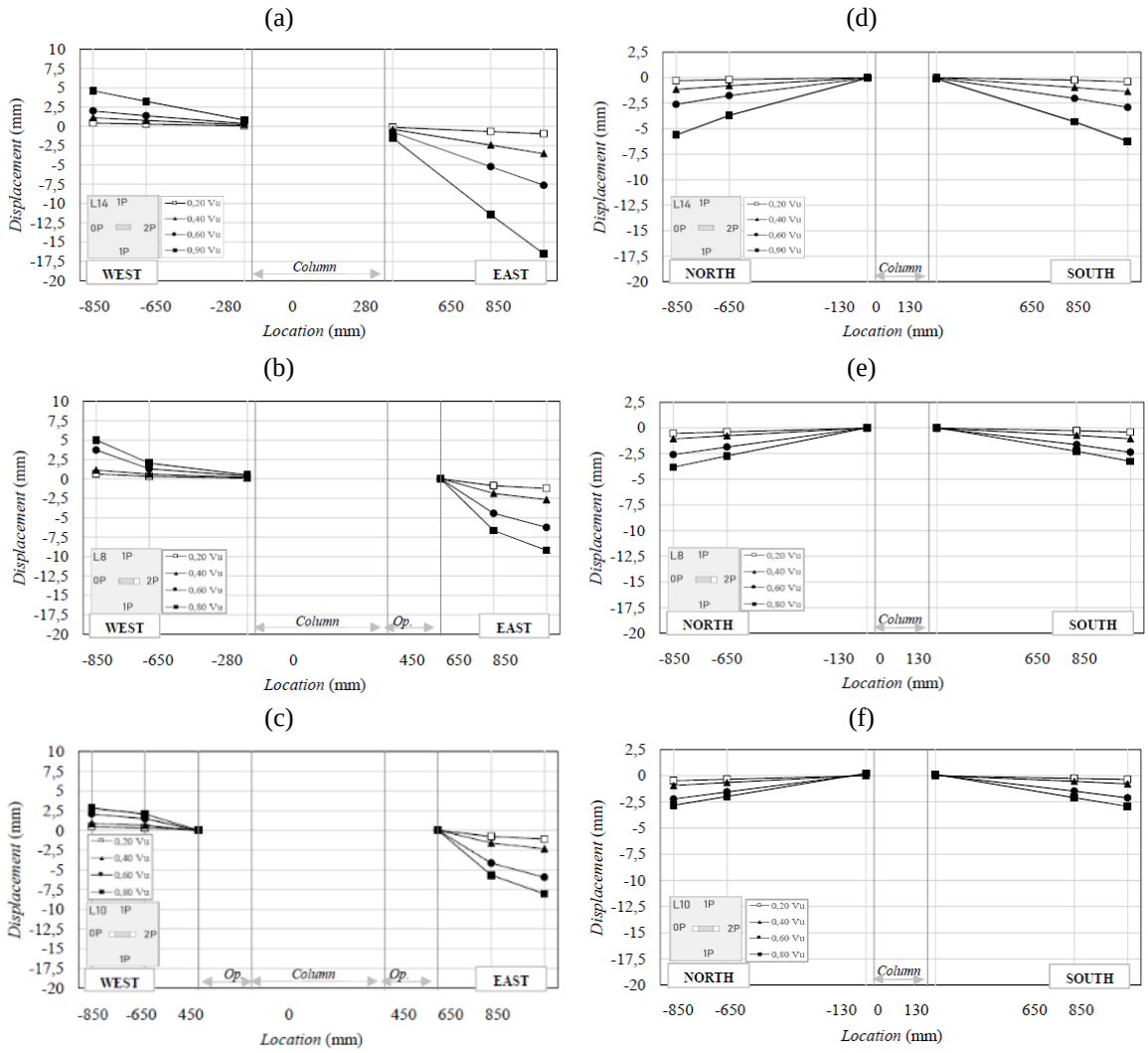

Figure 4.7 - Displacement-location of slabs in both directions, west-east direction: (a) L14 (b) L8 (c) L10, north-south direction: (e) L14 (f) L8 (g) L10

Figure 4.10d demonstrates the impact of the number of openings on slabs subjected to eccentricity in the y-axis. Notably, the results in the direction of moment transfer (north-south) were highly similar, even though slab L18 had two openings while slab L17 had one. In the west-east direction, the same observation can be made.

Examining Figure 4.10c, it becomes apparent that the additional opening on the west side of slabs L10 and L13 did not significantly impact the displacement in comparison to slabs with openings on the east side, L8 and L12. This implies that the effect of the unbalanced moment is more pronounced than that of the openings.

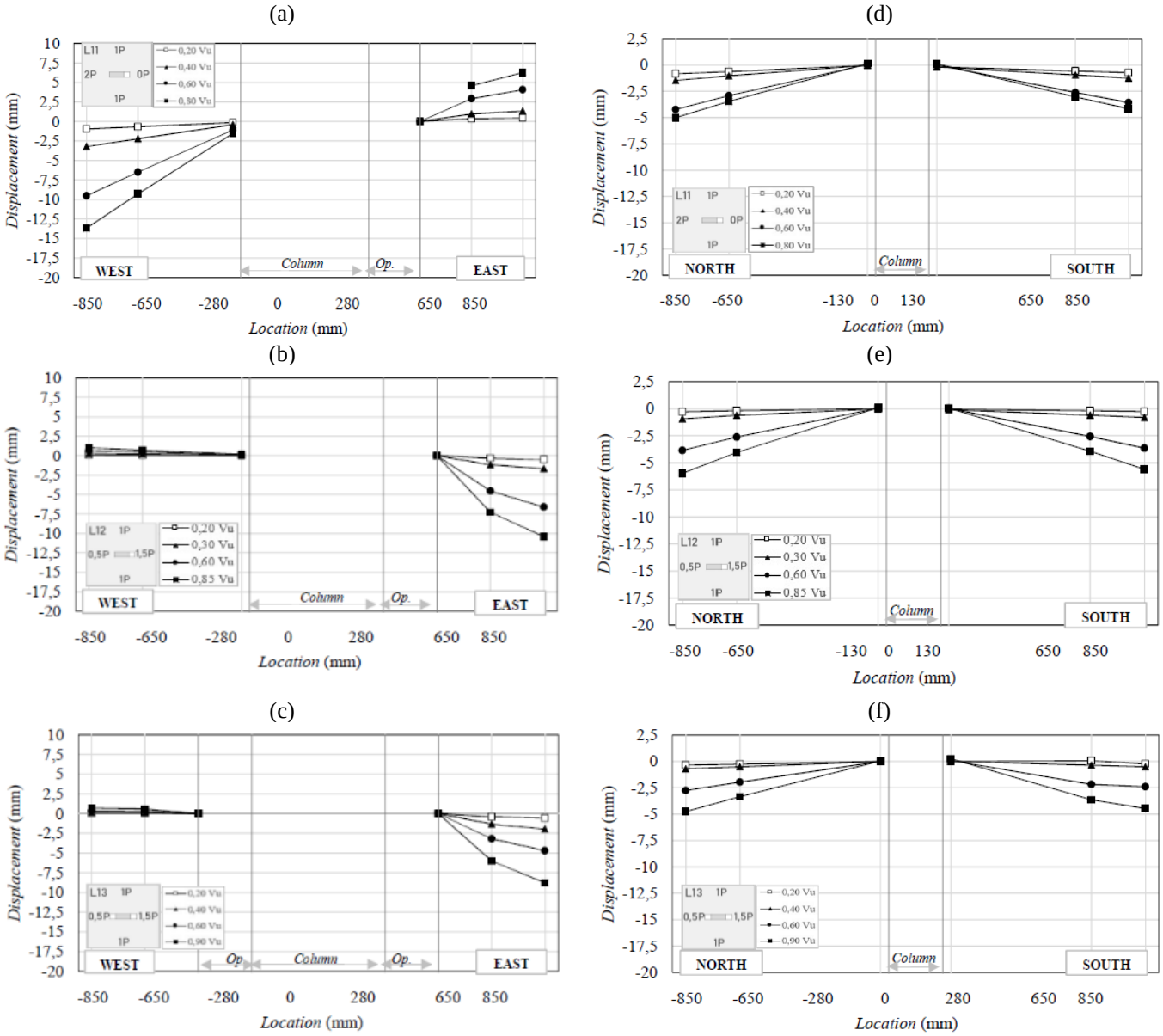

Figure 4.8 - Displacement-location of slabs in both directions, west-east direction: (a) L11 (b) L12 (c) L13, north-south direction: (e) L11 (f) L12 (g) L13

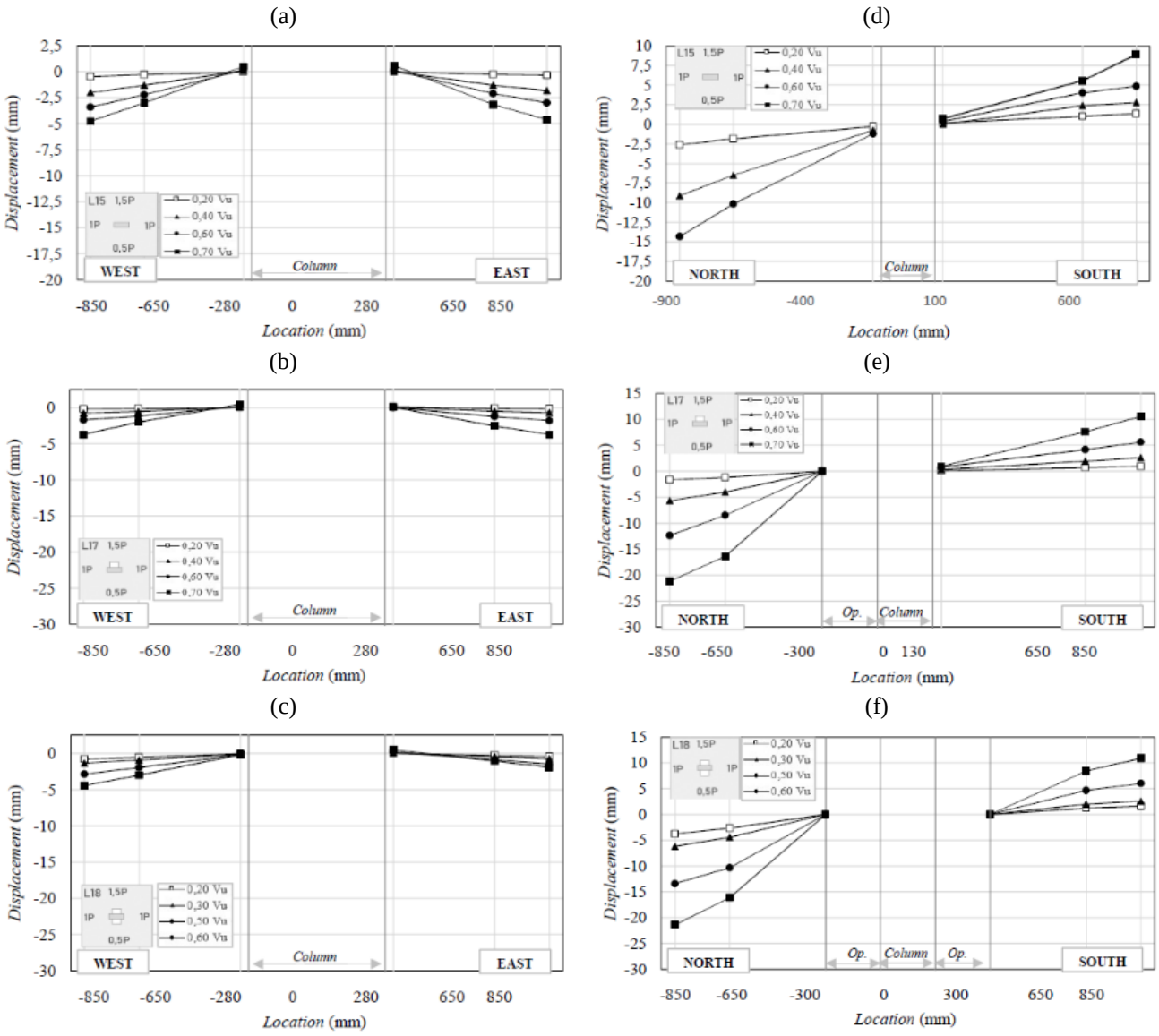

Figure 4.9 - Displacement-location of slabs in both directions, west-east direction: (a) L15 (b) L17 (c) L18, north-south direction: (e) L15 (f) L17 (g) L18

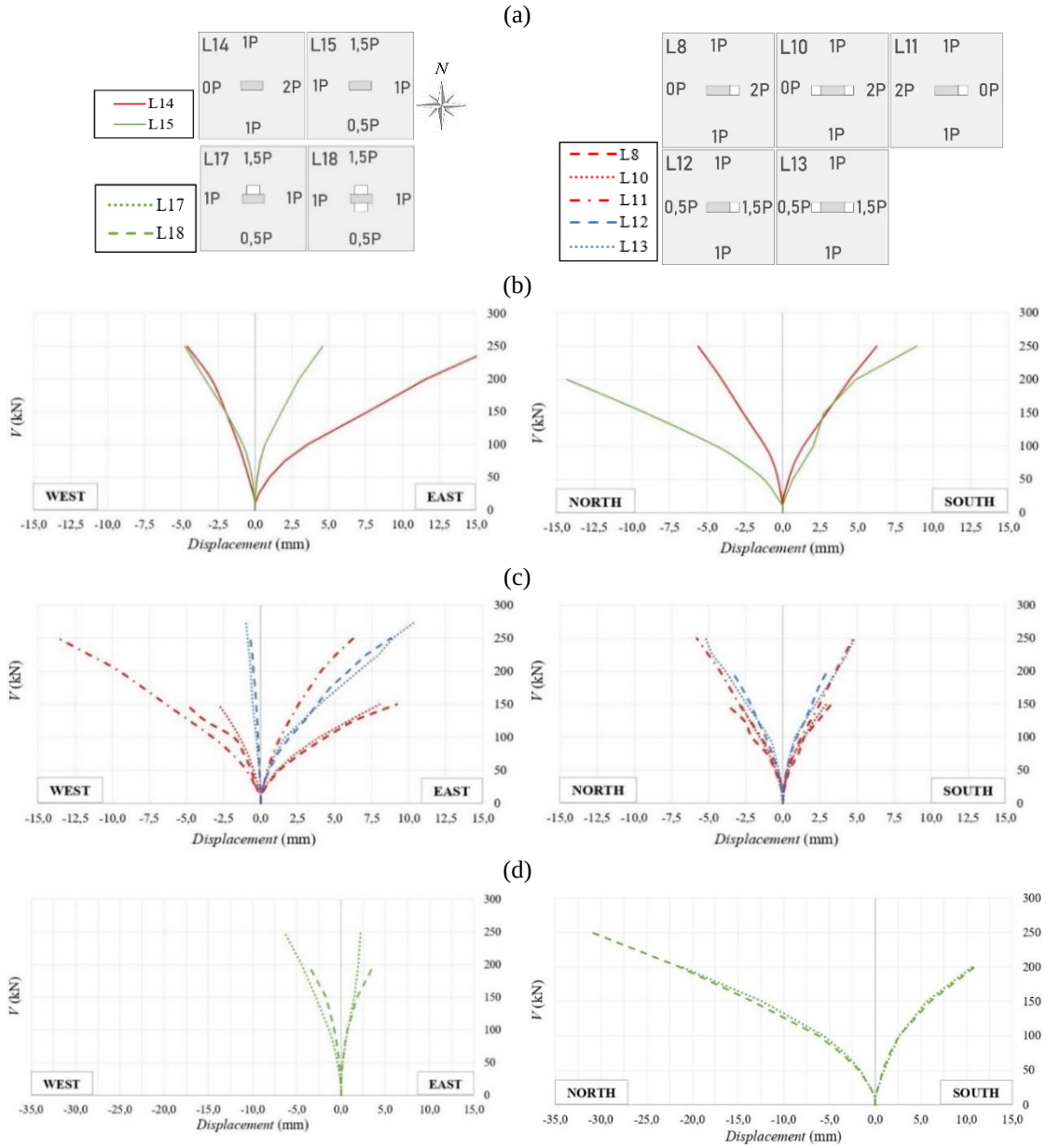

Figure 4.10 - Load-displacement in the west-east and north-south direction (a) Legend (b) Slabs without openings (14 and L15) (c) Slabs with openings and moment transfer in the west-east direction (L8, L10, L11, L12 and L13) (d) Slabs with openings and moment transfer in the north-south direction (L17 and L18)

4.3.4 Concrete strains

Figure 4.11-Figure 4.13 compare the concrete strain at bottom surface among different slabs. Figure 4.11 presents the concrete strain comparison to demonstrate the effect of unbalanced moment compared to the reference slab with moment L14 and the reference slab with axis-symmetric loading L1 from [12]. The effect of moment orientation can be observed in Figure

4.11c, where tensile concrete strain was observed in slab L11, and in Figure 4.11g, where greater compressive strain was recorded on the west side. Interestingly, L8 showed opposite results: compressive strains on the east side, as Figure 4.11c, and tensile tangential strains on the west side, Figure 4.11g. Additionally, Figure 4.11b shows that higher concrete strain occurred close to the opening of slab L8 compared to the slab without an opening, L14, which was higher than the strains recorded in the slab without a moment, L1. In the region of the column axis, the tangential strains were approximately the same for all slabs, Figure 4.11e, while the radial strains of slabs with moments were higher than those of the slab with symmetric loading (Figure 4.11d).

Figure 4.12 compares the effect of unbalanced moments on slabs with openings by analysing the concrete strains of different slabs. The slabs under consideration are L15, L17, and L18, which have different numbers of openings and are subjected to moments about the x-axis. The corresponding slabs with axis-symmetric loading, namely L1, L16, and L19 (from Santos *et al.* (2022) [12]), are also analysed. The concrete strains close to the opening on the north side were highest for L17 and L18, followed by L16 and L19, L15, and finally L1, which showed the lowest level of strain (Figure 4.12b). The tangential concrete strain on the east side was highest for L15 and lowest for the other slabs (Figure 4.12c). The strain in the east side of the column also followed a similar trend (Figure 4.12d). Near the opening corner, slabs with moment exhibited slightly higher strains (Figure 4.12e).

Figure 4.13 compares the concrete strains of slabs with openings subjected to different eccentricities in the x direction, and also with their corresponding slabs without moments and with openings from [12]. Figure 4.13b shows that the slab with moment and without openings, L14, exhibited, for the same load level, higher radial strains on the northeast column corner. Figure 4.13c shows how the tangential concrete strain gradually increases in the region of the opening as the eccentricity grows from slab L1 to L13, and, finally, to L10.

From slab L1 to L9, an increase in concrete strain provoked by the opening in slabs with concentric loading can be observed. The effect of the opening can be noted from slab L1 to L7, and the effect of unbalanced moments in slabs with openings can be observed from L7 to L8.

The concrete strains in the region of the column axis were lower for slab L1 and higher for the other slabs, as shown in Figure 4.13d. The tangential strains in the middle of the column were similar for all slabs, but L8, L7, and L1 presented higher strains, as depicted in Figure 4.13e. In the northwest column corner (Figure 4.13f), the concrete strain increased as the eccentricity increased, but the deformation was lower due to the orientation of the moment. Figure 4.13g displays tension tangential strains in the northwest corner for slabs L8 and L10 subjected to moments.

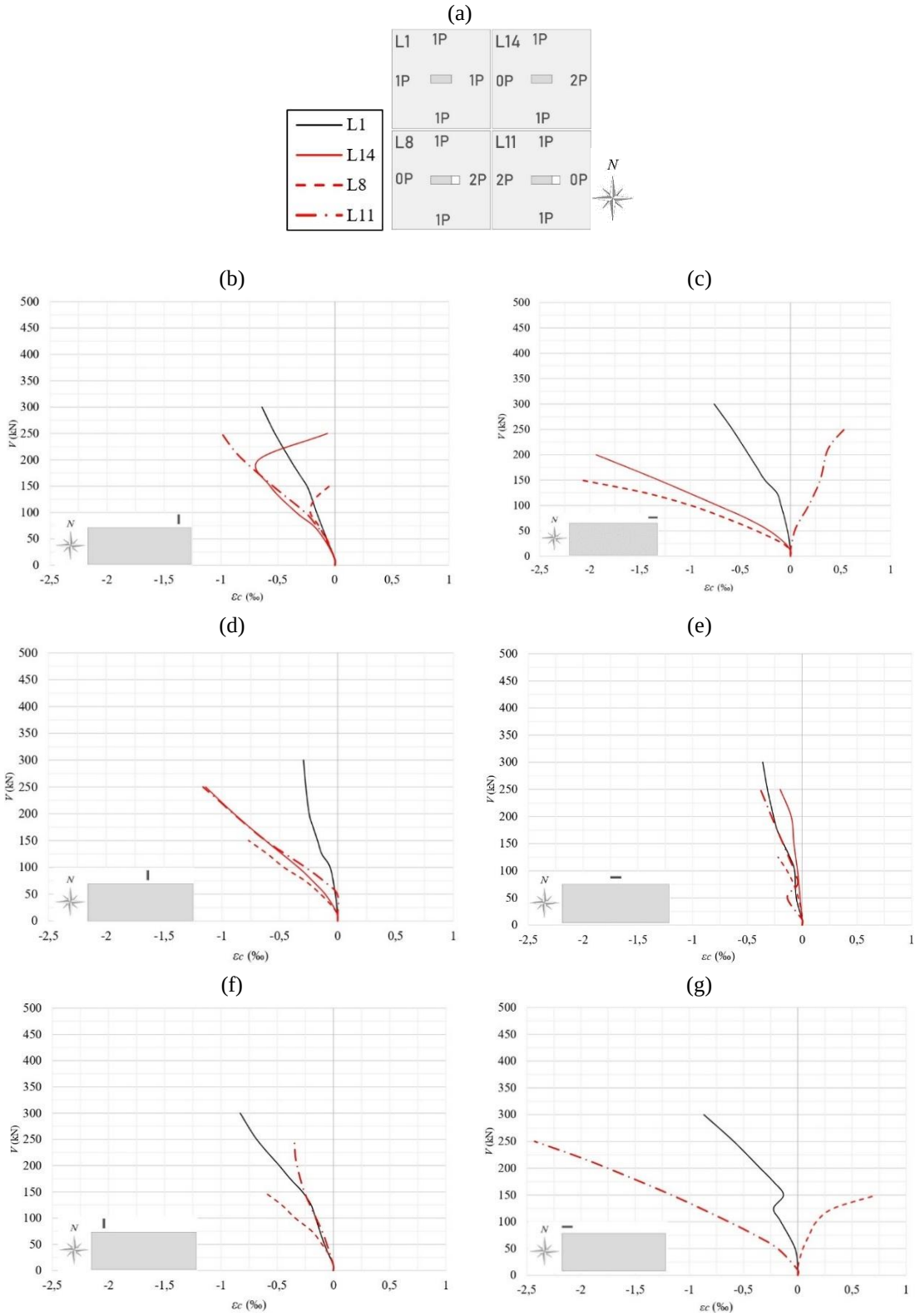

Figure 4.11 - Concrete strain comparison between slabs L1, L8, L11, L14 (a) legend (b) radial-northeast column corner (c) tangential-the northeast column corner (d) radial-column axis (e) tangential-column axis (f) radial-west column corner (g) tangential-west column corner

(a)

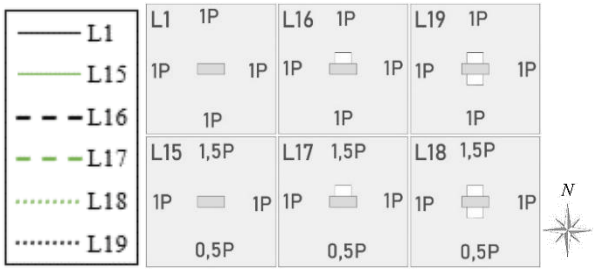

(b)

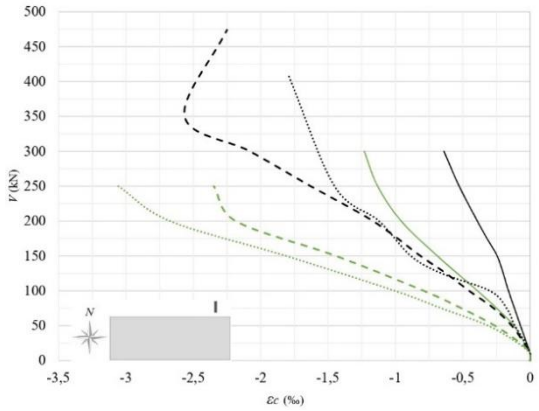

(c)

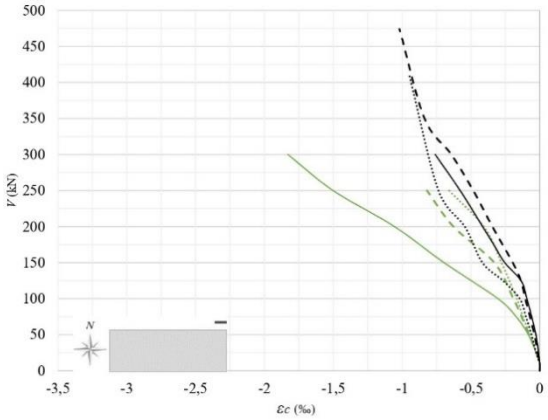

(d)

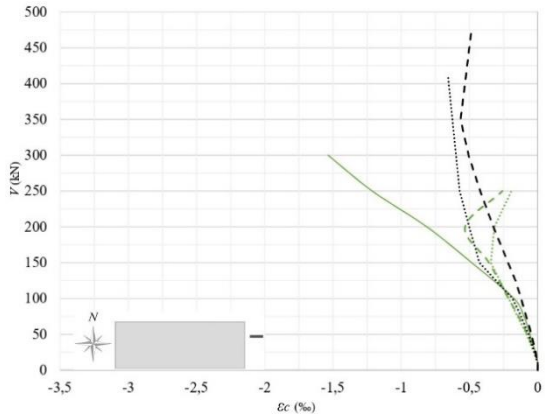

(e)

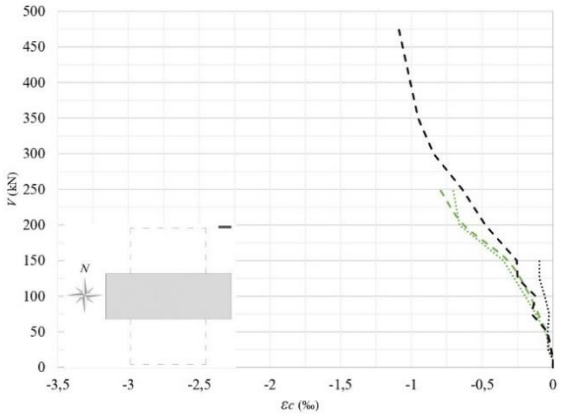

Figure 4.12 - Concrete strain comparison between slabs L1, L15, L16, L17, L18, L19 (a) legend (b) radial-northeast column corner (c) tangential-northeast column corner (d) radial-east column corner (e) tangential-northeast opening corner

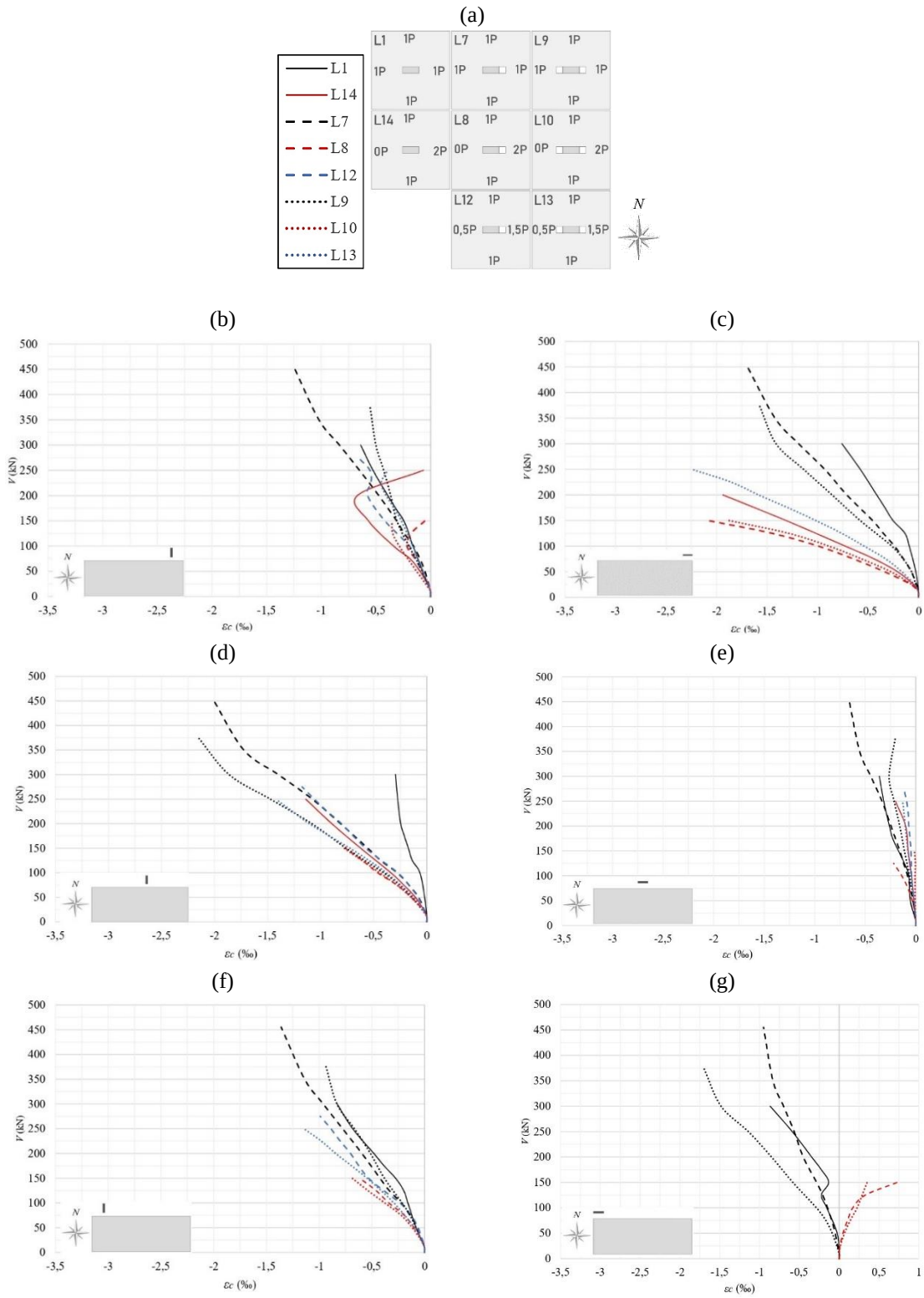

Figure 4.13 - Concrete strain comparison between slabs with moment transfer and slabs with axis-symmetric loading (a) legend and slabs characteristics (b) radial-northeast column corner (c) tangential-northeast column corner (d) radial-north column axis (e) tangential-north column axis (f) radial-northwest column corner (f) tangential-northwest column corner

4.4 COMPARISON OF THEORETICAL PREDICTIONS AND EXPERIMENTAL RESULTS

The formulae to calculate the punching resistance with moment transfer according to the investigated codes are summarized in the ANNEX A: CODE PROVISIONS.

Table 4.5 displays the findings derived from the theoretical analyses, wherein (a) signifies the current reduction of the control perimeter based on radial projections, and (b) corresponds to the recommended control perimeter proposed by [7]. The investigation involved analysing various approaches, and the corresponding notation used in Table 4.5 is as follows: (1) ACI 318:19 [25], (2) *fib* MC 2010:13 LoA II-ψ_{max} [26], (3) *fib* MC 2010:13 LoA III-ψ_{max}, (4) *fib* MC 2010:13 LoA III-$\psi_m = \sqrt{\psi_x \psi_y}$, (5) prEN 1992-1-1:21 $k_{pb(1)}$ [28] and (6) prEN 1992-1-1:21 $k_{pb(2)}$ [29].

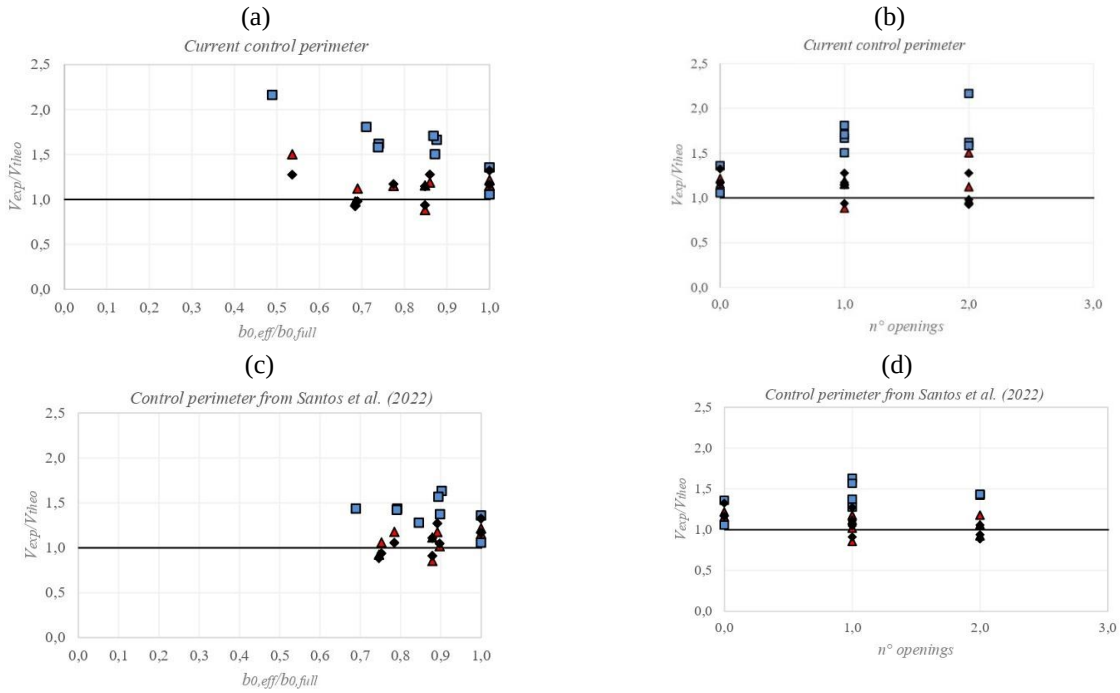

Figure 4.14 - Experimental-to-theoretical resistance considering the current control perimeter and (a) $b_{0,eff}/b_{0,full}$ (b) number of openings, considering the control perimeter from [7] and (c) $b_{0,eff}/b_{0,full}$ (d) number of openings

Figure 4.14 illustrates the experimental to theoretical resistance ratio as a function of two variables: the ratio of the effective control perimeter $b_{0,eff}$ of the slab with openings to the control perimeter of the slab without openings $b_{0,full}$, and the number of openings, according to the current control perimeter (a) and according to the control perimeter presented by [7] (b). Figure 4.14 shows only the results of ACI 318:19, *fib* MC 2010:13 LoA III-$\psi_m = \sqrt{\psi_x \psi_y}$ and prEN 1992-1-1:21 $k_{pb(1)}$. The summary of results from Figure 4.14 is shown in Table 4.4.

Table 4.4 - Summary of experimental-to-theoretical results of the codes shown in Figure 4.14

Code		Current		Santos *et al.* (2022) [7]	
		Av.	**CoV**	**Av.**	**CoV**
■	ACI 318:19	1,61	0,19	1,39	0,12
▲	*fib* MC 2010:13 $\psi_m = \sqrt{\psi_x \psi_y}$	1,15	0,15	1,08	0,12
◆	prEN 1992-1-1:21 $k_{pb(1)}$	1,13	0,13	1,08	0,14

Table 4.5 - Summary of experimental-to-theoretical provisions of codes according to the current control perimeter and the control perimeter proposed by Santos et al. (2022) [7]

	V_{exp}/V_{theo}											
Slab	**(1)**		**(2)**		**(3)**		**(4)**		**(5)**		**(6)**	
	(a)	**(b)**	**(a)**	**(b)**	**(a)**	**(b)**	**(a)**	**(b)**	**(a)**	**(b)**	**(a)**	**(b)**
L14	1,36	1,36	1,68	1,67	1,19	1,19	1,14	1,14	1,32	1,32	1,31	1,31
L8	1,51	1,37	1,08	1,04	0,88	0,85	0,85	0,82	0,95	0,92	1,00	0,91
L10	1,62	1,43	1,14	1,08	0,97	0,91	0,92	0,86	0,97	0,93	1,11	0,92
L11	1,67	1,63	1,47	1,45	1,22	1,20	1,15	1,13	1,29	1,28	1,36	1,27
L12	1,71	1,57	1,33	1,27	1,19	1,15	1,11	1,07	1,16	1,12	1,22	1,11
L13	1,58	1,42	1,32	1,22	1,11	1,05	1,05	0,98	1,03	0,98	1,17	0,98
L15	1,06	1,06	1,56	1,56	1,42	1,42	1,20	1,20	1,17	1,17	1,16	1,16
L17	1,81	1,28	1,55	1,37	1,34	1,17	1,13	1,00	1,17	1,05	2,41	1,26
L18	2,16	1,43	1,82	1,45	1,62	1,26	1,41	1,09	1,33	1,10	3,29	1,09
Av.	*1,61*	*1,39*	*1,44*	*1,35*	*1,22*	*1,13*	*1,11*	*1,03*	*1,15*	*1,10*	*1,56*	*1,11*
CoV.	*0,19*	*0,12*	*0,17*	*0,16*	*0,18*	*0,15*	*0,15*	*0,12*	*0,13*	*0,13*	*0,50*	*0,14*

Notes:

(1) ACI 318:19
(2) *fib* MC 2010:13 LoAII
(3) *fib* MC 2010:13 LoAIII
(4) *fib* MC 2010:13 $\psi_m = \sqrt{\psi_x \psi_y}$
(5) pr EN 1992-1-4:2021 $k_{pb(1)}$
(6) pr EN 1992-1-4:2021 $k_{pb(2)}$

(a) Current control perimeter
(b) Control perimeter from Santos *et al.* (2022) [7]

Table 4.5 demonstrates that the use of refined approaches led to a significant improvement in *fib* MC 2010:13 strength predictions. The approach of the geometric mean of the rotations [7], LoA III-$\psi_m = \sqrt{\psi_x \psi_y}$, provides a notable improvement of coefficient of variation and average of V_{exp}/V_{theo} compared to the approach LoA III-ψ_{max}, and even better if compared to LoA II-ψ_{max}. The prediction of the resistance can be very different in each direction, and the estimation of resistance along the direction with maximum rotation provides an overly conservative result. Taking into consideration the very different situations that can lead to non-axis-symmetrical punching in slabs with openings, the results are excellent from a practical perspective.

Table 4.5 presents the findings that refined approaches have significantly improved the accuracy of predicting the strength of *fib* MC 2010:13. Among the approaches, LoA III-$\psi_m = \sqrt{\psi_x \psi_y}$, (the geometric mean of the rotations proposed by [7]) had the best coefficient of variation and average of V_{exp}/V_{theo}, outperforming both LoA III-ψ_{max} and LoA II-ψ_{max}. This is particularly useful for slabs with openings and eccentric loading, where the resistance can vary considerably in each direction, and relying solely on the direction with the maximum rotation can lead to overly conservative estimates. Overall, these results are promising and have practical implications for designing non-axis-symmetrical punching in slabs with openings.

Furthermore, mechanical models, unlike empirical expressions calibrated on available test data such as ACI 318:19 provisions, strive to accurately represent the physical phenomena. This is evident in Figure 4.14, where it can be observed less scatter results obtained from *fib* MC 2010:13 LoA III-$\psi_m = \sqrt{\psi_x \psi_y}$ and prEN 1992-1-1:21 in comparison to the results obtained from ACI 318:19.

With respect to prEN 1992-1-1:21, the precision of the results obtained for slabs with openings is contingent on the k_{pb} equation selected. Figure 4.15 displays the experimental to

theoretical resistance ratio as a function of $b_0/b_{0.5}$ (b_0 is the perimeter at the edge of the column and $b_{0.5}$ is the control perimeter at 0,5d from the column), based on $k_{pb(1)}$ [28] and $k_{pb(2)}$ [29]. While in most of the slabs with openings the $b_0/b_{0.5}$ ratio remains approximately the same for slabs without openings, slabs L17 and L18 experienced a substantial impact on their ultimate strength due to the choice of k_{pb} equation (see Table 4.5). The premise of Eq. (4. 2) may not be valid for slabs with openings, depending on the location of the holes (see Figure 4.15b, c, d)). Therefore, the authors suggest the utilization of the $k_{pb(1)}$ [28] formula for slabs with openings, which can remain unaffected by potential cases of slabs with openings that do not satisfy Eq. (4. 2). As evident from Table 4.5 and Figure 4.14, the results obtained using the $k_{pb(1)}$ formula have proven to accurately forecast the capacity of such slabs, with excellent statistical outcomes.

The proposal of Santos *et al.* (2022) [7] consists in a less restrictive control perimeter reduction for openings located immediately adjacent to the column faces. Several researchers [2-7,12] have highlighted that radial projections for reducing the perimeter may not be suitable for a range of opening sizes, geometries, and locations in practical applications.

Figure 4.16 displays a comparison between the control perimeter length determined using the current radial approach (a) and the control perimeter obtained through the approach proposed by [7] (b). This alternative method leads to a longer control perimeter length, as can be seen in Figure 4.14, which permits the contribution of the shear forces at the edges of the openings, leading to less conservative results. In contrast, the radial approach ignores the shear forces in this region [2-7].

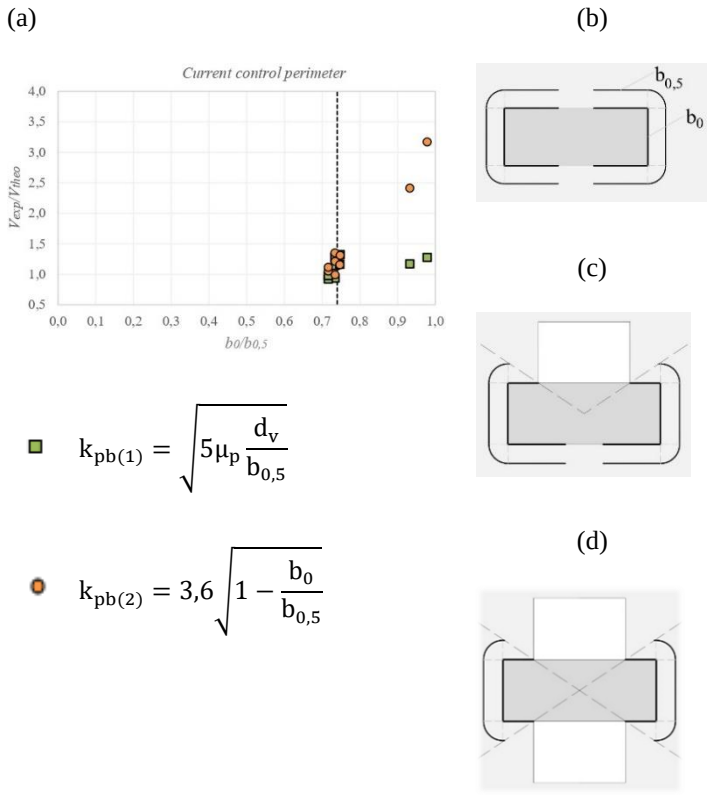

Figure 4.15 - (a) Comparison of coefficient k_{pb} from two different approaches of prEN 1992-1-1:21, perimeter at column edge b_0 and at 0.5d $b_{0,5}$ for: (b) slab without opening (c) L17 (d) L18

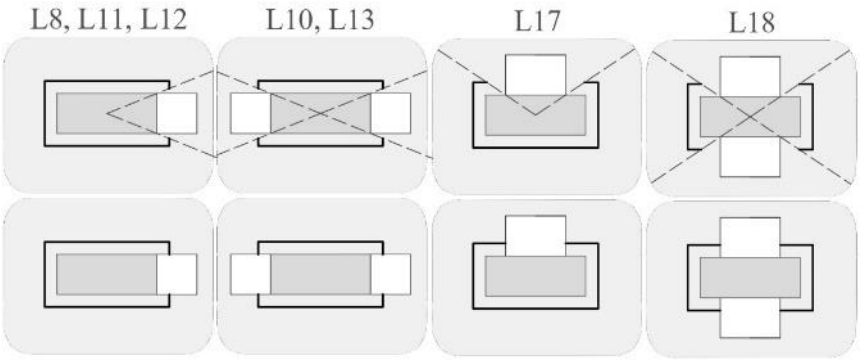

Figure 4.16 - Control perimeter of slabs with openings according to the current radial line approach, and according to the approach of Santos et al. (2022)

Figure 4.17 displays the normalized stress distribution along the control perimeter of the tested slabs in both the west-east (a) and north-south (b) directions. While ACI 318:19 assumes a linear shear stress distribution along the control perimeter, the results shown in Figure 4.17 are very consistent. Slabs with higher eccentricity had higher normalized shear stresses, and slabs with two openings had higher stresses compared to those with one opening, which had higher stresses compared to slabs with no openings. These trends are

overall consistent with the experimental concrete strain findings presented in Figure 4.11-Figure 4.13.

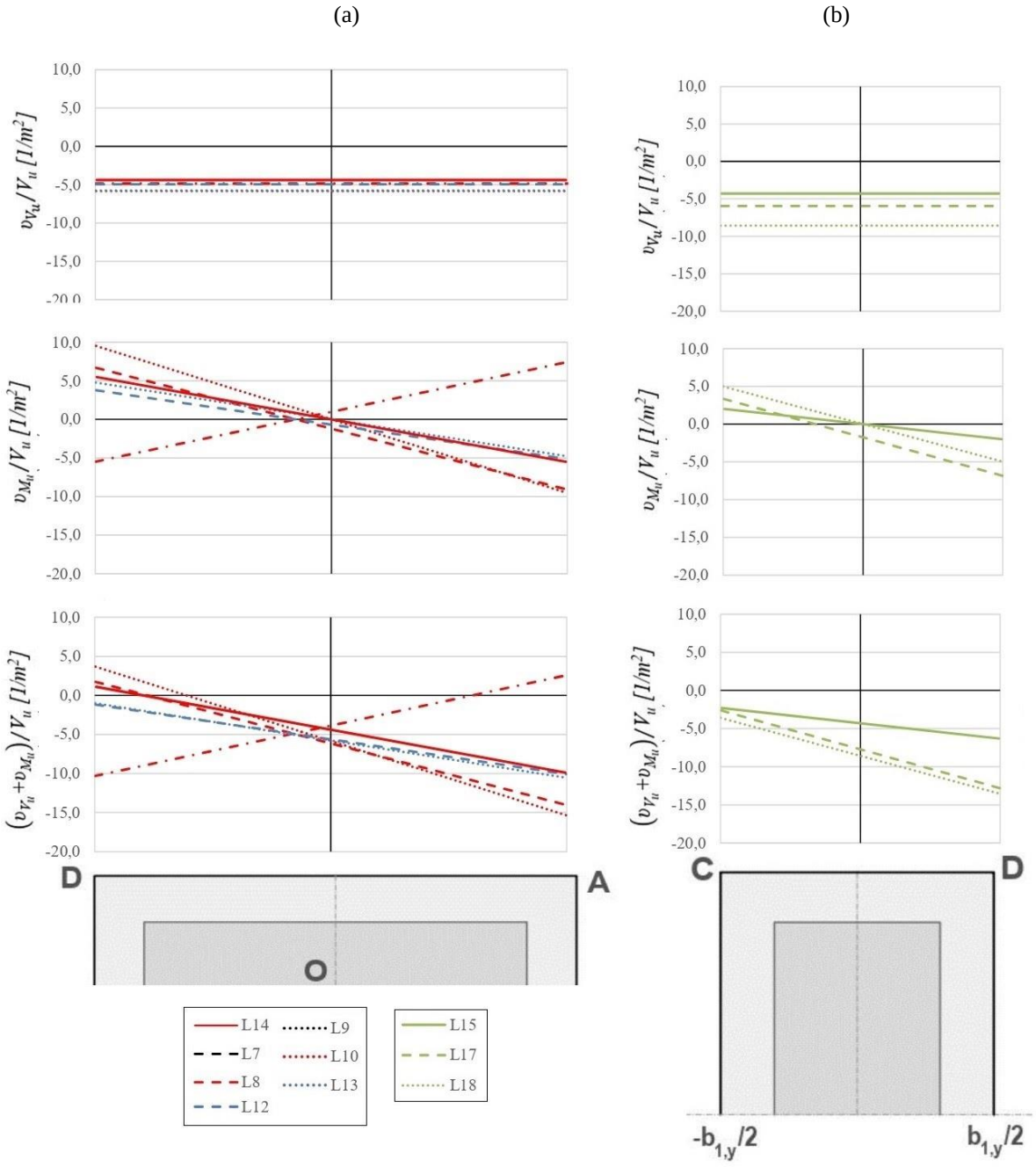

Figure 4.17 - Normalized stresses distribution according to ACI 318:19 (a) west-east direction of slabs L14, L8, L10, L11, L12 (b) north-south direction of slabs L15, L17, L18

4.5 CONCLUSIONS

This work presents the experimental results of nine full-scale slab-column connections with openings and subjected to unbalanced moments in various eccentricities and directions. Based on the obtained results, the following conclusions can be drawn:

1. Punching failure was observed in all the slabs, and the presence of openings and unbalanced moments significantly reduced their ultimate load-carrying capacity;
2. The effect of the unbalanced moment on resistance was found to be much more detrimental than the effect of the number of openings;
3. The moment orientation significantly affected the slab resistance with openings. Slabs subjected to moments in the opposite orientation to the openings position presented higher capacity;
4. Slabs with openings exhibited significantly lower levels of flexural strain than those without openings;
5. The concrete strains at the concrete surface were significantly influenced by the presence of openings and unbalanced moments. The tangential strains in the middle of the column were similar for all slabs, while the radial strains were higher for slabs with moments and openings, particularly close to the openings.

Regarding the comparison of theoretical and experimental results, the main conclusions are:

1. The theoretical results of ACI 318:19 and *fib* MC 2010:13 LoAII showed a high deviation when compared to experimental results;
2. The use of level of approximation III and the mean rotation significantly improved the *fib* MC 2010:13 results, with excellent results of average and coefficient of variation of experimental-to-calculated resistance;
3. The prEN 1992-1-1:2023 theoretical results demonstrated an excellent correlation with experimental results when using the early expression of k_{pb}. The equation of

this coefficient in the latter prEN 1992-1-1:2023 may not be suitable for analyzing slabs with openings. This is because the assumption that the control perimeter $b_{0.5}$ is equal to b_0 plus the length of rounded corners with a radius of $d_v/2$ may not be valid for slabs with openings;

4. The adoption of the control perimeter drawn to the faces of the openings, instead of the radial approach reduction, led to a noteworthy enhancement in both the average and coefficient of variation of experimental-to-calculated resistances according all the analysed codes.

4.6 REFERENCES

1. MOE J. *Shearing strength of reinforced concrete slabs and footing under concentrated loads*. Development department bulletin D47, Portland Cement Association, p. 135, 1961.
2. REGAN, P. E. Design for punching shear. The Structural Engineer, V. 52, n° 6, p. 197-207, 1974.
3. TENG S.; CHEONG H. K.; KUANG K. L., Geng J. Z. *Punching shear strength of slabs with openings and supported on rectangular columns*. ACI Structural Journal, V. 101, 678–87, 2004.
4. BORGES L. L. J.; MELO G. S.; GOMES R. B. *Punching shear of reinforced concrete flat plates with openings*. ACI Structural Journal, V. 110, p. 547-556, 2013.
5. AUGUSTIN T.; FILLO L.; HALVONIK, J. *Punching resistance of slab-column connections with openings*. Structural Concrete. p. 1–13, 2019. doi.org/10.1002/suco.201900158
6. KORMOŠOVÁ L.; HALVONIK J. *Punching shear behavior of flat slabs supported by elongated columns with openings*. Structural Concrete, p. 1–21, 2023. doi.org/10.1002/suco.202200450

7. SANTOS J. B.; MUTTONI A.; MELO G. S., *Enhancement of the punching shear verification of slabs with openings*. Structural Concrete, 18 p., 2022. dx.doi.org/10.1002/suco.202200714
8. MÜLLER F.; MUTTONI A.; THÜRLIMANN B. *Durchstanzversuche an Flachdecken mit Aussparungen*. Institut für Baustatik und Konstruktion, ETH Zürich, n° 7305-5 ISBN 3-7643-1686-1, 1984. *(In German)*
9. ANIL Ö.; KINA T.; SALMANI V. *Effect of opening size and location on punching shear behaviour of two-way RC slabs*. Magazine of Concrete Research, V. 66, n°18, p. 955-966, 2014. doi.org/10.1680/macr.14.00042
10. LIBERATI E. A. P.; MARQUES M. G.; LEONEL E. D.; ALMEIDA L. C.; TRAUTWEIN L. M. *Failure analysis of punching in reinforced concrete flat slabs with openings adjacent to the column*. Engineering Structures, V. 182, p. 331-343, 2019. doi.org/10.1016/j.engstruct.2018.11.073
11. LOURENÇO D. S.; LIBERATI E. A. P.; MARQUES M. G.; ALMEIDA L. C.; TRAUTWEIN L. M. *Reinforced concrete flat slabs with openings at different distances from the column*. IBRACON Structures and Materials Journal, V. 14, 2021. doi.org/10.1590/S1983-41952021000100011
12. SANTOS J. B.; SOUZA R. M.; MELO G. S.; GOMES R. B. *Punching resistance of flat slabs with openings adjacent to the columns*. ACI Structural Journal, V. 119, p. 41-53, 2022. doi: 10.14359/51734216
13. EL-SHAFIEY, T. F.; ATTA, A. M;; HASSAN, A.; ELNASHARTY, M. *Effect of opening shape, size and location on the punching shear behaviour of RC flat slabs. Engineering Structures*, V. 44, p. 1138-1151, 2022. doi.org/10.1016/j.istruc.2022.08.076

14. FERREIRA M. P.; OLIVEIRA M. H.; MELO G.S. *Tests on the punching resistance of flat slabs with unbalanced moments*. Engineering Structures, V. 196, 109311, 2019. doi.org/10.1016/j.engstruct.2019.109311
15. UNGERMANN J.; SCHMIDT P.; CHRISTOU G.; HEGGER J. *Eccentric punching tests on column bases - Influence of column geometry*. Structural Concrete. 2022, doi.org/10.1002/suco.202100744
16. VARGAS, D.; LANTSOGHT, E. O. L.; GENIKOMSOU, A. S. *Flat Slabs in Eccentric Punching Shear: Experimental Database and Code Analysis*. Buildings, V. 12, p. 2092, 2022. doi.org/10.3390/buildings12122092
17. HANSON, N. W.; HANSON, J. M. *Shear and Moment Transfer Between Concrete Slabs and Columns*. *Journal PCA Research and Development Laboratories*. Vol. 10, p. 2-16, 1968.
18. OLIVEIRA, D. C.,;GOMES, R. B.; MELO, G. S. *Punching shear in reinforced concrete flat slabs with hole adjacent to the column and moment transfer*. *IBRACON Structures and Material Journal*, V. 7, p. 1983-4195, 2014.
19. BURSAĆ, S.; BEŠEVIĆ, M.; PURČAR, M. V.; KOZARIĆ, L.; ĐURIĆ, N. *Experimental analysis of punching shear strength of eccentrically loaded slab with the opening along the face of the internal column*. *Engineering Structures*, V. 249, 113359, 2021. doi.org/10.1016/j.engstruct.2021.113359
20. ACI Committee 318. *Building code requirements for structural concrete (ACI 318-19) and commentary (318R-19)*. American Concrete Institute, Farmington Hills, MI, 2019, pp 623.
21. ACI Committee 421. *Guide for Shear Reinforcement for Slabs (ACI 421.1R-20)*. American Concrete Institute, Farming Hills, Mich., 2020, p. 27.

22. Fédération internationale du béton. *Fib Model Code for Concrete Structures 2010 (MC2010)*, fib , Lausanne, Switzerland, 2013, pp 390.
23. MUTTONI A. *Punching shear strength of reinforced concrete slabs without transverse reinforcement*. ACI Structural Journal, V. 105, n° 4, p. 440–50, 2008.
24. MUTTONI A.; FERNÁNDEZ RUIZ M. *The levels-of-approximation approach in MC 2010: application to punching shear provisions*. Structural Concrete, V. 13. doi: 2012.10.1002/suco.201100032
25. SAGASETA J.; MUTTONI A.; FERNÁNDEZ RUIZ M.; TASSINARI L. *Non-axis-symmetrical punching shear around of RC slabs without transverse reinforcement*. Mag Concr Res, V. 63, p. 441–57, 2011. doi.org/10.1680/macr.10.00098
26. SAGASETA J.; TASSINARI L.; Fernández Ruiz M.; Muttoni A. *Punching of flat slabs supported on rectangular columns.* Engineering Structures. V. 77, p. 17-33, 2014. doi.org/10.1016/j.engstruct.2014.07.007
27. MUTTONI A.; FERNÁNDEZ RUIZ M.; SIMÕES J. T. *The theoretical principles of the critical shear crack theory for punching shear failures and derivation of consistent closed-form design expressions*. Structural Concrete. V. 19, p. 174-190, 2018. doi.org/10.1002/suco.201700088
28. Background to prEN 1992-1-1:2020-11. *Background documents to prEN 1992-1-1*. Version of the draft of the 2nd generation of prEN 1992-1-1:2020-11, Report EPFL/RTWH-17-01-R5, May 2021, pp 500.
29. prEN 1992-1-1:2021. Eurocode 2-Design of concrete structures- Part 1-1: *General rules, rules for buildings, bridges and civil engineering structures,* Stable version of the draft of the 2nd generation of prEN 1992-1-1:2021, CEN, Brussels, Belgium, 2021, pp 410.

30. SOUZA, R. M. *Punção em lajes lisas de concreto armado com furos adjacentes ao pilar e transferência de momento*. Tese de Doutorado, Faculdade de Tecnologia, Departamento de Engenharia Civil e Ambiental, Universidade de Brasília, 2008, pp 442. *(In Portuguese)*
31. ŽIVKOVIĆ, S.; BEŠEVIĆ, M.; PURČAR, M. V.; KOZARIĆ, L. *Nonlinear Finite Element Analysis of Punching Shear Strength of Eccentrically Loaded RC Flat Slabs with Opening*. KSCE Journal of Civil Engineering, V. 23, p. 4771–4780, 2019. doi.org/10.1007/s12205-019-0075-5
32. ALROUSAN, R. Z.; ALNEMRAWI, B. R. *The influence of concrete compressive strength on the punching shear capacity of reinforced concrete flat slabs under different opening configurations and loading conditions*. Engineering Structures, V. 44, p. 101-119, 2022. doi.org/10.1016/j.istruc.2022.07.091
33. ALROUSAN, R. Z.; ALNEMRAWI, B. R. *Punching shear code provisions examination against the creation of an opening in existed RC flat slab of various sizes and locations*. *Engineering Structures*, V. 49, p. 875-888, 2023. oi.org/10.1016/j.istruc.2023.02.007
34. ISMAIL E-S. I. M. *Nonlinear finite element analysis of reinforced concrete flat plates with opening adjacent to column under eccentric punching loads*. Housing and Building National Research Center Journal, V. 14, p. 438–449, 2018. doi.org/10.1016/j.hbrcj.2018.01.001
35. SANTOS, E. V. *Punção em Lajes Lisas: Métodos de Cálculo, Prescrições Normativas e Exemplos de Aplicação*. Dissertação de Mestrado, Universidade de Brasília. Faculdade de Tecnologia, 2018, pp 225. *(In Portuguese)*

4.7 APPENDIX A

This section presents the code provisions for slabs with unbalanced moments. A detailed explanation of the property J_c according to ACI318:19 is provided, with specific considerations for slabs with openings.

4.7.1 J_c property according to ACI 318:19

ACI 318:2019 defines J_c as a property similar to polar moment of inertia. For connections without openings, J_c can be calculated using the given equation since the column centroid and control perimeter centroid coincide. However, in the case of slabs with openings, J_c calculation needs to be carried out based on the control perimeter axis. The following is a detailed derivation of the equations utilized to determine the J_c property for slabs with openings.

For a surface perpendicular to the moment axis (AD and BC in Figure 4.18), J_c is exactly the polar moment of inertia (Eq. 4. 14). For a surface parallel to the moment axis (AB and CD in Figure 4.18), J_c is the moment of inertia I_y (Eq. 4. 15). Santos (2018) [35] provides the mathematical explanation of J_c for interior, edge and corner connections.

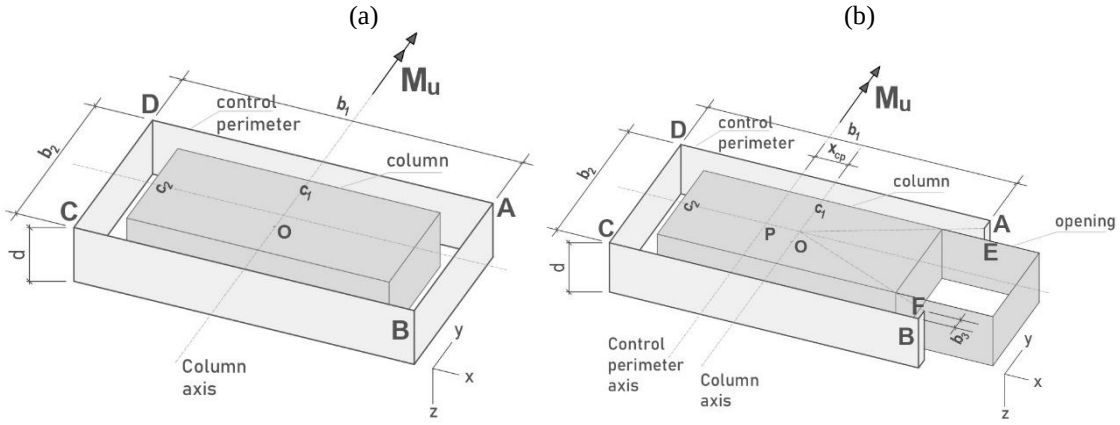

Figure 4.18 - Control perimeter areas for the J_c calculation of an interior connections subjected to moment transfer in the y-direction (a) connection without opening (b) connection with opening (P: control perimeter centroid, O: column centroid)

$$A_i \perp M_u: \quad J_y = \int_{A_i} (x^2 + z^2) dA \tag{4. 14}$$

$$A_i \parallel M_u: \quad J_y = I_y = \int_{A_i} x^2 dA \tag{4. 15}$$

Where: A_i is the control perimeter area, dA is the infinitesimal area.

For the interior connection without openings (see Figure 4.18a), J_c can be determined as:

$$J_{c,tot} = J_{c,DA} + J_{c,CB} + J_{c,DC} + J_{c,AB} \tag{4. 16}$$

$$J_{c,tot} = 2\left(\frac{db_1^3}{12} + \frac{b_1 d^3}{12}\right) + 2\left(b_2 d\left(\frac{b_1}{2}\right)^2\right) \tag{4. 17}$$

$$J_{c,tot} = \frac{db_1^3}{6} + \frac{b_1 d^3}{6} + \frac{(b_2 d) b_1^2}{2} \tag{4. 18}$$

Eq. (4. 18) is the equation given in section 8.4.4 of ACI 318:2019. Such equation is not exactly the polar moment of inertia, that is why ACI 318:2019 says it is 'analogous'.

For the interior connection with openings (see Figure 4.18b), the code does not give any equation. In this case, J_c must be calculated with respect to the centroid of the control perimeter and can be determined by Eq. (4. 20).

$$J_{c,tot} = J_{c,DA} + J_{c,CB} + J_{c,DC} + J_{c,AE} + J_{c,FB} \tag{4. 19}$$

$$J_{c,DA} = J_{c,CB} = \frac{db_1^3}{12} + (b_1 d) x_{cp}^2 + \frac{b_1 d^3}{12}$$

$$J_{c,DC} = (b_2 d)\left(\frac{b_1}{2} - x_{cp}\right)^2$$

$$J_{c,AF} = J_{c,FB} = (b_3 d)\left(\frac{b_1}{2} + x_{cp}\right)^2$$

$$J_{c,tot} = \frac{db_1^3}{6} + 2(b_1 d) x_{cp}^2 + \frac{b_1 d^3}{6} + b_2 d\left(\frac{b_1}{2} - x_{cp}\right)^2 + 2(b_3 d)\left(\frac{b_1}{2} + x_{cp}\right)^2 \tag{4. 20}$$

Similarly, J_c can be determined for other opening's location (Figure 4.19), according to Eq. (4. 21)-(4. 23).

(a)

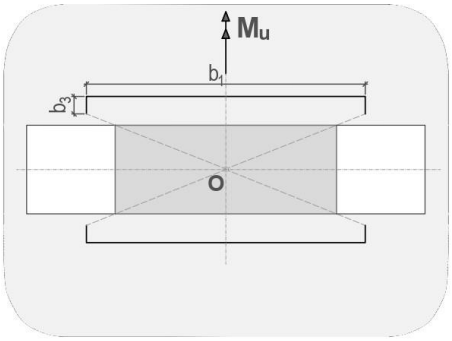

$$J_{c,tot} = \frac{db_1^3}{6} + \frac{b_1 d^3}{6} + (b_3 d) b_1^2 \qquad (4.\ 21)$$

(b)

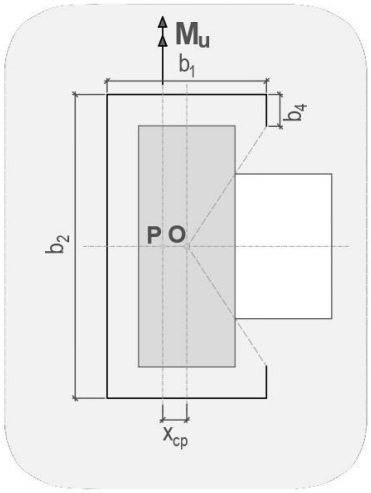

$$J_{c,tot} = \frac{db_1^3}{6} + 2(b_1 d) x_{cp}^2 + \frac{b_1 d^3}{6} + b_2 d\left(\frac{b_1}{2} - x_{cp}\right)^2 + 2(b_4 d)\left(\frac{b_1}{2} + x_{cp}\right)^2 \qquad (4.\ 22)$$

(c)

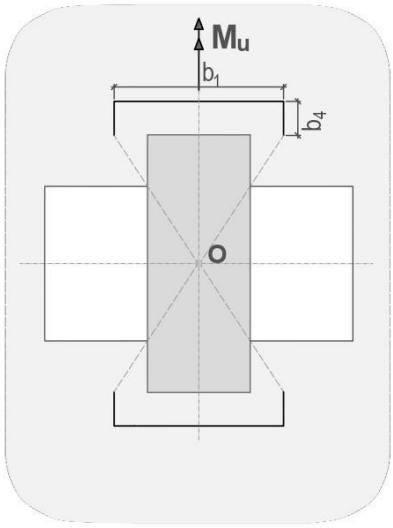

$$J_{c,tot} = \frac{db_1^3}{6} + \frac{b_1 d^3}{6} + (b_4 d) b_1^2 \qquad (4.\ 23)$$

Figure 4.19 - Control perimeter and parameters for J_c calculation for different opening's location (O: column centroid, P: control perimeter centroid)

5. PUNCHING PERFORMANCE OF FLAT SLABS WITH OPENINGS ACCOUNTING FOR THE INFLUENCE OF MOMENT TRANSFER AND SHEAR REINFORCEMENT

5.1 INTRODUCTION

In projects of flat slabs, openings are arranged in many cases near or adjacent to columns to allow for ducts and services connecting two floors, see Figure 5.1. Such choice, with clear benefits for the building services and architectural reasons, has however strong potential implications on the punching performance of slab-column connections. Namely, the punching resistance may be compromised, as the perimeter where the shear forces may develop is strongly reduced and arranging a shear reinforcement is typically adopted.

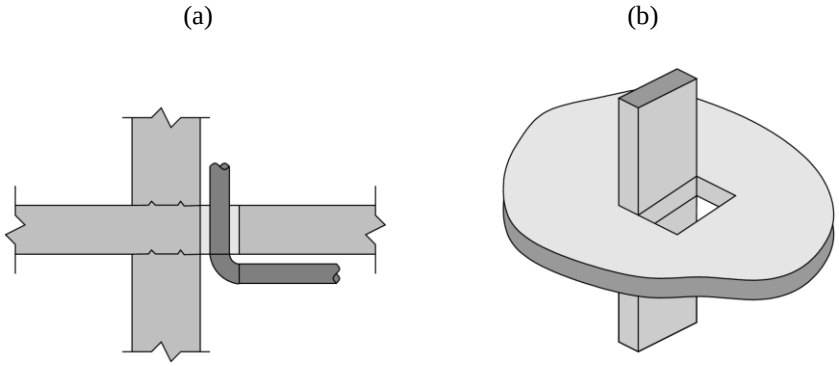

Figure 5.1 - Slab with an opening adjacent to a column: (a) section at the opening, and (b) view of the slab-column connection

Despite being a relatively common case in practice, there is scanty experimental research conducted on slabs with openings. As shown by Hernandez Fraile et al. [1], from the 73% of published tests on slab-column connections representing inner connections, only 8% focused on slabs with openings. Additionally, data collected by the authors [1-22] indicate that only 21% of tests on slabs with openings contained shear reinforcement. Remarkably, no published work was found on the performance of punching tests on slabs with openings and shear reinforcement in presence of a moment transfer between the slab and columns,

which is one of the most common situations in practice. For these cases, design has thus been performed so far by extending rules developed for other cases.

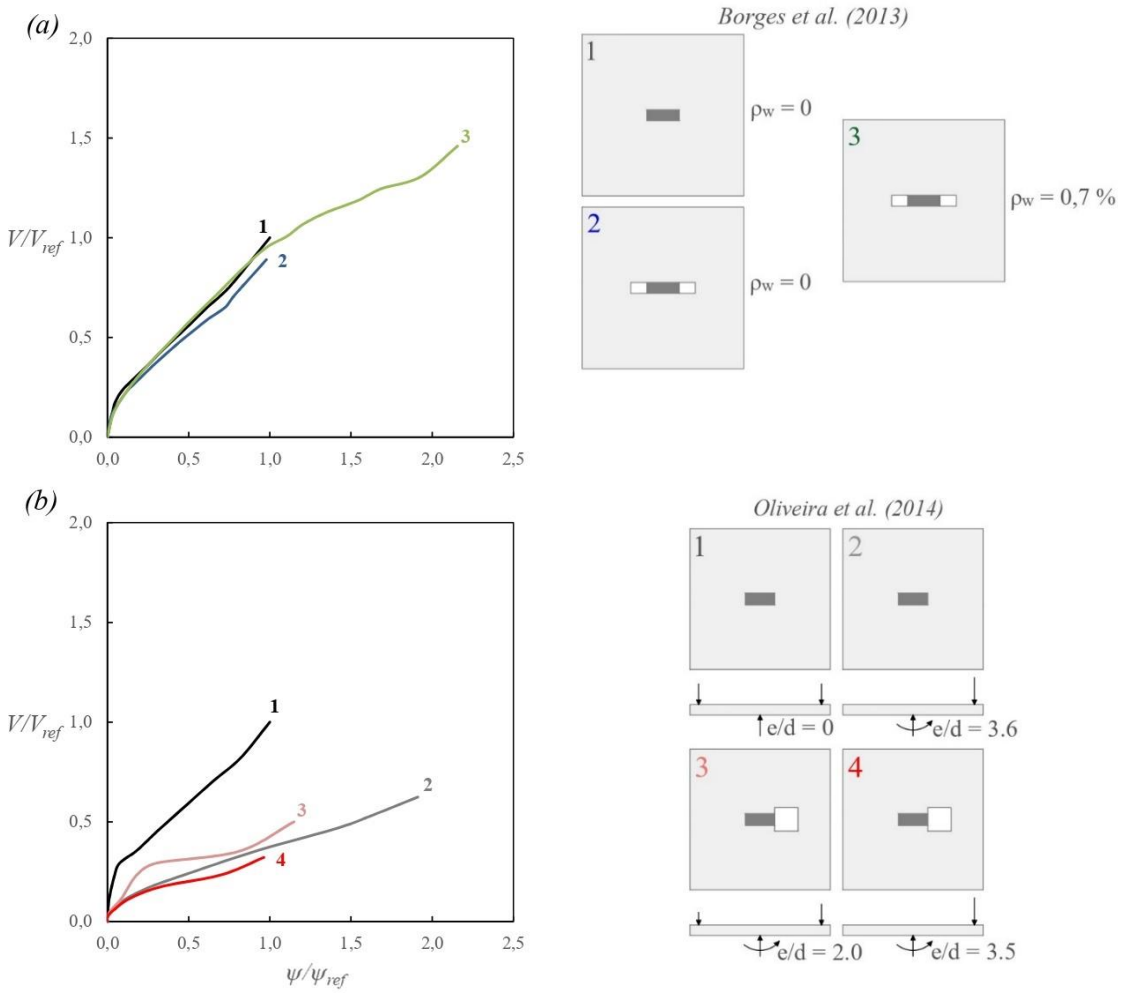

Figure 5.2 - Load-rotation of with and without openings (a) comparison of specimens with axis-symmetric loading, with and without shear reinforcement, tested by [13] (b) comparison of specimens with and without moment transfer, tested by [20] (Note: in both cases the reference specimen is 1-without openings, without shear reinforcement and with axis-symmetric loading)

Referring to previous experiences, it can be noted that the influence of shear reinforcement and transferred moment is notable in presence of openings. The first aspect can be clearly seen in Figure 5.2a (based on the tests by Borges et al. [13]) where three slabs are compared normalising the failure load and rotation to the values of specimen 1 (without openings and without shear reinforcement). While the presence of the opening reduces the punching resistance and deformation capacity, the shear reinforcement provides a significant

enhancement of both, in a similar manner as for slabs without openings [23]. In the second plot (Figure 5.2b, based on the experimental results by Oliveira et al. [20]), the influence of a moment transfer is also presented. As it can be noted, such moment is detrimental for the resistance of the connection (with or without opening), showing also a decrease on the deformation capacity in presence of an adjacent opening.

According to both experimental evidence and numerical investigations, the presence of openings in slabs near columns reduces the punching resistance depending on several parameters. Amongst them, some of the most relevant appear to be their location and geometry as well as the number of openings [2-22,24-30]. Despite the relatively complex physical phenomena occurring in presence of openings (such as concentrations of forces in the shear fields [11] or development of the critical shear crack [31]), codes of practice typically account for their influence by simply adapting the length of the critical control perimeter based on geometric rules [32-34]. Such approach raises however questions on whether such simplified rules are fully representative and safe for all potential cases. In addition, enhancement factors on the punching strength when shear reinforcement is arranged near openings (which is performed in many practical cases) are simply extrapolated from those of inner slab-column connections without openings. This may again be a crude approach accounting for the different confinement conditions of concrete and development of the critical shear crack in slabs with openings.

This paper is addressed at this gap in current state of knowledge. First, the results of a comprehensive test programme are presented in order to investigate the role of openings adjacent to columns in the punching performance. The tested connections were designed to allow for a moment transfer between the slab and the column, reproducing realistic practical conditions. In addition, several specimens were shear-reinforced to allow for direct comparisons on the observed performance. The test programme comprises five slabs,

including one without openings, one with openings but without shear reinforcement, and three with openings and double-headed studs for shear reinforcement. The experimental results are then compared to the strength predictions provided by codes of practice (ACI 318:19, *fib* MC 2010 as well as FprEN 1992-1-1:23) to check the accuracy of design formulations currently used in practice. Finally, based on this knowledge, the experimental tests are investigated in detail on the basis of the Critical Shear Crack Theory [31], suggesting the required adaptions to suitably apply this theory to the investigated case.

5.2 EXPERIMENTAL PROGRAMME

The experimental programme consisted of five reinforced concrete slabs tested to examine the effect of moment transfer and detailing of shear reinforcement on the punching resistance of slabs with openings adjacent to the column. All tests were performed in the Structural Laboratory of University of Brasilia, Brazil (LABEST).

5.2.1 Specimen description

The five specimens were square flat slabs with a side length equal to 2.5 m and a thickness equal to 180 mm. The slabs were supported at their centre by square column stubs with a size equal to 300 mm and protruding 800 mm on top and 600 mm on bottom (see Figure 5.3a). One specimen was cast without openings (LRSS, Figure 5.3a), while the remaining four had identical openings 300×300 mm^2 at two opposed sides of the column (Figure 5.3b). For the specimens with openings, one did not have shear reinforcement (LRFS) and the other three (LFS1, LFS2 and LFS3) had different shear reinforcement layouts. The main characteristics of the specimens and of their materials are summarized in Table 5.1.

The top reinforcement consisted of 16-mm rebars for all specimens. For the specimen without openings (LRSS), the average spacing of the top flexural reinforcement was 100 mm. For the specimens with openings (LRFS and LFS1-LFS3), the average spacing between

top bars was on average 120 mm and additional bars were provided at the edges of the openings (except at the column region, see Figure 5.4). Accounting for the reinforcement arrangement and actual values of the effective depths (measured after testing in saw-cuts), the average flexural reinforcement ratio ($\rho = \sqrt{\rho_x \cdot \rho_y}$) was $\rho = 1.37\%$ for the specimen without openings (LRSS) and varied between 1.00% and 1.13% for those with openings (LRFS and LFS1-S3). The bottom flexural reinforcement consisted for all specimens of 8-mm rebars spaced at 140 mm. Both top and bottom rebars were interrupted due to the presence of openings (see Figure 5.4a). Pins of 12.5-mm rebars were arranged at the edges of the slabs, but not at the edges of openings (the influence of this aspect was investigated later with the arrangement of shear reinforcement).

The column stub was cast monolithically with the slab (refer to Figure 5.3). The column reinforcement consisted of eight longitudinal 25.4 mm rebars, with four bars placed at each side adjacent to an opening (allowing for the moment transfer). These rebars were enclosed by 10-mm stirrups, spaced at 75 mm (see Figure 5.4a).

With respect to the shear reinforcement, double-headed studs with a diameter of 10 mm were used for specimens LFS1-S3. The detailing of the shear reinforcement varied for these specimens, according to the arrangements shown in Figure 5.4d,e.

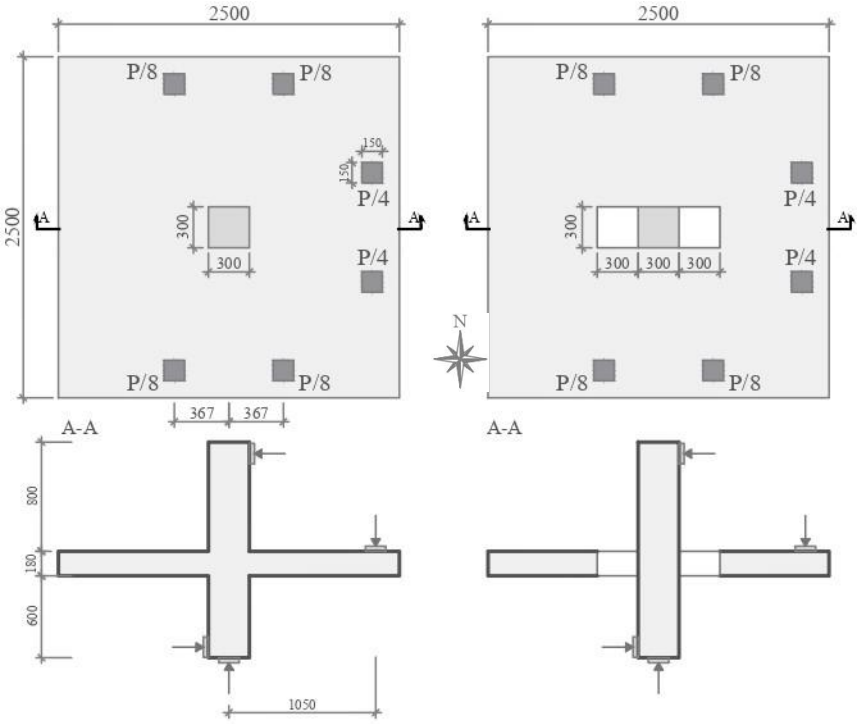

Figure 5.3 - Main dimensions and load arrangement (Note: dimensions in mm)

Table 5.1 - Main geometrical and material properties

specimen	f_c [MPa]	f_y [MPa]	f_{yw} [MPa]	d [mm]	ρ_x [%]	ρ_y [%]	ρ [%]	V_{flex} [kN]	V_R [kN]
LRSS	54.3	591	-	141	1.36	1.37	1.37	631	331
LRFS	54.3	591	-	136	1.18	0.90	1.03	396	173
LFS1	54.3	591	525	137	1.17	0.85	1.00	402	231
LFS2	44.9	532	525	131	1.16	1.06	1.11	356	285
LFS3	44.9	532	525	129	1.18	1.09	1.13	352	224

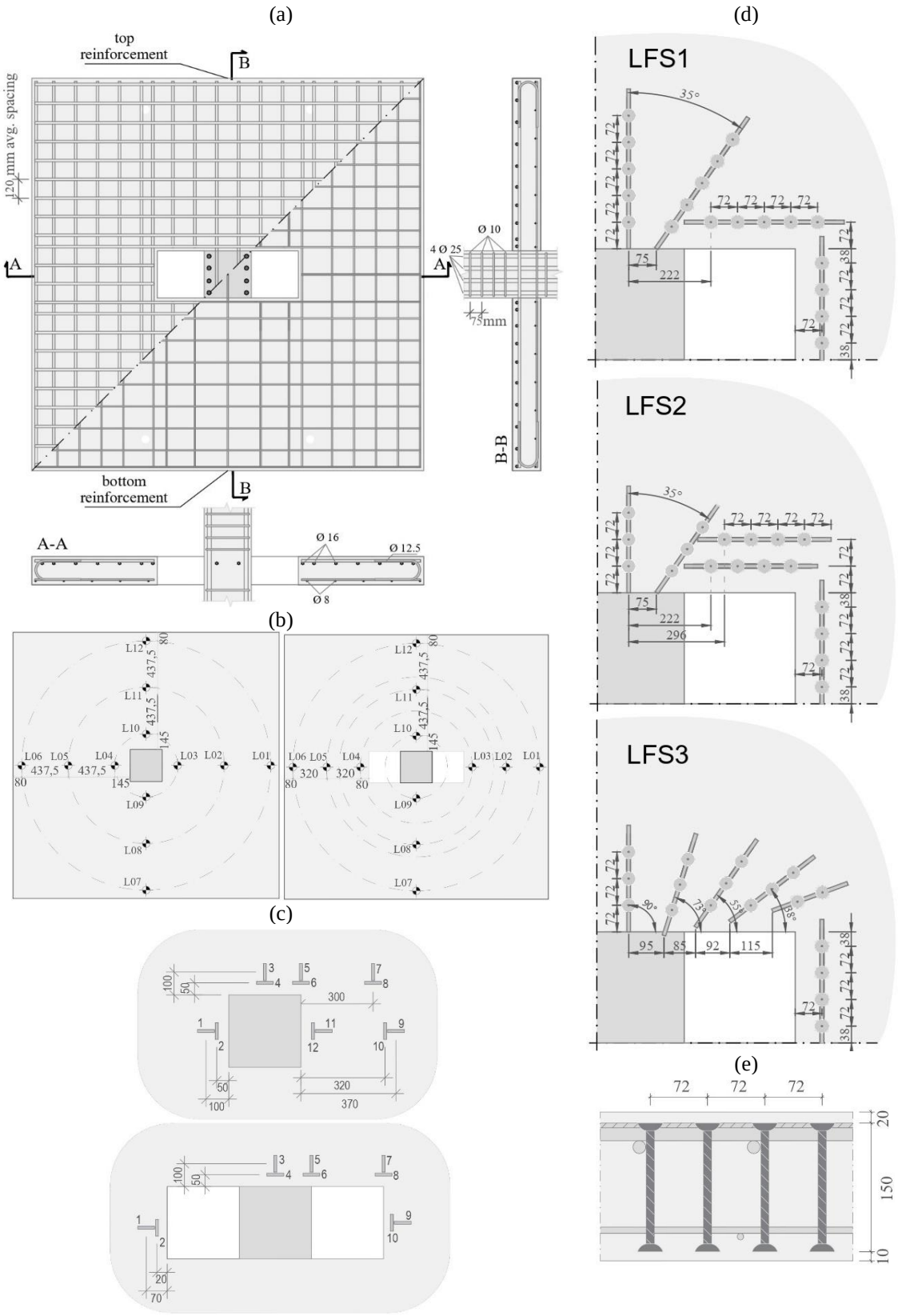

Figure 5.4 - Reinforcement arrangement and instrumentation of the slabs: (a) flexural and column reinforcement arrangement; (b) LVDTs; (c) bottom concrete strain gauge position; (d) shear stud arrangement; and (e) shear reinforcement detailing (Note: units in mm)

5.2.2 Material properties

Specimens LRSS, LRFS and LFS1 were cast and tested first. Once this first experimental series was finished, specimens LFS2 and LFS3 were cast and tested. For all specimens, concrete was provided by a local supplier. The specified compressive strength for the concrete was 40 MPa with crushed limestone sand and gravel used as aggregate. The maximum size for the coarse aggregate sieve was 12.5 mm. Conventional reinforcement with a specified yield strength of 500 MPa was also ordered from a local supplier.

The slabs of the same series were tested on consecutive days, to avoid significant time effects within each series (refer to concrete properties of Table 5.1). The actual compressive strength of concrete was determined for each slab by testing cylinders (100 mm diameter by 200 mm high). A total of fifteen cylinders were tested, three for each slab at the end of each series, with a measured compressive strength ranging between 44.9 and 54.3 MPa.

Concerning the flexural reinforcement, hot-rolled bars with a well-defined yield plateau were used. The measured yield strength in direct tension tests varied between 591 MPa and 532 MPa for the flexural bars of diameter 16 mm. Concerning the shear studs (diameter 10 mm), the average yield strength was 525 MPa.

5.2.3 Test setup and instrumentation

For testing, the slabs were positioned within a steel reaction frame, see Figure 5.5. The ends of the columns were laterally restraint and supported on the bottom surface. The loads were applied vertically, using three hydraulic jacks, that were supported on spreader beams distributing the load on six pads (150×150 mm^2). To transfer a moment from the slab to the column, the load was applied as shown in Figure 5.3b, with one half of the load applied on one axis but just on one side, and the remaining half on the perpendicular axis but

symmetrically. This load configuration is intended to represent scenarios involving slab-column connections with significant eccentricity.

The vertical displacement of the slabs was tracked by using LVDTs (Linear Variable Differential Transformers, model WA50 manufactured by HBM) in the locations indicated in Figure 5.4b (along the two main axes and at both sides). Such measurements were also used to determine the rotations of the slab at different locations of the main axes. Surface strains on the concrete were also measured on the bottom surface using strain gauges (manufactured by Kyowa Eletronic Instruments, with gage resistance of 119.8Ω ± 0.2%,) positioned as depicted in Figure 5.4c. In addition, strain gauges were used to monitor the flexural top rebars. Throughout the test, cracking progression of the slabs was tracked and marked at selected load steps and continuously recorded via video (top surface and both faces of the opening situated on the east side of the column).

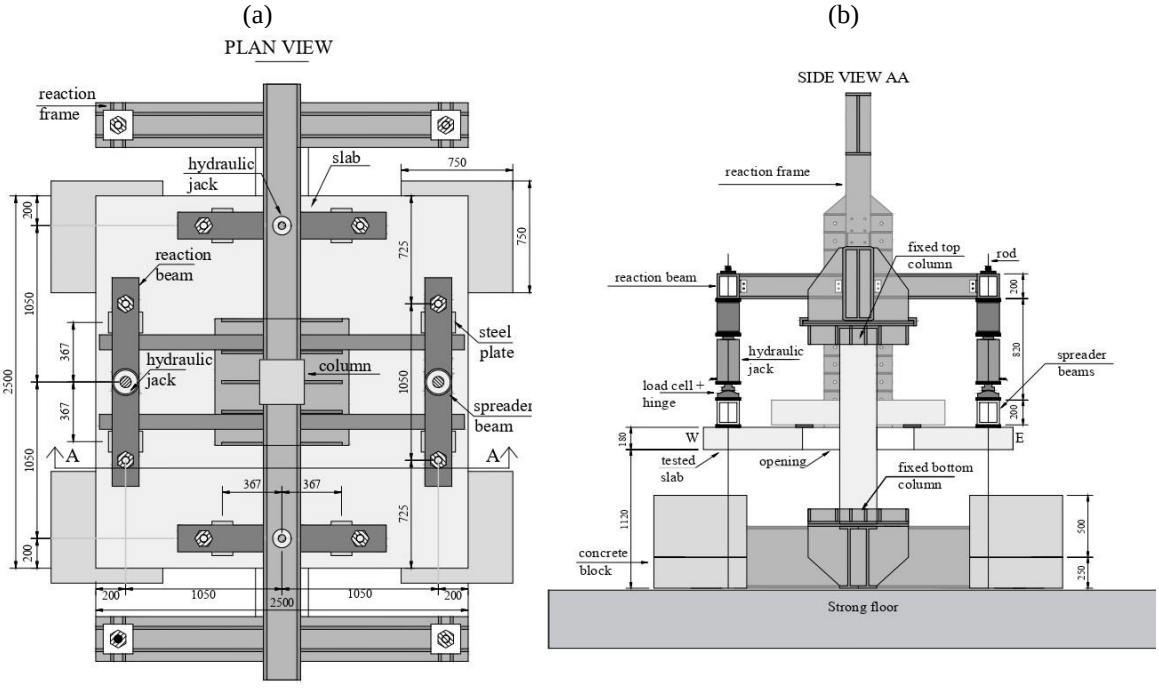

Figure 5.5 - Test setup: (a) plan view; and (b) side view

5.3 EXPERIMENTAL RESULTS

In this section the most relevant experimental results are discussed, highlighting the mechanical response of the specimens and the observed failure surfaces.

5.3.1 Global response and failure mode

All slabs failed in punching shear in a brittle manner (refer to Table 5.1 for actual failure loads and estimated flexural strengths according to). The results show that the presence of openings reduced significantly the failure load (by more than 50%), which can be attributed to the reduction of the punching control perimeter as well as to potential concentrations of shear forces. When the slabs are shear reinforced, the punching resistance is reduced with respect to the situation without openings but to a lower extent (reduction of approximately 25 to 30%, to be noted that some differences were also found on the compressive strength of concrete).

Figure 5.6 shows a comparison of the load-rotation curves for the different specimens, with rotations calculated at different directions and sides. In Figure 5.6, positive rotations indicate downward displacements of the slab, while negative rotations indicate upward displacements. As it can be observed, the slabs showed a different response along their main axis, with higher rotations and deflections in the WE direction. The presence of openings significantly decreased the rotation capacity, even in the direction of symmetric loading (north-south). However, the use of shear reinforcement could effectively enhance the deformation capacity of the slabs.

The observed global bending response is consistent with the strain measurements in the reinforcement, as shown in Figure 5.7 for one side of the specimen. Slabs LRSS and LFS3 achieved locally yielding in the rebars near the column, while the other slabs exhibited strains below the yielding strain. In any case, no generalized yielding was observed,

confirming that failures occurred below the flexural strength of the specimens (refer to 5.8 ANNEX A: FLEXURAL STRENGTH for flexural resistance analysis).

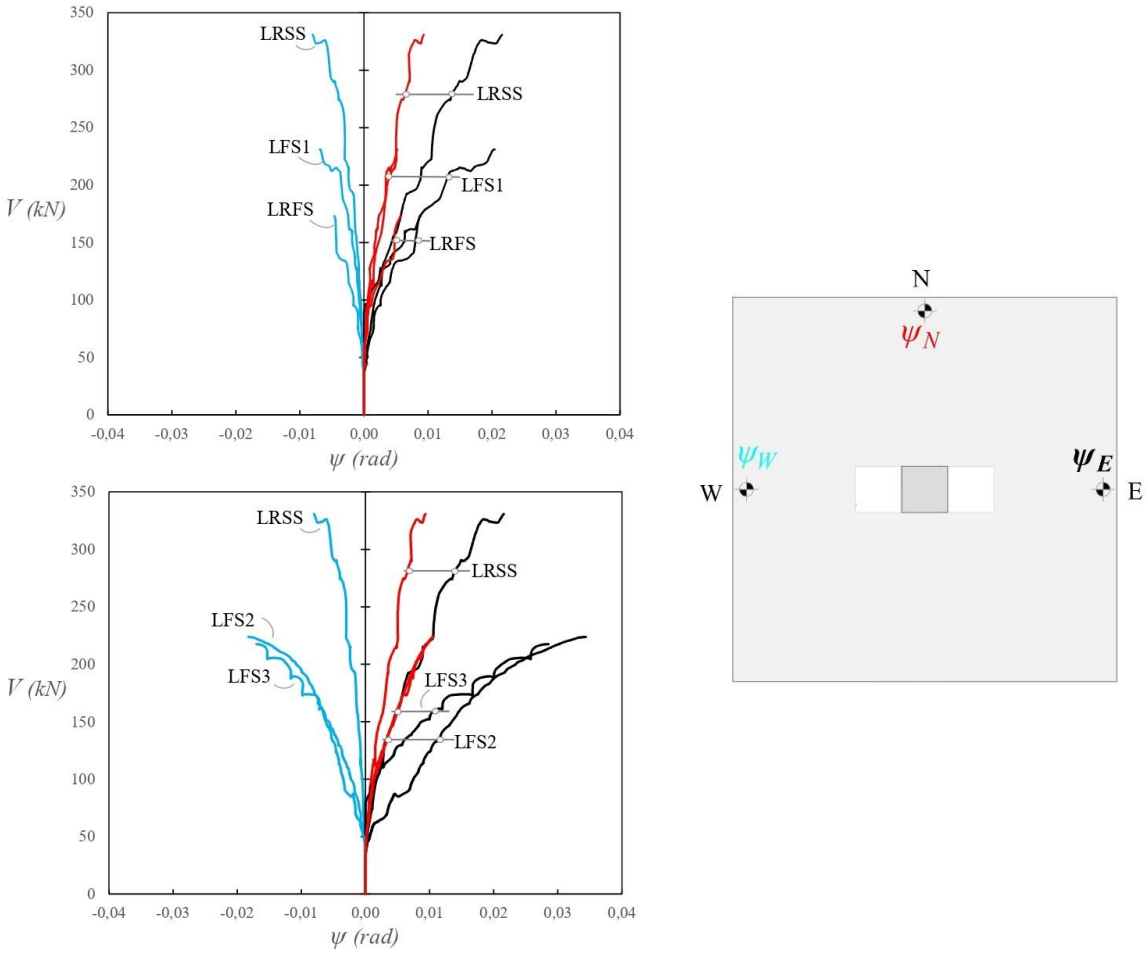

Figure 5.6 - Load-rotation relationships of the tested specimens (Note: LRSS: slab with moment, without openings and without shear reinforcement, LRFS: slab with openings, with moment and without shear reinforcement, LFS1-S3: Slabs with openings, with moment and with shear reinforcement, ψ_N, ψ_E, ψ_W: rotation in the north, east and west side, respectively)

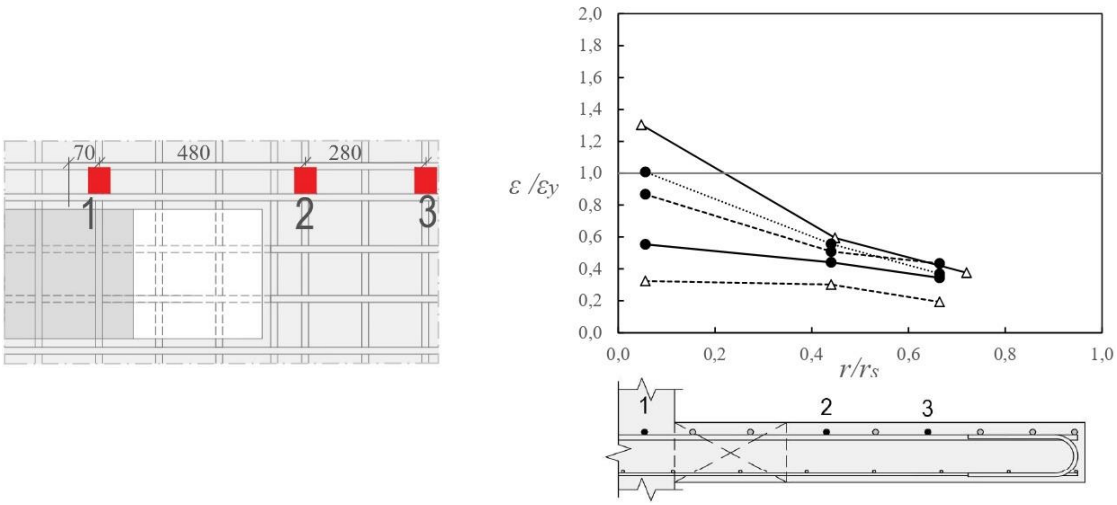

Figure 5.7 - Activation of flexural reinforcement

5.3.2 Cracking pattern

Figure 5.8 illustrates the observed cracking pattern on the top surface. Slabs without shear reinforcement (LRSS and LRFS) showed well-developed radial and tangential cracks according to the eccentric loading applied. A similar pattern was also observed for the shear-reinforced slabs (LFS1-S3), although the extent of cracking was more concentrated at the column region.

The critical shear crack after failure was also investigated by means of selected saw-cuts and views of the slabs. The saw-cuts of the slab without openings (LRSS) were performed along two perpendicular directions (WE (1) and NS (4)), see Figure 5.9a. Inspection of the saw cut revealed a critical shear crack developing at an angle of approximately 30º in the saw-cut (4) for the failure surface, developing on top in a sub horizontal manner (delamination crack).

For the slabs with openings, specimens LFS2 and LFS3 were saw-cut in the NS direction (4) and along a 45º direction (3), see Figure 5.9b and Table 5.2. As it can be noted, the cracking in the WE direction of the slabs with openings can be observed at the sides of the openings in the views (1) and (2), see Figure 5.9b. Inspection of the cracking pattern revealed a steeper

development of the critical shear crack (higher than 60º in most cases), both in the WE direction (views (1-2)) and in the NS or diagonal directions ((4) and (3) respectively). It was only reported a flatter angle than 45º in the view (2) of LRFS (specimen without shear reinforcement) for development of the first diagonal crack. Details on the measured angles in the saw-cuts (values for the critical shear crack) as well as of the time at which first diagonal cracking was observed are given in Table 5.2.

LRSS LRFS

LFS1 LFS2 LFS3

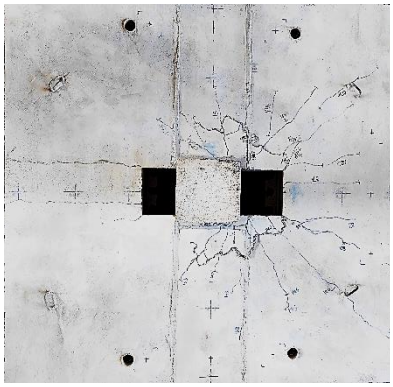

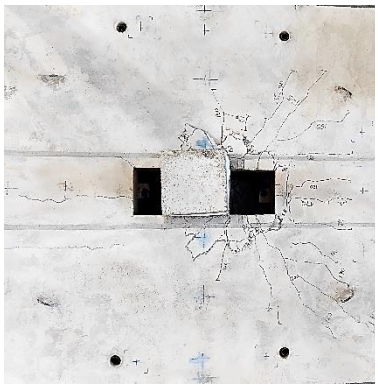

Figure 5.8 - Cracking pattern on the top surface of the slabs

Table 5.2 - Load levels at which shear cracking was observed and failure crack inclination

Specimen	$\theta_{(1)}$	$\theta_{(2)}$	$\theta_{(3)}$	$\theta_{(4)}$	V_{cr}/V_R
LRSS	25°/8°	-	-	31°/5°	-
LRFS	39°/8°	41°/7°	-	-	0.84
LFS1	51°/14°	32°/17°	-	-	0.76
LFS2	63°/7°	40°/10°	58°	53°/24°	0.63
LFS3	53°/9°	31°/11°	53°/25°	64°/19°	0.64

V_{cr}: Level of shear force at which first crack was observed on the sides of the opening

V_R: Level of shear force at which failure occurred

θ: crack inclination in the corresponding saw-cut

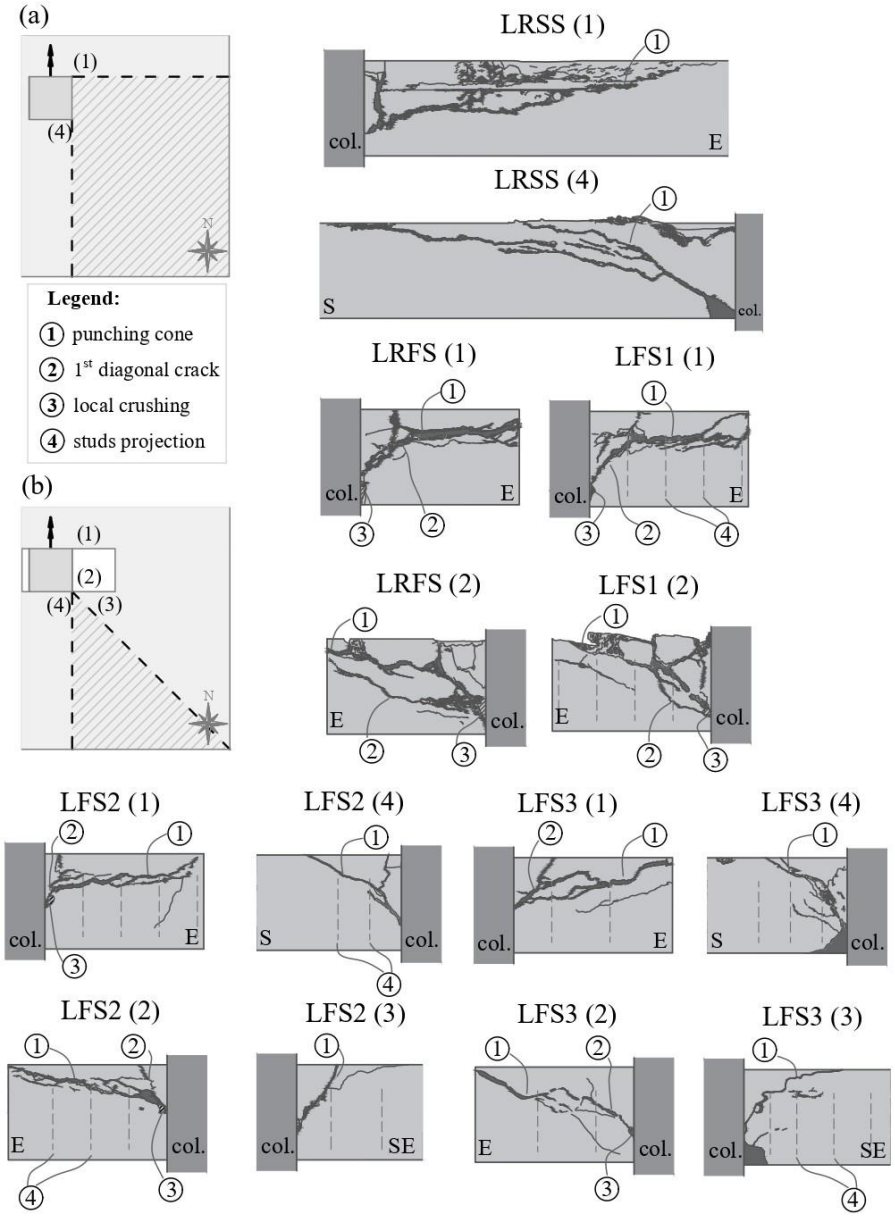

Figure 5.9 - Saw cuts and lateral views of specimens: (a) LRSS; and (b) LRFS, LFS1-S3

The presence of openings allowed also inspecting the cracking development during testing. It was possible to notice the appearance of a first diagonal crack at the opening sides, which was steeper for the slabs with shear reinforcement. Right before failure, it was observed that the top tangential crack at the punching cone propagated towards the supported corner of the openings. In some cases, it merged also with the diagonal cracks on the sides of the opening (LRFS and LFS1), that also propagated towards the supported corners. In other cases, the failure crack followed a different path from the inclined critical shear crack that had appeared

on the opening (LFS2 and LFS3). Local crushing of concrete was observed at failure for all specimens near to the column face. It can be noted that these observations are in agreement to previously reported manners in which a critical shear crack may develop and the possibility of the critical shear crack to fully or partly be coincident with the failure surface [35-36].

5.3.3 Strains on the concrete surface

The recorded surface strains on the concrete are shown in Figure 5.10 with respect to the distribution of strain gauges depicted in Figure 5.4. The radial strain gauges 1 and 2 positioned on the west side of the slab presented negligible strains and will not be discussed in the following.

In the region along the column axis, slab LFS3 exhibited higher radial strains compared to the other slabs (Figure 5.10a). Close to failure, the radial strains decreased or even turned positive, in agreement to the localisation of shear strains [31,36]. The trend for tangential strains was similar among all slabs with openings, with the lowest maximum strain observed in slab LRFS (Figure 5.9b). In the corner region of the column, slab LRSS displayed higher radial strains (Figure 5.9c), while the slabs with shear reinforcement demonstrated higher tangential strains compared to slabs without openings (Figure 5.9d). In the corner region of the opening, slabs LFS2 and LFS3 exhibited higher radial strains (Figure 5.9e), while the tangential strains were similar among all slabs (Figure 5.9f). On the east side of the opening, slab LRSS showed higher radial strain (Figure 5.9g), while the tangential strains were slightly higher in slabs LRFS and LFS3 (Figure 5.9h).

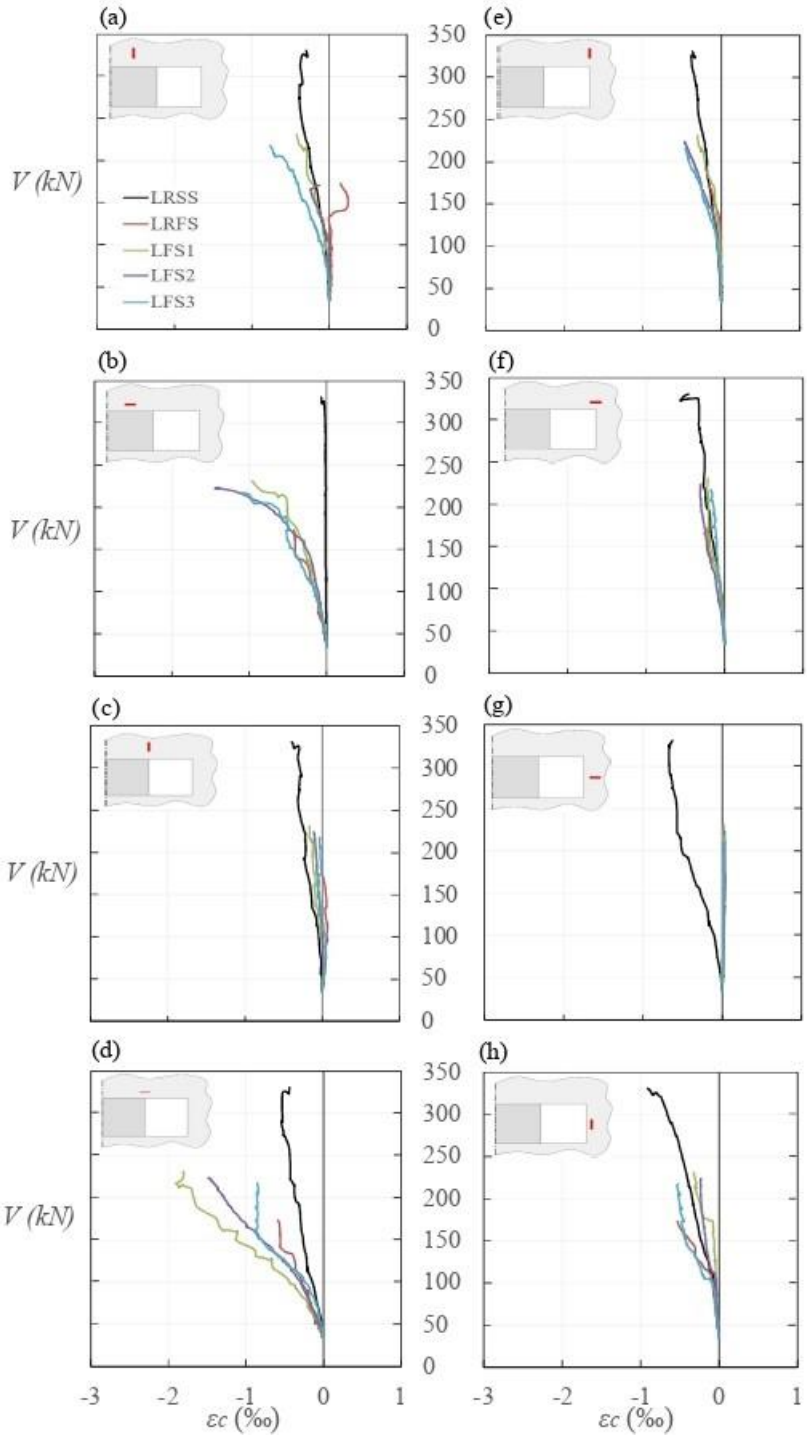

Figure 5.10 - Concrete strains: (a) EC03; (b) EC04; (c) EC05; (d) EC06; (e) EC07; (f); EC08; (g) EC09; and (h) EC10 (refer to Figure 5.4)

5.3.4 Activation of shear reinforcement

Figure 5.11 displays the load versus the ratio of recorded-to-yield strain for different shear reinforcement locations (the yield strain level was not reached in any of the instrumented studs). The activation of the shear reinforcement started first on the studs on the northeast column side (Figure 5.11a) towards the west side (Figure 5.11c), and later at the northeast opening region (Figure 5.11d), as expected following the regions of higher to lower stress. The activation of the second layer of the northeast stud started even later.

Figure 5.12 compares the strain levels in the shear reinforcement with their respective locations. In all three slabs, shear reinforcement strains reached a maximum of approximately 80% of the yield strain. In the first layer of shear reinforcement, the highest strain recorded occurred near to the northeast corner of the column for slabs LFS1 and LFS2, and along the north column axis for slab LFS3. In its turn, the second layer of LFS1 and LFS2 exhibited higher strains at the northeast corner of the column, and no significant difference in LFS3 was observed. The first layer displayed in all cases higher strains than in the second layer.

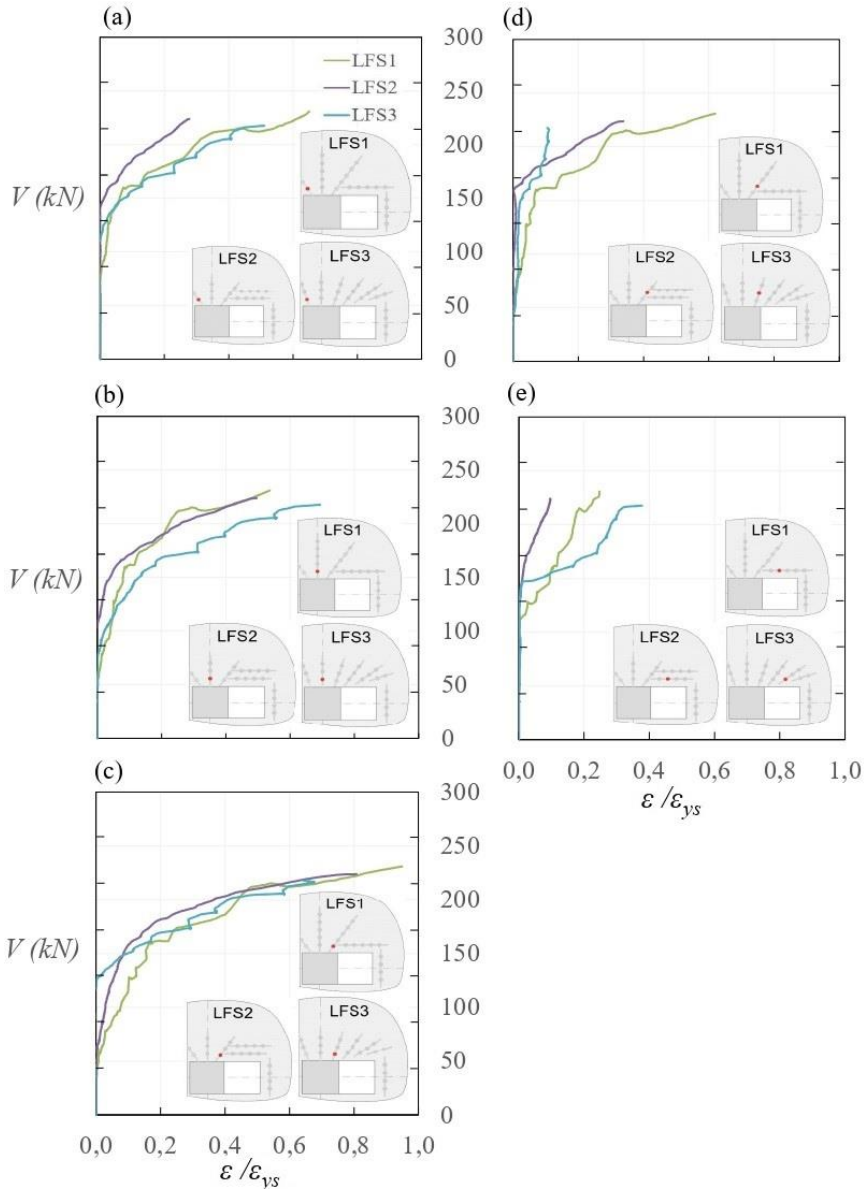

Figure 5.11 - Load-strain of shear reinforcement for different locations: (a) northwest (b) column north axis (c) northeast 1st layer (d) northeast 2nd layer (e) northeast opening region

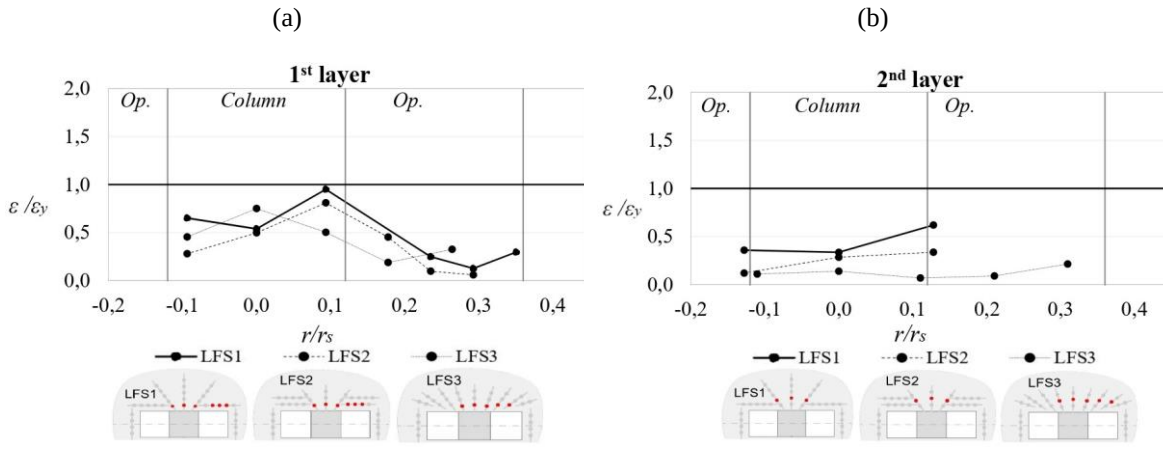

Figure 5.12 - Activation of shear reinforcement according to stud position: (a) 1st layer; and (b) 2nd layer

5.4 COMPARISON TO CODE PREDICTIONS

In this section, the experimental resistances of the various specimens are comparted to the predictions of codes of practice, including ACI 318:19 [32] and FprEN 1992-1-1:23 [33] as well as *fib*'s MC 2010:13 [34] with Level of Approximation (LoA) II. To that aim, the influence of the slabs will be considered in terms of presence of openings, moment transfer and shear-reinforcement. The formulations used for the different codes are provided in ANNEX A: CODE PROVISIONS. For comparison to tests, the characteristic values were replaced by mean values and all safety coefficients set to 1.0.

With respect to moment transfer, this effect is accounted for by increasing the action (ACI 318:19 or FprEN 1992-1-1:23) or by reducing the length of the control perimeter (MC2010). Concerning the influence of shear reinforcement, ACI 318:19 combines it with the concrete contribution of members without shear reinforcement, while FprEN 1992-1-1:23 and MC2010 reduce it (consistently with theoretical considerations on this issue [37]). All codes allow accounting for the presence of openings by modifying accordingly the length of the control perimeter, according to Figure A. 1 (refer to ANNEX A: CODE PROVISIONS).

Table 5.3 presents the ratio of experimental-to-theoretical resistance according to ACI 318:19, *fib*'s MC 2010 (LoA II), and FprEN 1992-1-1:23. All potential failure modes were checked in case of shear-reinforced slabs (comprising punching within the shear-reinforced region, crushing of concrete struts and punching outside of the shear-reinforced zone). In the analyses, the shear reinforcement contribution was determined by considering (according to the code recommendations) three studs parallel to each column face and one stud in each corner of the column, resulting in a total of 10 studs.

The results show that *fib*'s MC 2010 and the FprEN 1992-1-1:23, both based on the mechanical model of the Critical Shear Crack Theory (CSCT), provide more accurate estimates of resistance compared to the formulae of ACI 318:19 (with highest mean value

and coefficient of variation). The most reasonable estimates of the strength on the strength were, on average, provided by MC2010, whose scatter is however relatively high compared to other cases [38]. Concerning the FprEN1992-1-1:23, it depicted the lowest Coefficient of Variation (8%) but was rather safe on average. Despite both FprEN 1992-1-1:2023 and *fib*'s MC 2010 are based on the same mechanical model, the estimate of the concrete contribution to the punching resistance is higher in the present case for FprEN 1992-1-1:2023. Also, both codes present some differences when evaluating the maximum punching resistance (crushing of concrete struts), resulting into different failure modes and resistances as shown in Table 5.3.

On the basis of these results, it is observed that a mechanical model is required to better understand and to suitably account for the influence of the different phenomena implied. The CSCT (basis of *fib*'s MC2010) is identified as a promising tool, but where the design simplifications adopted for its LoA II may be refined. In particular, it is identified that the following aspects shall be incorporated in a consistent manner:

- Concentrations of shear stresses near openings [11]
- Consideration of the different response of the slab in its two main directions [39]

These issues will be discussed and addressed in the next section.

Table 5.3 - Comparison of experimental-to-calculated resistances according to codes of practice

Slab	**ACI 318:19**		***fib* MC 2010:13 (LoA II)**		**FprEN 1992-1-1:23**		**CSCT refined**	
	Failure	V_{test}/V_{calc}	**Failure**	V_{test}/V_{calc}	**Failure**	V_{test}/V_{calc}	**Failure**	V_{test}/V_{calc}
LRSS	V_c	1.31	V_c	1.41	V_c	1.19	V_c	0.95
LRFS	V_c	2.19	V_c	1.27	V_c	1.45	V_c	0.98
LFS1	V_{crush}	1.41	V_{within}	0.96	V_{crush}	1.18	V_{within}	0.97
LFS2	V_{crush}	1.65	V_{within}	1.01	V_{crush}	1.27	V_{within}	1.02
LFS3	V_{crush}	1.64	V_{within}	0.99	V_{crush}	1.24	V_{within}	1.00
	Av.	**1.64**		**1.13**		**1.27**		**0.98**
	CoV	**0.21**		**0.18**		**0.09**		**0.03**

5.5 A MECHANICAL APPROACH FOR PUNCHING DESIGN OF FLAT SLABS WITH OPENINGS AND UNBALANCED MOMENTS

In this section, the physics of the punching failures of slabs with openings and unbalanced moments is investigated in detail, considering the local development of the shear field and the various potentially governing failure modes. The aim of this section is to contribute towards a mechanical understanding of the phenomena implied, leading to a rational approach for its design. To that aim, the Critical Shear Crack Theory (CSCT) will be used in the following, as a basis to describe the failure criteria, activation of shear reinforcement and distribution of internal forces.

5.5.1 Mechanical background

The CSCT is a comprehensive theory describing failures in shear or punching shear where a localisation of strains occurs within a so-called Critical Shear Crack (CSC). The theory was originally developed for punching shear of members without shear reinforcement [31-40], but its principles were later successfully extended to shear of one-way slabs without shear reinforcement [41,42] and to punching of shear-reinforced members [43]. The theory has been adapted and verified to cover a large number of cases and was adopted for punching design recommendations, such as the *fib*'s MC2010 or FprEN1992-1-1:23 [44,45].

The mechanical model of the CSCT considers that the CSC (localizing the strains) governs the shear resistance. The two main parameters implied are the opening of the CSC (w) and the concrete properties (such as the concrete compressive resistance and crack roughness). Different refinements may be applied to estimate the opening of the CSC and the associated resistance. In its simplest form, the opening of the CSC is assumed to be correlated to the rotation of the slab (ψ) and its effective depth (d) [31]:

$$w \propto \psi \cdot d \tag{5. 1}$$

This simplified formula accounts actually for the fact that the opening of the CSC depends also on the column penetration (shear strains), but that this latter is correlated to the rotation

of the slab [41, 42]. On that basis, the capacity of concrete to transfer shear forces can be evaluated by direct integration of the shear-transfer components [35] or by means of a simplified failure criterion, accounting for their softening response with respect to the level of deformation (lower shear resistance associated to higher crack openings and lower crack roughness), see [31]:

$$\frac{V_R}{b_0 \cdot d_v \cdot \sqrt{f_c}} = \frac{3/4}{1+15\frac{\psi \cdot d}{d_{g0}+d_g}} \quad (5.2)$$

Where V_R stands for the shear resistance, b_0 for the length of the shear-resisting control perimeter, d_v for the shear-resisting effective depth (considering the penetration of the supported area), d_g for the maximum aggregate size and d_{g0} to a reference size (16 mm for ordinary concrete, see refined considerations for high-strength concrete in [45])

Within the CSCT, the contribution of shear reinforcement can also be accounted for, by considering the activation of the studs or stirrups as a function also of the crack opening [42]. In this case, several potential failure modes shall be checked, such as crushing of the concrete struts, failure within the shear-reinforced zone or failure outside of the shear-reinforced zone. It is of particular interest that the analyses based on the CSCT allow to determine the global response of a member, but also to investigate on its local response and redistributions of internal forces. This aspect is relevant for cases of non-axis-symmetric conditions, as those of members with elongated columns or non-symmetric reinforcement or loading conditions [39,46]. With this respect, Sagaseta et al. [39] proposed an approach based on the CSCT to consider a different response in sectors of the control perimeter (allowing also to investigate for potential redistributions of internal forces). Such approach will be adopted in the following to investigate the tests of the present experimental programme, together with the control perimeter suggested by Santos et al. [11] for slabs with openings adjacent to column faces.

5.5.2 Shear field analysis

The transfer of a moment from the slab to the column leads to concentrations in the shear field of a flat slab. For instance, Figure 5.12a shows the elastic distribution of shear forces for specimen LRSS at the basic control perimeter considered by the CSCT (at $0.5d_v$ from the column edge). The concentration of shear forces is usually taken into account by considering a reduced shear-resisting control perimeter whose length is calculated as Eq. (5. 3) [34].

$$b_0 = \frac{V}{v_{perp,max}} \tag{5. 3}$$

Where $v_{perp,\max}$ refers to the maximum value of the shear force projected in the direction perpendicular to the control perimeter. This consideration for the length of the control perimeter is in fact equal to assuming the maximum unitary shear force acting along the reduced shear-resisting control perimeter.

The presence of openings, as investigated in this paper, increases the peak value of the shear forces, see for instance the elastic shear forces shown in Figure 5.12b for specimen LRFS (considering the basic control perimeter defined by Santos et al. [11]). As it can be noted, the peak value raises to 1.7 times that of a slab without openings, reducing the length of the shear-resisting control perimeter (according to Eq. ((5. 3)) and thus the punching resistance (according to Eq. (5. 2)).

In Figure 5.12a,b, it is also shown the distribution of shear forces along the control perimeter considering four sectors as proposed by Sagaseta et al. [39]. It may be noted that in some sectors the shear field enters in the perimeter (positive values), while in others, it exits the perimeter (negative values). The negative values (in the tension side of the column) are due to the moment transfer, which actually increase the shear force at the shear-critical regions of the perimeter (those with highest shear forces). The methodology of Sagaseta et al. [39] considering different sectors allows considering the actual action and resistance potentially

developing in a local manner. This approach can consequently be used to examine potential softening of some sectors, although this effect is usually limited and may be neglected as a safe estimate [39].

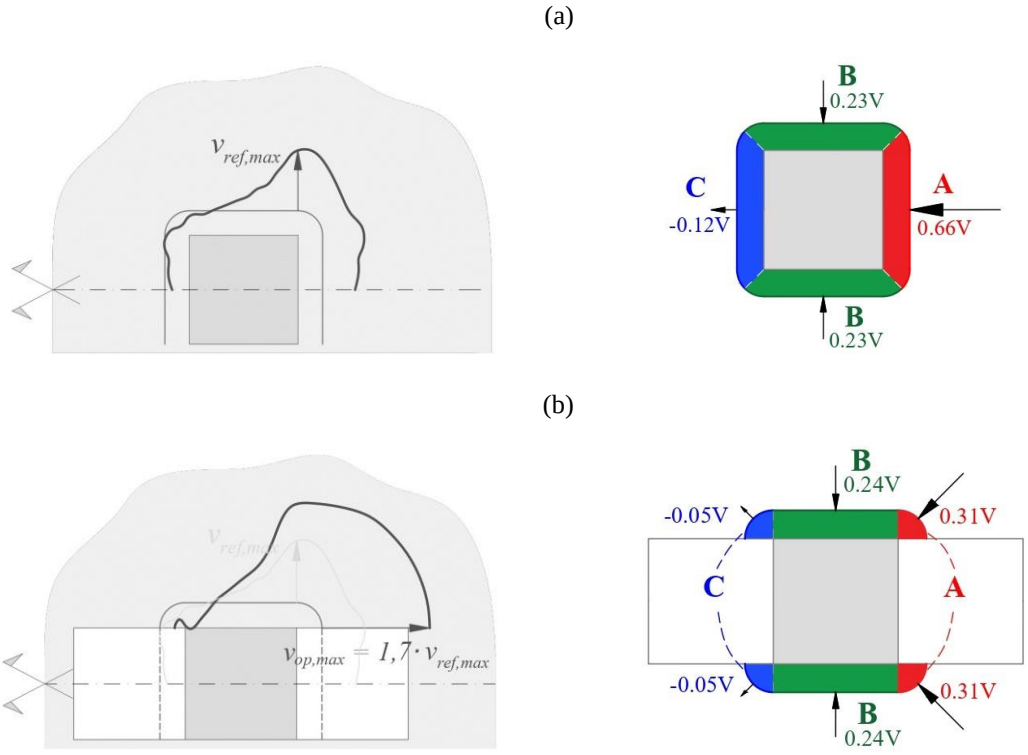

Figure 5.13 - Shear force distribution along the control perimeter of slabs with moment transfer: (a) slab without openings; and (b) slab with openings

According to the approach based on sectors, the total shear resistance (V_R) may be calculated by adding the shear force acting at the different sectors of the control perimeter. Considering to that aim the sectors A, B and C indicated in Figure 5.12, the contributions result in each sector result:

$$V_A = \int_{b_{1,A}} v_{perp} \cdot ds = \lambda_A \cdot V \tag{5. 4}$$

$$V_B = \int_{b_{1,B}} v_{perp} \cdot ds = \lambda_B \cdot V \tag{5. 5}$$

$$V_C = \int_{b_{1,C}} v_{perp} \cdot ds = \lambda_C \cdot V \tag{5. 6}$$

Where $b_{1,A}$, $b_{1,B}$ and $b_{1,C}$ stand for the basic control perimeter of sectors A, B and C respectively (refer to the control perimeters defined in Figure 5.12).

In the present case, two governing cases may occur: failure at sector A or B (sector C is not governing for the investigated range of eccentricities). For instance, in case the sector A is governing, $V_{R,A}$ refers to the punching resistance of the A-sector while V_B and V_C refer to the shear forces acting at that moment in the B- and C-sectors respectively. Conversely, if the sector B is governing, the terms $V_{R,B}$ and V_A, V_C will apply as shown in Eq. (5. 7).

$$V_R = min \begin{cases} V_{R,A} + V_B + V_C \\ V_A + V_{R,B} + V_C \end{cases} \quad (5.\ 7)$$

The terms $V_{R,A}$ and $V_{R,B}$ (shear strengths along sectors A and B respectively) are calculated using the failure criteria of the CSCT (as explained later) and the terms V_A, V_B and V_C (simultaneous components) are estimated on the basis of an elastic distribution of the shear field (Eqs. (4-6)). For instance, assuming that sector "*I*" is governing, the corresponding shear force at sector "*J*" will result in Eq. (5. 8).

$$V_J = \frac{\lambda_J}{\lambda_I} \cdot V_{R,I} \quad (5.\ 8)$$

It shall be noted that this approach does not consider any potential redistribution of shear stresses in the sectors of the control perimeter at failure. This consideration is safe as redistributions in the internal forces have the potential to increase the resistance (although such influence is typically limited in most cases [39]).

5.5.3 Failure criteria

In order to calculate the resistance at each sector, the following failure criteria will be considered:

5.5.3.1 Slabs without shear reinforcement

For slabs LRSS and LRFS, the resistance of each sector is only governed by the contribution of concrete, which will be evaluated in the following using Eq. (5. 2).

5.5.3.2 Slabs with shear reinforcement

When shear reinforcement is provided, three failure modes may govern [43]: crushing of the concrete struts, failure within the shear reinforced zone and failure outside the shear-reinforced zone. When failure occurs by development of a CSC within the shear-reinforced zone, the shear reinforcement shall be accounted for in addition to the concrete contribution (Eq. ((5. 2)). In the following, this will be performed by considering *fib*'s MC 2010 [34] recommendations, as given in Eqs. (9-10).

$$V_{R,s} = \Sigma A_{sw} k_e \sigma_{sw} \tag{5. 9}$$

$$\sigma_{sw} = \frac{E_s \psi}{6}\left(1 + \frac{f_b}{f_{yw}}\frac{d}{\emptyset_w}\right) \leq f_{yw} \tag{5. 10}$$

Where A_{sw} refers typically to the cross-sectional area of shear reinforcement located between $0.35d_v$ and d_v. In the present case, the stud arrangement is not perfectly radial or uniform. Thus, the number of effective studs is determined according to Muttoni et al. [47] in Eq. (5. 11):

$$A_{sw} = n_r \cdot (d/s) \cdot A_{\emptyset} \tag{5. 11}$$

Concerning crushing of the concrete struts, its resistance depends on the state of cracking and, as suggested in [43], it will be evaluated proportional to the contribution of concrete, as given in Eq. (5. 12).

The value of parameter k_{sys} depends upon the detailing rules and confinement conditions [48]. In absence of specific data, the value typically adopted for studs in inner slab-column connections k_{sys} = 2.8 [34] will be adopted in the following.

$$V_{R,max} = k_{sys} \cdot V_c \quad (5.\ 12)$$

5.5.4 Comparison with test results and discussion

The results following this methodology are shown in Figure 5.14 for slabs LRSS and LRFS without shear reinforcement and for slab LFS2 with shear reinforcement. The Figure shows the load-rotation relationship (estimated following the LoA II of the *fib*'s MC2010) and the governing failure criteria for directions *A* and *B* (the shear contribution in the other sectors was estimated using the elastic distribution according to Eq. (5. 7)). For slab LRSS, failure is governed by the concrete resistance in sector B. For slab LRFS, failure is governed by the concrete resistance in sector A, while for slabs LFS1-S3 failure is governed by the shear-reinforced zone in sector A.

The results show overall good agreement between the experimental results and the theoretical approach of the CSCT. It is particularly interesting to note also that the level of deformation in the shear studs seem well-captured. As shown in Fig. 15c, the studs at failure are not at yielding and remain at approximately 70% of their yield strain, which is in fine agreement to the experimental measurements shown in section 3. Table 5.3 compares the results of the proposed approach and the failure loads of the tests. When compared to the previous design models, it can be observed a significant improvement in terms of accuracy and scatter (lower Coefficient of Variation), showing the consistency of the CSCT approach.

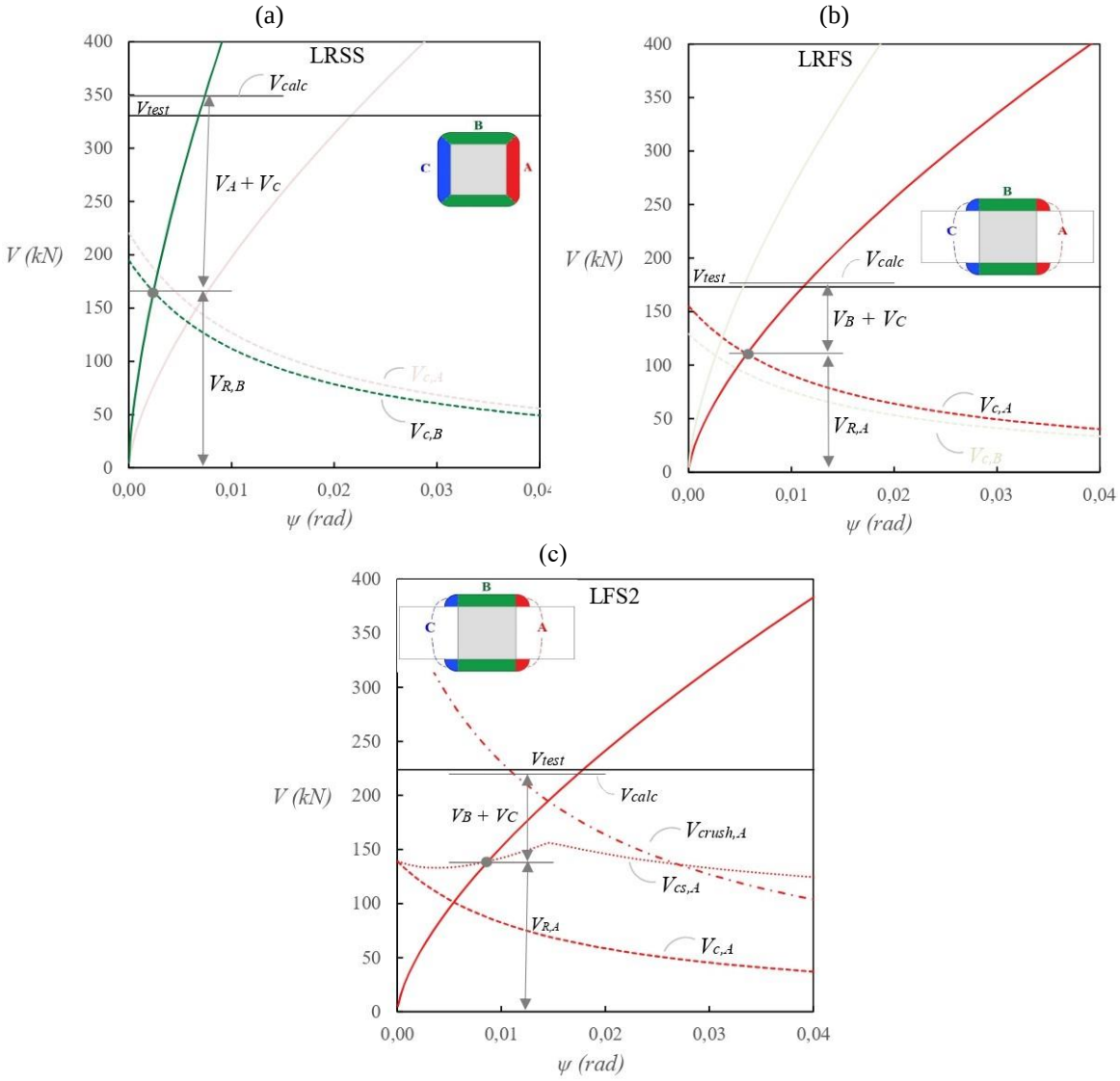

Figure 5.14 - Punching shear resistance approach according to the CSCT [39] adapted for slabs with openings and unbalanced moments: (a) LRSS, (b) LRFS and (c) LFS2

5.6 CONCLUSIONS

This paper investigates on the punching shear resistance of slab-column connections with moment transfer and shear reinforcement. The phenomenon is investigated by means of an experimental programme as well as a mechanical model developed on the basis of the CSCT. The main conclusions of this investigation are summarized below:

1. The presence of openings adjacent to columns reduces significantly the punching strength. This is the consequence of various effects, such as the reduction of shear-resisting perimeter and concentration of shear forces

2. Arranging shear reinforcement close to the openings is an efficient manner to enhance the resistance and deformation capacity;
3. For the investigated geometry, despite the fact that the openings develop fully at two sides of the columns, there is a significant amount of shear force entering in the corner regions. This is confirmed by means of analysis of the shear field and also by the location of the failure region;
4. Current design codes (such as ACI 318-19, *fib*'s MC2010 or FprEN1992-1-1:2023) provide relatively scattered or safe predictions of the punching resistance of this detail. It is observed that the comparison of strength is less accurate than for other cases (such as members without openings);
5. The Critical Shear Crack Theory provides a suitable frame for analysis of the punching resistance of this case, with accurate estimates of the strength and a low Coefficient of Variation. To that aim, different sectors may be considered in the control perimeter. One sector may reach its failure condition, while others not, allowing for potential redistributions of internal forces. This phenomenon may however be neglected as a safe estimate of the resistance but with sufficient accuracy;
6. The CSCT allows detecting the location of the governing region within the control perimeter. Also, the values of the stresses in the shear reinforcement are estimated in a consistent manner when compared to the test results.

5.7 REFERENCES

1. HERNÁNDEZ FRAILE, D.; SETIAWAN, A.; SANTOS J.B. MUTTONI, A. *Punching Tests on Edge Slab-Column Connections With Refined Measurements.* Engineering Structures, Elsevier, Vol. 288, 2023, pp. 1-24. doi.org/10.1016/j.engstruct.2023.116166
2. MOE J. *Shearing strength of reinforced concrete slabs and footing under concentrated loads.* Development department bulletin D47, Portland Cement Association, 1961. pp 135.

3. TENG S.; CHEONG H.K.; KUANG K.L.; GENG J.Z. *Punching shear strength of slabs with openings and supported on rectangular columns*. ACI Structural Journal, 2004, V. 101, pp. 678–87.
4. AUGUSTIN T.; FILLO L.; HALVONIK, J. *Punching resistance of slab-column connections with openings*. Structural Concrete. 2019, pp. 1–13. doi.org/10.1002/suco.201900158
5. KORMOŠOVÁ L.; HALVONIK J.; *Punching shear behavior of flat slabs supported by elongated columns with openings*. Structural Concrete, 2023, pp. 1–21. doi.org/10.1002/suco.202200450
6. ANIL Ö.; KINA T.; SALMANI V. *Effect of opening size and location on punching shear behaviour of two-way RC slabs*. Magazine of Concrete Research, Vol. 66, n°18, 2014, pp. 955-966. doi.org/10.1680/macr.14.00042
7. LIBERATI E.A. P.; MARQUES M.G.; LEONEL E.D.; ALMEIDA L.C.; TRAUTWEIN L.M. *Failure analysis of punching in reinforced concrete flat slabs with openings adjacent to the column*. Engineering Structures, Elsevier, Vol. 182, 2019, pp. 331-343. doi.org/10.1016/j.engstruct.2018.11.073
8. LOURENÇO D.S.; LIBERATI E.A. P.; MARQUES M.G.; ALMEIDA L.C.; TRAUTWEIN L. M. *Reinforced concrete flat slabs with openings at different distances from the column*. IBRACON Structures and Materials Journal, Vol. 14, 2021. doi.org/10.1590/S1983-41952021000100011
9. SANTOS J.B.; SOUZA R.M.; MELO G.S.; GOMES R.B. *Punching resistance of flat slabs with openings adjacent to the columns*. ACI Structural Journal, Vol. 119, 2022, pp. 41-53. doi: 10.14359/51734216
10. EL-SHAFIEY, T.F.; ATTA, A. M.; HASSAN, A.; ELNASHARTY, M. *Effect of opening shape, size and location on the punching shear behaviour of RC flat slabs*.

Engineering Structures, Elsevier, Vol. 44, 2022, pp. 1138-1151. doi.org/10.1016/j.istruc.2022.08.076

11. SANTOS J. B.; MUTTONI A.; MELO G. S. *Enhancement of the punching shear verification of slabs with openings*. Structural Concrete, 18 p., 2022. dx.doi.org/10.1002/suco.202200714
12. REGAN, P. E. *Punching Tests of Reinforced Concrete Slabs with and without shear reinforcement with openings adjacent to columns*. School of the Built Environment, University of Westminster, London, 1999.
13. BORGES L. L. J.; MELO G. S.; GOMES R. B. *Punching shear of reinforced concrete flat plates with openings*. ACI Structural Journal, Vol. 110, 2013, pp. 547-556.
14. MÜLLER F.; MUTTONI A.; THÜRLIMANN B.; *Durchstanzversuche an Flachdecken mit Aussparungen*. Institut für Baustatik und Konstruktion, ETH Zürich, n° 7305-5 ISBN 3-7643-1686-1, 1984. *(In German)*
15. GOMES, R. B.; ANDRADE, M. A. S. *Punching in Reinforced Concrete Flat Slabs With Holes*. Civil-Comp Press, Edinburgh, UK, 1995, pp. 185-193.
16. SOUZA R.M, *Punção em lajes cogumelo de concreto armado com furos adjacentes ou distantes de um pilar interno*. Dissertação de Mestrado, Faculdade de Tecnologia, Departamento de Engenharia Civil e Ambiental, Universidade de Brasília, 2004. pp 171. (*In Portuguese*)
17. MARQUES M.G.; LIBERATI E.A.P.; GOMES, R.B.; ALMEIDA L.C.; TRAUTWEIN L.M. *Study of Failure Mode of Reinforced Concrete Flat Slabs with Openings and Studs*. ACI Structural Journal, Vol. 117, 2020, pp. 39-48 (Title no. 117-S75). doi: 10.14359/51723518
18. MARQUES M. G.; LIBERATI E. A. P.; GOMES, R. B.; CARVALHO, A. L.; TRAUTWEIN L. M. *Punching Shear Strength Model for Reinforced Concrete Flat*

Slabs with Openings. J. Struct. Eng. Vol. 147(7), 2020, pp. 01-16 (Title no. 117-S75). doi: 10.1061/(ASCE)ST.1943-541X.0003043

19. HANSON, N. W.; HANSON, J. M. *Shear and Moment Transfer Between Concrete Slabs and Columns*. Journal PCA Research and Development Laboratories, Vol. 10, 1968, pp. 2-16.
20. OLIVEIRA, D. C.; GOMES, R. B.; MELO, G. S. *Punching shear in reinforced concrete flat slabs with hole adjacent to the column and moment transfer*. IBRACON Structures and Material Journal, 2014, Vol. 7, pp. 1983-4195.
21. BURSAĆ, S.; BEŠEVIĆ, M.; PURČAR, M.V.; KOZARIĆ, L.; ĐURIĆ, N. *Experimental analysis of punching shear strength of eccentrically loaded slab with the opening along the face of the internal column*. Engineering Structures, Elsevier, Vol. 249, 2021, 113359. doi.org/10.1016/j.engstruct.2021.113359
22. SANTOS J. B.; SOUZA R. M.; MELO G. S.; GOMES R. B. *Investigating Punching Shear in Slabs With Unbalanced Moments and Openings.* Engineering Structures, Elsevier, 2023. (*Under Review*)
23. LIPS, S.; FERNÁNDEZ RUIZ, M.; MUTTONI, A. *Experimental investigation on the punching strength and the deformation capacity of shear-reinforced slabs*. American Concrete Institute, Structural Journal, Vol. 109, No. 6, 2012, pp. 889-900. doi: 10.14359/51684132
24. BALOMENOS, G.P.; GENIKOMSOU, A.S.; POLAK, M.A. *Investigation of the effect of openings of interior reinforced concrete flat slab*. Structural Concrete, Wiley, 2018, Vol. 19, pp. 1672–1681. doi.org/10.1002/suco.201700201
25. GENIKOMSOU, A.S.; POLAK, M.A. *Finite-Element Analysis of Reinforced Concrete Slabs with Punching Shear Reinforcement.* American Society of Civil Engineers, 2017. doi: 10.14359/51689871

26. MOSTOFINEJADA, D.; JAFARIANA, N.; NADERIA, A.; MOSTOFINEJAD, A.; SALEHIA, M. *Effects of openings on the punching shear strength of reinforced concrete slabs.* Engineering Structures, Elsevier, 2020. doi.org/10.1016/j.istruc.2020.03.061
27. ŽIVKOVIĆ, S.; BEŠEVIĆ, M.; PURČAR, M. V.; KOZARIĆ, L. *Nonlinear Finite Element Analysis of Punching Shear Strength of Eccentrically Loaded RC Flat Slabs with Opening.* KSCE Journal of Civil Engineering, Vol. 23, 2019, pp. 4771–4780. doi.org/10.1007/s12205-019-0075-5
28. ALROUSAN, R.Z.; ALNEMRAWI, B.R. *The influence of concrete compressive strength on the punching shear capacity of reinforced concrete flat slabs under different opening configurations and loading conditions*. Engineering Structures, Elsevier, Vol. 44, 2022, pp. 101-119. doi.org/10.1016/j.istruc.2022.07.091
29. ISMAIL E-S. I. M. *Nonlinear finite element analysis of reinforced concrete flat plates with opening adjacent to column under eccentric punching loads*. Housing and Building National Research Center Journal, 2018, V. 14, pp. 438–449. doi.org/10.1016/j.hbrcj.2018.01.001
30. ALROUSAN, R.Z.; ALNEMRAWI, B.R. *Punching shear code provisions examination against the creation of an opening in existed RC flat slab of various sizes and locations*. Engineering Structures, Elsevier, Vol. 49, 2023, pp. 875-888. doi.org/10.1016/j.istruc.2023.02.007
31. MUTTONI A. *Punching shear strength of reinforced concrete slabs without transverse reinforcement.* ACI Structural Journal, V. 105, No 4, 2008, pp. 440–50.
32. ACI Committee 318. *Building code requirements for structural concrete (ACI 318-19) and commentary (318R-19).* American Concrete Institute, Farmington Hills, MI, 2019, pp 623.

33. FprEN 1992-1-1:23. Eurocode 2-Design of concrete structures- Part 1-1: *General rules, rules for buildings, bridges and civil engineering structures*. Stable version of the draft of the 2nd generation of prEN 1992-1-1:23, CEN, Brussels, Belgium, 2023, pp 405.
34. Fédération internationale du béton. *Fib Model Code for Concrete Structures 2010 (MC2010). fib* , Lausanne, Switzerland, 2013, pp 390.
35. SIMÕES J.T.; FERNÁNDEZ RUIZ M.; MUTTONI A. *Validation of the Critical Shear Crack Theory for punching of slabs without transverse reinforcement by means of a refined mechanical model*. Structural Concrete, Vol. 19, pp. 191-216, 2018. dx.doi.org/10.1002/suco.201700280
36. EINPAUL J.; FERNÁNDEZ RUIZ M.; MUTTONI A. *Measurements of internal cracking in punching test slabs without shear reinforcement*. Magazine of Concrete Research, 13 p., 2017. doi.org/10.1680/jmacr.16.00099
37. MUTTONI A.; FERNÁNDEZ RUIZ M. *The levels-of-approximation approach in MC 2010: application to punching shear provisions*. Structural Concrete, Wiley, Vol. 13, 2012. doi: 10.1002/suco.201100032
38. SIGRIST, V.; BENTZ, E.; FERNÁNDEZ RUIZ, M.; FOSTER, S.; MUTTONI, A. *Background to the fib Model Code 2010 shear provisions – part I: beams and slabs*. Structural Concrete, Wiley, Vol. 14, No 3, 2013. doi: 10.1002/suco.201200066
39. SAGASETA J.; MUTTONI A.; FERNÁNDEZ RUIZ M.; TASSINARI L., *Non-axis-symmetrical punching shear around of RC slabs without transverse reinforcement.* Mag Concr Res, 2011, Vol. 63, pp. 441–57. doi.org/10.1680/macr.10.00098
40. MUTTONI A.; SCHWARTZ J. *Behaviour of beams and punching in slabs without shear reinforcement.* IABSE Colloquium, Vol. 62, Zurich, Switzerland; 1991, pp. 703–708.

41. MUTTONI, A.; FERNÁNDEZ RUIZ, M. *Shear strength of members without transverse reinforcement as function of critical shear crack width*. American Concrete Institute, Structural Journal, Vol. 105, No. 2, 2008, pp. 163-172.
42. CAVAGNIS, F.; SIMÕES, J. T.; FERNÁNDEZ RUIZ, M.; MUTTONI, A. *Shear strength of members without transverse reinforcement based on development of critical shear crack*. American Concrete Institute, Structural Journal, Vol. 117, No. 1, 2020, pp. 103-118. doi: 10.14359/51718012
43. FERNÁNDEZ RUIZ, M.; MUTTONI A. *Applications of Critical Shear Crack Theory to Punching of Reinforced Concrete Slabs with Transverse Reinforcement*. ACI Struct Journal, Vol. 106, No 46, 2009, pp. 485–94.
44. MUTTONI, A.; FERNÁNDEZ RUIZ, M. *From experimental evidence to mechanical modelling and design expressions: the Critical Shear Crack Theory for shear design.* Structural Concrete, Wiley, Vol. 20, 2019, pp. 1464-1480. doi.org/10.1002/suco.201900193
45. MUTTONI, A.; SIMÕES, J. T.; FARIA, D. M. V.; FERNÁNDEZ RUIZ, M. *A mechanical approach for the punching shear provisions in the second generation of Eurocode 2*. Hormigón y Acero, ACHE, Madrid, Spain, in press (doi.org/10.33586/hya.2022.3091)
46. SAGASETA J.; TASSINARI L.; FERNÁNDEZ RUIZ M.; MUTTONI A. *Punching of flat slabs supported on rectangular columns.* Engineering Structures, Elsevier, Vol. 77, 2014, pp. 17-33. doi.org/10.1016/j.engstruct.2014.07.007
47. MUTTONI, A.; FERNÁNDEZ RUIZ, M.; BENTZ, E.; FOSTER, S.; SIGRIST, V., *Background to the fib Model Code 2010 shear provisions – part II: punching shear*. Structural Concrete, Wiley, Vol. 14, No 3, 2013. doi: 10.1002/suco.201200064

48. HERNÁNDEZ-FRAILE, D.; SIMÕES, J.T.; FERNÁNDEZ RUIZ, M.; MUTTONI, A. *A mechanical approach for the maximum punching resistance of shear-reinforced slab-column connections*. fib Symposium, Lisbon, Portugal, 14-16 June, 2021, 10 p.
49. LimitState products. *LimitState: slab*. Version 2.3. University of Sheffield. www.limitstate.com/slab

5.8 ANNEX A: FLEXURAL STRENGTH

The yield-line method can be used to estimate the flexural strength of the slab specimens subjected to non-axis-symmetric loading, as depicted in Figure 5.15. The governing yield line was initially identified using the yield line software LimitState [49], and subsequently, the flexural strength V_{flex} (Eq. (5. 13) and (5. 14)) was derived analytically.

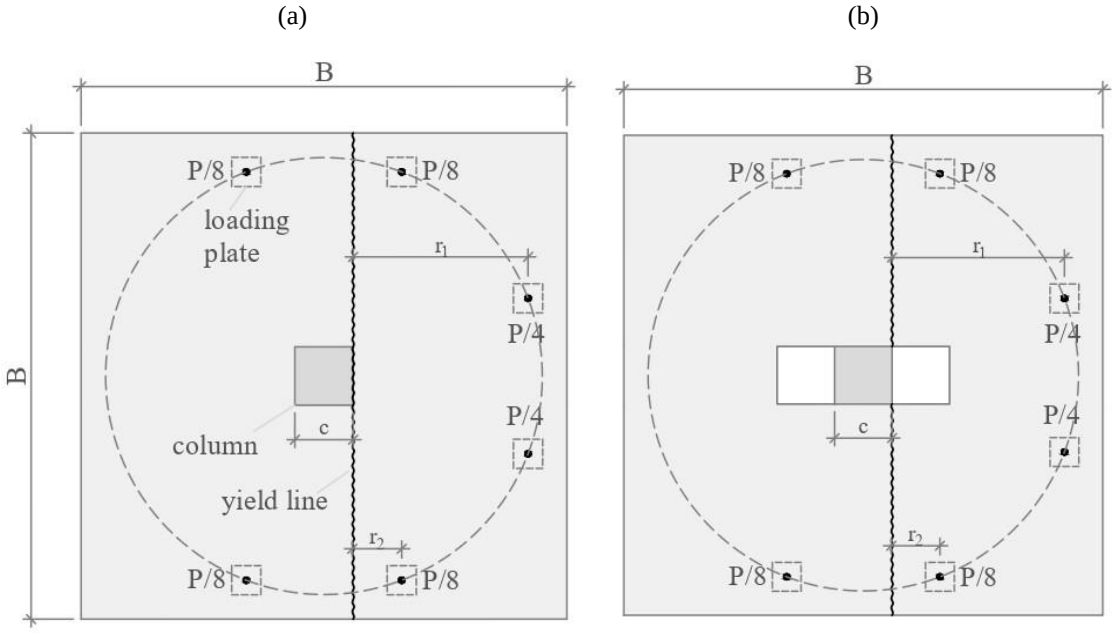

$$V_{flex} = \frac{m_R \cdot B}{r_1/4 + r_2/2} \qquad (5.\ 13)$$

$$V_{flex} = \frac{m_R \cdot (B-c)}{r_1/4 + r_2/2} \qquad (5.\ 14)$$

Figure 5.15 - Governing yield-line pattern: (a) LRSS (b) LRFS, LFS1-S3

5.9 ANNEX B: EXPERIMENTAL DATA

A few specific load steps were chosen to present the experimental results. The results of rotations were shown in Table 5.4 to Table 5.8. The instrumentation of flexural rebars is shown in Figure 5.16 and Figure 5.17. The results of flexural strains were shown in Figure 5.18 . The instrumentation of shear reinforcement is shown in Figure 5.19. The results of shear reinforcement strains were shown in Table 5.9 to Table 5.11.

Table 5.4 – Slab LRSS: results of rotations

LRSS			
V (kN)	**ψ_E**	**ψ_W**	**ψ_N**
0,0	0,0000	0,0000	0,0000
50,8	0,0003	-0,0001	0,0001
60,7	0,0005	-0,0002	0,0002
70,2	0,0009	-0,0003	0,0004
80,3	0,0011	-0,0004	0,0005
90,2	0,0014	-0,0004	0,0007
100,5	0,0018	-0,0005	0,0009
110,4	0,0024	-0,0007	0,0011
120,9	0,0028	-0,0008	0,0015
130,9	0,0030	-0,0008	0,0016
140,9	0,0037	-0,0010	0,0018
150,1	0,0043	-0,0011	0,0023
160,5	0,0051	-0,0013	0,0028
170,8	0,0056	-0,0014	0,0030
180,9	0,0060	-0,0015	0,0032
190,3	0,0065	-0,0016	0,0034
200,2	0,0085	-0,0023	0,0036
210,8	0,0089	-0,0024	0,0043
220,3	0,0100	-0,0028	0,0050
230,5	0,0106	-0,0030	0,0050
240,7	0,0108	-0,0030	0,0050
251,1	0,0110	-0,0030	0,0051
261,7	0,0115	-0,0031	0,0052
271,2	0,0126	-0,0035	0,0057
280,2	0,0138	-0,0040	0,0065
290,5	0,0149	-0,0046	0,0071
301,0	0,0165	-0,0053	0,0071
310,9	0,0170	-0,0055	0,0070
319,9	0,0176	-0,0057	0,0074
321,2	0,0176	-0,0057	0,0075
330,8	0,0216	-0,0080	0,0093

Table 5.5 - Slab LRFS: results of rotations

LRFS			
V (kN)	**ψ_E**	**ψ_W**	**ψ_N**
0,0	0,0000	0,0000	0,0000
40,1	0,0002	-0,0001	0,0000
50,1	0,0004	-0,0002	0,0001
60,7	0,0007	-0,0004	0,0002
70,6	0,0013	-0,0008	0,0004
80,7	0,0015	-0,0009	0,0006
90,1	0,0018	-0,0010	0,0006
100,1	0,0026	-0,0016	0,0013
110,1	0,0033	-0,0020	0,0018
120,9	0,0042	-0,0024	0,0027
130,5	0,0047	-0,0027	0,0033
140,5	0,0077	-0,0042	0,0047
170,2	0,0086	-0,0045	0,0055
173,1	0,0089	-0,0046	0,0057

Table 5.6 - Slab LFS1: results of rotations

LFS1			
V (kN)	**ψ_E**	**ψ_W**	**ψ_N**
0,0	0,0000	0,0000	0,0000
40,6	0,0000	-0,0001	0,0000
50,4	0,0000	-0,0001	0,0002
60,8	0,0000	-0,0002	0,0002
70,2	0,0000	-0,0004	0,0002
80,1	0,0000	-0,0004	0,0003
90,4	0,0001	-0,0006	0,0004
100,4	0,0007	-0,0008	0,0006
110,2	0,0014	-0,0009	0,0008
120,4	0,0024	-0,0011	0,0010
130,6	0,0039	-0,0014	0,0010
140,3	0,0045	-0,0015	0,0016
150,7	0,0063	-0,0018	0,0017
160,3	0,0067	-0,0019	0,0020
170,1	0,0086	-0,0024	0,0022
180,5	0,0101	-0,0028	0,0029
190,1	0,0120	-0,0034	0,0034
202,2	0,0128	-0,0036	0,0034
211,1	0,0134	-0,0037	0,0035
220,4	0,0192	-0,0063	0,0047
231,0	0,0204	-0,0069	0,0052

Table 5.7 - Slab LFS2: results of rotations

LFS2			
V (kN)	**ψ_E**	**ψ_W**	**ψ_N**
0,0	0,0000	0,0000	0,0000
40,1	0,0001	0,0000	0,0001
50,0	0,0007	-0,0002	0,0002
60,1	0,0012	-0,0004	0,0004
70,3	0,0034	-0,0015	0,0006
80,4	0,0039	-0,0017	0,0008
90,3	0,0068	-0,0032	0,0011
100,1	0,0075	-0,0035	0,0013
110,2	0,0085	-0,0039	0,0017
120,0	0,0094	-0,0043	0,0023
130,0	0,0105	-0,0048	0,0029
140,0	0,0119	-0,0054	0,0036
150,0	0,0135	-0,0062	0,0045
160,4	0,0148	-0,0067	0,0050
170,3	0,0166	-0,0075	0,0057
180,3	0,0185	-0,0083	0,0063
190,7	0,0208	-0,0094	0,0070
200,0	0,0234	-0,0108	0,0078
210,0	0,0269	-0,0129	0,0087
220,0	0,0314	-0,0161	0,0099
223,8	0,0344	-0,0183	0,0106

Table 5.8 - Slab LFS3: results of rotations

LFS3			
V (kN)	**ψ_E**	**ψ_W**	**ψ_N**
0,0	0,0000	0,0000	0,0000
40,0	0,0000	-0,0001	0,0000
50,9	0,0000	-0,0003	0,0002
60,1	0,0000	-0,0008	0,0004
70,4	0,0000	-0,0008	0,0006
80,6	0,0001	-0,0011	0,0007
90,1	0,0008	-0,0017	0,0010
100,0	0,0017	-0,0023	0,0013
110,1	0,0026	-0,0027	0,0019
120,1	0,0043	-0,0036	0,0026
130,1	0,0057	-0,0042	0,0031
140,0	0,0073	-0,0049	0,0036
150,1	0,0088	-0,0057	0,0042
160,8	0,0119	-0,0072	0,0051
170,7	0,0126	-0,0074	0,0057
180,2	0,0167	-0,0098	0,0068
190,1	0,0200	-0,0117	0,0074
200,0	0,0213	-0,0122	0,0078
210,0	0,0258	-0,0153	0,0090
217,5	0,0285	-0,0170	0,0094

Figure 5.16 – LRSS: instrumentation of flexural rebars

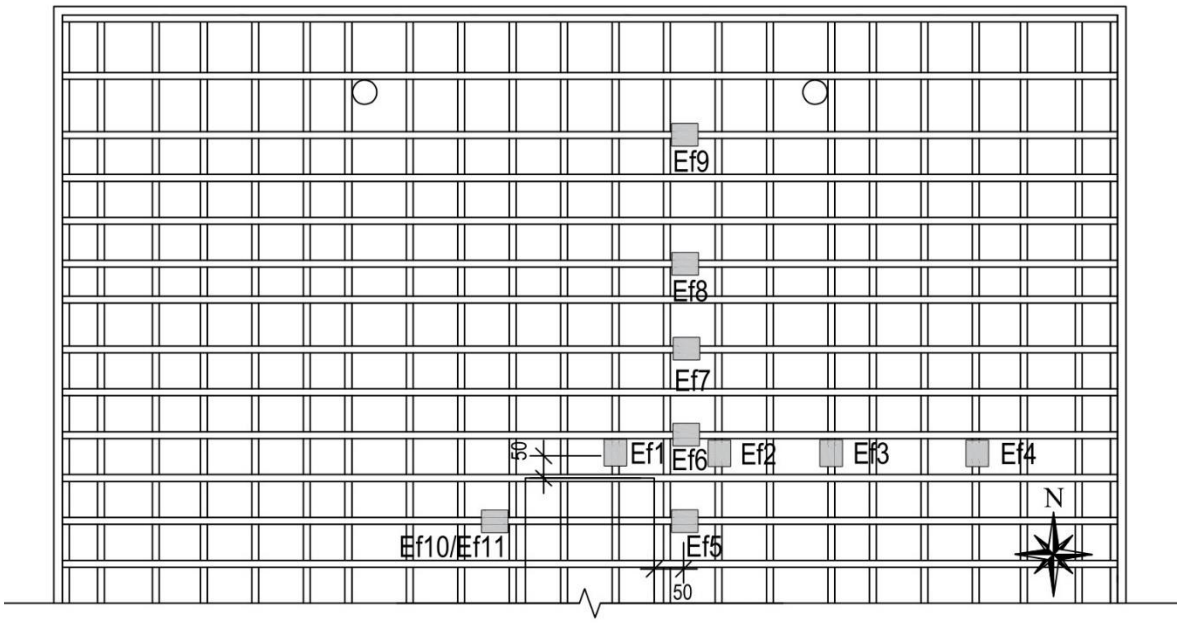

Figure 5.17 – LRFS: instrumentation of flexural rebars

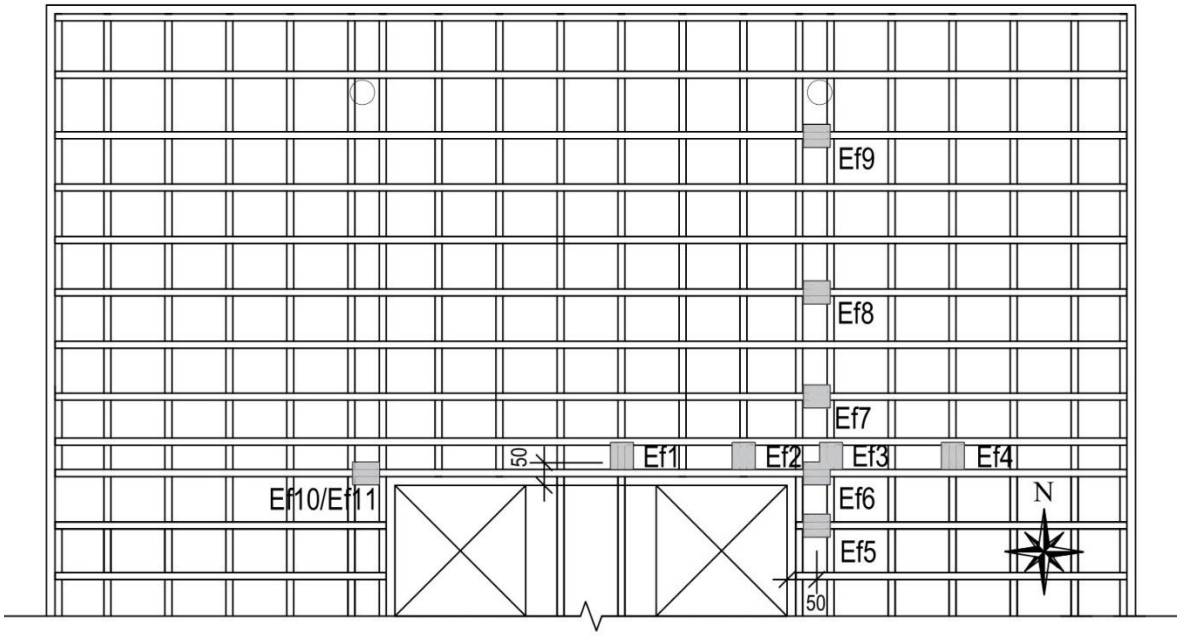

Figure 5.18 – Strains of flexural rebars: (a) LRSS (b) LRFS (c) LFS1 (d) LFS2 (e) LFS3

(a)

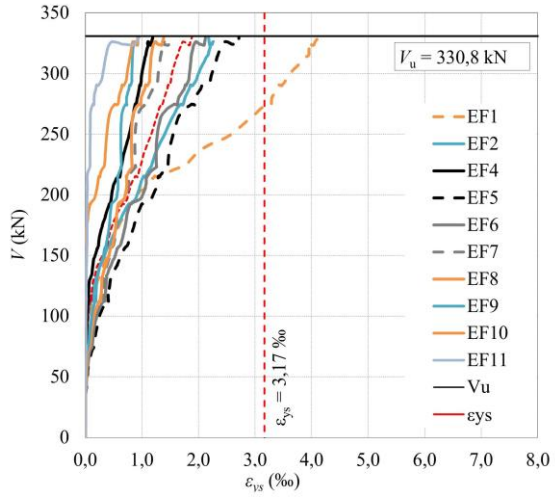

(b)

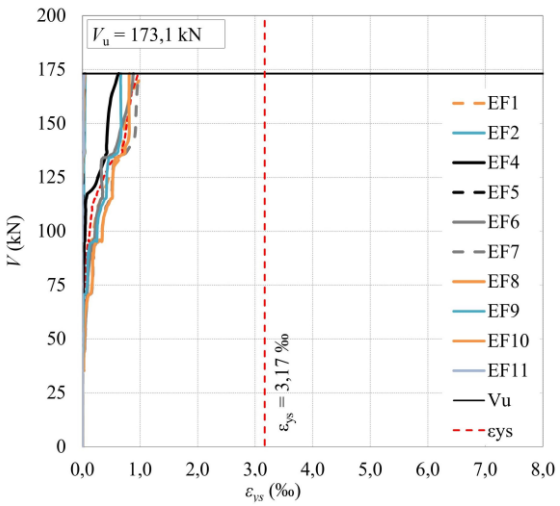

(c)

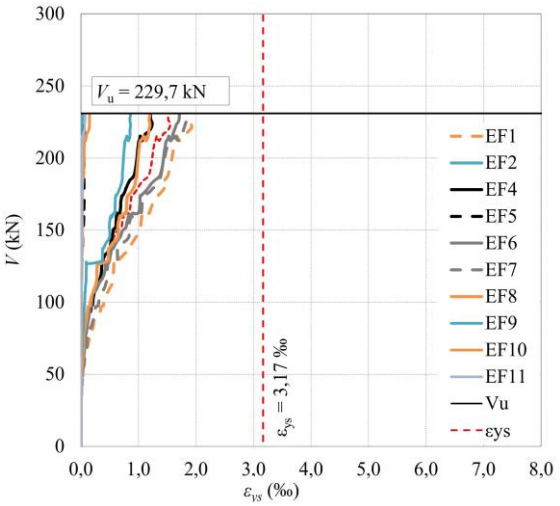

(d)

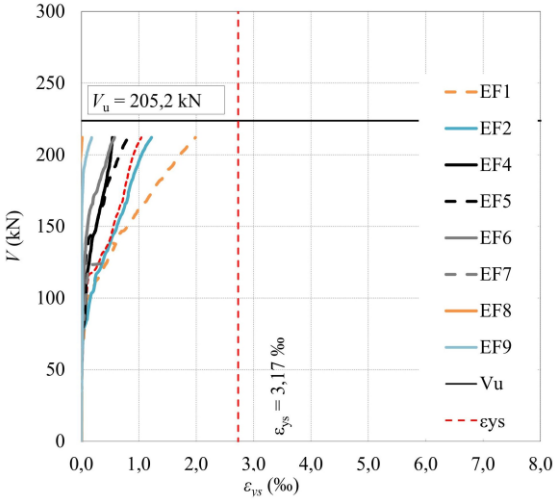

(e)

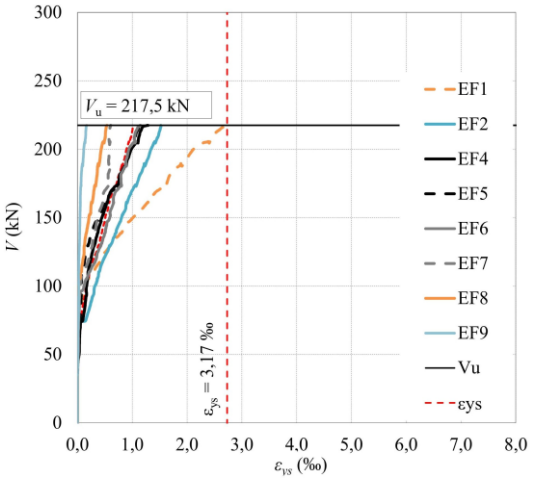

Figure 5.19 – Instrumentation of shear reinforcement (a) LFS1 (b) LFS2 (c) LFS3

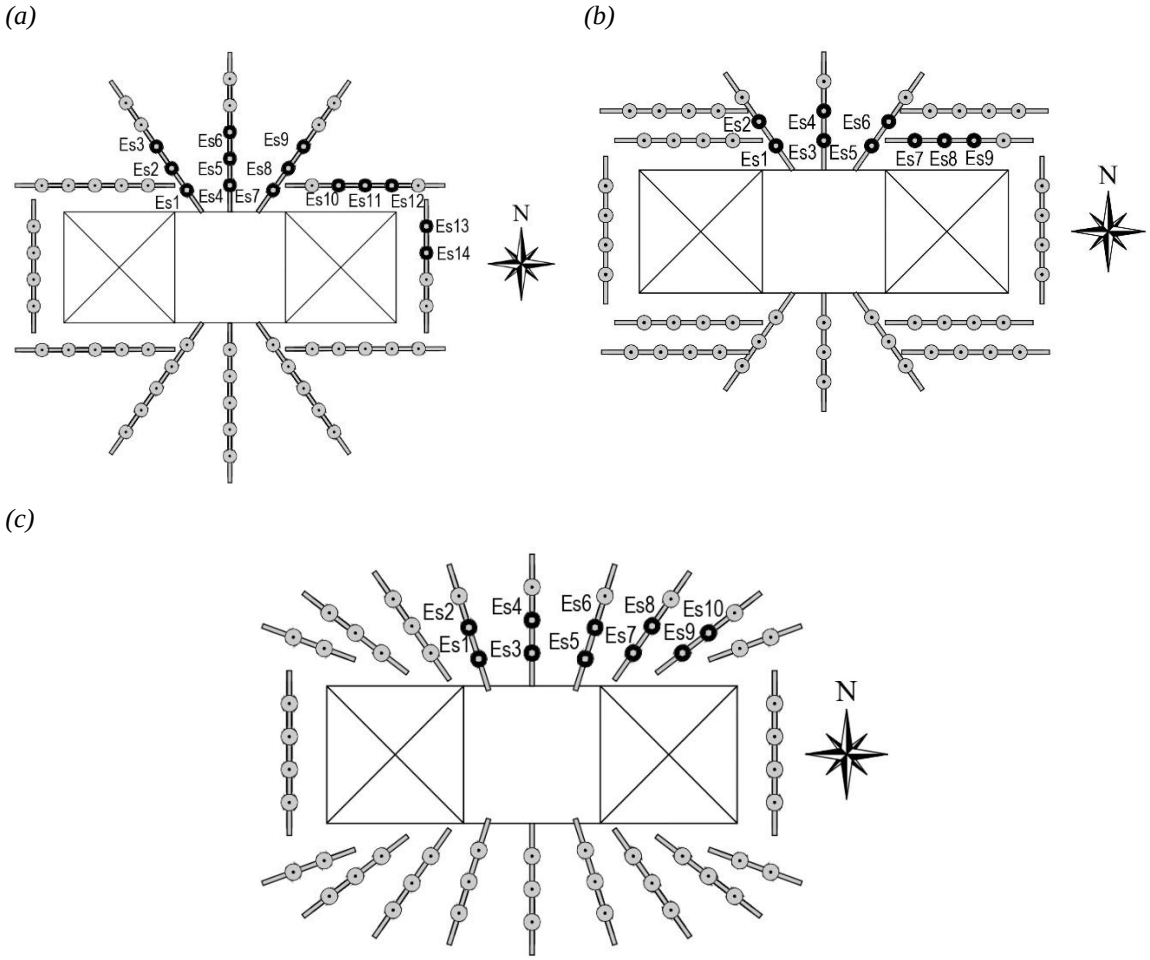

Table 5.9 – Slab LFS1: ratio of recorded-to-yield shear reinforcement strain ($\varepsilon / \varepsilon_{ys}$)

LFS1					
V (kN)	**ES1**	**ES4**	**ES7**	**ES8**	**ES10**
35,2	0,00	0,00	0,00	0,00	0,00
40,6	0,00	0,00	0,00	0,00	0,00
50,4	0,00	0,00	0,01	0,00	0,00
60,3	0,00	0,01	0,02	0,01	0,00
70,2	0,00	0,01	0,03	0,01	0,00
80,1	0,00	0,02	0,04	0,02	0,00
90,4	0,01	0,03	0,05	0,03	0,00
100,4	0,02	0,04	0,08	0,03	0,00
110,2	0,02	0,05	0,09	0,04	0,00
121,0	0,02	0,05	0,10	0,04	0,02
130,2	0,03	0,06	0,12	0,05	0,05
140,7	0,05	0,07	0,14	0,06	0,07
150,3	0,06	0,08	0,16	0,07	0,09
160,3	0,08	0,09	0,17	0,08	0,11
170,1	0,14	0,12	0,24	0,14	0,12
181,2	0,21	0,17	0,35	0,22	0,15
190,1	0,26	0,20	0,41	0,26	0,16
202,2	0,30	0,22	0,44	0,28	0,17
211,9	0,35	0,25	0,48	0,30	0,18

220,4	0,58	0,44	0,76	0,50	0,22
231,0	0,65	0,54	0,95	0,62	0,25

Table 5.10 – Slab LFS2: ratio of recorded-to-yield shear reinforcement strain ($\varepsilon / \varepsilon_{ys}$)

LFS2					
V (kN)	**ES1**	**ES3**	**ES5**	**ES6**	**ES8**
35,2	0,00	0,00	0,00	0,00	0,00
40,1	0,00	0,00	0,00	0,00	0,00
50,4	0,00	0,00	0,00	0,00	0,00
60,1	0,00	0,00	0,00	0,00	0,00
70,0	0,00	-0,01	0,01	0,00	0,00
80,2	0,00	-0,01	0,02	0,00	0,00
90,3	0,00	-0,01	0,02	0,00	0,00
100,1	0,00	-0,01	0,03	0,00	0,00
110,2	0,00	0,00	0,04	0,01	0,00
120,0	0,00	0,01	0,04	0,01	0,00
130,0	0,00	0,02	0,06	0,01	0,00
140,0	0,00	0,02	0,07	0,01	0,01
150,4	0,01	0,04	0,09	0,01	0,01
160,1	0,03	0,06	0,11	0,00	0,02
170,3	0,06	0,09	0,15	0,03	0,02
180,6	0,08	0,15	0,19	0,07	0,04
190,1	0,12	0,21	0,28	0,14	0,05
200,0	0,17	0,26	0,37	0,19	0,07
210,0	0,22	0,35	0,50	0,24	0,08
220,2	0,26	0,44	0,68	0,30	0,09
223,8	0,28	0,50	0,81	0,34	0,10

Table 5.11 – Slab LFS3: ratio of recorded-to-yield shear reinforcement strain ($\varepsilon / \varepsilon_{ys}$)

LFS3					
V (kN)	**ES1**	**ES3**	**ES5**	**ES6**	**ES9**
35,1	0,00	0,00	0,00	0,00	0,00
40,2	0,00	0,00	0,00	0,00	0,00
50,9	0,00	0,00	0,00	0,01	0,00
60,1	0,00	0,00	0,00	0,01	0,00
70,4	0,00	0,00	-0,01	0,01	0,00
80,2	0,00	0,01	0,00	0,02	0,00
80,6	0,00	0,01	0,00	0,02	0,00
80,9	0,00	0,01	0,00	0,02	0,00
90,4	0,00	0,01	0,00	0,02	0,01
100,7	0,00	0,02	0,00	0,01	0,00
110,1	0,00	0,04	0,00	0,01	0,00
120,1	0,01	0,06	0,00	0,02	0,00
130,4	0,02	0,08	0,02	0,02	0,00
140,4	0,04	0,11	0,05	0,02	0,01
150,1	0,07	0,13	0,10	0,02	0,07
160,4	0,13	0,17	0,16	0,05	0,15
170,2	0,17	0,23	0,22	0,07	0,21
180,7	0,23	0,31	0,29	0,08	0,24

190,1	0,30	0,40	0,37	0,10	0,27
200,0	0,33	0,44	0,41	0,10	0,28
210,4	0,41	0,56	0,59	0,11	0,30
217,5	0,51	0,69	0,64	0,11	0,38

6. CONCLUSIONS AND OUTLOOK

6.1 CONCLUSIONS

This thesis focuses on the punching shear behaviour of slabs with openings under axis-symmetrical and non-axis-symmetrical loading conditions, without shear reinforcement and with shear reinforcement. In addition to Chapters 1 (Introduction) and 6 (Conclusions and Future Research), the thesis comprises four main chapters, each corresponding to a journal article addressing specific aspects within the research topic.

To present the main conclusions in an organized manner, this section is divided by chapters, with each chapter's key findings summarized individually.

6.1.1 Punching resistance of flat slabs with openings adjacent to the column

Previous studies on the presence of openings in flat slabs without shear reinforcement primarily focused on slabs with square columns. However, rectangular columns are more representative of real buildings. An experimental programme consisted of eight interior slab-column connections to study the influence of adjacent holes on rectangular columns, considering their quantity, dimensions, and orientation with respect to column dimensions. Current normative predictions for the control perimeter reduction do not adequately consider the position of openings relative to the column. Comparing experimental and theoretical resistances can improve the design recommendations for punching with openings. The main conclusions are:

- The presence of openings in slab-column connections affects the punching shear behaviour, reducing the loading carrying capacity of flat slabs;
- The dimensions, location, and number of holes influence the distribution of the punching cone and the inclination of the critical shear crack;

- The code provisions reduce the control perimeter based on the distance of the hole from the column. It is desirable to have more detailed guidelines that consider the geometry and position of the hole;
- For slabs with large and non-symmetrical openings, considering the bending moment transfer leads to theoretical resistance values closer to experimental results, across all analysed design codes;
- However, for slabs with small holes, considering the moment transfer results in more conservative values for punching resistance;
- There is a clear need to enhance the design guidelines that consider the presence, size, and location of openings in flat slabs. Such improvements are crucial to accurately predict the structural behaviour and punching resistance of such slabs.

6.1.2 Enhancement of the punching shear verification of slabs with openings

Even though slabs with openings have been investigated since the 1960s, available experimental evidence on the behaviour of slabs with openings without shear reinforcement is scarce and some effects are neglected in current design codes. A database of 68 flat slab specimens with openings was analysed according to ACI 318:2019, current Eurocode 2 (EN 1992-1-1:2004) and the draft for the 2nd generation (prEN 1992-1-1:2021), *fib* MC 2010:2013 and the Critical Shear Crack Theory. The main conclusions are:

- Analysis of 68 slabs without shear reinforcement revealed some issues: overly conservative predictions for openings adjacent to the column, meaning that the radial line approach's is unsuitable for various geometries;
- Code provisions for slabs with unsymmetrical openings neglect the effect of moment transfer, leading to unsafe predictions;

- A new approach that increases the control perimeter for openings adjacent to columns and explicitly considers the eccentricity of slabs with unsymmetrical configurations resulted in better correlations with experimental and numerical results;
- The proposed approach for reducing the control perimeter considers the influence of the column, opening geometry, and effective depth;
- Mechanical models such as MC 2010:13 and CSCT show promising results for slabs with openings, demonstrating the closest mean value to one and the smallest coefficient of variation of experimental-to-calculated resistances;
- *fib* MC 2010:13 and CSCT effectively account for the non-linearity between the reduced control perimeter and resistance;
- *fib* MC 2010:13 and CSCT successfully evaluate the non-axis-symmetrical punching caused by column geometry and different reinforcement ratios;
- The Critical Shear Crack Theory is a powerful tool to model non-axis-symmetrical behaviour by considering the geometric mean of rotations in both directions.

6.1.3 Investigating punching shear in slabs with unbalanced moments and openings

The impact of openings and moment transfer on punching shear resistance was investigated by conducting tests on nine interior slab-column. The connections were subjected to different unbalanced moment orientations and eccentricities, all slabs without shear reinforcement. The experimental punching strength was compared to theoretical predictions according to ACI 318:19, fib MC 2010:13 for different levels of approximation and the 2nd generation of Eurocode 2 prEN 1992-1-1:23. The main conclusions are:

- The presence of openings and unbalanced moments significantly reduced the ultimate load-carrying capacity of the slabs;
- The effect of the unbalanced moment on resistance was found to be much more detrimental than the effect of the number of openings;
- The moment orientation significantly affected the slab resistance with openings: slabs subjected to moments in the opposite orientation to the openings position presented higher capacity;
- Slabs with openings exhibited significantly lower levels of flexural strain than those without openings;
- The concrete strains were significantly influenced by the presence of openings and unbalanced moments;
- The theoretical results of ACI 318:19 and fib MC 2010:13 LoAII showed a high deviation when compared to experimental results;
- The use of level of approximation III and the mean rotation significantly improved the *fib* MC 2010:13 results, with excellent results of average and coefficient of variation of experimental-to-calculated resistance;
- The theoretical results according to prEN 1992-1-1:21 demonstrated an excellent correlation with experimental values when using the early expression of k_{pb}. The equation of this coefficient in the latter version of prEN 1992-1-1:23 may not be suitable for analysing slabs with openings;
- The adoption of the control perimeter drawn to the faces of the openings, instead of the radial approach reduction, led to a noteworthy enhancement in both the average and coefficient of variation of experimental-to-calculated resistances according to all analysed codes.

6.1.4 Punching performance of flat slabs with openings accounting for the influence of moment transfer and shear reinforcement

There is currently no experimental evidence on the response of shear-reinforced slab-column connections with adjacent openings and unbalanced moments. Design is thus performed on the basis of simplified rules, modifying the resistance of connections without openings. A comprehensive test programme addressed at this issue is presented in an effort to improve the current state-of-knowledge. Five slabs representing several practical cases and potential arrangements of shear reinforcement were tested. The experimental results were investigated in detail and compared to codes of practice, highlighting a number of deficiencies of current simplified rules. The main conclusions are:

- Openings adjacent to columns significantly reduce the punching strength of slab-column connections due to effects such as shear-resisting perimeter reduction and shear force concentration;
- Placing shear reinforcement near the openings effectively improves the resistance and deformation capacity of the connections;
- In the investigated geometry, shear forces enter the corner regions despite the openings developing fully on two sides of the columns. This is confirmed by analysing the shear field and observing the failure location;
- Current design codes (ACI 318-19, fib MC2010, FprEN1992-1-1:23) provide scattered or conservative predictions of the punching resistance for slab-column connections with openings compared to other cases without openings.
- The Critical Shear Crack Theory (CSCT) offers an appropriate framework for analysing the punching resistance of these connections, providing accurate strength estimates with a low coefficient of variation. The CSCT allows for considering

different sectors in the control perimeter, where some sectors may fail while others remain intact, allowing for potential internal force redistributions;

- The CSCT accurately determines the location of the governing region within the control perimeter and provides consistent estimates of stresses in the shear reinforcement compared to test results.

6.2 OUTLOOK

Some questions remain open with respect to the punching shear behaviour of slabs with openings. Further experimental, numerical and theoretical investigation is still required to approach a consensus in this topic. Some possible ideas for future research are listed below:

- With respect to experimental works:
  - Further experimental programs are required to enhance the understanding of the impact of openings on the punching shear behaviour of flat slabs with moment transfer, particularly those involving different types of shear reinforcement and varying column and opening geometries. These studies would contribute to advancing the existing knowledge in this field;
- With respect to code design improvements:
  - Further research is required to establish the ideal relationships between the dimensions of openings and the critical perimeter for accurately consider the moment transfer in slabs with non-symmetrical openings;
  - The recommendations regarding the codes approach for slabs with openings and without shear reinforcement could also be validated for comprehensive database of slabs with shear reinforcement;

- With respect to the shear fields analyses:
  - Further investigation is desired to analyse the effects of openings on shear field perturbations in slabs with moment transfer, considering a variety of column and opening geometries;
- With respect to the Critical Shear Crack Theory models suggested in this thesis:
  - The application of the refined mechanical model of the Critical Shear Crack Theory (CSCT) for slabs with openings, moment transfer, and shear reinforcement can be extended to a comprehensive database of slabs with openings and moment transfer;
  - Additional experimental results focusing on slabs with openings, moment transfer, and various types of shear reinforcement could further validate the proposed refined approach of the CSCT for such slabs.

ANNEX A: CODE PROVISIONS

Figure A. 1 shows the control perimeter reduction according to the current code provisions. Table A. 1 summarizes the provisions for ACI 318:19, Table A. 2 for *fib*'s MC 2010:13, and Table A. 3 for FprEN 1992-1-1:23.

(a) (b)

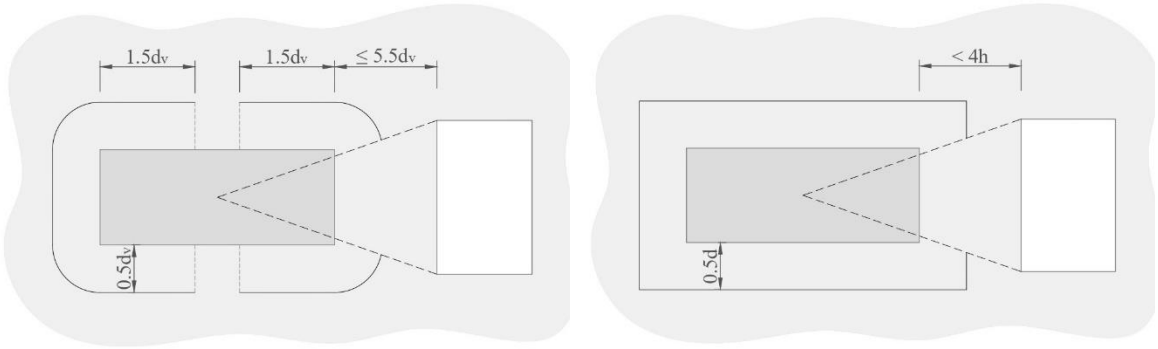

Figure A. 1 - Control perimeter reduction of slabs with openings according to: (a) fib MC 2010:13 and FprEN 1992-1-1:23 (b) ACI 318:19

Table A. 1 - Summary of ACI 318:19 provisions

Design equations for punching resistance – ACI 318:19		
$V_R \leq \begin{cases} V_{R,max} \\ V_{R,cs} \\ V_{R,out} \end{cases}$	$V_{R,máx} = \begin{cases} 0{,}5\sqrt{f_c}\ (stirrups) \\ 0{,}66\sqrt{f_c}\ (studs) \end{cases}$	$V_{R,cs} = \begin{cases} 0{,}17\sqrt{f_c} + \frac{A_{sw} \cdot f_{ywk}}{b_{0,5} s_r}\ (stirrups) \\ 0{,}25\sqrt{f_c} + \frac{A_{sw} \cdot f_{ywk}}{b_{0,5} s_r}\ (studs) \end{cases}$
$v_u = \frac{V}{b_{0.5}\, d} \pm \frac{\gamma_v M_u x}{J_c}$	$\gamma_v = 1 - \frac{1}{1 + \frac{2}{3}\sqrt{\frac{b_1}{b_2}}}$	J_c for a slab with two openings at column face: $J_{c,tot} = \frac{d b_1^3}{6} + \frac{b_1 d^3}{6} + (b_3 d) b_1^2$
OBS: see list of symbols		

Table A. 2 - Summary of fib MC 2010:13 provisions

Design equations for punching resistance - *fib* MC 2010:13

$$V_R \leq \begin{cases} V_{R,max} = k_{sys} k_\psi \sqrt{f_c} b_{0,5} d_v \leq \sqrt{f_c} b_{0,5} d_v & k_{dg} = \dfrac{32}{16 + d_g} \geq 0.75 \\ V_{R,cs} = k_\psi \sqrt{f_c} b_{0,5} d_v k_e + \left(\sum A_{sw}\right) k_e \sigma_{sw} & \psi = k_m \cdot \dfrac{r_s}{d} \dfrac{f_y}{E_s} \left(\dfrac{m_E}{m_R}\right)^{3/2} \\ V_{R,out} \end{cases}$$

$$k_\psi = \frac{1}{1.5 + 0.9 \cdot k_{dg} \cdot \psi \cdot d} \leq 0.6$$

$$b_{0.5} = k_e \cdot b_{1,red} \qquad k_e = \frac{1}{1 + {e_u}/{b_u}}$$

$$k_{sys} = \begin{cases} 2{,}4 \text{ (stirrups)} \\ 2{,}8 \text{ (studs)} \end{cases} \qquad \sigma_{sw} = \frac{E_s \psi}{6} \left(1 + \frac{f_b}{f_{yw}} \frac{d}{\phi_w}\right) \leq f_{yw}$$

LoAII for inner connections:

$$m_E = V \left(\frac{1}{8} + \frac{|e_{u,i}|}{2 b_s}\right)$$

OBS: see list of symbols

Table A. 3 - Summary of FprEN 1992-1-1:23 provisions

Design equations for punching resistance - FprEN 1992-1-1:23

$$V_R \leq \begin{cases} V_{R,cs} = \eta_c V_c + \eta_s \rho_w f_{yw} b_{0.5} d \geq \rho_w f_{yw} b_{0.5} d \\ V_{R,max} = \eta_{sys} \cdot V_c \\ V_{R,out} \end{cases}$$

$$\rho_l = \sqrt{\rho_{l,x} \cdot \rho_{l,y}}$$

$$d_{dg} = 16 + d_g \leq 40 \text{ mm}$$

$$1 \leq k_{pb} = 3{,}6 \sqrt{1 - \frac{b_0}{b_{0,5}}} \leq 2.5$$

$$d_a = \sqrt{\frac{a_p}{8} \cdot d_v} \geq d_v$$

$$a_p = \sqrt{a_{p,x} \cdot a_{p,y}}$$

where:

$$V_c = 0.6 \cdot k_{pb} \left(100 \rho_l f_c \cdot \frac{d_{dg}}{d_a}\right)^{1/3} \cdot b_{0.5} \cdot d_v$$

$$\eta_c = \frac{V_c}{V_E}$$

$$\eta_s = \frac{d_v}{150 \phi_w} + \left(15 \frac{d_{dg}}{d_v}\right)^{1/2} \cdot \left(\frac{1}{\eta_c \cdot k_{pb}}\right)^{3/2} \leq 0.8$$

$$\eta_{sys} = \begin{cases} 0{,}70 + 0{,}63 \left(\dfrac{b_0}{d_v}\right)^{1/4} \geq 1{,}0 \text{ (studs)} \\ 0{,}50 + 0{,}63 \left(\dfrac{b_0}{d_v}\right)^{1/4} \geq 1{,}0 \text{ (stirrups)} \end{cases}$$

$$\tau_E = \beta_e \frac{V}{b_{0.5} \cdot d_v}$$

$$\beta_e = 1 + 1.1 \frac{e_b}{b_b}$$

$$b_b = \sqrt{b_{bmin} b_{bmax}}$$

For internal columns: $e_b = \sqrt{e_{b,x}^2 + e_{b,y}^2}$

OBS: see list of symbols